Doctoral School in Environmental Engineering

Hydrothermal carbonization of waste biomass

Daniele Basso

UNIVERSITÀ DEGLI STUDI DI TRENTO
Dipartimento di Ingegneria Civile,
Ambientale e Meccanica

2016

Doctoral thesis in Environmental Engineering, XXVIII cycle
Department of Civil, Environmental and Mechanical Engineering
University of Trento
Academic year 2015/2016
Internal supervisor: Luca Fiori, University of Trento (IT)
External supervisor: Marco Baratieri, Free University of Bolzano (IT)

University of Trento
Trento, Italy
2016

Dedication

A Fede e Minù.

"... per chi viaggia in direzione ostinata e contraria
col suo marchio speciale di speciale disperazione
e tra il vomito dei respinti muove gli ultimi passi
per consegnare alla morte una goccia di splendore
di umanità di verità
...
ricorda Signore questi servi disobbedienti
alle leggi del branco
non dimenticare il loro volto
che dopo tanto sbandare
è appena giusto che la fortuna li aiuti
come una svista
come un'anomalia
come una distrazione
come un dovere."
F. De André, Smisurata Preghiera

Aknowledgements

Many people helped me during my Ph.D., though in different ways.
The first person I want to thank is the person who gave me the strength and the motivation to start this adventure and gave me (and is continuing to give me) the all her love and support. This person is Federica, my wife. She introduced me into a magic world, the world of knowledge, curiosity and science. There is another special person I want to thank: she is the other my big love of my life, my daughter Miriam. I started my Ph.D. when she was only one year old. Miriam followed me in Trento, in Stuttgart, in the labs. Thank you Miriam for having let your daddy work. I want to apologize to both Federica and Miriam for all the times I was working hard and I cannot stay relaxed with them.
I want to thank prof. Luca Fiori and prof. Marco Baratieri for their precious hints on my research. Thanks to Elsa Weiss Hortala, Francesco Patuzzi and all the other friends of the Free University of Bolzano. Thank to prof. Andrea Kruse, Dominik Wüst and all the friends of the University of Hohenheim for having hosted me and helped me. Thank you all even for your precious friendship. A special thank to prof. Marco Tubino for his precious fatherly advices. Thanks even to Giuliano Chies.
Thanks to my parents, Giorgio and Germana. A special thank to Gabriella, Roberto, Lucia and Jacopo, Tita and Enrichetta Mazzon, Patrizia and Flavio Bianchi, aunt Daniela and uncle Gianni, Andrea and Davide Colleoni. Thanks to my cousin Riccardo.
Thanks to Contarina S.p.A. for the financial support of this work.
Thank to all the other friends and relatives that remained with me, Federica and Miriam during this long period.

Contents

List of Figures

Chapter 5

Chapter 6

Chapter 7

Chapter 8

List of Tables

Chapter 5

Chapter 6

Chapter 7

Chapter 8

List of acronyms and symbols

B/W: biomass to water weight ratio (g/g)

EWC: European waste catalogue

GM: grape marc

HTC: hydrothermal carbonization

HHV: Higher heating value (MJ/kg)

LHV: Lower heating value (MJ/kg)

OC: off-specification compost, coded as EWC 19.05.03

P: pressure (bar)

RDF: Refuse derived fuel

T: temperature (°C)

τ: residence time (h)

UW: unsorted residual waste, coded as EWC 19.12.12

Summary

Hydrothermal carbonization (in acronym, HTC) is a thermochemical conversion process through which it is possible to directly transform wet organic substrates into a carbonaceous material, referred as hydrochar. Hydrochar has chemical and physical characteristics that make it similar to fossil peats and lignite. Depending on the process conditions, mostly temperature and residence time, this material can be enriched in its carbon content, modifying its structure and providing it interesting characteristics that make it possible to be used for several applications, such as for energy production, as a soil conditioner and improver, for carbon dioxide sorption and sequestration, and some others reported in literature. HTC is a different process, if compared to other common thermochemical processes, such as pyrolysis, torrefaction, gasification, etc., because it works in wet conditions (humidity content higher than 60%). As a matter of fact, biomass is transformed into hydrochar because of the properties of hot pressurized water, that acts both as a reactant and as a catalyst. The HTC process has been studied from many years, although at present not all the chemical reactions that occur during the process are completely known. Moreover, the application of this quite new process to different substrates can bring to different results. Even though HTC can be applied to any kind of organic material (of both animal and vegetable derivation), the possible uses of hydrochar can strongly be influenced by the characteristics of the feedstock. This, for example, can be due to legislative constraints. In Chapter 1, an overview of the existing literature is presented.

To get insights on this process, a small bench scale batch reactor has been designed and built at the Department of Civil, Environmental and Mechanical engineering of the University of Trento, Italy. This reactor has

been tested, prior to be used with real substrates. In Chapter 2 the reactor and the preliminary tests done are described.

In this work, the HTC process applied to three different substrates have been studied: grape marc, the EWC 19.05.03 residue and the EWC 19.12.12 residue. In Chapter 3 the three raw substrates are described.

Grape marc is produced by the winery industries or by distilleries. This feedstock is composed by woody seeds and holocellulosic skins and it presents an average humidity content of about 60%. At present, it is used for the production of animal food or it is landfilled. In this case, the application of HTC can be an interesting alternative to these end uses because, through this process, grape marc can be recovered, for example, for energy production. The hydrochar produced from this feedstock could be even used as a soil conditioner. In Chapter 4 several analyses on the hydrochar, on the process water and on the gaseous phase obtained during the carbonization tests are presented.

The EWC 19.05.03 residue is a by-product of the composting treatment applied to the organic fraction of municipal solid waste (MSW). In collaboration with Contarina S.p.A., a company that collects and treats MSW in the province of Treviso, in the North-East of Italy, this by-product was carbonized and tested both as a soil conditioner and for energy production. Results of the analyses on the solid, liquid and gaseous phases produced by the HTC process are reported in Chapter 5.

The EWC 19.12.12 residue is a by-product of the refuse derived fuel (RDF) production, from the residual fraction of the MSW. This substrate was provided by Contarina S.p.A. and preliminary tests on the exploitability of the hydrochar for energy production are reported in Chapter 6, together with analyses on both the liquid and gaseous phases.

A rigorous energy balance has been proposed in Chapter 8, based on the experimental data obtained for grape seeds. In this chapter, all the hypotheses and the assumptions taken to evaluate the enthalpy of the HTC reaction at different process conditions (namely, three different temperatures and three residence times) are described.

In Chapter 8 a kinetic model is proposed, based on a two-step reaction mechanism. The activation energy and pre-exponential factor of the various degradation reactions were determined by means of least square optimization versus the experimental data of grape marc. A thermo fluid model is even proposed in this chapter. The model integrates mass, momentum and heat equations within the reactor domain by means of the finite volumes method (f.v.m.) approach. Convective and radiative exchange between the reactor and the fluid within the reactor have been implemented in the f.v.m. model. Under two strong assumptions (mono-component and mono-phase fluid, which fulfils the reactor), it was possible to estimate the behaviour of an equivalent fluid (eq_fluid), in terms of thermal properties of the fluid (thermal capacity, thermal conductivity and thermal diffusivity). Moreover, a simplified dynamic analytic model is also presented – based on lumped capacitance method – in order to simulate the thermal behaviour of the system, using the actual temperature profile imposed by the reactor external heater. A resistance-capacitance network was used to describe the system. Finally, the Henry's law has been applied to assess the amount of gas really produced during the HTC process.

In Chapter 9, the main conclusions of this work are reported.

Chapter 1

Hydrothermal carbonization of waste biomass

1.1 Introduction

The exploitation of natural resources, with characteristics of environmentally friendliness, renewability and low green house gases (GHGs) emission, for energy production is a great challenge that has been investigated for many years. In this field, biomass has been evaluated for the production of solid, liquid and gaseous fuels through a large variety of processes. For the sake of simplicity, these processes can be divided into biological and thermochemical treatments. The former are processes in which living organisms (such as bacteria, fungi and other micro organisms) are involved in many chemical reactions, aimed to oxidize and stabilize the organic matter and to produce energy-value streams, typically gaseous products. In this category of processes, it is possible to contemplate, for example, the anaerobic digestion through which a biogas and a digestate are produced. The composting is another biological treatment applied to waste organic materials to obtain a fertilizer and soil amendment. These processes usually require specific operating conditions to guarantee the organisms to acclimate and survive, and usually take several days to be completed.

Conventional thermochemical processes permit to obtain heat, heat and electricity, syngas, and pyrolysis oils and by-products from the dry biomass.

These conversion technologies are represented by the combustion of the biomass, the co-firing of woody and herbaceous biomasses, the gasification and the pyrolysis [1]. All these processes require the biomass to be dried prior to be converted. The current thermochemical technologies used to exploit solid biomasses arrange the process conditions (e.g., temperature, pressure, residence time, wt.% of humidity) in order to obtain gaseous, liquid or solid products. A quiet new family of processes that have been studied in recent years and that are currently object of many researches are the hydrothermal processes. These processes are performed in a hot compressed water environment, condition that permits the direct treatment of wet substrates, avoiding any drying pretreatment. Depending on the process conditions (temperature and pressure), the hydrothermal processes can be divided into hydrothermal carbonization (HTC), hydrothermal liquefaction (HTL) and hydrothermal gasification (HTG). At temperature ranging from 180 to 250°C (HTC conditions) very little amount of gas is produced downstream of the process and the major product is in the solid state. Enhancing the temperature up to near 400°C, more liquid is formed and the amount of gas becomes higher. These are typical HTL conditions. A further enhancement of temperature, brings to reach the HTG conditions. In this case, water is in its supercritical state and the primary product is gaseous.

Typical solid products are obtained through the chemical decomposition of the feedstock, resulting in a carbon rich solid material, with an high chemical stability.

Liquid products resulting from an HTL process are mainly composed of liquid hydrocarbons and heavy oils.

Gaseous products are composed of hydrogen (H2), methane (CH4), carbon dioxide (CO2) and others compounds, that can be both combusted (after a cleaning procedure, e.g. in a gas turbine, or in a Biomass Integrated Gasification/Combined Cycle) and used to produce pure hydrogen [2].

In this paper, the focus is on the hydrothermal carbonization process, with the aim of presenting an overview on all the aspects and characteristics of this

process so far studied, in terms of parameters governing an HTC treatment, the characteristics and the possible applications of the products, the main challenges and the possible objectives of further researches.
This paper is based on two previous works on the hydrothermal treatments by Funke and Ziegler [3] and Libra et al. [4] and summarizes the state of the art after these two reviews.

1.2 Hydrothermal carbonization

Description of the process

The hydrothermal carbonization process is a thermochemical process in which the wet biomass is converted into a solid product, called hydrochar, in milder operational conditions if compared to the other conversion technologies. The HTC temperatures usually range from 180°C to 250°C, even though some authors have explored the behavior of the process up to 300°C or at higher temperatures [5, 6, 7, 8, 9, 10, 11, 12, 13]. The pressure is held as high as to maintain water in the liquid phase (10 – 40 bar). In these conditions, the hot pressurized water exhibits higher ion production than at ambient conditions, behaving as an acid/base catalyst precursor and acting both as a solvent and as a reactant, as a catalyst or product [14]. Enhancing temperature and pressure above the critical point (374.15°C, 220.64 bar), water changes its property by lowering its density and dielectric constant [15], becoming more capable to solve organic non-polar compounds. In subcritical conditions, the HTC converts the wet biomass in a carbonaceous hydrochar, which is a solid phase enriched in its carbon content. The hydrochar has a heating value higher than the original input material, with lower hydrogen/carbon and oxygen/carbon ratios and with a chemical structure that make it similar to natural coal [16]. The Van Krevelen diagram represents adequately this similarity (Figure 1.1). The structure of the hydrochar results to be homogeneous independently of the original

feedstock, representing an advantage in the use of the hydrochar as a solid fuel in heat and/or power generation plants. The process usually is conducted at alkaline conditions (pH lower than 7). Typical residence times range between minutes to several hours, mainly depending on the characteristics of the products to obtain. The higher the temperature, and hence the higher the pressure, the higher the carbon content of the hydrochar, even though the total solid yield becomes smaller.

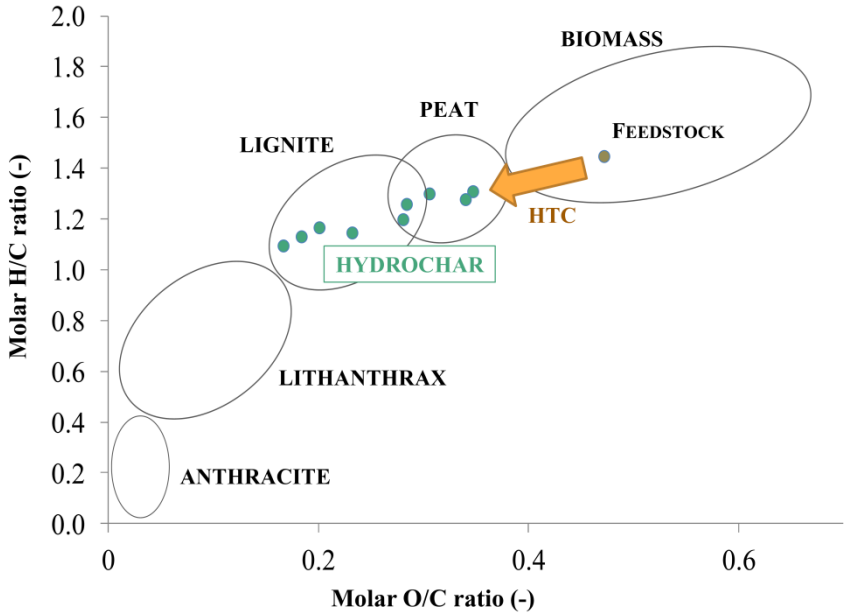

Figure 1.1. Van Krevelen diagram.

From a design and application point of view, the hydrothermal treatment has the advantage to take only hours (when compared to traditional biological treatments) resulting in smaller plants; it allows the elimination of organic contaminants and pathogen organisms; typically it does not produce odors. Moreover, the hydrothermal treatment can be exploited to store carbon,

limiting the emissions of CO2 and contributing to the mitigation of green-house gases with effects on the climate change (this is valid only when hydrochar is used as a soil amendment or as carbon-storage material).

Chemical reactions and mechanisms involved

Lots of reactions could occur during the hydrothermal process at subcritical temperature, the majority of them being the same that occur during pyrolysis. The HTC is mainly governed by hydrolysis, which breaks the ester and ether bonds of cellulose (at T > 200°C), hemicellulose (at T > 180°C) and lignin (at T > 200°C) [3] by addition of water. The hydrolysis pathway has been suggested by many authors [5, 17, 18, 19, 20, 21, 22, 23, 24, 25, 26]. Hydrolysis of hemicellulose produces acetic acid, D-xilose, D-manose, D-galactose and D-glucose. These last three are typically converted into 5-hydroxy-methyl-furfural (5-HMF) and then in formic or levulinic acid. The cellulose follows an analogous pathway, hydrolyzing into D-glucose, producing 5-HMF and subsequently into formic or levulinic acid. Lignin typically forms phenolic compounds (Figure 1.2).

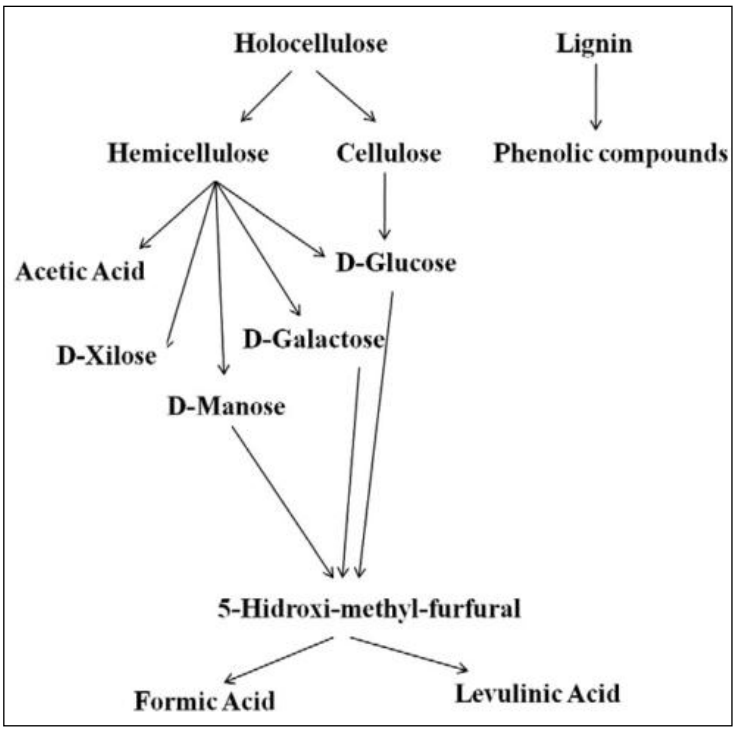

Figure 1.2. Degradation products and sub products during hydrolysis of lignocellulosic biomass (from ref. [18]).

The lowering of the H/C and O/C ratios during the HTC is mainly explained by dehydration and decarboxylation mechanisms. Hydroxyl groups are generally eliminated by dehydration, while carboxyl and carbonyl groups are involved during decarboxylation. In the Van Krevelen diagram, dehydration pathway follows a straight line which decreases both H/C and O/C ratios, moving from top right to bottom left; decarboxylation moves from bottom right to top left, thus enhancing the H/C ratio and lowering the O/C ratio. During the HTC process typically dehydration is a more important mechanisms than decarboxylation. This fact explains why the products of HTC are mainly located on the bottom left. Hydrolysis fragments formed during the process could be highly reactive, condense and polymerize to

form the hydrochar. As suggested by Quadariyah et al. [7] at subcritical and near critical temperatures, ionic reactions appears to be the main mechanism of formation, while at supercritical temperatures free-radical reactions may dominate. At high reaction conditions of temperature and pressure, mechanisms of formation of aromatic structures can occur in hydrothermal conditions [27, 28]. The trend of the enhancement of the formation of aromatic structures with the enhancement of temperature and pressure during an HTC process has been demonstrated experimentally with 13C-NMR measurements [29]. The formation of aromatic bonds during the hydrothermal process could decrease the total carbon content of the hydrochars. The residence time can have an influence on the aromatization process, but its influence has not been investigated yet.

Other mechanisms occurring during the hydrothermal carbonization can be summarized as:

- demethylation;
- transformation reactions;
- pyrolytic reactions;
- Fischer-Tropsch-type reactions.

Demethylation is the chemical process through which a phenol becomes part of a cathecol-like structure of the coal [30], and consists in the removal of a methyl group (CH3) from the molecule.

Transformation reactions in lignin may occur when the hydrolysis and the subsequent condensation cannot take place, mainly for stable compounds with crystalline structure and oligomer fragments [31, 32].

Pyrolytic reactions may occur at temperatures higher than 200°C and contribute to form carbonaceous products from the fragments of feedstock that could not come into contact with water, because they are trapped by precipitation of condensed fragments [33]

Products of HTC

The products resulting from HTC treatment are a solid phased enriched in carbon content, the hydrochar, a liquid phase with phenolic compounds and furan derivatives [24] dissolved and a small quantity of a gas mostly composed of carbon dioxide [22].

The hydrochar is a solid phase with H/T and O/C ratios lower than the original biomass (though higher with respect to char obtained during pyrolysis). Chemically, the hydrochar presents a significant amount of functional groups compared to natural bituminous coals, but lower amounts in carboxyl and hydroxyl groups. Thus hydrochar presents a lower hydrophilicity than the original biomass. Berge et al. [35] have reported that hydrochar is mainly composed of fused aromatic rings, which could improve its stability for example in the use of hydrochar as an amendment. Some authors [34, 35, 36] show that most of the carbon present in the initial biomass remains within the hydro-char (up to 80% by weight [**Errore. Il segnalibro non è definito.**]), if compared to both the liquid and gas phases. The energy content of the hydrochar with respect to the original feedstock is enhanced by the HTC by 1.01 to 1.41 times (on weight basis) and 6.39 and 9.0 times (on volume basis) [36]. Roman et al. [17] found that the hydrochar has a heating value ranging between 28.9 and 29.3 MJ/kg, corresponding to an increase of 1.50–1.71 (on weight basis) of the heating value of the original feedstock. Other authors [24, 34, 36, 38] confirm this energy values, which underline the potential of an energetic exploitation of this solid product. Experimental analyses of the N2 adsorption isotherms at 77 K [39] showed that the apparent surface area of hydrochars ranges between 25 and 30 m^2g^{-1}, and that adsorption isotherms fitting the experimental data are all of type II, according to IUPAC classification.

Furthermore, the hydrochar has shown a clear aptitude on adsorption applications and as a activated carbon precursor [7, 40, 41].

The liquid phase presents several organic compounds, such as acetic acid, aldehydes and alkenes, and aromatics such as furanic and phenolic compounds, as it has been detected experimentally [36, 37]. Heilmann et al. [i] found non-agglomerated colloidal carbonized material in the aqueous filtrates. Other studies [13] observed the formation of a tar fraction consisting of polar compounds of high molecular mass. From GC-MS analyses performed by Xiao et al. [23], the presence of sugar derived compounds and lignin derived compounds has been investigated. Furfural, 2-ethyl-5-methyl-furan and 2-hydroxy-3-methyl-2-cyclopenten-1-one were the main sugar derived products detected, while phenols were the major lignin derived products found (particularly phenol monomers such as 2,6-dimethoxyl, butyl-2-methylpropy-lester-1,2-benzenedicarboxylic acid and butyl 4-ethoxy-2,5-dimethoxy-benzaldehyde). COD, BOD and TOC concentrations of the liquid obtained downstream of the process are similar to those typically found in landfill leachate. BOD/COD was found to be higher than 0.3 [36]. Because of the presence of organic acids, the pH of the liquid phase is usually acidic.

HTC produces also a small amount of gaseous phase. This phase is mainly composed by CO2 with traces of CO, CH4 and H2 [22, 36]. The amount of carbon present into the gaseous phase is mainly due to decarboxylation. Lu et al. [37] have detected also other hydrocarbons in appreciable concentrations (ethane, ethane and propene). The lower yield of gaseous oxidation compounds during HTC, if compared to direct combustion or pyrolysis, could be attributed to the fact that the amount of oxygen available is limited given the reaction conditions.

It is important to note that the yield of the products is strongly dependent on the HTC conditions (mainly temperature and retention time) and on the biomass used as feedstock. The influence of the process parameters is discussed below.

Influence of reaction parameters

The HTC process is mainly governed by the following parameters: temperature, biomass to water (B/W) ratio, pressure, residence time, pH, feedstock composition.

Temperature is considered to be the most influencing parameter of an HTC process. Many experiments have been developed to understand how variations of temperature may affect the total carbon recoverable and the solid yield (hydrochar) downstream the hydrothermal carbonization. All authors agree that an enhancement of temperature produces an increase of carbon content of the hydrochar, while the hydrochar yield undergoes a general decrease [42, 22, 23]. As a matter of fact, the enhancement of temperature favours the dehydration and the decarboxylation reactions, which correspond to a decrease of the oxygen and of the hydrogen contents of the treated feedstock and consequently the O/C ratio decreases enhancing the carbon content of the hydrochar. On the other hand, higher temperatures drive the reaction to generate more liquid and gaseous products, hence a decrease of the solid phase occurs. Furthermore, higher temperatures may cause the degradation of part of the hydrochar produced, contributing to the lowering of the mass yield [43]. At temperatures lower than 180°C carbonization is considered to occur with difficulty, because cellulose and hemicellulose typically decompose at temperatures higher than 180 – 200°C [3, 22]. Also Weidner et al. [43] suggested a negligible temperature influence on the chemical composition of hydrochar at temperatures below 180°C, indicating a dominance of the kind of feedstock, at these temperature values. As a matter of fact, the higher the temperature the more homogeneous, dense and uniform the solid product of the HTC reaction. Muller et al. [12] suggested the formation of two different type of solid product: a primary char (lower temperatures), produced from hard plant tissue of lignocellulosic

biomass, and a secondary char (at 350 – 370°C, named coke), produced from water soluble biomass components, such as phenols and 5-hydroxy-methyl-furfurals (5-HMF). The primary char presents a structure similar to the original biomass and results in a significant surface area and pore volume. Secondary char, which is formed by liquefaction of the biomass, is richer in oxygen and hydrogen, presents no inner surface area or pores and has no structural resemblance with the original feedstock. Weidner et al. [43] suggested that at lower temperatures most of the polysaccharides do not degrade, resulting in a hydrochar more similar to the original feedstock. As a matter of fact, the lignin content generally decrease with increasing temperature, mainly because of the enhancement of its degree of oxidation with temperature. The decrease of the O/C ratio, which correspond to a removal of oxygen from the feedstock, may explain the enhancement of the higher heating value (HHV) of the hydrochar with an increase of temperature, as suggested by Du et al. [44]. From an energy point of view, given the fact that both dehydration and decarboxylation have negative heat of reaction [19], it could be expected that the amount of energy released must increase and hence that the HTC process becomes exothermal at higher temperatures.

Authors [10, 12, 19] agree that temperature controls the reaction kinetics. As it will be discussed in the following, the typical reaction kinetics proposed are the pseudo first-order kinetic and an Arrhenius-type description [3]. In the modelling of the HTC process, important differences have been observed on the reaction constant rates (k) of a first-order kinetic description with the enhancement of temperature, as well as the variations of the apparent activation energy (E). This could be due to the fact that at lower temperatures the decomposition of cellulose and hemicellulose prevails, while at higher temperatures the effect of lignin is more evident [12]. Furthermore, higher E values at higher temperatures may be due to lowering of the dielectric constant when approaching the supercritical conditions. It has been shown that at lower temperatures condensation and depolymerisation are the main

conversion pathways, while at higher temperatures polymerization and aromatization prevail [3, 45]. Temperature also increases the pH of the hydrochar, gives it a higher cation exchange capacity and a higher surface area [7]. Considering a possible use of hydrochar as soil improver or for carbon sequestration, Gajić et al. [9] found that the reduction of the O/C ratio of the hydrochar (i.e., reduction of oxygen content) enhances the stability of the hydrochar. Analyzing the possibility to recover a solid fuel from municipal solid wastes through a hydrothermal carbonization process [35], it has been shown that the chlorine content due to the presence of PVC can be degraded into soluble chlorine compounds and hence washed away to improve the hydrochar quality as a solid fuel.

The process has to be developed in hydrous conditions. Experiments of carbonization of biomass within other substrates (e.g., oil) have been investigated, but the hydrothermal carbonization in water seems to be the best pathway for biomass carbonization [45, 46, 47, 48]. In general, the experiments developed by authors [6, 11, 13, 16, 34, 35] were conducted with water contents which ranged from 50% to 95%. The majority of these experiments has not investigated in deep the influence of the biomass to water ratio on the products. Funke and Ziegler [18] found no influence on the HTC reaction kinetics, of a solid loading in the range of 20 – 50%. The modelling of the process proposed by Heilmann et al. [41] has suggested an influence of the percentage of the solid loading on the percentage of mass yield obtained downstream of an HTC process. On the other hand, from the same analysis the solid yield seems not to be determinant in respect to the efficiency of the carbonization (i.e., the percentage of carbon recovered through the HTC process). Moreover, they have noted that the recirculation of the process water, which contains small amounts of non-agglomerated materials, does not significantly contribute to the whole yield of the process. The experiments were developed varying the percentage of input solids in a range of 5 – 25%. Different results were obtained by Román et al. [17]. In their work, the enhancement of the biomass to water (B/W) ratio produced a

decrease on the solid yield and lower carbonization. These results may be explained by the fact that the higher water quantity enhances the hydrolysis reactions. Studying the glycerol degradation into tar and char [12], it has been found that the higher the feed concentration, the faster the glycerol degradation into solid products. The amount of glycerol initially present within the water decreased faster as this amount was enhanced.

Pressure is mostly considered to be an indirect parameter of the process, because it is strongly dependent on the temperature. As a matter of fact, to develop an hydrothermal carbonization process it is compulsory to maintain the water in the liquid phase. However, the influence of pressure has been investigated in simulating lithostatic pressure [49, 50]. It is considered that the variations of pressure moves the equilibrium of an HTC process according to the Le Chatelier's principle. The typical reactions which occur during an hydrothermal carbonization (i.e., dehydration and decarboxylation) appear to be weakened by higher pressures; on the other hand, an easier dissolution in water of extractables present in the biomass, increasing the process pressure, has been detected [32, 51].

The residence time of an HTC process has a rising interest especially for practical processing design and operating. Usually, the HTC process takes a time that ranges between some minutes and several hours. The majority of the experiments analyzed in this review has shown that enhancing the residence time of the biomass inside of the HTC reactor generally results in a higher carbon content of the hydrochar [12, 42, 21, 41, 52] and a consequently higher HHV. With respect to the characteristics and properties of the products, the residence time permits an improvement of the dehydration and decarboxylation reactions [3], thus avoiding the use of catalysts to obtain higher conversions of the feedstocks, even though higher residence times may cause further degradations of the products into other compounds [7]. Residence time is also generally considered to reduce the total solid yield downstream of the HTC process, favouring the formation of higher quantities of water soluble compounds. Modelling the process,

Heilmann et al. [41] found that the residence time has an influence on the carbon yield comparable to that of temperature, while its influence is near an order of magnitude lower with respect to the total mass yield. A different behaviour was found by Mumme et al. [16], who found that both temperature and residence time reduces the solid carbon yield with the same strength. Roman et al. [17] found almost no influence of this parameter both on carbon and solid yields. Some authors [6] have pointed out the influence of residence time on the surface area and porosity of the hydrochar, because of the recondensation and repolymerization reactions of water soluble compounds. Moreover, Kruse [21] suggested that cellulose could carbonize at lower temperatures (200°C) in case higher residence times are employed.

During an HTC reaction, the pH usually drops because of the formation of several acidic compounds, such as acetic, formic, levulinic and lactic acids, as suggested by many works [19, 50, 53, 54, 55, 56]. The influence of different acids and bases on the characteristics and properties of the products have been investigated [15, 47, 57]. Generally acidic conditions catalyze the carbonization of the biomass [57], facilitating the hydrolysis of cellulose, while the influence on the other processes, such as decarboxylation and condensation polymerization, is still unknown. Some authors [15, 58, 59, 60] observed that the enhancement of the pH in a HTC process result in products with higher H/C ratios, which correspond to more bituminous hydrochars. Funke and Ziegler [18] found that the addition of acids to the process does not result in different amounts of heat release during an HTC process. Besides autocatalysis of produced organic acids results more difficult as the pH lowers below 3. Different conclusions on the influence of the pH on the hydrothermal carbonization process were found by some authors. Mumme et al. [16] observed an interference on the carbonization process at low pH conditions, while the hydrochar's carbon content seems not to be affected by this parameter. Titirici et al. [57] suggested a catalytic effect of acidic conditions on the HTC process. Heilmann et al. [41] did not find such an effect on the HTC process in the presence of citric acid. Funke and Ziegler

[3] observed that weakly acidic conditions improve the overall rate of the HTC reaction.

It is widely considered that the HTC process is a more effective treatment, if compared to pyrolysis or to the biological treatments, because of its independence on the characteristics of the inlet biomass. HTC can treat the biomass as it is, without the need for a drying pre-treatment, and it is not affected by the presence of toxic compounds, in contrast to a typical biological treatment. At temperatures near 180°C the hydrothermal carbonization yields products with characteristics and properties similar to those of the original feedstock. At these conditions, the typical HTC reactions cannot wholly occur, thus the feedstock becomes the parameter dominating the reaction products [43]. HTC is regarded as a treatment which permits to obtain homogeneous products, regardless of the feedstock characteristics.

1.3 Modelling of the HTC process

Although a complete mathematical description of the process is still lacking, several authors have proposed relationships to examine the behavior of the HTC process, mainly in terms of the amount of carbon recovered within the hydrochar and of the amount of solid phase obtainable downstream the process.

The approach followed by Heilmann et al. [41] and by Mumme et al. [16] was to build linear regression equations for the carbon content, C_Y, and for the mass yield, M_Y. The former have correlated these two process outputs to the temperature, the residence time and the solid load through dimensionless variables (equations (1.1) and (1.2)).

$$C_Y = 64.98 + 1.78 \cdot X_1 + 1.32 \cdot X_2 + 0.08 \cdot X_3 \quad (1.1)$$

$$M_Y = 37.44 - 1.34 \cdot X_1 - 0.44 \cdot X_2 + 6.01 \cdot X_3 \quad (1.2)$$

In these relations, X_1 is the dimensionless temperature, X_2 is the dimensionless residence time and X_3 is the dimensionless percentage of solids in the inlet.
The linear regression analysis conducted by Mumme et al. [16] is reported in what follows (equations (1.3) and (1.4)).

$$C_Y = -38.4 + 0.21 \cdot \vartheta_P + 0.54 \cdot t_R \quad (1.3)$$

$$M_Y = 184 - 0.24 \cdot \vartheta_P - 0.44 \cdot t_R + 2 \cdot pH \quad (1.4)$$

In this case, ϑ_P represents the temperature (in Kelvin), t_R the residence time (in hours) and pH is the pH of the reaction.
Equations (1.1) and (1.2) were built for the hydrothermal carbonization of distiller's grains, whereas equations (1.3) and (1.4) were used to describe the HTC of anaerobically digested maize silage. Both descriptions agree with the positive correlation of temperature and residence time with respect to the hydrochar's carbon content, while the same parameters act through an inverse proportionality regarding the mass yield. This is in agreement with the mechanisms evolved during an HTC process, as discussed before.
Quadariyah et al. [7] have proposed a kinetic model for the degradation of glycerol during an hydrothermal process, with temperature in the range 473 – 673 K and residence times from 20 to 60 minutes. They have considered the initial and the final concentrations of glycerol, defining

$$\frac{dC_A}{dt} = k_1 \cdot {C_A}^a \cdot {C_B}^b \quad (1.5)$$

$$\frac{dC_A}{dt} = k_1{}' \cdot C_A{}^a \qquad (1.6)$$

where k_1 is the kinetic constant of glycerol consumption, C_A and C_B are the concentrations of glycerol and water, respectively and $k_1{}' = k_1 \cdot C_B{}^b$.
The authors suggested equations (1.5) and (1.6) to be pseudo-first-order kinetics. It was observed that the reaction rate constant k_1 increases with reaction temperature in sub-critical conditions; on the contrary it decreases below the critical temperature (Table 1.1). The explanation for this behavior in supercritical conditions could be found considering the different reaction mechanisms (ionic vs. radical) prevailing in the different water phases (subcritical vs. supercritical), as suggested by [61], or referring to the fact that self-dissociation of water at these temperatures also decreases [62].

T (K)	$\boldsymbol{k_1{}'}$ **(min^{-1})**
473	0.009
523	0.065
573	0.095
623	0.106
673	0.073

Table 1.1: Reaction rate constant for equation (1.6) at different temperatures (data from [7]).

Liu and Balasubramanian [11] have proposed a first-order kinetic reaction to describe the hydrothermal carbonization of waste biomass (1.7).

$$\frac{da}{dt} = A \cdot exp\left(-\frac{E}{RT}\right) \cdot (1 - a) \quad (1.7)$$

In equation (1.7), a is the weight loss, calculated by the following expression (1.8),

$$a = \frac{m_0 - m_t}{m_0 - m_f} \quad (1.8)$$

in which, m_0 is the initial weight of the biomass, whilst m_t and m_f are the weight at time t and at the final temperature (i.e., time). A is the pre-exponential factor, E is the apparent activation energy, T and t are the absolute temperature and time, respectively, and R is the gas constant. The authors proposed a logarithm form of the equation (1.7), in the case of constant heating rate $\beta = \frac{dT}{dt}$, (1.9):

$$ln\left[-\frac{ln(1-a)}{T^2}\right] = ln\left[\frac{AR}{\beta E}\left(1 - \frac{2RT}{E}\right)\right] - \frac{E}{RT} \quad (1.9)$$

The authors characterized the description of the HTC process into two different temperature ranges (150 – 300°C and 300 – 375°C), according to the different reaction rates at sub- and near-critical temperature. Plotting equation (1.8) on a $\ln\left[-\frac{\ln(1-a)}{T^2}\right]$ versus $\frac{1}{T}$, they found different apparent activation energy values for both the temperature ranges (Table 1.2).

Biomass	**T (°C)**	***E*** **(kJ/mol)**	***A*** **(-)**
Coconut fiber	150 - 300	67.5	4.08e+12
	300 - 375	179.5	1.23e+21
Eucalyptus leaves	150 – 300	59.2	4.38e+11
	300 – 375	173.7	2.05e+20

Table 1.2: Kinetic parameters for HTC (data from [11]).

This different behavior at different temperatures was explained by the authors by the fact that varying the temperature, carbohydrates (such as hemicellulose and cellulose) and lignin are submitted to different reactions, resulting in different E values.

Gajićet al [9] have suggested a mathematical description of the stability of hydrochar in soil, when it is used for carbon sequestration as well as a soil conditioner (1.10).

$$C_{tot} = C_1\left(1 - e^{-k_1 t}\right) + C_2\left(1 - e^{-k_2 t}\right) \quad (1.10)$$

In equation (1.10), C_{tot} is the total amount of carbon mineralized, C_1 is the labile carbon fraction with a high turnover rate (k_1), and C_2 is the stable carbon fraction with a slower turnover rate (k_2). Hence, the authors have evaluated a mean residence time MRT of the carbon in soil, as the summation of the MRT_1 (referred to C_1) and of the MRT_2 (referred to C_2):

$$MRT = MRT_1 + MRT_2 = \frac{\left({}^{1}/_{k_1}\right)}{365} + \frac{\left({}^{1}/_{k_2}\right)}{365} \quad (1.11)$$

Through equation (1.10), the authors have mathematically described the decomposition of the organic matter and organic carbon with respect to the action of soil organisms, the physic-chemical environmental conditions of the soil and the properties of the organic matter itself.

1.4 Hydrochar applications

The possible applications of the hydrochar have been studied by many authors [4, 6, 8, 9, 11, 42, 17, 18, 23, 34, 35, 36, 37, 38, 39, 40, 41, 43, 44, 52, 63, 64, 65, 66, 67] and are listed here below:

- for energy production and storage;
- as soil improver;
- for CO2 sorption and carbon sequestration;
- as activated carbon adsorbents (or as precursor for activated carbon);
- for the generation of nanostructured materials;
- as a catalysts.

The majority of the studies that have been conducted in these last years have focused their attention mainly on the possibilities to recover energy from the biomass, through the hydrothermal carbonization. Reported higher heating values (HHV) obtainable downstream of an HTC process depend largely on the process conditions and feedstock compositions, ranging from values of 13.8 MJ/kg (for HTC of municipal solid wastes [34]) to 36 MJ/kg (for HTC of anaerobically digested maize silage [16]). Typical values of HHV from HTC of lignocellulosic biomasses are of about 30 MJ/kg, which are values similar to those of coals. The HTC treatment has been proved by many authors [4, 10, 11, 16, 17, 23, 34, 36, 37, 38, 41] to be effective in the production of a solid fuel which could be used together with or in substitution of coal. As a matter of fact, the HTC process permits to obtain a practically

homogeneous hydrochar, suitable for the co-combustion with coal, with low moisture content, regular shape and high bulk density [37]. With respect to the combustion of the raw biomass, the hydrochar has higher ignition temperatures, higher combustion temperature regions and higher weight loss rates [11]. Furthermore, under hydrothermal carbonization conditions, the chlorine content (deriving from the presence of PVC and salt of food, in the municipal solid wastes) has been proved to be removable because of its decomposition into soluble chlorine compounds during HTC and through a subsequent washing [34, 38]. With respect to others harmful or toxic compounds, the HTC process leads to a product which is less aromatic and less condensed than biochar. The presence of polycyclic aromatic hydrocarbons (PAHs) is mainly due to their presence on the initial feedstock. However, their harmful and carcinogenic effect could mostly be effective if the hydrochar is used irrationally as soil improver [43]. To obtain a better hydrochar to be used as a solid fuel, Kang et al. [10] have proposed to perform an HTC process in presence of a 2.8 wt.% of formaldehyde. In these conditions the hydrochar showed higher yield, higher HHV, higher carbon recovery efficiency, higher total energy recovery efficiency and lower sulfur and ash content. Focusing on the municipal solid waste management, Lu et al. [36] have observed that the potential energy obtained by using the hydrochar as a solid fuel is greater than the energies that could be recovered from landfilling (CH4), incineration (combustion gas) and anaerobic digestion (CH4) of the same waste materials.

Because of its high carbon content and chemical and physical characteristics, a more direct use of the hydrochar as a soil conditioner and for long term carbon storage has been suggested [68]. To this purpose, the behavior and the characteristics of hydrochar have been explored by some authors [4, 8, 9, 16, 36, 43], mainly focusing on how the HTC process could affect parameters such as the stability of hydrochar in soils, the presence within the hydrochar of hazardous or inhibitor chemicals and green-house gas emissions from soils containing hydrochar. With respect to the biochar (obtained through a

pyrolysis conversion), the hydrochar has less aromatic structures and higher percentage of labile carbon species, which give it less stability when applied to soils. Similar results have been obtained by Weidner et al. [43], who have observed a low aromatic condensation of the hydrochars, which implies a lower stability in soils. Furthermore, it has been observed [9] that the hydrochar could have also higher chemical reactivity due to its more reactive hydrophilic (e.g., carboxylic) groups content. The analysis of mineralization performed by Gajić et al. [9] has shown that the stability of the hydrochars is typically higher than that of wheat straw, but lower with respect to white peat. The authors reported that the mean residence time of the biochar obtained from the same feedstock is numerous order of magnitude higher, if compared to that of the hydrochar. However, the hydrochar can have a potentially benign effect in preserving and restoring the soil organic carbon (SOC) stocks, thus ensuring soil quality. Becker et al. [8] have focused their work on the potential presence of harmful volatile organic compounds (VOCs), present in the inlet feedstock or generated during an HTC process, which could be released to the environment when hydrochar is applied as soil amendment. An interesting comparison in terms of grams of CO2-equivalent (g CO2-equivalent) emissions between the HTC of municipal solid waste and current waste management techniques has been performed by Lu et al. [36]. In this study, they highlighted that usually fugitive emissions of CO2-equivalent associated with waste degradation during landfilling were higher than the HTC g CO2-equivalent emissions per gram of wet waste. Similarly, gas emissions from composting or from incinerating resulted significantly larger than those associated with HTC. However, they underlined that their discussion is valid only if the hydrochar is used as a soil amendment or as carbon-storage material. Even though further studies have to be developed to analyze the effects on applying the hydrochar to soils, in terms of improving soil fertility and GHGs emissions, hydrochar seems to be a useful product both for carbon sequestration and as a soil amendment, as observed by Libra et al. [4].

The hydrochar characteristics have been studied by some authors [6, 17, 39, 40] also to understand its direct applicability as an adsorbent or as a precursor for activated carbons. For example, the macromolecular and porous structure of the hydrochar observed by Kumar et al. [6] and the presence of oxygen-rich functional groups on its surface, give it the potentiality to be used to remove uranium from contaminated sites. With the Brunauer–Emmett–Teller (BET) analysis, typical surface areas range between values of 12.3 m2/g [16] to values of 25 – 30 m2/g [17], which represent interesting values for the application of the hydrochar as an adsorbent. If performed at mild conditions, the HTC process of lignocellulosic biomass maintains the original texture of the biomass and typically forms a carbonaceous network of nanostructured elements [69]. Unfortunately, this network is non-porous and with low specific surface area [40], which are fundamental characteristics determining the adsorption efficiency of the hydrochar. Thus, in order to improve these adsorption characteristics of the products of the HTC process, some authors [40, 70] have tried to couple the hydrothermal treatment with traditional activation methods. Typical activation agents used are potassium hydroxide (KOH) or sodium hydroxide (NaOH). KOH generally reacts with the carbon at lower temperatures (~400°C) than NaOH does (~570°C) and this permits to achieve higher activation [71]. Activating the hydrochar with KOH Unur [40] was able to obtain a nanostructured carbon with specific surface area of 1700 m2/g and with optimal pore size distribution.

The employment of the hydrochar as nanostructured material, for example as a surrogate of the currently used carbon black, or in the building industry to produce reinforced concrete or lightened pavements, has been studied by some authors [72, 73, 74]. Other uses of the hydrochar, for example in electrochemical applications, have been investigated [75]. Typically, adjusting the carbonization time, the feedstock characteristics and the biomass to water ratio, and employing additives or stabilizers, it is possible to vary the characteristics of the hydrochar.

Due to its characteristic of high stability in processes which employ elevated temperatures or harsh conditions, the hydrochar have been reported to be a good material to be used directly as a catalyst or as a catalyst support [4].

1.5 Conclusions of Chapter 1

Hydrothermal carbonization (HTC) is a process that allows the treatment of wet biomass without the need for a drying pretreatment, which is necessary for traditional thermochemical processes (combustion, air gasification, pyrolysis). Foreseeing milder operational conditions (180 - 250 °C and 20 - 40 bar) with respect to the other treatments, HTC presents a more affordable and easier technical applicability. The products resulting from a HTC treatment are primarily a solid phase enriched in carbon, called hydrochar, a liquid phase with dissolved organic compounds and a small quantity of a gas phase mainly composed of carbon dioxide.

Hydrochar can be utilized in co-combustion with low-rank fossil coals, which can be a very effective and economically feasible way to exploit biomass for energy generation. Hydrochar can also be utilized in high-value applications, such as soil improver and for carbon sequestration, as adsorbent (i.e., activated carbon), as catalyst or as catalyst support, and for the generation of nano-structured materials.

In this chapter, an overview of the literature published on the HTC is presented.

References of Chapter 1

[1] Rosillo-Calle F., De Groot P., Hemstock S.L., Woods J., 2007. The biomass Assessment Handbook, Bioenergy for a Sustainable Environment, EarthScan, London (UK).

[2] Dewulf J., Van Langenhove H., 2006. Renewables-Based Technology: sustainability assessment.

[3] Funke A., Ziegler F., 2010. Hydrothermal carbonization of biomass: A summary and discussion of chemical mechanisms for process engineering, Biofuels, Bioproducts & Biorefining, vol. 4, p. 160-177.

[4] Libra J.A., Ro K.S., Kammann C., Funke A., Berge N.D., Neubauer Y., Titirici M.M., Fühner C., Bens O., Kern J., Emmerich K.H., 2011. Hydrothermal carbonization of biomass residuals: a comparative review of the chemistry, processes and applications of wet and dry pyrolysis, Biofuels, vol. 2(1), p. 89-124.

[5] Ying G.A.O., Han-ping C., Jun W., Tao S.H.I., Hai-ping Y., Xian-hua W., 2011. Characterization of products from hydrothermal liquefaction and carbonation of biomass model compounds and real biomass, Journal of Fuel Chemistry and Technology, vol. 39(12), p. 893–900.

[6] Kumar S., Loganathan V.A., Gupta R.B., Barnett M.O., 2011. An Assessment of U (VI) removal from groundwater using biochar produced from hydrothermal carbonization, Journal of Environmental Management, vol. 92(10), p. 2504–2512.

[7] Qadariyah L., Machmudah S., Sasaki M., 2011. Degradation of glycerol using hydrothermal process, Bioresource Technology, vol. 102(19), p. 9267–9271.

[8] Becker R., Dorgerloh U., Helmis M., Mumme J., Diakité M., Nehls I., 2013. Hydrothermally carbonized plant materials : Patterns of volatile organic compounds detected by gas chromatography, Bioresource Technology, vol. 130, p. 621–628.

[9] Gajić A., Ramke H.G., Hendricks A., Koch H.J., 2012. Microcosm study on the decomposability of hydrochars in a Cambisol, Biomass and Bioenergy, vol. 47, p. 250-259.

[10] Kang S., Li X., Fan J., Chang J., 2012. Solid fuel production by hydrothermal carbonization of black liquor, Bioresource Technology, vol. 110, p. 715–718.

[11] Liu Z., Balasubramanian R., 2012. Hydrothermal Carbonization of Waste Biomass for Energy Generation, Procedia Environmental Sciences, vol. 16, p. 159–166.

[12] Müller J.B., Vogel F., 2012. Tar and coke formation during hydrothermal processing of glycerol and glucose . Influence of temperature , residence time and feed concentration, The Journal of Supercritical Fluids, vol. 70, p. 126–136.

[13] Kruse A., Dinjus E., 2007. Hot compressed water as reaction medium and reactant 2. Degradation reactions, Journal of Supercritical Fluids, vol. 41, p. 361–379.

[14] Kronholm J., Hartonen K., Riekkola M.L., 2007. Analytical extractions with water at elevated temperatures and pressures, Trends in Analytical Chemistry, vol. 26(5), p. 396-412.

[15] Schuhmacher J.P., Huntjens F.J., Van Krevelen D.W., 1969. Chemical structure and properties of coal XXVI – Studies on artificial coalification, Fuel, vol. 39, p. 223-234.

[16] Mumme J., Eckervogt L., Pielert J., Diakité M., Rupp F., Kern J., 2011. Hydrothermal carbonization of anaerobically digested maize silage, Bioresource Technology, vol. 102, p. 9255-9260.

[17] Román S., Nabais J.M.V., Laginhas C., Ledesma B., González J.F., 2012. Hydrothermal carbonization as an effective way of densifying the energy content of biomass, Fuel Processing Technology, vol. 103, p. 78–83.

[18] Funke A., Ziegler F., 2011. Heat of reaction measurements for hydrothermal carbonization of biomass. Bioresource Technology, vol. 102(16), p. 7595–7598.

[19] Sevilla M., Fuertes A.B., 2009. The production of carbon materials by hydrothermal carbonization of cellulose, Carbon, vol. 47(9), p. 2281–2289.

[20] Tymchyshyn M., Xu C.C, 2010. Liquefaction of bio-mass in hot-compressed water for the production of phenolic compounds, Bioresource Technology, vol. 101(7), p. 2483–2490.

[21] Kruse A., 2011. Hydrothermal Carbonization – 1 . Influence of Lignin in Lignocelluloses *, Chemical & Engineering Technology, vol. 12, p. 2037–2043.

[22] Brunner G., 2009. Near critical and supercritical water . Part I . Hydrolytic and hydrothermal processes, The Journal of Supercritical Fluids, vol. 47, p. 373–381.

[23] Xiao L., Shi Z., Xu F., Sun, R., 2012. Hydrothermal carbonization of lignocellulosic biomass, Bioresource Technology, vol. 118, p. 619–623.

[24] Liu Z., Zhang F., Wu J., 2010. Characterization and application of chars produced from pinewood pyrolysis and hydrothermal treatment, Fuel, vol. 89(2), p. 510–514.

[25] Titirici M.M., Antonietti M., 2010. Chemistry and materials options of sustainable carbon materials made by hydrothermal carbonization, Chemical Society reviews, vol. 39(1), p. 103–16.

[26] Tsukashima H., 1967. Alkaline permanganate oxidation of artificial coals prepared from lignin and cellulose, Fuel, vol. 46, p. 177-185.

[27] Luijkx G.C.A., 1994. Hydrothermal conversion of carbohydrates and related compounds, Technical University of Delft, p. 31-45.

[28] Sugimoto Y., Miki Y., 1997. Chemical structure of artificial coals obtained from cellulose, wood and peat. In: A. Ziegler, K.H. van Heek,

J. Klein and W. Wanzi editors, Proceedings of the 9th International Conference on Coal Science ICCS ’97, vol. 1, DGMK, p. 187-190.

[29] Lewman M.D., 1985. Evaluation of petroleum generation by hydrous pyrolysis experimentation, Philos. Trans. R. Soc. London, Ser A 350, p. 123-134.

[30] Peterson A.A., Vogel F., Lachance R.P., Fröling M., Antal M.J., 2008. Thermochemical biofuel production in hydrothermal media: A review of sub- and supercritical water technologies, Energy Environmental Science, vol. 1, p. 32-65.

[31] Mok W.S.L., Antal M.J., 1992. Uncatalyzed solvolysis of whole biomass hemicellulose by hot compressed liquid water, Industrial & Engineering Chemical Research, vol. 31, p. 1157-1161.

[32] Hashaikeh R., Fang Z., Butler I.S., Hawari J., Kozinski J.A., 2007. Hydrothermal dissolution of willow in hot compressed water as a model for biomass conversion, Fuel, vol. 86, p. 1614-1622.

[33] Ramke H.G., Bloshe D., Lehmann H.J., Fetting J., 2009. Hydrothermal carbonization of organic waste, Preceeding of the Twelfth International Waste Management and Landfill Symposium, Sardinia, Italy.

[34] Hwang I.H., Aoyama H., Matsuto T., Nakagishi T., Matsuo T., 2012. Recovery of solid fuel from municipal solid waste by hydrothermal treatment using subcritical water, Waste Management, vol. 32, p. 410-416.

[35] Berge N.D., Ro K.S., Mao J., Flora J.R.V., Chappell M., Bae S., 2011. Hydrothermal carbonization of municipal waste streams, Environmental Science and Technology, vol. 45(13), p. 5696-5703.

[36] Lu X., Jordan B., Berge N.D., 2012. Thermal conversion of municipal solid waste via hydrothermal carbonization: comparison of carbonization products to products from current waste management techniques, Waste Management, vol. 32(7), p. 1353–1365.

[37] Lu L., Namioka T., Yoshikawa K., 2011. Effects of hydrothermal treatment on characteristics and combustion behaviors of municipal solid wastes, Applied Energy, vol. 88(11), p. 3659–3664.

[38] Prawisudha P., Namioka T., Yoshikawa K., 2012. Coal alternative fuel production from municipal solid wastes employing hydrothermal treatment, Applied Energy, vol. 90(1), p. 298–304.

[39] Bernardo M., Lapa N., Gonc M., Mendes B., Pinto F., Fonseca I., Lopes H., 2012. Physico-chemical properties of chars obtained in the co-pyrolysis of waste mixtures, Journal of Hazardous Materials, vol. 219– 220, p. 196– 202.

[40] Unur E., 2013. Microporous and Mesoporous Materials Functional nanoporous carbons from hydrothermally treated biomass for environmental purification, Microporous and Mesoporous Materials, vol. 168, p. 92–101.

[41] Heilmann S.M., Jader L.R., Sadowsky M.J., Schendel F.J., Von Keitz M.G., Valentas K.J., 2011. Hydrothermal carbonization of distiller' s grains, Biomass and Bioenergy, vol. 35(7), p. 2526–2533.

[42] Erlach B., Harder B., Tsatsaronis G., 2012. Combined hydrothermal carbonization and gasification of biomass with carbon capture, Energy, vol. 45(1), p. 329–338.

[43] Wiedner K., Naisse C., Rumpel C., Pozzi A., Wieczorek P., Glaser B., 2013. Organic Geochemistry Chemical modification of biomass residues during hydrothermal carbonization – What makes the difference, temperature or feedstock ?, Organic Geochemistry, vol. 54, p. 91–100.

[44] Du Z., Mohr M., Ma X., Cheng Y., Lin X., Liu Y., Zhou W., Chen P., Ruan R., 2012. Hydrothermal pretreatment of microalgae for production of pyrolytic bio-oil with a low nitrogen content, Bioresource Technology, vol. 120, p. 13–18.

[45] Bergius F., 1928. Beiträge zur theorie der kohleentstehung, Naturwissenschaften, vol. 1, p. 1-10.

[46] Terres E., 1952. Über die entwässerung und veredlung von rohtorf und rohbraunkohle, Brennstoff-Chemie, vol. 33, p. 1-12.

[47] Leibnitz E., Könnecke H.G., Schröter M., 1958. Zur kenntnis der druckinkohlung von braunkohlen in gegenwart von wasser. IV, J. Prakt. Chem., vol. 6, p. 18-24.

[48] Mok W.S.L., Antal M.J., Szabo P., Varhegyl G., Zelei B., 1992. Formation of charcoal from biomass in a sealed reactor, Industrial & Engineering Chemistry Research, vol. 31, p. 1162-1166.

[49] Davis A., Spackman W., 1964. The role of cellulosic and lignitic components of wood in artificial coalification, Fuel, vol. 43, p. 215-224.

[50] Orem W.H., Neuzil S.G., Lerch H.E., Cecil C.B., 1996. Experimental early-stage coalification of a peat sample and a peatified wood sample from Indonesia, Organic Geochemistry, vol. 24, p. 111-125.

[51] Afonso C.A.M. and Cerspo J.G. eds., 2005. Green separation processes, Wiley VCH, Weinheim, p. 323-337.

[52] Erlach B., Tsatsaronis G., 2010. Upgrading of biomass by hydrothermal carbonisation: analysis o fan industrial-scale plant design, In: Proc. ECOS – 23rd International Conference, 2010 Jun 14-17, Lausanne, Switzerland.

[53] Berl E., Schimdt A., 1928. Über das verhalten der cellulose bei der druckerhitzung mit wasser, Liebigs. Ann. Chem., vol. 461, p. 192-220.

[54] Kuster B.F.M., 1990. 5-hydroxymethylfurfural (HMF). A review focusing on its manufacture, Starch/Staerke, vol. 42, p. 314-321.

[55] Antal M.J., Mok W.S.L., Richards G.N., 1990. Mechanism of formation of 5-(hydroxymethyl)2-furaldehyde from D-fructose and sucrose, Carbohydrate Research, vol. 199, p. 91-109.

[56] Wallman H., 1995. Laboratory studies of a hydrothermal pretreatment process formunicipal solid waste, US Department of Energy, W-7405-Eng-48.

[57] Titirici M.M., Thomas A., Antonietti M., 2007. Back in the black: hydrothermal carbonization of plant material as an efficient chimica process to treat the CO2 problem?, New Journal of Chemistry, vol. 31, p. 787-789.

[58] Funasaka W., Yokokawa C., 1951. On the formation of coal, Mem. Fac. Eng. Kyoto, vol. 12, p. 128-137.

[59] Khemchandani G.V., Ray T.B., Sarkar S., 1974. Studies on artificial coal. 1. Caking power and chloroform extracts, Fuel, vol. 53, p. 163-167.

[60] Blazsó M., Jakab E., Vargha A., Székely T., Zoebel H., Klare H., Keil G., 1986. The effect of hydrothermal treatment on a Merseburg lignite, Fuel, vol. 65, p. 337-341.

[61] Buhler W., Dinjus E., Ederer H.J., Kruse A., Mas C., 2002. Ionic reactions and pyrolysis of glycerol as competing reaction pathwayin near- and supercritical water, Journal of Supercritical Fluids, vol. 22, p. 37-53.

[62] Ott L., Bicker M., Vogel H., 2006. Catalytic dehydration of glycerol in sub- and supercritical water: a new chemical process for acroleinproduction, Green Chemistry, vol. 8, p. 214-220.

[63] Lehmann J., Czimczik C., Laird D., Sohi S., 2009. Stability of biochar in soil. In: Biochar for Environmental Management – Science and Technology. Lehmann J, Joseph S (Eds). Earthscan, London, UK, p. 183–205.

[64] Schmidt M.W.I., Skjemstad J.O., Gehrt E., Kögel-Knabner I., 1999. Charred organic carbon in German chernozemic soils, European Journal of Soil Science, vol. 50(2), p. 351–365.

[65] Lehmann J., Skjemstad J., Sohi S., Carter J., Barson M., Falloon P., Coleman K., Woodbury P., Krull E., 2008. Australian climate-carbon cycle feedback reduced by soil black carbon, Nature Geoscience, vol. 1(12), p. 832–835.

[66] Glaser B., Haumaier L., Guggenberger G., Zech W., 2001. The 'Terra preta' phenomenon: a model for sustainable agriculture in the humid tropics, Naturwissenschaften, vol. 88(1), p. 37–41.

[67] Tremel A., Stemann J., Herrmann M., Erlach B., Spliethoff H., 2012. Entrained flow gasification of biocoal from hydrothermal carbonization, Fuel, vol. 102, p. 396–403.

[68] Lehmann J., 2007. A handful of carbon, Nature, vol. 447, p. 143-144.

[69] Thomas A., Kuhn P., Weber J., Titirici M.M., Antonietti M., 2009. Porous polymers: Enabling solutions for energy applications, Macromolecular Rapid Communications, vol. 30, p. 221-236.

[70] Zhao L., Fan L., Zhou M., Guan H., Qiao S., Antonietti M., Titirici M.M., 2010. Nitrogen-containing hydrothermal carbons with superior performance in supercapacitors, Advanced Materials, vol. 22, p. 5202-5206.

[71] Lillo-Ródenas M.A., Cazorla-Amorós D., Linares-Solano A., 2003. Undertanding chimica reactions between carbons and NaOH and KOH. An insight into the chemical activation mechanism, Carbon, vol. 41, p. 267-275.

[72] Baccile N., Laurent G., Babonneau F., Fayon F., Titirici M.M., Antonietti M., 2009. Structural characterization of hydrothermal carbon spere by advanced solid-state MAS 13C NMR investigations, The Journal of Physical Chemistry, vol. 113, p. 9644-9654.

[73] Titirici M.M., Antonietti A., Baccile N., 2008. Hydrothermal carbon from biomass: a comparison of the local structure from poly- to monosaccharides and pentoses/hexoses, Green Chemistry, vol. 10, p. 1204-1212.

[74] Titirici M.M., Thomas A., Yu S., Müller J., Antonietti M., 2007. A direct synthesis of mesoporous carbons with bicontinuous pore morphology from crude plant material by hydrothermal carbonization, Chemistry of Materials, vol. 19, p. 4205-4212.

[75] Titirici M.M., Antonietti M., Thomas A., 2006. A generalized synthesis of metal oxide hollow spheres using a hydrothermal approach, Chemistry of Materials, vol. 18(16), p. 3808-3812.

Chapter 2

Experimental apparatus design

A part of this chapter has been published in [1] and [2].

2.1 Experimental apparatus

The HTC process involves temperatures and pressures that have to be considered when designing the experimental apparatus. In particular, the pressures reached during the process can generate both sealing and safety problems. Another issue concerns heat providing. As the process involves high percentages of water, considering the dry biomass treated (B/W = 0.1 to 0.3), and having the reactor a not negligible mass, the heat providing system must be adequate to warm up the reactor to the process temperatures in a way to make the thermal transient as shorter as possible compared to the process residence time. Moreover, the heating system should avoid significant temperature profiles within the reactor, limiting the formation of convective motions.

Thus, a HTC experimental apparatus was designed, consisting of a stainless steel (AISI 316) batch reactor with an internal volume of about 50 mL. Figure 2.1 shows the piping and instrumentation diagram (P&ID) of the experimental system and a drawing of the HTC flanged top and reactor, while Figure 2.2 shows a picture of the apparatus.

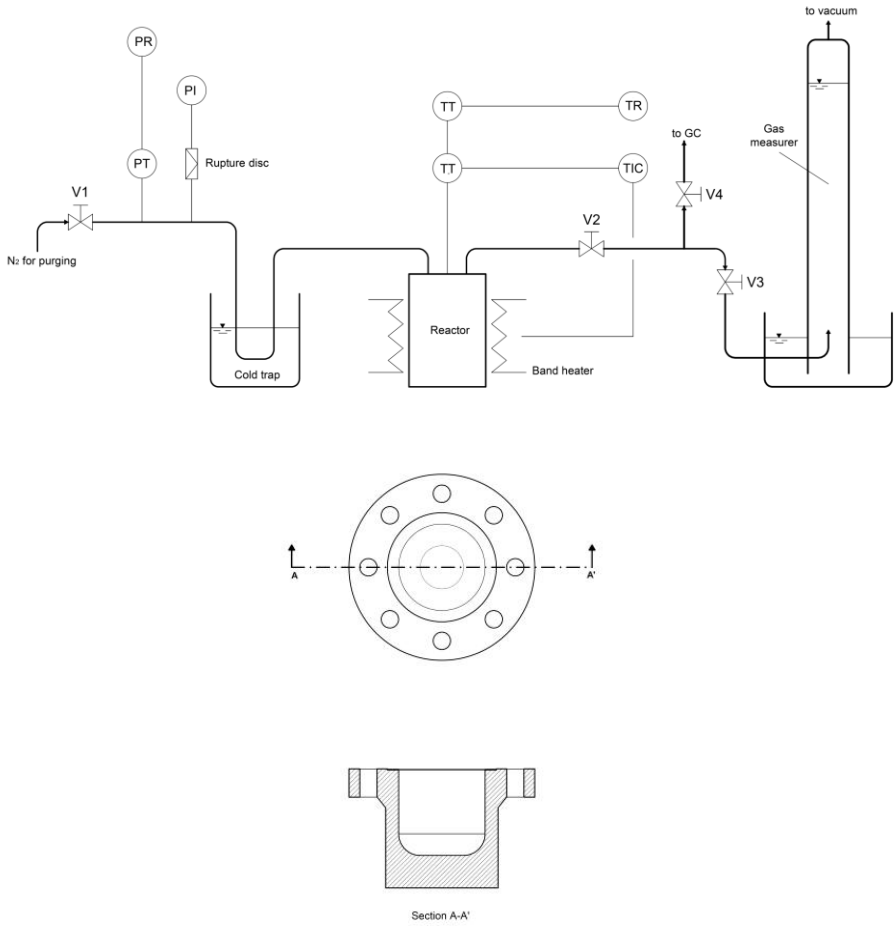

Figure 2.1. P&I diagram of the experimental apparatus and details of the reactor.

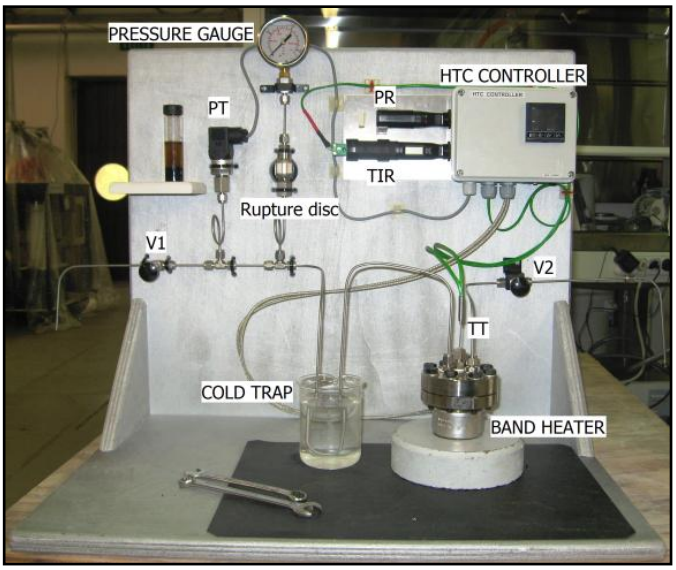

Figure 2.2. Experimental apparatus.

Two pipes of 2 mm internal diameter are connected to the reactor flanged cover. At the ends of the pipes, two needle valves are positioned, V1 and V2. Through V1, an inert gas (N2) can be fluxed inside the reactor to purge it from the presence of air; V2 is used to exit the gaseous products, which are formed during the HTC process, at the end of the process. On the left pipe, a pressure transmitter (PT) and a pressure gauge (PI) are placed. For safety reasons, a rupture disc is positioned in the pipe upstream the PI. Moreover, a water bath is foreseen on the left pipe to avoid that hot fluids from the reactor could come into contact with the PT or the PI. A thermocouple (TT) is embedded inside the reactor, passing through the reactor flanged cover. Both the thermocouple and the pressure transmitter send data to the HTC controller, which provides temperature and pressure data to a temperature indicator and recorder (TIR) and to a pressure recorder (PR), respectively. The HTC controller (TIC) is also connected to a band heater, in order to heat the reactor and to hold its temperature at the desired set point. The reactor is closed by the flanged cover with eight screws and positioned over a support

consisting of a stone disc. The seal of the HTC reactor is realized through a copper gasket, housed between the reactor flange and the flanged cover. To avoid clogging of the pipes when carbonizing small particles materials, for example coffee dregs, an aluminium coffee filter was positioned under the flanged cover, placing it over the inner reactor walls. In this way, when the particles start moving during the reaction, the filter prevent them to dirty the inner walls of the two pipes connected to the cover.

For the measurements regarding the gaseous phase, an additional apparatus has been installed. Referring to Figure 2.1, after the V2 valve, the pipe is divided in two lines: the first one is the part governed by the V4 valve, the other is the one governed by the V3 valve. Through the first line, the pipe can be connected to a gas chromatograph, with which it is possible to evaluate the composition of the gas formed during HTC. On the contrary, to evaluate the mass of gas formed during the reaction, V4 has to be closed allowing the gas flowing through the pipe line governed by the V3 valve (that, in this case is open) and letting it fill a graduate cylinder, prior filled with water. In this way, measuring the position of water meniscus before and after the flux of the gas, the volume of the gaseous phase produced by the HTC process can be calculated.

2.2 Preliminary tests

The reactor was tested before using it to perform the carbonizations.

The first test performed had the objective to test the tightness of the reactor, by filling it with cold distilled water using a HPLC pump, connected to the left pipe, near the V1 valve. By this pump, the reactor was filled up to a pressure of 130 bar, that was the rupture disc calibration pressure. The reactor was kept in pressure for one hour to observe if some leaching occurred. After one hour, the water was made to flow away from the reactor, by opening the needle valve (V2).

To assess the behaviour of the reactor when enhancing the temperature, a test was performed filling the reactor with distilled water, warming it up to several different temperatures and leaving it at these conditions for about twenty minutes for each temperature (Figure 2.3). During this test, both the temperature and the pressures were recorded. The reactor was in this way tested at 100 °C, 150 °C, 200 °C, 250 °C and 300 °C. By following the values of the pressure, it was possible to determine that no leaching occurred during this test.

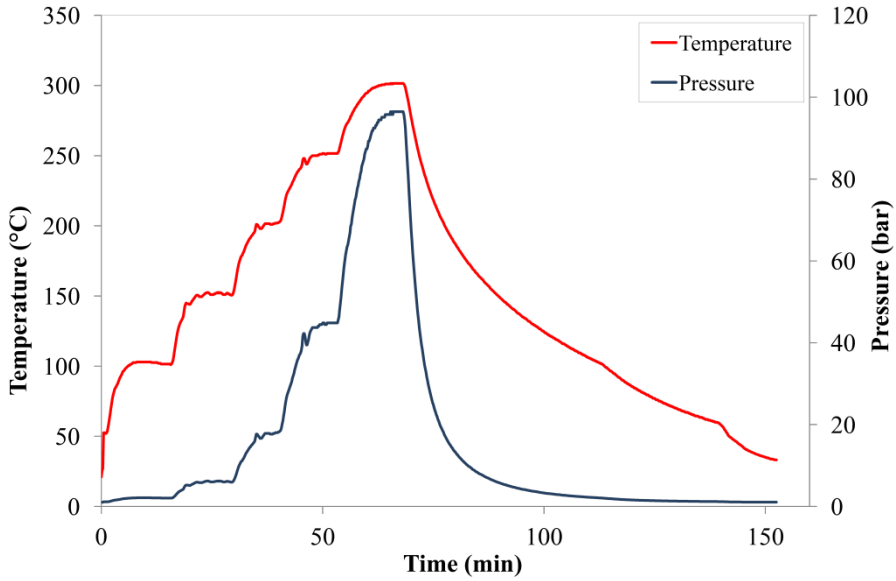

Figure 2.3. Tightness test with distilled water at different temperatures.

Figure 2.4 shows the measurements obtained testing two different methods to cool down the reactor once the reaction was finished. The main objective of the quenching is to shorten as much as possible the cooling transient, so that it could be considered negligible or, at least, irrelevant when compared to the process time, namely HTC residence time (i.e. the time between the moment

in which the reactor reaches the process temperature and the moment in which the quenching starts). Another important parameter that has been evaluated was the time in which the reactor reaches a temperature below 100°C. As a matter of fact, the hypothesis that no reactions occur below this temperature has been taken. Moreover, it must be considered that the reactor takes about 30 min to reach the temperature of 250 °C.

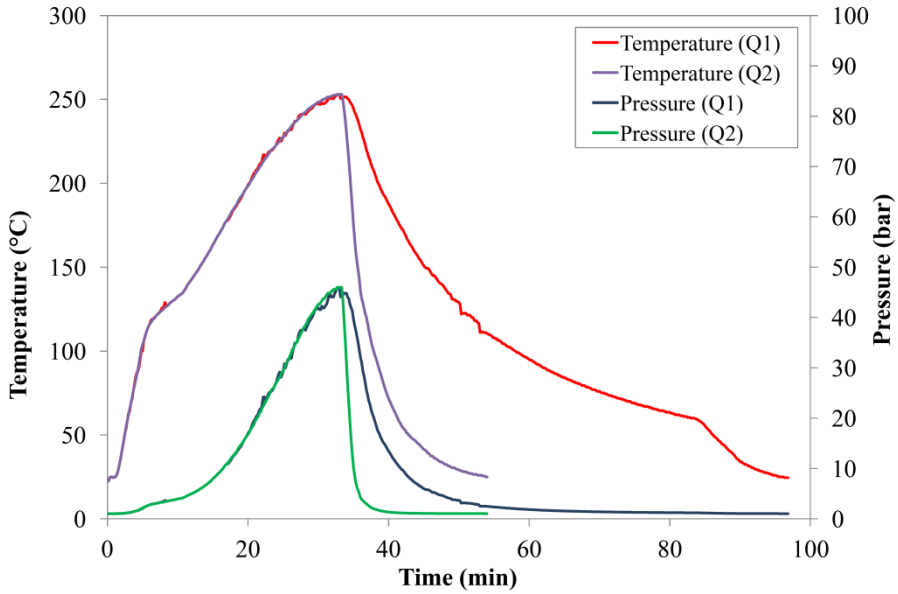

Figure 2.4. Quenching tests.

Thus, the first quenching method (Q1) foresaw the substitution of the stone disc with a steel disc, of the same dimensions of the stone one, at a temperature of -24 °C, after having removed the band heater from the reactor. In this case, the heat exchange between the reactor and the steel disc occurs only through the bottom surface, while the reactor walls and top exchange

heat with the surrounding air. Through this method, the inner temperature decreases down to 100 °C in about 23 min and the reactor reaches the temperature of 25 °C in about 1 hour. These long transients, especially the time taken to cool down to 100 °C, cannot be considered negligible if compared to both the warming up transient and the HTC residence time. In particular, the description of the residence time of the process can be affected by this cooling down transient.

To improve the quenching operation, after having removed the band heater and put the cold steel disc under the reactor, the heat exchange of the walls was promoted by blowing compressed air at an average temperature of 20 °C. In Figure 2.4, this procedure is referred as Q2. In this case, the inner temperature took about 4 min and a half to pass from 250 °C to 100 °C, and the reactor took about 33 min to reach the temperature of 25 °C. Thus, through this second quenching procedure, the errors in the description of the process parameter (i.e., the HTC residence time) are strongly limited.

2.3 Tests with real substrates

Three real substrates have been carbonized to evaluate the behaviour of the experimental apparatus in real HTC conditions. Sucrose was chosen as a model compound representing holocellulose compounds, while both coffee dregs and grape marc were chosen as possible candidates for a real HTC application. Figures 2.5, 2.6 and 2.7 show the carbonization process of these three substrates. In the three figures, the process temperature is drawn with a solid red line and the pressure with a solid blue line. The green dots labelled "H2O vap. press.", represent the water vapour pressure at the actual process temperatures. The Antoine equation (2.1) was used to determine the vapour pressure of water at the different process conditions.

$$lnP^{sat} = A - \frac{B}{T+C} \tag{2.1}$$

in which T is the process temperature expressed in degree celsius, and the constants A, B and C were taken from [3]. The vapour pressures evaluated through the equation 2.1 were then aligned with respect to the process time, so that in each instant it was possible to calculate the difference between the pressure registered by the data logger and the water vapour pressure, indicating the amount of gas formed at each process time.

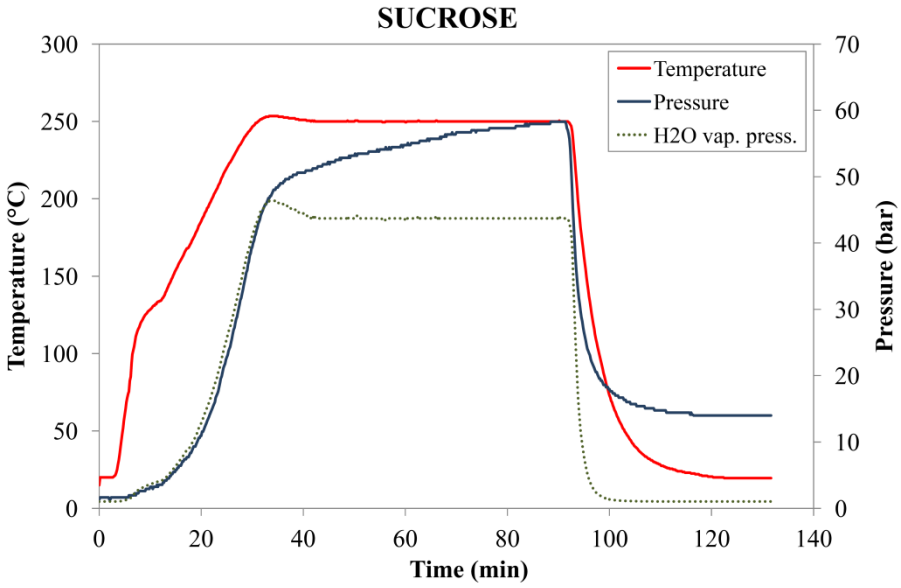

Figure 2.5. Test with real substrates (sucrose).

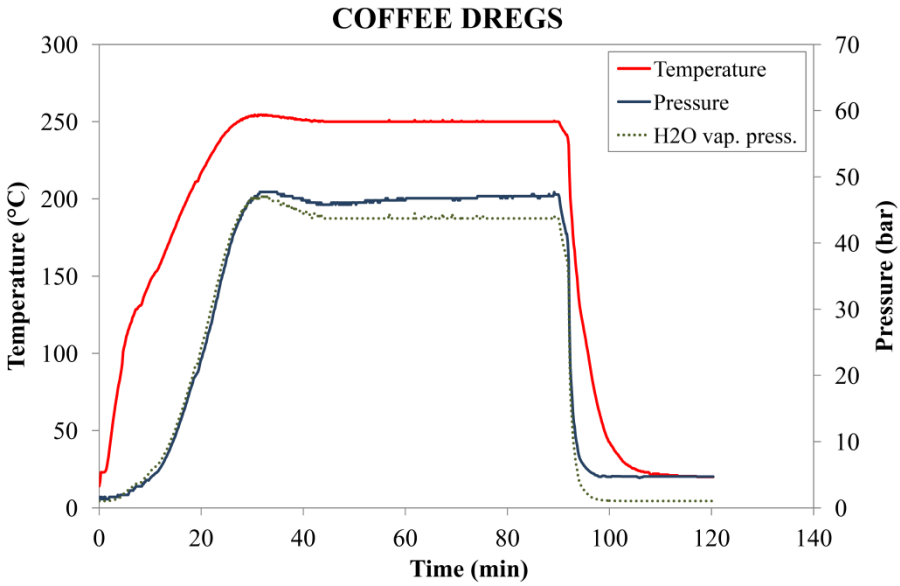

Figure 2.6. Test with real substrates (coffee dregs).

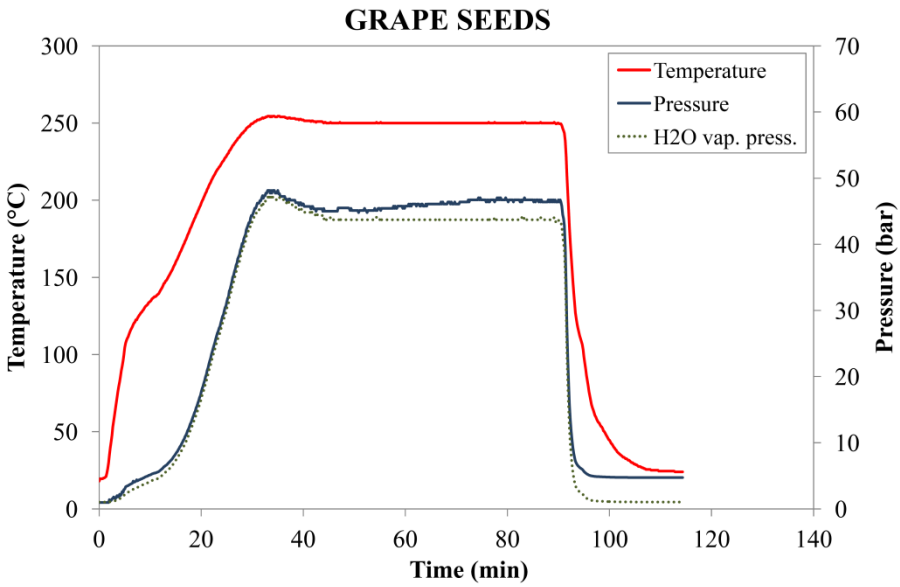

Figure 2.7. Test with real substrates (grape seeds).

The pressures registered during the process and at the end can be easily correlated to the gasification mechanisms, through which the molecules of the feedstock are degraded into gaseous compounds, being mainly carbon dioxide, carbon monoxide, methane and hydrogen. Both coffee dregs and grape marc degraded less than sucrose, because of their more complex structure. The total amount of gas formed during the HTC process can be calculated from the residual pressure measured after quenching the reactor, through the ideal gas equation of state (2.2).

$$P \cdot V = n \cdot R \cdot T \tag{2.2}$$

in which P is expressed in atmospheres, V in litres, n in moles, T in kelvins and is R = 0.0820574614 l·atm·K-1·mol-1. Thus, considering the three tests showed in the above, the carbonization of sucrose produced about 0.014 mol of gas, while the carbonization of coffee dregs and grape marc produced about 0.005 mol and 0.006 mol, respectively. When considering all the gas formed composed only by carbon dioxide, the mass of gas produced during the three tests are 0.62 g, 0.22 g and 0.26 g, representing respectively the 5.9 %, 3.6 % and 4.3 % of the initial mass of the feedstocks.

2.4 Conclusions of Chapter 2

In this chapter, the experimental apparatus used to perform the carbonization tests has been described. In particular, at the Department of Civil, Environmental and Mechanical engineering of the University of Trento (IT), a 50 mL bench scale batch reactor has been designed and realized. This reactor has been equipped with two thermocouples, one for the measurement of the inner temperature, with the purpose to control the band heater, which was used to warm up and keep the temperature of the reactor, and the other to register the actual temperature inside the reactor. A pressure transmitter and

register was even used to continuously register the pressure inside the reactor. An external apparatus has been designed and used to evaluate the gaseous phase produced during the carbonization process. This apparatus consists on a graduate cylinder through which it was possible to measure the volume of gas produced. A separate connection allowed the connection of a micro-GC, to evaluate the gas composition.

Several tests were performed to assess the behaviour of the reactor at real test conditions. In particular, the tightness of the reactor, the best quenching conditions and the behaviour of the HTC processes with different testing feedstocks were tested.

All the preliminary tests performed and described in this chapter, have allowed to become confident with HTC and to develop an appropriate testing protocol.

References of Chapter 2

[1] Fiori L., Basso D., Castello D., Baratieri M., 2014. Hydrothermal Carbonization of Biomass: Design of a Batch Reactor and Preliminary Experimental Results, Chemical Engineering Transactions, vol. 37, ISBN 978-88-95608-28-0; ISSN 2283-9216.

[2] Basso D., Weiss-Hortala E., Patuzzi F., Castello D., Baratieri M., Fiori L., 2015. Hydrothermal carbonization of off-specification compost: a byproduct of the organic municipal solid waste treatment, Bioresource Technology, vol. 182, p. 217-224.

[3] Reid R.C., Prausnitz J.M. and Poling B.E., 1987. The Properties of Gases and Liquids, 4th Ed., McGraw-Hill.

Chapter 3

Description of the feedstocks

3.1 Grape marc

Grape marc (Figure 3.1) is a residue coming from the wine production industry. This substrate is then used in distilleries for the production of distillates, such as grappa. The distillation process foresees the stripping of the impregnating alcohols and, after this stage, the substrate is referred as "exhausted grape marc".

Figure 3.1. Exhausted grape marc.

In the Trentino region, in which this work was performed, the yearly production of grape marc is about 17000 ton (data provided from the Consorzio di Tutela Vini del Trentino, 2008), while the world production is estimated around 67.1 million tons per year [1]. The grape marc provided

was dried for at least 8 h at 105 °C, and then manually separated into skins and seeds. The average composition found by Fiori and Florio [2] was about 46 % of skins, 52 % of seeds and 2 % of stalks, on dry basis. These data were in good agreement with those found by Jordan [3]: 51 % skins, 47 % seeds and 2 % stalks, on dry basis. These data can slightly vary considering different cultivars. Thus, to avoid differences while performing the HTC tests, it was decided to reproduce grape marc by composing it with 50 % of skins and 50 % of seeds; in this case, considering that, when referring to macromolecules (i.e., hemicellulose, cellulose and lignin), grape stalks are more similar to seeds than to skins, this operative hypothesis was assumed to be acceptable.

Preliminary analyses were performed on this substrate. In Table 3.1, the elemental analyses of both grape seeds and grape skins are reported.

ID	C (%)	H (%)	N (%)	S (%)	O (%)	Ash (%)
Seed	54.4	6.6	1.6	0.0	34.2	3.2
Skin	46.8	5.4	2.6	0.00	36.1	8.9

Table 3.1: Ultimate analyses of grape seeds and grape skins.

The elemental analyses were carried out in a Thermo NA 2100 to obtain C, H, N, and S mass fractions. The ash content was then determined by incineration at 550 °C according to EN 14775 procedure. The O content was deduced by difference.

As reported by Corbin et al. [4], grape marc is composed by 31–54% w/w of carbohydrates, of which 47–80% water soluble carbohydrates, namely glucose and fructose, and structurally complex polysaccharides, such as polyphenols, pectins, heteroxylans, xyloglucan and cellulose.

3.2 Waste residue EWC 19.05.03

The raw material was provided by Contarina S.p.a.

This residue is produced downstream of a composting treatment process. In particular, in the province of Treviso, near Venice (Italy), the organic fraction of the municipal solid waste (hereinafter OFMSW) is collected, through a "door to door" system, which foresees that every family collects separately the organic fraction from the recyclables, and twice a week the company that manages and treats the wastes in the province, carry away the OFMSW. This organic fraction is subsequently conveyed to the composting treatment plant and mixed with the lignocellulosic material coming from the mowing and pruning activities (called "green residue"), in the ratio 60/40 (mass basis, as it is). Figure 3.2 represents the treatment process.

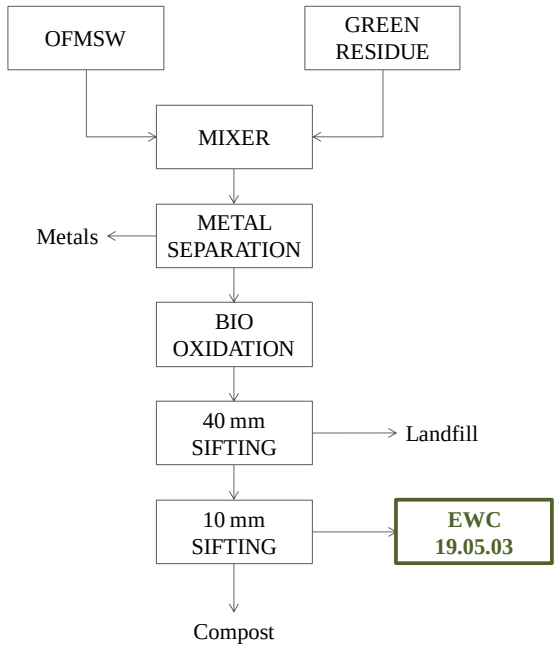

Figure 3.2. Scheme of the treatment process of the OFMSW.

The material undergoes to a metal separation process, and then the bio-oxidation process starts. It takes about 30 days, afterwards the bio-stabilized material is sifted first with a 40 mm sifting, and then with a 10 mm one. The material passing through both the siftings is recognized as compost, while the material which passed the 40 mm sifting but not the 10 mm one, is referred to be the "off-specification compost", catalogued with the code 19.05.03 by the European Waste Catalogue (EWC 19.05.03). Table 3.2 reports the main characteristics of the OFMSW. The analysis was performed on a 100.55 kg sample, taken in June 2013.

Parameter	**U.o.M.**	**Value**
Compostable material	% (mass)	98.7
Paper and cardboard	% (mass)	4.5
Organic materials	% (mass)	91.1
Biodegradable bags	% (mass)	3.1
Not compostable material	% (mass)	1.3
Plastics	% (mass)	0.5
Metals	% (mass)	0.1
Glass	% (mass)	0.1
Inert material	% (mass)	< 0.1
Other materials	% (mass)	0.6

Table 3.2: Characterization of the OFMSW.

Table 3.3 reports the chemical and physical analyses of the EWC 19.05.03 residue. The sampling was performed according to the legislation UNI EN

14899:2006. The sample was obtained after the mechanical homogenization of the material, taking 16 increments from the starting cumulation, homogenization and quartering. The elements and molecules not reported in Table 3.3, were under the detectable limit.

Parameter	U.o.M.	Value
Humidity	%	30.3[1]
pH	--	7.6
TOC	%	23
Dry matter	%	66
Dry residue (at 550 °C)	%	19
Flash point	°C	> 80
Chromium	mg/kg	16
Copper	mg/kg	32
Zinc	mg/kg	83

Table 3.3: Characterization of the EWC 19.05.03 residue.

Prior to use, the substrate was milled and manually homogenized to better guarantee the reproducibility of the tests. Then, the substrate was divided into 30 grams samples, stored in closed plastic bags at -24 °C.

[1] This is an average value, obtained drying five samples of the residue at 105 °C for at least 8 h.

Figure 3.3 shows the EWC 19.05.03 residue.

Figure 3.3. EWC 19.05.03 residue.

3.3 Waste residue EWC 19.12.12

The raw material was provided by Contarina S.p.a.

This residue is defined by the European Waste Catalogue as "other wastes (including mixtures of materials) from mechanical treatment of wastes other than those mentioned in 19.12.11", were the EWC 19.12.11 is referred as "other wastes (including mixtures of materials) from mechanical treatment of waste containing dangerous substances". This substrate is produced downstream of the treatment of the residual fraction of municipal solid waste, that is the fraction of wastes that is not recyclable (such as, paper, cardboard, PET, tin, glass, etc.) and not OFMSW. Figure 3.4 shows the process through which the EWC 19.12.12 is produced.

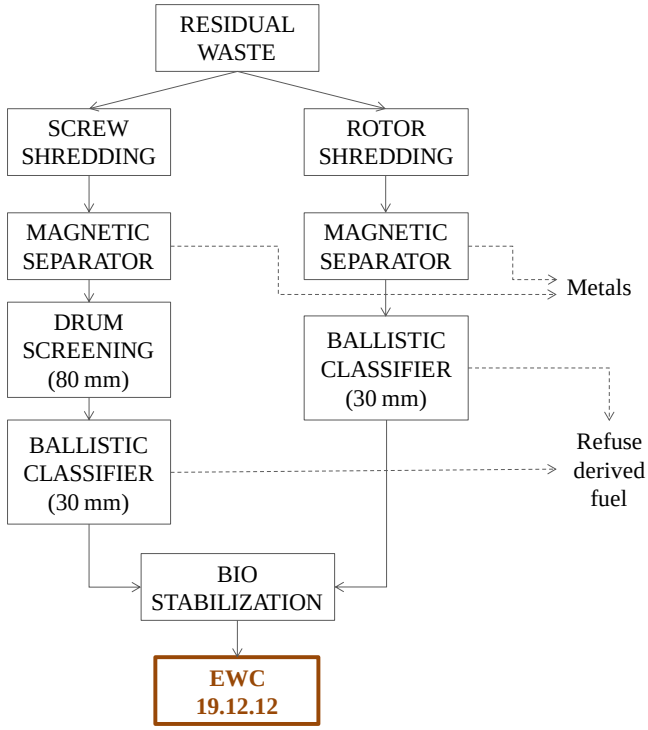

Figure 3.4. Scheme of the treatment process of the residual waste.

Depending on the size, the residual waste undergoes a shredding pre-treatment. This is performed by a screw shredding (for the bigger material) or by a rotor shredding (for the fine material). After a magnetic separation, the large size material is screened (80 mm) and then separated through a ballistic classifier (30 mm). For what concerns the fine material treatment process, there is not a drum screening, but only a ballistic classifier (30 mm). The material that passes through the 30 mm holes, is subsequently bio-stabilized, the resulting material being the EWC 19.12.12.

Parameter	**U.o.M.**	**Value**
Humidity	%	39.7[2]
pH	--	5.4
TOC	%	14
Dry matter	%	47
Organic matter	%	28
Bulk density	g/cm^3	0.34
Flash point	°C	> 80
Dry residue (600 °C)	%	20
LHV	MJ/kg	5.53
Barium	mg/kg	62
Carbon	%	40
Hydrogen	%	6.3

[2] This is an average value, obtained drying five samples of the residue at 105 °C for at least 8 h.

Oxygen	%	33
Nitrogen	%	0.21
Sulfur	%	0.11
Chlorine	%	0.38
Organic chlorine	%	0.17
Copper	mg/kg	647
Lead	mg/kg	125
Manganese	mg/kg	152
Tin	mg/kg	14
Zinc	mg/kg	253
Heavy hydrocarbons (C>12)	mg/kg	700
Total hydrocarbons	mg/kg	710

Table 3.4: Characterization of the EWC 19.12.12 residue.

Figure 3.5 shows the EWC 19.05.03 residue.

Figure 3.5. EWC 19.12.12 residue.

Prior to use, the substrate was milled and manually homogenized to better guarantee the reproducibility of the tests. Then, the substrate was divided into 30 grams samples, stored in closed plastic bags at -24 °C.

3.4 Discussion on the residues EWC 19.05.03 and EWC 19.12.12

As mentioned before, these two residues are produced by two municipal solid waste treatment plants, which are located in the province of Treviso (North-East of Italy). These two plants are hold by the society Contarina S.p.A., which collects and treats the wastes of 50 municipalities, spread on an area of 1300 km^2, corresponding to about 554000 inhabitants. The society can recycle up to 85% [5] of the total amount of MSW managed, being the remaining 15% the residual waste, with which Contarina S.p.A. produces the refuse derived fuel (hereinafter, RDF), that is sent to the incinerators to be burnt for energy production.

For what concerns the organic fraction, from which the EWC 19.05.03 residue is produced, the society annually collects about 17700 ton of OFMSW and 12900 ton of green residue. After the treatment of these residues, about 9000 ton of "off-specification compost" are produced annually [5]. This material is at present landfilled and has a landfilling price of about 90 €/ton. Because it is mainly composed by not completely composted lignin materials, it can be a suitable feedstock for hydrothermal carbonization. As a matter of fact, it can be carbonized and the hydrochar produced can be exploited as an amendment for agronomical purposes. For example, it could be mixed to the fresh material entering the composting plant. In this way, both the environmental and economical impacts of landfilling the EWC 19.05.03 could be avoided. Results concerning the EWC 19.05.03 residue are presented in Chapter 5.

Similarly, the residue coming from the residual fraction of the MSW treatment is bio-stabilized and landfilled. Contarina S.p.A. treats about

60000 ton/y of residual waste, producing about 10000ton/y of RDF and about 14000 ton/y of EWC 19.12.12 [5]. The landfilling costs for this last residue are about 96 €/ton. In this case, the chemical composition of the residue restricts and strongly limits the application of the hydrochar produced from it, in the agronomical field. Thus, to gain both environmental and economical benefits, while avoiding the EWC 19.12.12 to be landfilled, other hydrochar applications have to be investigated, the simplest one being the production of energy Preliminary results on the possibility to carbonize the EWC 19.12.12 residue are presented in Chapter 6.

3.5 Conclusions of Chapter 3

In this chapter, three specific feedstocks have been presented. In particular, grape marc is a residue coming from the winery industry, while both the EWC 19.05.03 and EWC 19.12.12 residues are by-products of the treatment of municipal solid waste. The main characteristics of these three substrates are reported in this chapter and some perspectives on the possible utilization of the hydrochars produced from these feedstocks are reported.

The raw material coded as EWC 19.05.03 and EWC 19.12.12 were kindly provided by Contarina S.p.a.

References of Chapter 3

[1] Food and Agriculture Organization of the United Nations Statistics Division (FAO), 2015. http://faostat3.fao.org/home/E (last accessed 19.02.15).

[2] Fiori L. and Florio L., 2010. Gasification and combustion of grape marc: comparison among different scenarios, Waste Biomass Valor, vol. 1, p. 191-200.

[3] Jordan R., 2008. Ecorecycle Australian report on grape marc utilisation - cold pressed grape seed oil and meal by the Cooperative Research Centre for International Food Manufacture and Packaging Science. http://www.ecorecycle.vic.gov.au.

[4] Corbin K.R., Hsieh Y.S.Y., Betts N.S., Byrt C.S., Henderson M., Stork J., De Bolt S., Fincher G.B. and Burton R.A., 2015. Grape marc as a source of carbohydrates for bioethanol: Chemical composition, pre-treatment and saccharification, Bioresource Technology, vol. 193, p. 76-83.

[5] Contarina S.p.A., 2014. Bilancio sostenibilità 2013. (www.contarina.it)

Chapter 4

Grape marc: experimental tests and results

In this chapter grape seeds, grape skins and grape marc were carbonized at different process conditions, namely 180 °C, 220 °C and 250 °C, at 0.5 h, 1 h, 3 h and 8 h. Several analyses were performed on the solid, liquid and gaseous phases obtained after the HTC process.
The analyses described in this chapter were partly performed in collaboration with prof. Elsa Weiss-Hortala, from the Centre Rapsodee in Mines-Albi (FR) and with Ph.D. Francesco Patuzzi from the Free University of Bolzano (IT).

4.1 Experimental procedure

This procedure was followed to perform the HTC tests.
The tare of the reactor was measured and the following weights were registered: reactor with the feedstock, reactor with both feedstock and distilled water, reactor with feedstock, distilled water and copper seal. The reactor was filled at about 75% of its inner volume. Then, the reactor was closed with the flanged top. Prior to the heating up, nitrogen was fluxed for at least 4 minutes to create an inert atmosphere inside the reactor and avoiding the presence of oxygen. Subsequently, the two needle valves (V1 and V2, in Figure 2.2) were closed, and the reactor was heated up. According to the set point temperature, the heating up took about 20 minutes. When the set point temperature was reached, the residence time was started to be measured. Both temperature and pressure were registered every 10 seconds by the two

data logger (TIR and PR, in Figure 2.2). During the experiment, the HTC controller continuously checked the temperature value provided by the thermocouple: if the temperature was lower than the set point, additional heat was provided through the band heater, activated by the HTC controller. If the temperature was equal or higher than the set point, the HTC controller switched off the band heater. Once passed the defined residence time, the set temperature was put equal to 20 °C and the band heater was removed. Simultaneously, a steel disc of about 3 kg and at -24 °C, was put under the reactor, substituting the stone one. To faster the quenching, compressed air was blown, as described in Chapter 2. When the temperature inside the reactor was about 25 °C, the quenching was stopped and the residual pressure was lowered by opening the needle valve V2 and fluxing the gas through the apparatus used to measure or the gas volume or its composition (Figure 2.1). Hence, the reactor was opened by removing the flanged top, and its gross weight (reactor, copper seal, water and hydrochar) was measured. The gross weight without the copper seal was measured too. Then, the content (i.e., water and hydrochar) was filtered with a 0.45 μm Whatman filter. The liquid was stored in brown glass vials and kept in a fridge at 4 °C, while both the reactor and the dirty filter were dried in an oven at 105 °C for at least 8 h. Finally, by measuring the weights of both the dried reactor and filter, all the data to calculate the mass of hydrochar obtained were collected. The hydrochar was stored in glass vials at -24 °C, before its analyses.

4.2 Grape seeds, skins and marc: experimental results

Several carbonizations have been performed at different process conditions. In particular, to get insights on the HTC process, three temperatures and four residence times were chosen: 180 °C, 220 °C, 250 °C and 0.5 h, 1 h, 3 h and 8 h. The biomass to water ratio (B/W) was kept equal to 0.3, 0.1 and 0.2 for grape seeds, grape skins and grape marc, respectively. Moreover, to better understand the differences in the behavior of feedstocks with a prevailing

lignin content and feedstocks with a predominant cellulose content, the above mentioned tests were performed separately on grape seeds, on grape skins and finally on grape marc. As previously described in Chapter 3, grape marc was reproduced by adding 50% mass of seeds and 50% mass of skins. In this paragraph, the three phases, (solid, liquid and gas) are analyzed. At the end of the paragraph, the overall balances are reported.

Solid phase

As previously mentioned, hydrochar was produced at different process conditions and from three different substrates, namely grape seeds, grape skins and grape marc. Both the feedstocks and the hydrochars were analyzed through an elemental analyzer (Vario Macro Cube). Sulfur was absent or detected in negligible percentages: for this reason the sulfur content was not reported in the tables. The ash content was determined according to the ISO 18122:2015 method, used for the determination of ash content of solid biofuels. Oxygen was calculated by difference. Tables 4.1, 4.2 and 4.3 report the ultimate analyses of the three feedstocks and of the hydrochars obtained at different process conditions.

Temperature (°C)	Time (h)	C (%)	H (%)	N (%)	O (%)	Ash (%)
SEEDS	0	54.4	6.6	1.6	34.2	3.2
180	0.5	59.5	6.7	1.4	30.1	2.2
	1	60.2	6.6	1.3	27.8	2.5
	3	60.6	6.5	1.4	27.4	2.7
	8	62.3	6.8	1.4	25.4	3.5
220	0.5	63.7	6.8	1.5	25.3	2.6
	1	63.4	6.7	1.6	24.0	2.8
	3	63.6	6.4	1.6	23.8	2.9
	8	68.4	6.7	1.9	18.3	3.1
250	0.5	67.3	6.5	1.7	20.8	3.6
	1	66.5	6.4	1.8	20.5	3.0
	3	69.5	6.6	1.9	17.0	3.1
	8	70.7	6.5	2.0	15.7	3.9

Table 4.1. Elemental analysis of grape seeds and hydrochar obtained from grape seeds at different process conditions.

Temperature (°C)	Time (h)	C (%)	H (%)	N (%)	O (%)	Ash (%)
SKINS	0	46.8	5.4	2.6	36.2	9.0
180	0.5	54.9	6.5	2.5	31.9	3.9
	1	54.5	6.0	2.6	32.2	4.6
	3	55.4	6.2	2.3	30.8	5.1
	8	58.2	5.7	2.1	28.3	5.6
220	0.5	59.7	6.4	2.3	25.6	5.6
	1	58.8	6.3	2.3	26.7	5.4
	3	61.0	6.0	2.3	25.4	5.2
	8	62.3	5.5	2.7	23.4	5.9
250	0.5	64.7	6.2	2.3	20.7	5.8
	1	63.9	5.6	2.7	21.2	6.6
	3	66.3	6.1	3.0	18.9	5.6
	8	68.2	5.3	3.1	18.4	4.3

Table 4.2. Elemental analysis of grape skins and hydrochar obtained from grape skins at different process conditions.

Temperature (°C)	Time (h)	C (%)	H (%)	N (%)	O (%)	Ash (%)
MARC	0	49.7	6.2	2.4	35.5	6.1
180	0.5	56.9	6.5	2.0	31.1	3.3
	1	56.2	5.9	2.5	30.8	4.5
	3	57.0	5.6	2.6	30.3	4.5
	8	57.2	5.7	2.8	29.7	3.7
220	0.5	60.4	6.4	2.0	27.3	3.7
	1	59.8	5.7	2.6	28.0	3.8
	3	62.5	5.4	2.7	25.9	3.5
	8	64.1	5.7	2.2	24.0	4.0
250	0.5	64.7	6.4	2.2	21.8	4.8
	1	64.9	5.8	2.8	22.3	3.9
	3	65.6	6.0	2.8	20.3	5.3
	8	68.1	5.8	2.6	19.4	4.2

Table 4.3. Elemental analysis of grape marc and hydrochar obtained from grape marc at different process conditions.

Looking at the ultimate analyses of these feedstocks, is it possible to state that the more severe the process conditions, the more oxygen is lost, while the carbon content increases in the solid phase. In particular, both grape seeds and skins loose from 12% to 54% of the oxygen, consistently with the process temperature and residence time. Interestingly, the ash loss is stronger in skins than in seeds: this can be due to the fact that while skins are mainly composed by hemicellulose and cellulose, seeds have higher lignin content. Thus, for seeds the degradation is less pronounced. This affect the carbon densification: as a matter of fact, the carbon densification in skins is more marked (from + 16% to + 46%), while in seeds these values reduce from + 9% to + 30%. For what concerns the combination of these two substrates into grape marc, the carbon densification range is 13 - 37%, values that are quite similar to the average of the ranges of skins and seeds. A part from skins, the hydrogen content seems to remain relatively constant, even though data

regarding grape marc shows a slight decrease at longer residence times. At lower temperatures and, in particular, at short residence times, nitrogen tends to solve into the liquid phase. On the contrary, at more severe process conditions, the nitrogen content increases within the hydrochar. Figure 4.1 shows the average molar increment of carbon, hydrogen, nitrogen, oxygen and ash, referred to grape marc. The data are expressed as mol/g,$_{TOT}$ %.

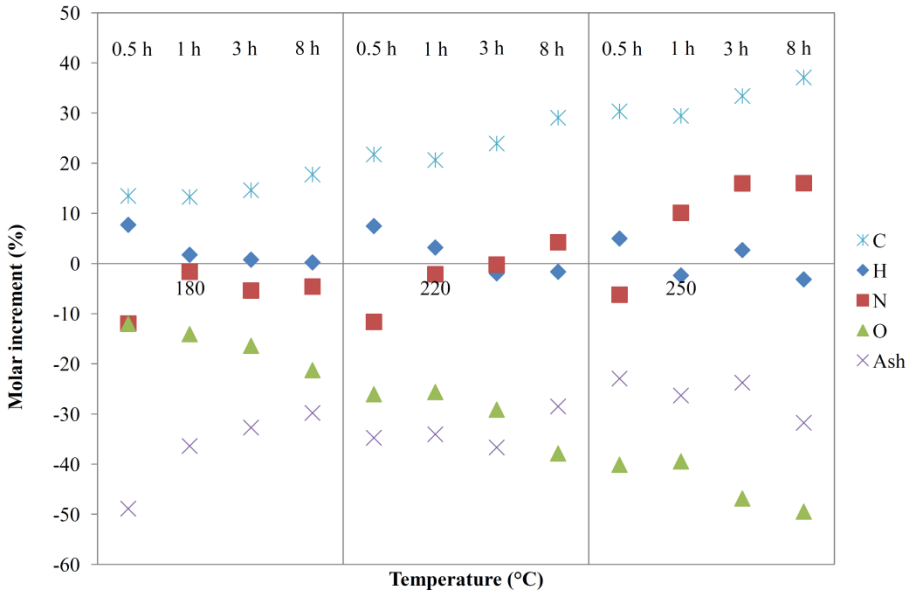

Figure 4.1. Molar increment of C, H, N and ash, during the HTC of grape marc.

The data shown in Figure 4.1 have been calculated as average values between the molar fractions of C, H, N, O and ash measured in the seeds, skins and marc respectively, referred to the total mass of the substrate. This figure clearly shows the carbon densification and oxygen depletion. A part at 250 °C, the hydrogen content increases in the early stages of the process, reducing its molar percentage at longer residence times. The hydrochar loses some amount of nitrogen in the early stages of the carbonization.

Subsequently, the moles of nitrogen increases within the solid phase, in particular at higher temperatures and residence times. An interesting behavior is shown by ash: it seems that there is a limit in the ash depletion, around - 30%, that is get quite immediately at 250 °C, while it is reached at longer residence times for 180 °C and 220 °C.

Figure 4.2 reports the Van Krevelen [2] diagram obtained from the data of grape marc.

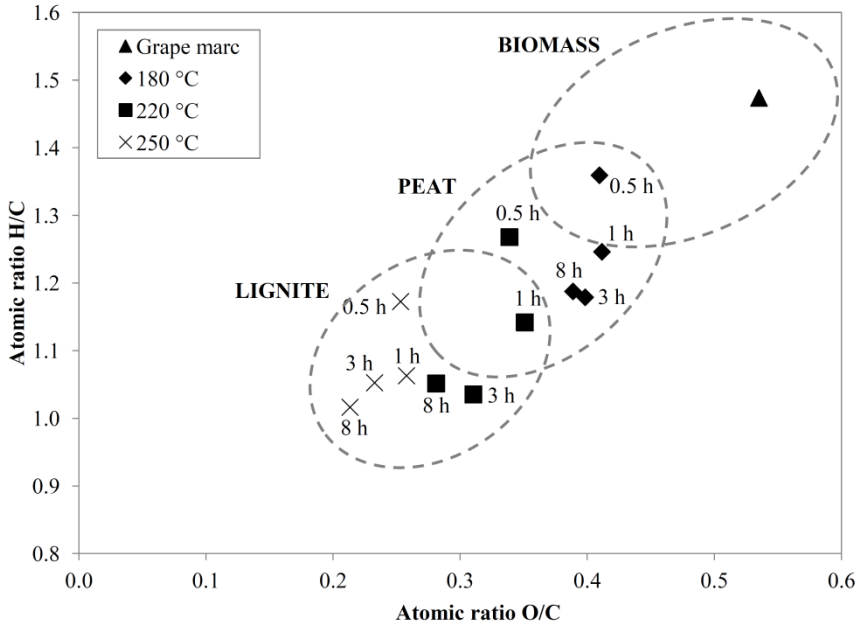

Figure 4.2. Van Krevelen diagram of grape marc.

In the Van Krevelen diagram, the influences of both temperature and residence time are clearly shown. These process parameters influence both the dehydration and decarboxylation reactions, promoting the loss of water and carbon dioxide during the process. An interesting information that can be recovered from Figure 4.2 is that temperature seems to linearly increase the

loss of hydrogen and oxygen atoms. As a matter of fact, considering constant the residence time, the three points (concerning respectively, 0.5 h, 1 h and 8 h) can be arranged in three straight lines, with positive intercept. A particular behavior is followed by the point 3 h at 250 °C: it is positioned in a higher point respect to the expectations. This can be due to errors in the experimental procedure or to a variation on the humidity content of the sample. As a matter of fact, even though the samples were dried prior to be analyzed, during the sample preparation small amounts of humidity can have altered the hydrogen content of the hydrochar. However, the data used for the construction of Figure4.2 were obtained performing the elemental analysis in triplicate. Moreover, temperature affects more than residence time the O/C ratio, while the H/C ratio seems to be more sensible to residence time.

In the early stages of the process (residence times up to 0.5 h), the main reaction that seems to occur is the physical dewatering of the biomass. This is in agreement with what was found by Funke and Ziegler in 2010 [3]. Interestingly, after this early reaction stage, from 0.5 h to 1 h, the O/C ratio seems to be nearly constant, while a strong reduction in the H/C ratio occurs. This can be explained considering the solution of sugars (like glucose and fructose) within the liquid. As suggested by Funke and Ziegler [4], other sugars can be solved in the liquid, for example D-xylose, D-mannose and D-galactose. Moreover, acetic acid can be a degradation product of hemicellulose. Considering the results obtained for the temperatures of 220 °C and 250 °C, the O/C ratio at 1 h is slightly higher than that at 0.5 h. Apparently, this effect is not evident at 180 °C. The explanation can be found considering that at temperatures below 200 °C, the degradation of lignin is more difficult, especially at lower residence times. Because lignin mainly degrades into phenolic compounds, as indicated by Funke and Ziegler [4], in this case the loss of carbon and hydrogen atoms is more marked if compared to that of oxygen. Thus, the O/C ratio could slightly increase.

As the residence time increases, other reaction mechanisms begin to act. In particular decarboxylation leads to the removal of carboxyl groups, as

suggested by many authors [5, 6, 7]. Finally, at longer residence times (i.e., from 3 h to 8 h) the variations on both H/C and O/C ratios are less pronounced, a part from what happens at higher temperatures, namely 250 °C. This can represent an important hint while designing the process parameters for a real application plant. In fact, the efforts due to the extension of the residence time may be not justified only considering the coalification degree of the feedstock.

Table 4.4 reports the higher heating values of grape seeds, grape skins and marc, while Figure 4.3 shows the HHV of grape marc, at the different process conditions. The HHV of all these three feedstock were evaluated through a calorimetric bomb (IKA 200C). Isoperibolic method was applied in accordance with UNI EN 14918:2010.

Temperature (°C)	**Time (h)**	**HHV seeds (MJ/kg)**	**HHV skins (MJ/kg)**	**HHV marc (MJ/kg)**
Feedstock	0	22.52	18.66	20.59
180	0.5	22.84	19.16	21.51
	1	24.92	19.38	22.46
	3	24.36	20.69	22.72
	8	24.36	23.84	23.52
220	0.5	22.70	21.84	21.03
	1	22.91	24.36	20.95
	3	26.35	23.11	21.71
	8	26.09	26.72	24.01
250	0.5	22.97	21.88	23.24
	1	23.33	24.56	24.86
	3	27.81	24.85	26.09
	8	28.79	27.54	26.19

Table 4.4. Heating values of grape seeds, skins and marc at different process conditions.

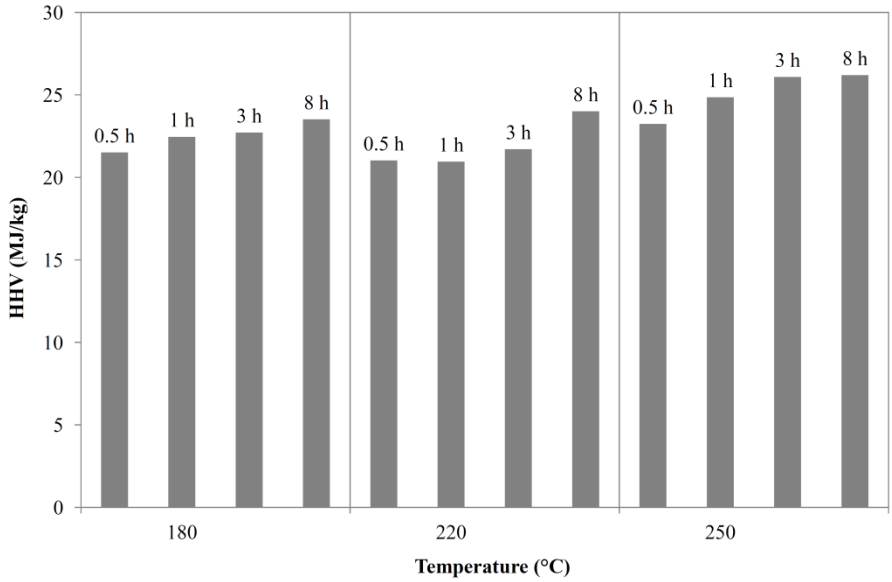

Figure 4.3. Higher heating value of carbonized grape marc.

As expected, increasing the severity of the process, the energy content of the hydrochar is enhanced. Although it was not possible to determine which of the two process parameters (temperature and residence time) was more effective to enhance the heating value of the hydrochar, the average tendency is that at higher temperatures the increase of the HHV is higher than at lower temperatures. This is in agreement with the information provided by the Van Krevelen diagram of Figure 4.2. At higher temperatures the oxygen content of the hydrochar is lower, thus the heating value results to be higher. The increase in HHV of carbonized grape marc is significant, ranging from 4.47% (residence time: 0.5 h; temperature: 180 °C) to 27.2% (residence time: 8 h; temperature: 250 °C). The data for grape seeds and skins are: 1.4% (0.5 h, 180 °C) - 27.8% (8 h, 250 °C) and 2.7% (0.5 h, 180 °C) - 47.6% (8 h, 250 °C), respectively. These values of energy densification seem to be consistent with those obtained by Pala et al. [8].

Performing HTC of several municipal solid wastes, Lu et al. [9] obtained an increase in HHV ranging from 1% to 41% (residence time: 30 min; temperature: 220 C), values comparable to those here obtained.
Many authors [10, 11, 12, 13, 14, 15] have proposed correlations for the estimation of the higher heating value of solid substrates, exploiting the data of their ultimate analyses. The correlations proposed by the authors are reported in Table 4.5.

Eq.	Correlation	Unit of Measurement	Ref.
4.1	$HHV = 0.3491 \cdot C + 1.1783 \cdot H - 0.1034 \cdot O - 0.0211 \cdot Ash + 0.1005 \cdot S - 0.0151 \cdot N$	MJ/kg	[10]
4.2	$HHV = 0.3259 \cdot C + 3.4597$	MJ/kg	[11]
4.3	$HHV = -1.3675 + 0.3137 \cdot C + 0.7009 \cdot H + 0.0318 \cdot O^*$ $O^* = 100 - C - H - Ash$	MJ/kg	[11]
4.4	$HHV = 3.55 \cdot C^2 - 232 \cdot C - 2230 \cdot H + 51.2 \cdot C \cdot H + 131 \cdot N + 20600$	kJ/kg	[12]
4.5	$HHV = 0.3491 \cdot C + 1.1783 \cdot H + 0.1005 \cdot S - 0.1034 \cdot O - 0.0151 \cdot N - 0.0211 \cdot Ash$	MJ/kg	[13]
4.6	$HHV = -0.763 + 0.301 \cdot C + 0.525 \cdot H + 0.064 \cdot O$	MJ/kg	[14]
4.7	$HHV = 0.4373 \cdot C - 1.6701$	MJ/kg	[15]

Table 4.5. Summary of correlations used for predicting the HHV of biomass.

All the correlations reported in Table 4.5 were tested on the basis of the ultimate analyses performed on the three substrates. Table 4.6 reports the average percentage errors obtained comparing the HHVs of grape seeds, skins and marc measured, to the calculated ones.

	Eq. 4.1 [10]	Eq. 4.2 [11]	Eq. 4.3 [11]	Eq. 4.4 [12]	Eq. 4.5 [13]	Eq. 4.6 [14]	Eq. 4.7 [15]
Grape seeds	-12.1%	1.1%	1.6%	-11.5%	-12.1%	4.3%	-7.0%
Grape skins	-10.0%	-1.0%	0.9%	-8.7%	-10.1%	2.8%	-7.4%
Grape marc	-10.0%	-1.1%	0.9%	-9.4%	-10.0%	2.8%	-8.0%

Table 4.6. Average percentage errors of HHV prediction.

Considering the results shown in Table 4.6, it is possible to conclude that, for the type of feedstocks and process evaluated, the correlations proposed by Sheng and Azevego [11] are those who better predict the heating value of the solid substrate.

Thermogravimetric analyses (TGA) were performed on grape marc. Results from TGA testify that the mass loss of the hydrochar samples during analysis greatly reflects the HTC operational conditions: the mass loss is in the range of 65.7–67.9 wt.% for the hydrochars obtained at 180°C, while it is comprised between 51.8 and 57.2 wt.% for the hydrochars obtained at 250 °C (the complete set of results is shown in Appendix I).
The derivative mass loss (DTG) is reported in Figure 4.4 for five samples including the raw material and the hydrochars obtained after 1 or 8 h HTC treatment at 180 or 250 °C.

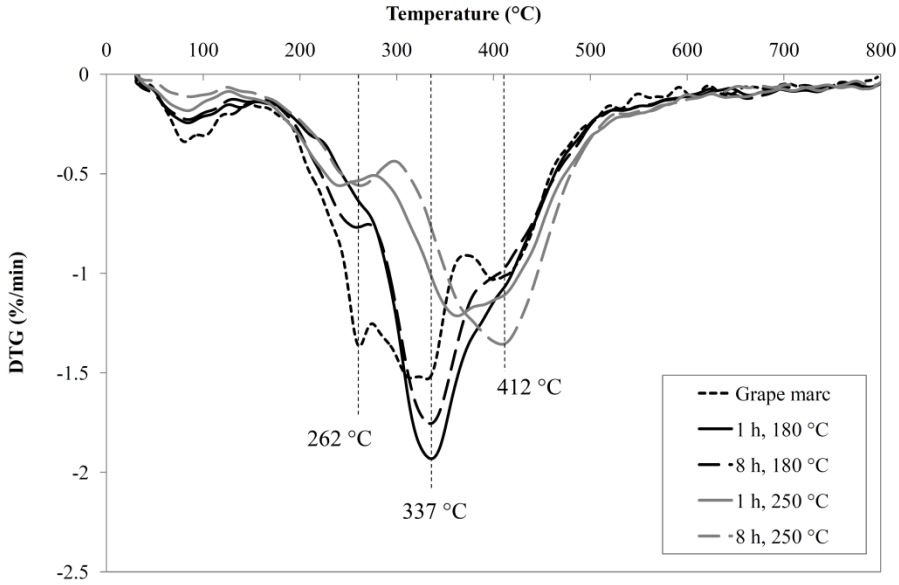

Figure 4.4. DTG curves of carbonized grape marc.

For the raw sample, a large peak of DTG is observed at low temperature with three relative minima at 80, 102 and 134 °C. These peaks are due to dehydration and release of volatile compounds. After HTC treatment, the peak appears to be only centered at 80 °C, likely due to residual water content. Therefore, the HTC treatment impacts the presence of volatile compounds in the remaining solid. Raw sample shows three other main peaks centered at 262, 310, and 408 °C. These peaks correspond to the thermo-degradation of organic compounds present in the grape marc. Considering hydrochars obtained at low temperature (180 °C), the main mass loss is represented by a peak centered at a temperature of about 337 °C. Interestingly, such peak is more intense than the peaks of grape marc, meaning that new compounds are produced during HTC. Moreover, this peak is slightly shifted to a higher temperature if compared to the peak detected for the raw material (310 °C), meaning that the new compounds are

slightly more stable. At the highest treatment temperature (temperature: 250 °C; residence time: 1 h), the peak is shifted to 371 °C, testifying that the new formed compounds are even more stable. HTC has a clear impact on the compounds which are degraded at 262 °C, as the peak is much less intense after HTC. Thus, a large part of these compounds were removed during HTC. The peak centered at 410 °C is also impacted by HTC, as its intensity increases with the increase of temperature and residence time. The highest impact is found for the most severe conditions (temperature: 250 °C; residence time: 8 h).

To summarize the information contained in Figure 4.4, the increase of temperature and residence time causes a decrease in the amount of volatile compounds and thermo-sensitive molecules, and results in an increase in thermal stable compounds in the hydrochar. This is in complete agreement with the data on elemental analyses reported in Table 4.3: the increase in carbon content indicates an increase in ‘‘fixed carbon’’, which is testified by the increased thermal stability proved by TGA. In addition, the increase of carbon content sustains the higher HHV of the hydrochar produced at the most severe conditions, as shown in Figure 4.3.

Liquid phase

On the liquid phases obtained from the carbonization of the three substrates, total organic carbon (TOC) and inductively coupled plasma (ICP) analyses were performed. In this section, the TOC data are reported in histograms (Figures 4.5, 4.6 and 4.7), in function of the process conditions. The precise data are reported in Appendix I (Table I.1).

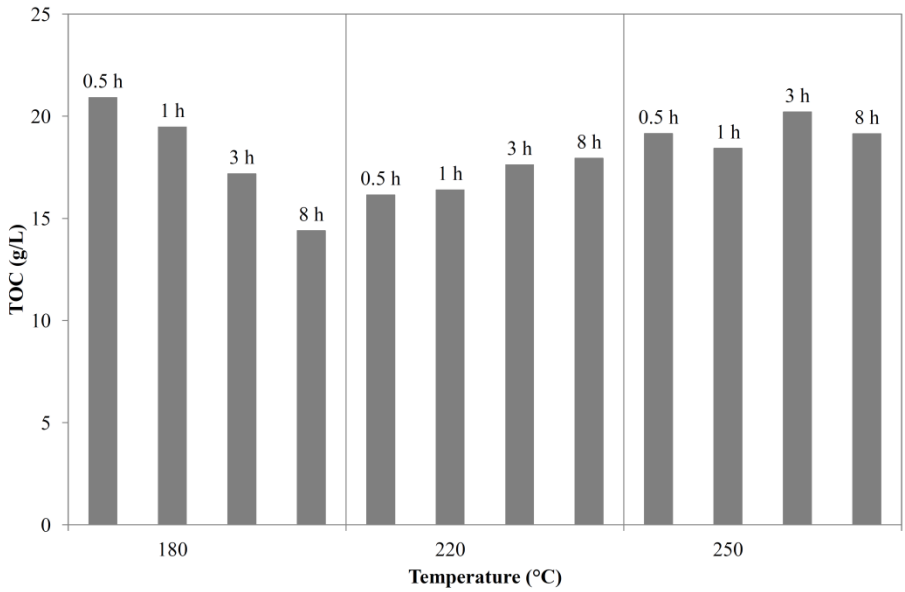

Figure 4.5. TOC data of the liquid phase after HTC of grape seeds.

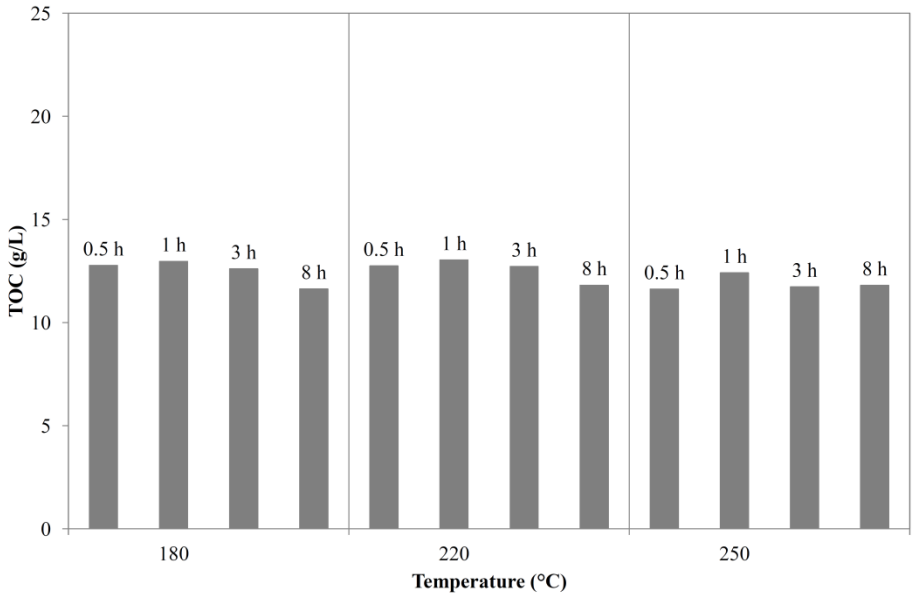

Figure 4.6. TOC data of the liquid phase after HTC of grape skins.

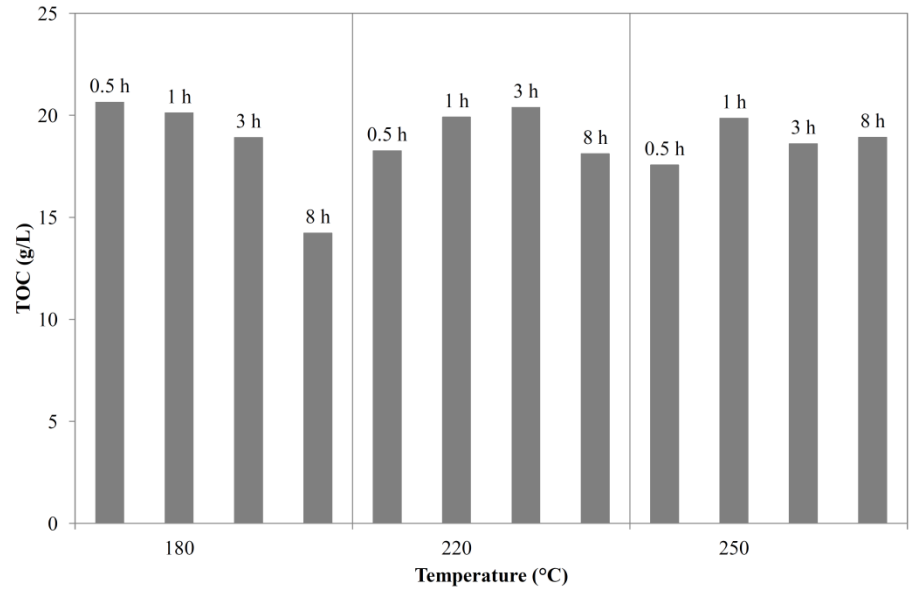

Figure 4.7. TOC data of the liquid phase after HTC of grape marc.

The TOC data are very variable and a clear trend cannot be seen. In general, at 180 °C the TOC values tend to decrease with time. This can be due to the polymerization reactions that can occurs from the molecules in liquid phase, that solidify producing secondary char, according to the definition given by Müller and Vogel [16]. Another cause of TOC decrease can be the formation of gaseous compounds (for example, carbon dioxide and carbon monoxide) from the carbonaceous molecules within the liquid phase. Moreover, this high variability on the results can be due to the high reactivity of the molecules in the liquid phase. In fact, not all the liquid was produced and collected at the same time (sometimes the HTC tests were done even after some weeks), while all the analyses were performed nearly in the same period. Thus, the liquid molecules can have formed some polymer solid molecules that, before measuring the TOC, were eliminated by filtration, even though the samples were stored closed and in a fridge at 4 °C.

Regarding grape seeds (Figure 4.5), the TOC values in the liquid phase are decreasing with time at 180°C, while it is slightly increasing at higher temperature. Regarding grape skin, not clear correlation is obtained. However, it seems that the maximum value of TOC in the liquid phase is reached after 1 hour of treatment whatever the temperature. Using table, it can be seen that the most interesting variation is for grape seeds at 180°C.

From literature, "seeds are rich in extractable phenolic antioxidants such as phenolic acid, flavonoids, procyanidins and resveratrol, while grape skins contain abundant anthocyanins", Yu and Ahmedna [17]. In addition, "grape seeds contain 13–19% oil, which is rich in essential fatty acids, about 11% protein, 60–70% of non-digestible carbohydrates, and non-phenolic antioxidants" [17]. "Drying of grape seeds at 100 and 140 °C resulted in 18.6 and 32.6% reduction in extractable total polyphenols, respectively, and reduced antioxidant activity of grape seeds compared to freeze-drying (Larrauri *et al.*, 1997" [18] ")" [17]. "Grape seeds procyanidins interact strongly with proteins leading to the rapid formation of protein–tannin

aggregates, and the binding increases with the degree of polymerization and molecular weight of procyanidins (de Freitas & Mateus, 2001) " [19] ". Present knowledge indicates that this interaction is affected by parameters of the protein (molecular size, hydrophobicity, structural flexibility), the polyphenol (degree of polymerisation, extent of galloylation, structural flexibility) and the environment (temperature, pH, ionic strength, presence of organic solvents and presence of carbohydrates) (Carvalho *et al.*, 2006)" [20] ".

"The oil content of grape seeds was reported in range of 11.6–19.6% depending on the variety and maturity of grapes (Rao, 1994" [21] "; Llobera & Cañellas, 2007" [22] "). The fatty acid composition of grape seed oil also variety and maturity dependent. Major fatty acids of grape seed oil are linoleic (66.76–73.61%) acid, oleic acid (17.8–26.5), palmitic acid (6.35–7.93%) and stearic acid (3.64–5.26%), respectively (Beveridge *et al.*, 2005" [23] "; Rubio *et al.*, 2009" [24] ")".

Pala et al. [25] about grape pomace wrote: "However, distribution of carbon in aqueous phase (around 12 wt%) did not significantly change over the temperature range of 175–275°C."

Moreover, Pala et al. [25] reported that the increase of extraction temperature from 175 to 250°C significantly enhances the antioxidant activity. "This behavior might be due to effect of temperature on the polarity of water (e.g. dielectric constant), because the dielectric constant of water is considerably decreased by increasing the temperature. This result is in agreement with previous studies relating to subcritical water extraction of plants and fruits (Aliakbarian et al., 2012" [26] "; Singh et al., 2011" [27] "). The decrease in AA above 250°C might be due to the degradation of flavonoids and anthocyanins at high temperatures. As conclusion, one can conclude that grape pomace can be converted to not only solid fuel but also chemicals through hydrothermal carbonization."

Prado et al. [28] wrote: "The solid residue at the end of the experiments decreased with temperature for all the raw materials, which indicates that the

lignocellulosic complex was degraded at 250°C. On the other hand, 200°C was not enough to break it down; therefore, only the hemicellulosic fraction could be recovered at lower temperature.". Moreover, "For the three raw materials the total reducing sugars recovered increased with temperature. This fact combined with the decrease in the solid residue at the end of the process indicates that only the hemicellulosic fraction was hydrolysed under 203–212°C, and that the cellulosic fraction was hydrolysed at 256–259°C." "For defatted grape seed the monosaccharides yield remained approximately constant and the inhibitors yield increased little with temperature increase." "… total reducing sugars yield increased with temperature, which indicates that more oligosaccharides were formed at higher temperature (89% oligosaccharides at 258°C vs. 79% oligosaccharides at 203°C). However, for defatted grape seeds the total sugars yield is very low compared to the other raw materials, because cellulose and hemicellulose content in the raw material is low".

To summarize, it seems that the composition of skin and seeds is different, especially regarding the distribution between cellulose, hemicelluloses and lignin. The seeds contain more lignin than skins; this could explain that the amount of organic carbon in the liquid phase accounts for 8-13% and 24-28% for seeds and skins respectively. The value of 8-13% of C in the aqueous phase for experiments with seeds is in agreement with literature [25]. At 180°C, it seems to be clear that the TOC value decreases in the liquid phase for HTC experiments with seeds. One of the explanations could be that the lignin and part of cellulose are not completely degraded to liquid phase at this temperature, even if the reaction time increases. By increasing the reaction time two phenomena could occur: organics are broken into little molecules and gas is produced or phenols react following repolymerization. Regarding the solid phase the carbon content increased more significantly after 8h and O content decreased significantly that can be linked to repolymerization reactions. At higher temperature, hemicelluloses and lignin are attacked by water and the walls of the seeds are expected to be thinner that could release

organics in the liquid phase. ESEM pictures (Appendix I) does not support a thinner wall, however it seems that the external surface and inner content are more degraded at higher temperature. In addition, seeds may contain oily products that can be more or less dispersed in the aqueous phase due to surfactant properties of some of the fatty acids in basic media.

The ICP data are reported in Appendix I at the Tables I.2, I.3, I.4.1, I.4.2 and I.4.3. In Tables I.4.2 and I.4.3, values of Al, B, Ba, Ca, Fe, K, Mg, Mn, Na, S, Si Sr and Zn were measured by Inductively Coupled Plasma (ICP), while P was measured through Atomic Absorption Spectroscopy (AAS).
Even in this case, it is not possible to highlight a correlation between the process conditions (above all, temperature and residence time) and the results obtained with this analysis. The potassium content in the process water is higher at 180 °C, presenting a peak for all the three substrates carbonized at 180 °C for 1 h. After 1 h, the potassium content tends to decrease. At higher temperatures, this inorganic elements tend to lower his presence.

Tables 4.7 and 4.8 report the liquid phase analyses performed through a gas chromatograph with flame ionization detector (GC-FID). The data are related to grape marc obtained at different process conditions and at B/W = 0.2.

Temp. (°C)	Res. time (h)	Guaiacol (mg/L)	Phenol (mg/L)	Acetic acid (mg/L)	Hydroxyacetone (mg/L)
180	1	<200	<200	2195	473
	3	<200	<200	2560	450
	8	<200	<200	2826	442
220	1	<200	<200	2760	329
	3	<200	<200	2720	259
	8	200	<200	2540	132
250	1	270	<200	2400	125
	3	354	<200	2070	0
	8	365	<200	2020	0

Table 4.7. GC-FID analyses of the liquid phase (data related to grape marc).

Temp. (°C)	Res. time (h)	2-Cyclopenten-1-one (mg/L)	Cyclopentanone (mg/L)
180	1	0	0
	3	0	0
	8	0	0
220	1	<100	0
	3	<100	0
	8	<100	<100
250	1	<100	<100
	3	<100	<100
	8	<100	<100

Table 4.8. GC-FID analyses of the liquid phase (data related to grape marc).

Gaseous phase

Table 4.9 reports the masses of gas formed from the carbonization of the three feedstocks at several process conditions.

Res. time	180 °C			220 °C			250 °C		
	SD (g)	**SK (g)**	**MR (g)**	**SD (g)**	**SK (g)**	**MR (g)**	**SD (g)**	**SK (g)**	**MR (g)**
0.5 h	0.09	0.08	0.10	0.23	0.13	0.21	0.36	0.21	0.36
1 h	0.11	0.08	0.11	0.24	0.15	0.23	0.38	0.25	0.35
3 h	0.15	0.09	0.14	0.31	0.18	0.29	0.42	0.27	0.42
8 h	0.18	0.11	0.17	0.37	0.22	0.35	0.45	0.28	0.45

Table 4.9. Total mass of gas formed during HTC of grape seeds (SD), skins (SK) and marc (MR), at different process conditions.

The masses of gas formed during the carbonization of grape seeds (SD), grape skins (SK) and grape marc (MR), seem to be influenced by the biomass to water ratio. As a matter of fact, from Table 4.9 it can be seen that comparing the amount of gas produced by HTC of grape seeds and that produced by grape skins, the first one is always higher than the second one. This can appear in contrast to the expectations: because grape skins have higher and more easily available holocellulose material, at fixed temperature and residence time, this substrate should degrade faster than a mostly lignocellulosic one (i.e., grape seeds), resulting in a higher mass of gas generated. But when considering the B/W ratio as an influencing process parameter, the data reported clearly show that a higher B/W ratio promotes the gas formation. As a matter of fact, grape seeds were carbonized with a B/W equal to 0.3, while grape skins were carbonized with a B/W equal to 0.1.

For this reason, these values were made independent from the B/W parameter, by dividing them with the corresponding B/W ratio (i.e., 0.3 for grape seeds, 0.1 for grape skins and 0.2 for grape marc). Equation (4.8) shows the calculation made to obtain the normalized mass of gas (NMG) values, starting from the actual mass of gas formed during the HTC tests (M_{gas}) and the biomass to water ratio ($^{B}/_{W}$) used in each test.

$$NMG = \frac{M_{gas}}{^{B}/_{W}} \tag{4.8}$$

Table 4.10 reports the NMG values, calculated for each substrate at different process conditions.

Res. time	180 °C			220 °C			250 °C		
	SD (g/-)	SK (g/-)	MR (g/-)	SD (g/-)	SK (g/-)	MR (g/-)	SD (g/-)	SK (g/-)	MR (g/-)
0.5 h	0.31	0.76	0.51	0.77	1.34	1.04	1.20	2.11	1.80
1 h	0.36	0.79	0.55	0.81	1.50	1.13	1.29	2.54	1.76
3 h	0.49	0.93	0.69	1.03	1.79	1.45	1.41	2.72	2.11
8 h	0.61	1.07	0.85	1.25	2.18	1.73	1.51	2.83	2.23

Table 4.10. NMG values calculated for grape seeds (SD), skins (SK) and marc (MR), at different process conditions.

Considering the data of Table 4.10, it is now possible to highlight the differences on the production of gas, considering the composition of each substrate, in terms of hemicellulose, cellulose and lignin content. In this case, it is clear that grape skins produce more gas than grape seeds. Moreover, the gas produced from grape marc is quite in the middle between the values of grape seeds and those of grape marc. This is completely in agreement with

the experimental procedure adopted to reproduce grape marc as composed by seeds and skins in the proportion 50% and 50%.

Table 4.11 reports the mass percentages of gas with respect to the mass of the dry feedstock charged inside the reactor. Table 4.11 clearly shows that the mass of feedstock that degrades into gas increases both enhancing temperature and time. The mass of gas formed during the carbonization, with respect to the initial dry charge, ranges between 1.50% and 9.42%, with an average value of 5.03%.

Res. time	180 °C			220 °C			250 °C		
	SD (%)	**SK (%)**	**MR (%)**	**SD (%)**	**SK (%)**	**MR (%)**	**SD (%)**	**SK (%)**	**MR (%)**
0.5 h	1.50	2.53	1.87	3.76	4.47	3.87	5.88	7.03	6.67
1 h	1.75	2.62	2.05	3.99	4.99	4.18	6.30	8.46	6.52
3 h	2.42	3.12	2.54	5.05	5.96	5.38	6.92	9.07	7.80
8 h	2.97	3.57	3.14	6.11	7.27	6.42	7.40	9.42	8.24

Table 4.11. NMG values calculated for grape seeds (SD), skins (SK) and marc (MR), at different process conditions.

The gaseous phase produced during each carbonization test, was analyzed through a mobile micro-gas chromatograph unit, equipped with a PLOT-U and a MOLSIEVE column, capable to detect the following molecules: H_2, N_2, O_2, CO, CH_4, CO_2, C_2H_6 and C_2H_4. The main results are graphically reported in the histograms of Figures 4.8, 4.9 and 4.10. These figures refer to the gas produced during the carbonization process of grape marc at different process conditions. The complete set of data, regarding even the grape seeds and the grape skins feedstocks are reported in Appendix I. The data related to the gas formed during HTC of grape seeds and skins are even reported in histograms (Figures I.27 to I.32.).

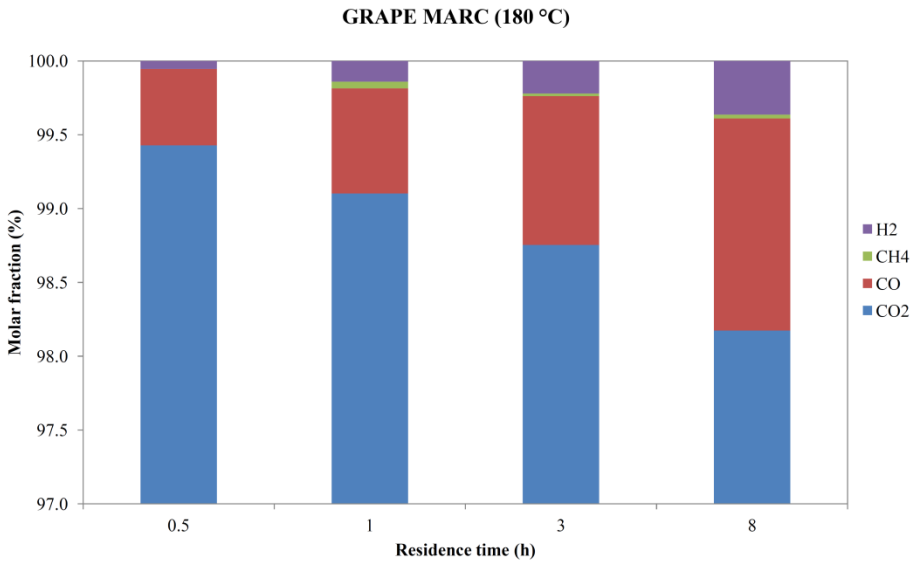

Figure 4.8. HTC of grape marc at 180 °C: gases molar fractions.

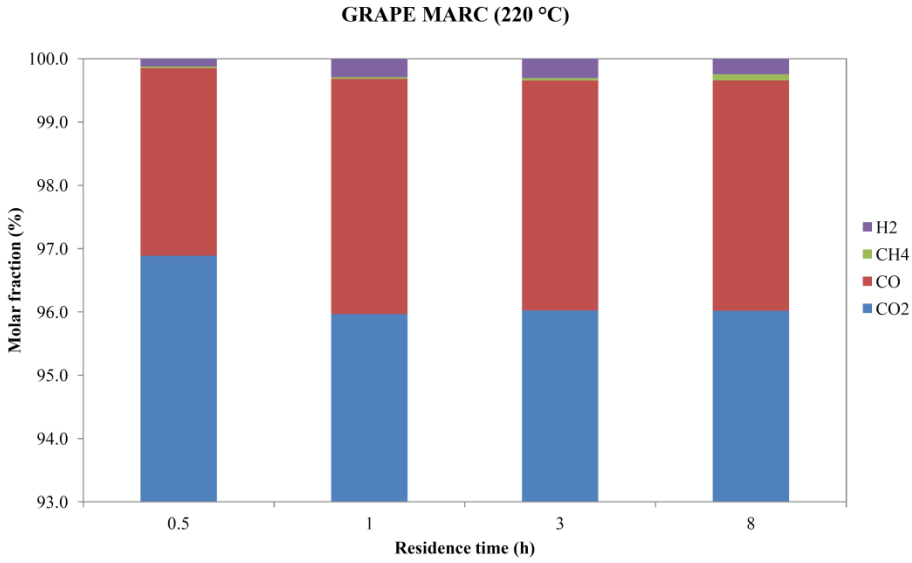

Figure 4.9. HTC of grape marc at 220 °C: gases molar fractions.

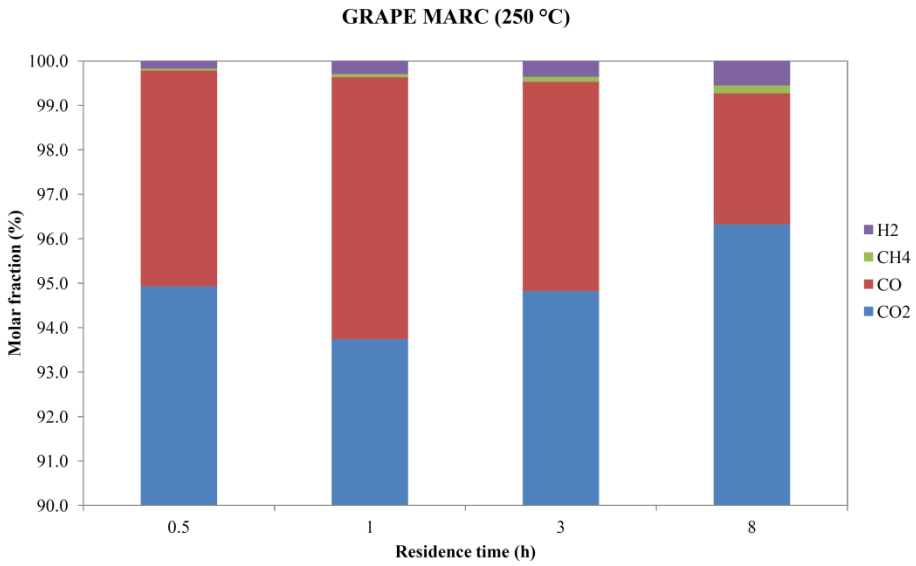

Figure 4.10. HTC of grape marc at 250 °C: gases molar fractions.

From the figures here reported and from those reported in Appendix I, it is clear that the gas formed during a HTC process is mainly composed by carbon dioxide. In particular, for what concerns grape marc, the molar fractions of carbon dioxide range between 93.7 to 99.4%. Carbon monoxide is present in a range of 0.5 to 5.9%, while traces of methane (0.0 - 0.17%) and hydrogen (0.05 - 0.55%) are found. Focusing on grape marc and considering the trend of formation of these gases, at lower temperatures (180 °C) the percentage of carbon dioxide tends to decrease with the residence time, while the formation of carbon monoxide and hydrogen (even though at very small percentages) are promoted. Methane has a peak after 1 h (0.05%), and then it tends to decrease with time. At 220 °C the trend previously described cannot be clearly appreciated, even though a slight decrease in the carbon dioxide percentage can be seen, in particular from 0.5 h to 1 h. Then, the molar fraction of this gas seems to remain constant (95.97% at 1 h, 96.02% at both 3 and 8 h). Interestingly, if the carbon dioxide percentage remains constant, the

carbon monoxide production has a peak at 1 h (3.72%), presenting a slight decrease at longer residence times (3.63% at 3 h, and 3.64 at 8 h). Hydrogen has a peak after 3 h (0.3%) but tends to decrease at 8 h (0.24%). On the contrary, the presence of methane increases with time. At 250 °C, carbon dioxide seems to decrease in the early stages of the process (from 0.5 h to 1 h), while it increases at longer residence times. On the other side, carbon monoxide increases its percentages from 0.5 h to 1 h, decreasing it at 3 h and 8 h. As expected, at higher temperatures more methane and hydrogen are formed, and their production increases at longer residence times.

Considering all the data reported in Appendix I, some considerations can be made. For what concerns carbon dioxide, that represents averagely the 96.4% in molar fraction of the gas and ranges between 92.6% (at 250 °C, 8 h) and 99.4% (at 180 °C, 1 h), generally at lower temperatures its amount tends to slightly decrease with time. One exception is represented by grape seeds carbonized at 180 °C. In fact, looking at Figure I.27, its molar fraction increases from 0.5 h to 1 h. After one hour, carbon dioxide begins to decrease. This particular behavior cannot be appreciated for the other substrates at the same HTC temperature. One hypothesis can be that, being grape seeds composed mainly by lignin, the process conditions are not too strong to make the gasification mechanisms to completely start after only 0.5 h. If compared with the molar fraction of carbon dioxide produced by grape skins after the same residence time at 180 °C, the more easily degradable molecules composing this substrate can faster initiate all the gasification mechanisms.

The molar percentages of carbon monoxide formed at 180 °C and at 220 °C, generally tend to increase both with temperature and residence time, while at 250 °C they tend to decrease after 3 h. One exception is represented by data of grape seeds carbonized at 250 °C. In this case, carbon monoxide increases from 0.5 h to 1 h, then it decreases from 1 h to 3 h, and finally it increases again from 3 h to 8 h.

Methane is present in very low concentrations. None or negligible amounts of methane were formed during the carbonization of grape skins. When carbonizing grape seeds and marc, its molar fraction tends to increase at higher temperatures. The hydrogen production generally tends to increase both with temperature and residence time, and traces of this element were always found in every carbonization. The hydrogen production can not only be due to gasification mechanisms, but also to reactions of the inorganic ions solved in the liquid phase. Equations (4.9) and (4.10) represent possible reactions causing hydrogen formation.

$$K^+ + H_2O \leftrightarrow KOH + H^+ \quad (4.9)$$

$$Mg^{2+} + 2\,H_2O \leftrightarrow Mg(OH)_2 + 2\,H^+ \quad (4.10)$$

Overall balances

Figures 4.11, 4.12 and 4.13 report the mass balances obtained at different process conditions.

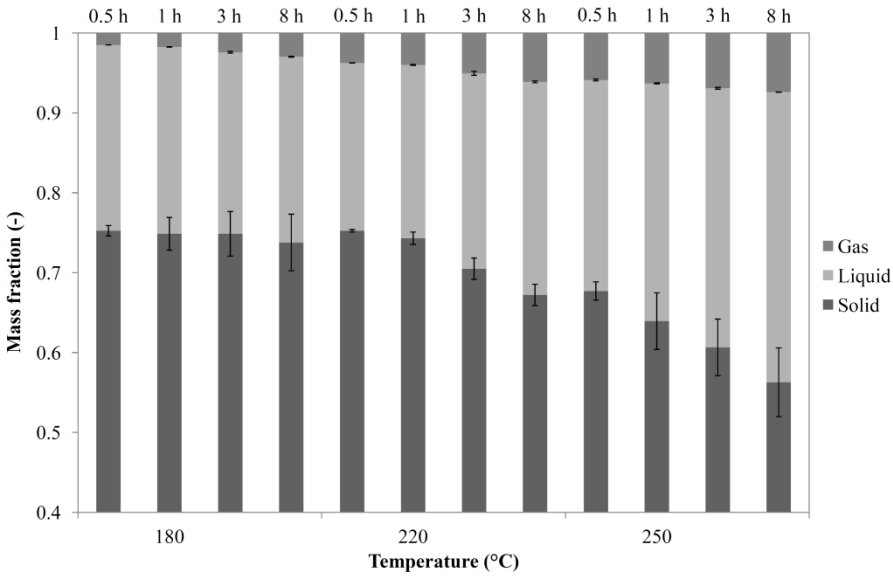

Figure 4.11. Grape seeds. Mass balance at different process conditions.

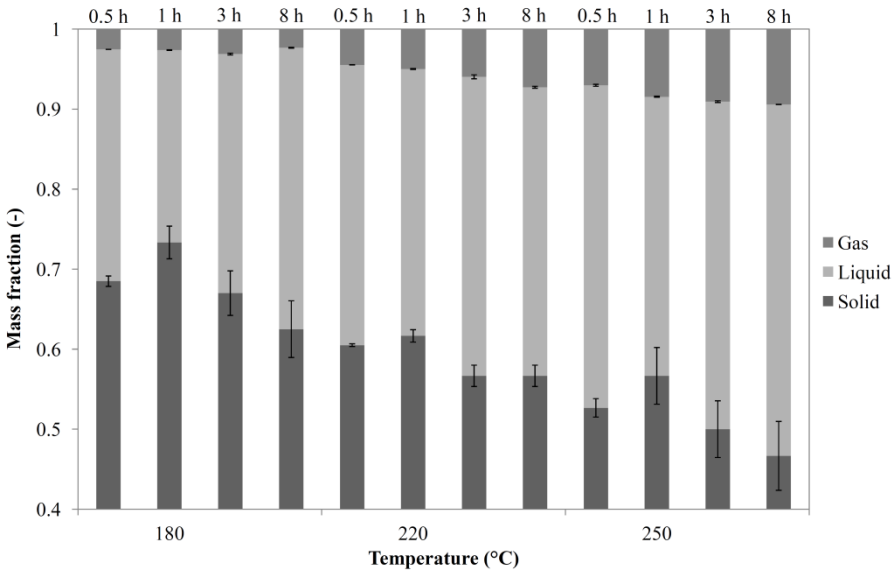

Figure 4.12. Grape skins. Mass balance at different process conditions.

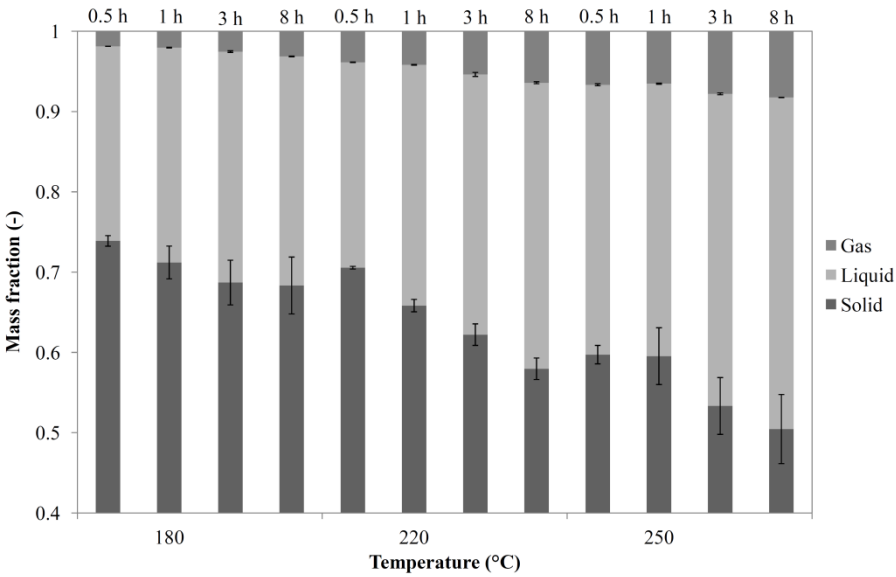

Figure 4.13. Grape marc. Mass balance at different process conditions.

The trend that can be appreciated looking at these figures, reflects the fact that increasing the process conditions (i.e., longer residence times and higher temperatures), the hydrochar yield decreases. Moreover, as can be seen in Figure 4.14, the mass lost by the feedstock during the process, tends in percentage to move more into the gaseous phase than in the liquid one. In particular, considering the mass loss within the solid phase, at longer residence times the percentage of gas formed tends to be lower, while the gas production is slightly enhanced. This fact can be explained considering that, as the residence time progresses, the molecules of the compounds which were solved in the liquid phase, more and more degrade into gaseous compounds. Thus, a part of the liquid compounds contributes to the formation of the gases. At higher temperatures, the gasification reactions occur faster than at lower temperatures: this fact can explain why at 250 °C the distribution of the mass lost during HTC between liquid and gas seems to be slightly time independent.

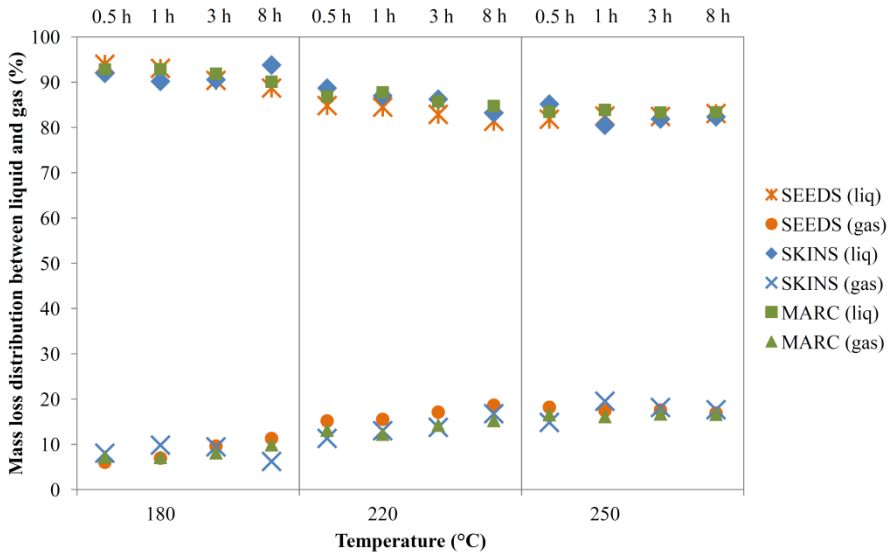

Figure 4.14. Distribution of the mass lost by the feedstock, between the liquid and the gas phases.

The carbon balance of grape seeds is reported in Figure 4.15. The data of carbon balance of the three substrates are reported in Appendix I, in Tables I.8, I.9 and I.10.

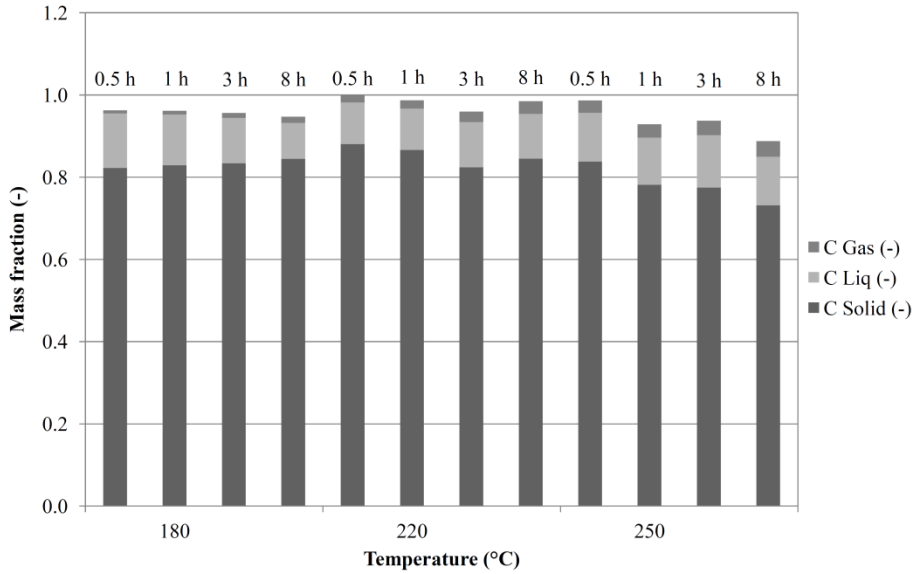

Figure 4.15. Carbon balance of grape seeds.

The carbon mass fractions in solid, liquid and gas were obtained calculating the mass of carbon present within each phase and dividing this datum by the mass of carbon initially present within the raw feedstock.

As expected, carbon mainly remains in the solid phase, ranging between 73% and 88% of the carbon initially present within the feedstock. Interestingly, the mass fraction of carbon within the hydrochar obtained at 180 °C tends to increase with time, while the mass of carbon contained within the hydrochars obtained at 220 °C and 250 °C tends to decrease with time. The higher carbon fraction in the hydrochar is obtained after 0.5 h at 220 °C, while the lower value is obtained after 8 h at 250 °C. The carbon mass fraction in the liquid phase ranges between 8.7% and 13.3%, being the lower value referred to the test performed for 8 h at 180 °C, and the higher value to the test performed for 0.5 h at 180 °C. In the gas, the carbon mass fraction ranges between 0.8% (0.5 h, 180 °C) and 3.8% (8 h, 250 °C).

For what concerns grape skins and marc, the carbon mass fraction tends to decrease with time, and this behavior can be appreciated for each testing temperature. Considering the hydrochars obtained from grape skins, this value ranges between 67.9% (8 h, 250 °C) and 85.4% (1 h, 180 °C); in the liquid, 24.9% (0.5 h, 250 °C) and 28.2% (1 h, 220 °C); in the gas 1.4% (8 h, 180 °C) and 5.6% (8 h, 250 °C). For what concerns grape marc, the ranges are: solid, 69.1% (8 h, 250 °C) and 85.7% (0.5 h, 220 °C); liquid, 14.4% (8 h, 180 °C) and 20.8% (3 h, 220 °C); gas, 1.0% (0.5 h, 180 °C) and 4.6% (8 h, 250 °C).

4.3 Conclusions of Chapter 4

In this chapter, several analyses were performed on the hydrochars, on the liquid phase and on the gas formed during hydrothermal carbonizations of grape seeds, skins and marc. These analyses were performed mainly with the objective to get insights on the main chemical pathways occurring during a HTC process and to assess the feasibility to valorize exhausted grape marc for energy purposes. In particular, it was found that up to 75% of the mass of the feedstock introduced inside the reactor can be recovered within the hydrochar at lower temperatures and residence times, without the addition of any catalyst. At stronger process conditions, namely 250 °C and long residence time, the mass recovery reaches a percentage of 50%. On the contrary, the carbon densification that directly affects the energy content of the hydrochar, increases with both temperature and residence time. For what concerns grape marc, considering both the hydrochar yield and its energy content, the carbonization of this material at 180 °C for 8 h gives the most favorable result: high energy content and considerable mass yield. However, under the perspective of real scale application, this result has to be coupled with the energy need to maintain the reactor at that temperature for 8 h. In this case, an interesting compromise is given by the carbonization of grape marc at 180 °C at 1 to 3 h: in this case, the higher heating value of the

hydrochar is slightly lower but the mass of hydrochar produced is higher. Thus, when considering possible HTC industrial applications, data shown in this chapter suggest not proceeding with the process more than 3 h.

All the ultimate analyses performed on the three substrates, reported negligible sulfur content and this fact has a strong influence when considering the possibility to substitute hydrochar from grape marc to fossil lignite. As a matter of fact, sulfur oxides (SO_X) are one of the most polluting products of the combustion process and they are considered to be one of the main causes of lung damages and pulmonary and respiratory damages [28]. Moreover, considering that the hydrochar is produced from an organic residue, when exploiting it for energy purposes no net carbon dioxide emissions are released in the atmosphere, while a net positive increment of carbon dioxide in the atmosphere is promoted by the utilization of fossil resources, like fossil lignite. This again represents an environmental benefit. Finally, the ash content decreases averagely by 32.8%. Fossil lignite has an ash content that ranges between 6% to 19%, while bituminous coals have an ash content from 6% to 12%. The hydrochar obtained at different process conditions presents ash contents that range between 3.3% and 5.3%, and this lower ash content represents another benefit when exploiting the hydrochar for energy purposes.

The process water contains a high TOC value, comparable to that found by Stemann et al. [29], who carbonized poplar wood chips at 220 °C for 4 h. In particular, the TOC of grape seeds carbonized at 220 °C for 3 h was 17.62 g/L, while the TOC found by the authors was 17.4 g/L. Therefore, for real scale or industrial applications, the process water could be recirculated as suggested by these authors, in this way catalyzing the carbonization process, causing an increase in the carbon content of the hydrochar and better dewaterability. At 180 °C from 1 to 3 h, the potassium content within the liquid phase is significantly high. In the optic of real scale implementation of a HTC plant, this can constitute an interesting inorganic element to be recovered from the liquid.

The mass percentages of the gas produced during the HTC process range between 1.5% and 7.4% (grape seeds), 2.3% and 9.4% (grape skins) and 1.9% and 8.2% (grape marc) and it is mainly composed by carbon dioxide (up to 96.7%, molar fraction). Traces of carbon monoxide, hydrogen and methane can be found in very small percentages, varying with the process conditions. Generally, the molar fraction of carbon dioxide decreases both with temperature and time, promoting mainly the production of carbon monoxide and hydrogen. However, if compared to other common thermochemical or biological processes commonly used for the treatment of wet organic materials, the gaseous emissions of HTC are much lower than those of these processes. When considering real scale application, this constitutes a big advantage of HTC technology, in terms of both environmental and legislative constraints.

References of Chapter 4

[1] Food and Agriculture Organization of the United Nations Statistics.

[2] Van Krevelen D.W., 1950. Graphical-statistical method for the study of structure and reaction processes of coal. Fuel, vol. 29, p. 269-284.

[3] Funke A. and Ziegler F., 2010. Hydrothermal carbonization of biomass: A summary and discussion of chemical mechanisms for process engineering. Biofuels, Bioproducts and Biorefining, vol. 4, p. 160-177.

[4] Funke A., Ziegler F., 2011. Heat of reaction measurements for hydrothermal carbonization of biomass. Bioresource Technology, vol. 102(16), p. 7595–7598.

[5] Lau F.S., Roberts M.J., Rue D.M., Punwani D.V., Wen W.W., Johnson P.B., 1987. Peat beneficiation by wet carbonization. International Journal of Coal Geology, vol. 8, p. 111-121.

[6] Blaszò M., Jakab E., Vargha A., Székely T., Zoebel H., Klare H., Keil G., 1986. The effect of hydrothermal treatment on Merseburg lignite. Fuel, vol. 65, p. 337-341.

[7] Schafer H.N.S., 1972. Factors affecting the equilibrium moisture content of low rank coals. Fuel, vol. 51, p. 4-9.

[8] Pala M., Kantarli I.C., Buyukisik H.B., Yanik J., 2014. Hydrothermal carbonization and torrefaction of grape pomace: a comparative evaluation. Bioresource Technology, vol. 161, p. 255–262.

[9] Lu L., Namioka T., Yoshikawa K., 2011. Effects of hydrothermal treatment on characteristics and combustion behaviors of municipal solid wastes. Applied Energy, vol. 88 (11), p. 3659–3664.

[10] Gaur S., Reed T.B., 1998. Thermal data for natural and synthetic fuels, Marcel Dekker. Inc.: New York, NY, USA.

[11] Sheng C, Azevedo J.L.T., 2005. Estimating the higher heating value of biomass fuels from basic analysis data. Biomass Bioenergy, vol. 28, p. 499–507.

[12] Friedl A., Padouvas E., Rotter H., Varmuza K., 2005. Prediction of heating values of biomass fuel from elemental composition. Analytica Chimica Acta, vol. 544, p. 191–198.

[13] Channiwala S.A., Parikh P.P., 2002. A unified correlation for estimating HHV of solid, liquid and gaseous fuels. Fuel, vol. 81, p. 1051–1063.

[14] Jenkins B.M., Ebeling J.M., 1985. Correlations of physical and chemical properties of terrestrial biomass with conversion. In: Proceedings of 1985 symposium energy from biomass and waste IX IGT, California, p. 371.

[15] Tillman D.A., 1978. Wood as an energy resource. New York: Academic Press.

[16] Müller J.B., Vogel F., 2012. Tar and coke formation during hydrothermal processing of glycerol and glucose. Influence of temperature, residence time and feed concentration. The Journal of Supercritical Fluids, vol. 70, p. 126-136.

[17] Yu J., Ahmedna M., 2013. Functional components of grape pomace: their composition, biological properties and potential applications. International Journal of Food Science & Technology, vol. 48, p. 221-237.

[18] Larrauri J.A., Ruperez P., Saura-Calixto F.,1997. Effect of drying temperature on the stability of polyphenols and antioxidant activity of red grape pomace peels. Journal of Agricultural and Food Chemistry, vol. 45, p. 1390-1393.

[19] de Freitas V.A.P., Mateus N., 2001. Structural features of procyanidin interactions with salivary proteins. Journal of Agricultural and Food Chemistry, vol. 49, p. 940-945.

[20] Carvalho E., Póvoas M.J., Mateus N., de Freitas V., 2006. Application of flow nephelometry to the analysis of the influence of carbohydrates on protein-tannin interactions. Journal of the Science of Food and Agriculture, vol. 86, p. 891-896.

[21] Rao P.U., 1994. Nutrient composition of some less-familiar oil seeds. Food Chemistry, vol. 50, p. 378-382.

[22] Llobera A., Cañellas J., 2007. Dietary fibre content and antioxidant activity of Manto Negro red grape (*Vitis vinifera*), pomace and stem. Food Chemistry, vol. 101, p. 659-666.

[23] Beveridge T.H.J., Girard B., Kopp T., Drover J.C.G., 2005. Yield and composition of grape seed oils extracted by supercritical carbon dioxide and petroleum ether: varietal effects. Journal of Agricultural and Food Chemistry, vol. 53, p. 1799-1804.

[24] Rubio M., Alvarez-Orti M., Fernández E., Pardo J.E., 2009. Characterization of oil obtained from grape seeds collected during berry development. Journal of Agricultural and Food Chemistry, vol. 57, p. 2812-2815.

[25] Pala M., Kantarli I.C., Buyukisik H.B., Yanik J., 2014. Hydrothermal carbonization and torrefaction of grape pomace: A comparative evaluation. Bioresource Technology, vol. 161, p. 255-262.

[26] Alikabarian B., Fathi A., Perego P., Dehghani F., 2012. Extraction of antioxidants from winery wastes using subcritical water. The Journal of Supercritical Fluids, vol. 65, p. 18-24.

[27] Singh P.P., Saldana M.D.A., 2011. Subcritical water extraction of phenolic compounds from potato peel. Food Research International, vol. 44, p. 2452-2458.

[28] World Health Organization, 2005. WHO Air quality guidelines for particulate matter, ozone, nitrogen dioxide and sulphur dioxide.

[29] Stemann J., Putschew A., Ziegler F., 2013. Hydrothermal carbonization: Process water characterization and effects of water recirculation. Bioresource technology, vol. 143, p. 139-146.

Chapter 5

EWC 19.05.03: experimental tests and results

In this chapter, the tests and the analyses performed on the waste residue coded by the European Waste Catalogue as EWC 19.05.03 are presented. Analyses were performed on the three phases obtained after the carbonization process, namely on the hydrochar, on the liquid and on the gas. The hydrochars obtained at different process conditions were tested in germination tests, to assess the feasibility to exploit this material as a soil conditioner.
A part of this chapter was developed on the basis of the work of Basso et al. [1].

5.1 Analyses and results

Solid phase

The carbonizations were performed at three temperatures (180 °C, 220 °C and 250 °C) and at three residence times (1 h, 3 h and 8 h). Table 5.1 reports the ultimate analysis of the raw material and of the hydrochars obtained at different process conditions. In the table the hydrochar yields are even reported. The solid phase was characterized in terms of C, H, N, and S mass

fractions, with the equipment Thermo NA 2100. The ash content was determined by incineration at 550 C according to EN 14775 procedure. The O content was then deduced by difference.

Temperature (°C)	Time (h)	C (%)	H (%)	N (%)	O (%)	Ash (%)	HC yields (%)
EWC 19.05.03	0	37.72	4.80	2.79	36.13	18.56	-
180	1	4408	5.40	1.26	36.03	13.17	0.806
	3	44.01	5.44	1.56	36.11	12.88	0.679
	8	45.02	4.92	1.60	33.49	14.97	0.653
220	1	45.01	4.76	1.81	35.41	13.00	0.576
	3	48.72	4.95	2.05	25.05	19.24	0.659
	8	52.53	4.87	2.70	19.31	20.60	0.420
250	1	49.32	4.58	2.51	23.72	19.84	0.408
	3	52.58	4.38	2.02	19.74	21.28	0.567
	8	53.84	5.10	2.46	12.91	25.69	0.396

Table 5.1. Elemental analysis and hydrochar yields at different process conditions.

The carbon content of the hydrochar increases both with the residence time and temperature, passing from a value of 44.08%, for a carbonization at 180 °C for 1 h, to a value of 53.84%, obtained at 250 °C after 8 h. The hydrogen mass percentage tends to decrease with time during the carbonization, a part for the datum at 250 °C and 8 h that shows a slight increase. This can be due to the heterogeneity of the sample that could have affected this measurement. As a matter of fact, the ultimate analyses were done at least three times, and the standard deviation referred to that datum was calculated as 0.409%. The nitrogen content tends to increase with the residence time, remaining averagely under the nitrogen mass percentage of the raw feedstock. As expected, the oxygen content decreases both with temperature and residence time, passing from a value of 36.13% (raw feedstock) to a value of 12.91% at 250 °C after 8 h. The ash content decreases in the early stages of the process

(i.e., after 1 h), tending to increase with time. Hydrochar yields smoothly decrease with time at 180 °C, while at higher temperatures this trend is not evident.

In Figure 5.1 the experimental data from ultimate analysis were arranged in a van Krevelen's diagram.

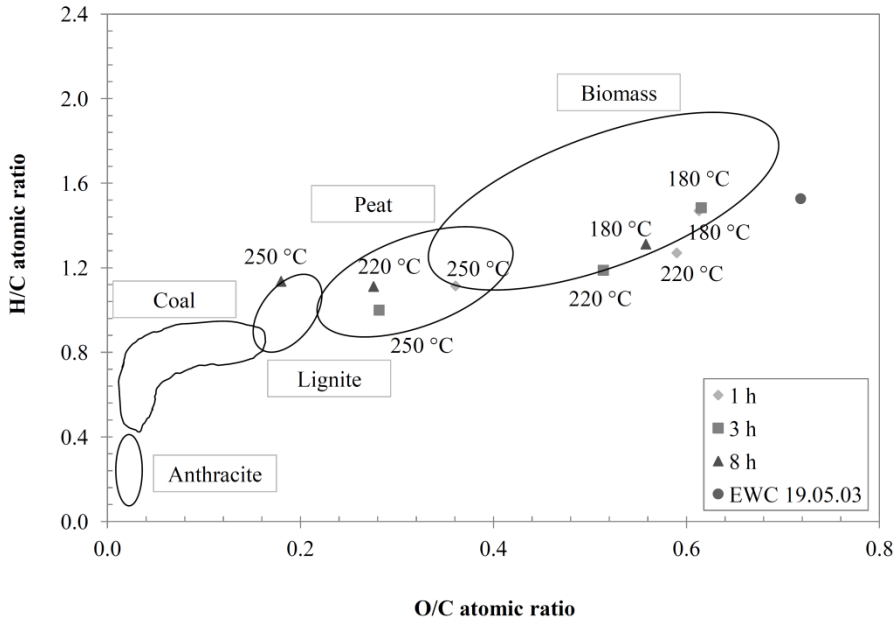

Figure 5.1. Van Krevelen diagram, referred to HTC of the residue EWC 19.05.03.

HTC acts as a process for concentrating the carbon content of biomass. As a consequence, both H/C and O/C atomic ratios are expected to decrease due to the treatment. The results confirm such trend. Notably, the raw feedstock presents a very high O/C atomic ratio, due to the fact that it previously underwent a long oxidation process like composting. For many experimental points the reduction of the O/C ratio does not appear to be very high. As a consequence, despite the HTC treatment, many samples may be still

classified as ‘‘biomass’’, without significant carbonization effects. This is particularly true for the mildest process conditions, which were applied for all the points obtained at 180 °C and for those obtained at 220 °C with a residence time up to 3 h. On the contrary, harsher process conditions allow obtaining a significant increase of hydrochar quality, with the experimental points falling in the regions of peat and lignite.

Figure 5.2 shows the higher heating value (HHV) of the produced hydrochar as a function of the hydrochar yield. The complete set of HHV data are reported in Appendix II (Table II.1).

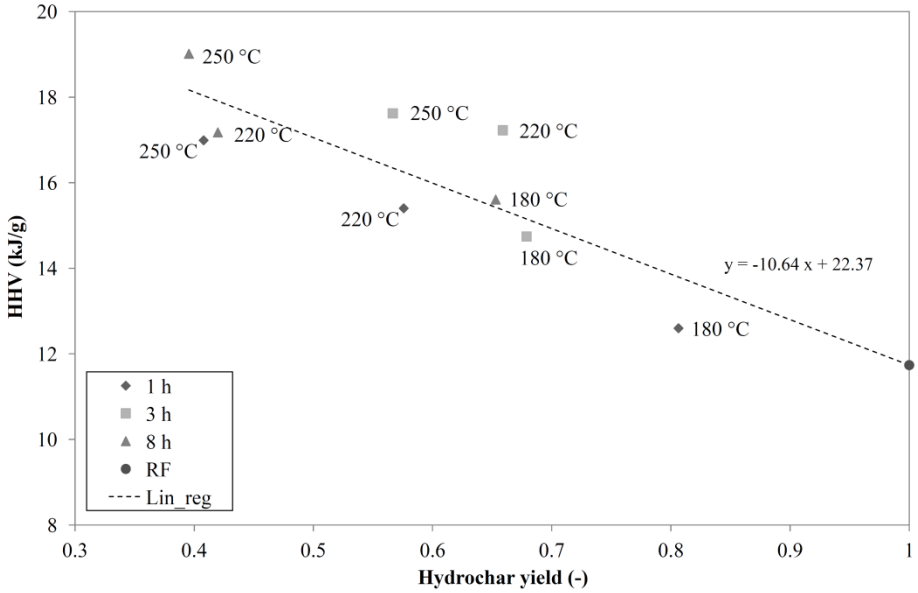

Figure 5.2. Hydrochar HHV versus hydrochar yield.

The point having a yield equal to one actually refers to the HHV of the raw material. There is a net increase of the HHV of hydrochar if compared to that of the raw substrate. The effect is more evident in correspondence of low solid yields. As the solid yields reduces, the HHV of hydrochar increases.

Similar trends have been reported previously in the literature [2, 3, 4]. This is a consequence of the carbon enrichment which takes place during HTC. The enrichment in carbon is due to the migration of oxygen and hydrogen, originally included in the solid matter, into the liquid and gaseous phases. As a result, when hydrochar has a high carbon concentration, which also implies a high HHV, solid yields are necessarily lower. From the points in Figure 5.2, it is possible to obtain a linear correlation between the hydrochar yield and its HHV:

$$HHV = 22.37 - 10.64 \cdot Y \tag{5.1}$$

where Y is the solid yield (i.e. hydrochar yield). The regression is quite satisfactory, with a mean relative error of 5.2%.

Some conclusions can be stated as far as the dependence on the operating conditions is taken into account. For the tests at 180 °C, the points are arranged on a straight line, in order of residence time. As the residence time increases, solid yields are lower and HHV is higher. Such strong correlation could not be observed at the other temperatures. However, it can be generally concluded that an enhancement of the severity of the process in terms of both residence time and temperature implies a stronger energy densification of the final solid substrate. Similarly to the results by Pala et al. [5], the HHV of the hydrochar produced here is comparable to that of peat and lignite. The HHV increase with respect to raw feedstock ranges from 7% to 61%. In terms of elemental composition, Table 5.2 reports the values of energy densification (ED), defined by equation (5.2), and energy yields (EY), defined by equation (5.3).

$$ED = \frac{HHV_{hydrochar}}{HHV_{raw\ material}} \quad (5.2)$$

$$EY = \frac{HHV_{hydrochar} \cdot mass_{hydrochar}}{HHV_{raw\ material} \cdot mass_{raw\ material}} \quad (5.3)$$

When referring to the $mass_{raw\ material}$, it is considered the raw material as received. The HHV of the hydrochar and hence ED increases with the increase of the severity of the process, i.e. for higher temperatures and higher residence times: the data fully respect this (Table 5.2). Conversely, EY decreases with the increase of the severity of the process: the trend is clear even if in this case the data are more scattered, due to the scatter affecting hydrochar yield.

Temperature (°C)	Time (h)	ED	EY
180	1	0.60	1.07
	3	0.59	1.26
	8	0.60	1.33
220	1	0.52	1.31
	3	0.67	1.47
	8	0.43	1.46
250	1	0.41	1.45
	3	0.59	1.50
	8	0.44	1.62

Table 5.2. Energy densification and energy yields.

The hydrochars obtained at the different process conditions, were analyzed thermo-gravimetrically (TGA analyses) with a LabSys Evo (Setaram). About 20 mg of sample was heated from 25 to 800 °C in a nitrogen atmosphere at 5 °C min^{-1}. In Table 5.3, the mass losses are reported.

Temperature (°C)	Time (h)	Total mass loss (%)	Mass loss up to 150 °C (%)	Mass loss at 150-800 °C (%)
EWC 19.05.03	0	-62.08	-6.85	-55.23
180	1	-60.97	-4.14	-56.83
	3	N.A.	N.A.	N.A.
	8	-64.47	-3.34	-61.13
220	1	-54.90	-3.20	-51.70
	3	-56.67	-2.80	-53.87
	8	-48.18	-2.47	-45.71
250	1	-53.83	-1.88	-51.95
	3	-47.64	-0.87	-46.77
	8	-47.99	-0.47	-47.52

Table 5.3. TGA experimental results: mass losses. (N.A. means "not available").

Table 5.3 shows that the mass loss between 150 and 800 °C is quite similar for the raw material (i.e., EWC 19.05.03 residue) and the hydrochars obtained at 180 °C. Conversely, the mass loss relevant to hydrochars obtained at higher HTC temperatures is lower. The data show a univocal trend, but significant scatter occurs.

Figure 5.3 reports the derivative mass loss (DTG) relevant to the raw material (labeled as EWC 19.05.03) and the hydrochars obtained at the four limit conditions (RT = 1 h, T = 180 °C; RT = 8 h, T = 180 °C; RT = 1 h, T = 250 °C; RT = 8 h, T = 250 °C).

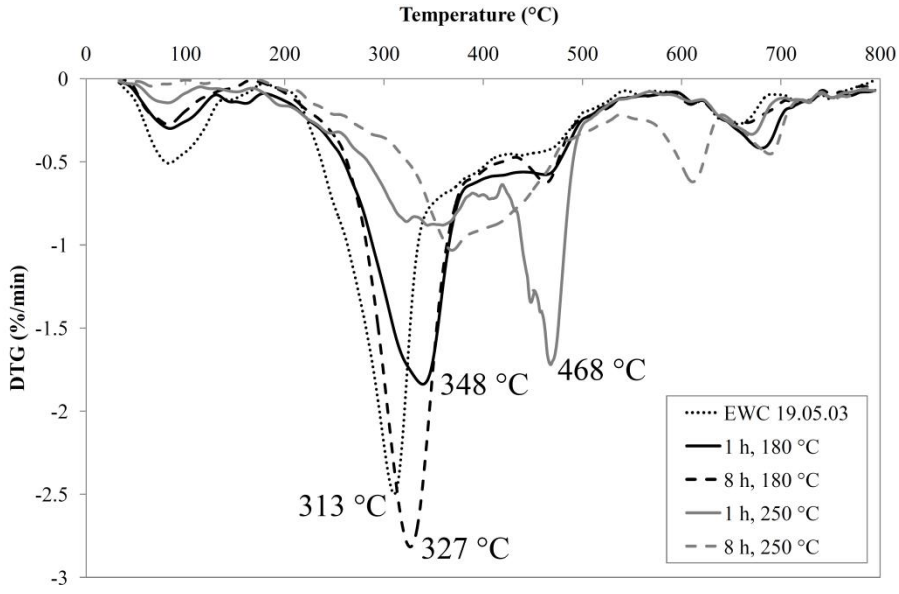

Figure 5.3. TGA analyses.

The DTG curves show that a large part of the solid constituents is degraded between 200 and 400 °C. The peaks of the DTG are centered on about 330 °C. A slight shift of the peak from 313 °C (OSC) to 348 °C (RT = 1 h, T = 180 °C) and 327 °C (RT = 8 h, T = 180 °C) indicates that the organics were only slightly modified during HTC occurring at 180 °C. The hydrochars obtained at a higher HTC temperature (250 °C) show a greater thermal stability: the compounds degraded between 200 and 400 °C are significantly reduced as the DTG is less intense and the peaks are shifted to higher temperatures (Figure 5.3). A new peak appears centered on 468 °C for the hydrochar obtained at RT = 1 h and T = 250 °C. This indicates that new compounds were formed during HTC performed at 250 °C even at a short residence time. Increasing the HTC residence time makes these new compounds more stable, as indicated by the new peak at about 600 °C relevant to the hydrochar obtained at RT = 8 h and T = 250 °C.

As a whole, the higher was the severity of the HTC treatment, the higher the thermal stability of the hydrochar produced. In particular, the thermal stability of the hydrochar (and thus its organic composition) was far from that of the raw feedstock (OSC) for RT = 8 h and T = 220 °C and for T = 250 °C whatever was the residence time, which is totally in agreement with Figure 5.1. As far as appearance of the solid substrates is concerned (visual observation by digital microscope are reported in Appendix II, in Figures II.1 to II.4), the raw material exhibit numerous fibers that wrap wood pieces, which confirms its heterogeneous nature. The width of the fibers was statistically determined at about 20 μm. By increasing the severity of the process, at first fibers reduced in length, then completely disappeared (RT = 3 h and T = 220 °C). The microscopic observations also reveal a significant transformation of the wood pieces: as long as the carbonization process proceeded, they moved from their natural brown color, to a darker color, till they became completely black. During such carbonization path, the statistical size of wood pieces reduced and bright spots started to appear on the hydrochar surface, probably due to the presence of minerals at the surface.
Thus, increasing the severity of the HTC process on the one hand reduces EY (Table 5.2), on the other hand allows obtaining a product, hydrochar, whose thermal and chemical characteristics make it suitable for utilization as a fuel, differently from the original raw material. The hydrochar produced at such severe conditions could be thus potentially utilized as a solid fuel in common coal burners. It is worth noticing that, when operating at 250 °C, a solid comparable to peat can be obtained after only 1 h of treatment. This opens interesting perspectives for the energy valorization of off-specification compost (i.e., the EWC 19.05.03 residue), with possible economic benefits for the whole cycle of organic municipal waste. Future work should analyze the economic feasibility of such process, by taking into account the capital and operating costs and the optimal configuration of the plants.

Liquid phase

The liquid phase was characterized in terms of total organic carbon (TOC) concentration. The total carbon (TC) and the total inorganic carbon (TIC) were measured in a TOC-Analyzer (Shimadzu, TOC V-CSH). The TOC was deduced by subtracting the TIC value from the TC value. TC concentration (mg of C L^{-1}) was obtained by combustion in synthetic air of the solution at 720 °C on a platinum fixed bed catalyst. The CO2 released from organics combustion and carbonate volatilization was then measured by Fourier transform infrared (FTIR) spectroscopy. A second analysis consisted in the acidification by phosphoric acid coupled with outgassing to remove carbonates as CO2: in this way the TIC value was measured. The mineral content in the liquid phase was measured using inductively couple plasma optical emission spectroscopy (ICPOES, ICP JOBIN YVON-ULTIMA 2).

Table5.4 reports the TOC of the liquid phase obtained downstream the HTC process. TOC values are in the range 7–13 g/L, corresponding to 27–48% of the initial carbon present in the solid feedstock. Such TOC values are comparable to the values obtained by Gao et al. [6] when processing at 300 °C for 30 min different real biomass and biomass model compounds: the authors measured TOC values in the range 4–4.7 g/L (about half of the values measured here) when working with a biomass to water ratio of 0.05 (about half of the value used here).

Temperature (°C)	Time (h)	TOC ± σ (g L^{-1})	Total minerals in liquid (mg L^{-1})	% of minerals from initial ash
180	1	7.0 ± 0.2	1556.2	12.0
	3	7.5 ± 0.1	1644.4	12.7
	8	7.3 ± 0.1	1643.7	12.7
220	1	8.8 ± 0.2	1641.25	12.7
	3	10.5 ± 0.4	1929.35	14.9
	8	11.2 ± 0.3	1911.5	14.8
250	1	12.2 ± 0.2	2027.15	15.7
	3	12.7 ± 2.2	2066.75	16.0
	8	12.0 ± 0.2	2239.1	17.3

Table 5.4. TOC and mineral content in the aqueous phase from HTC at different operating conditions.

TOC is strongly dependent on the temperature: operating at higher temperature results in a higher value of TOC. Indeed, the temperature enhances the decomposition of the biomass into the liquid phase, which is consequently richer in organic compounds. As far as residence time is concerned, the TOC shows a slight increase from 1 h to 3 h of residence time, while being almost stable (or even decreasing) for longer residence times. However, this trend is not very evident and the residence time seems to play a quite marginal role. TOC data testify that the organic matter passes from the solid to the liquid phase in the initial stage of the HTC process: the TOC concentration does not change to an appreciable extent in the range of reaction times studied. It is worth noticing that the data show a very good reproducibility, which is witnessed by the small values of the standard deviation (SD). For all the data but one, the relative standard deviation (RSD) ranges between 0.7% and 4.1%. The only exception is represented by the run at 3 h and 250 °C, whose RSD is equal to 17.5%.

Besides the organic compounds dissolved in the liquid, the presence of ions in the aqueous phase was analyzed. Such piece of information was obtained

by means of ICP analyses. The total mineral content in liquid and the percentage of minerals from initial ash are shown in Table 5.4, while data about ions are presented in Table 5.5.

Temperature (°C)	Time (h)	Concentration in liquid phase (mg L^{-1})					
		K	Ca	Si	Mg	S	Fe
180	1	1096.0	221.5	112.1	80.3	31.1	6.6
	3	1162.8	257.1	90.7	87.2	34.2	7.2
	8	1093.9	335.6	86.2	90.0	26.0	9.2
220	1	1059.7	348.0	100.6	84.4	33.3	9.1
	3	1231.5	443.5	106.0	104.1	34.7	5.4
	8	1198.1	468.9	117.5	94.0	24.8	5.0
250	1	1236.9	570.3	110.6	71.5	29.1	3.2
	3	1433.8	308.0	155.2	133.7	22.3	10.5
	8	1253.7	827.9	102.4	35.7	16.2	0.8

Table 5.5. Mineral content in the aqueous phase from HTC at different operating conditions.

The total minerals concentration in the liquid phase was calculated from the large spectra of elements quantified. The main significant concentrations where those of K, Ca, Si, Mg, S and Fe, are reported in Table 5.5. The complete set of data are reported in Appendix II, Tables II.2.1, II.2.2 and II.2.3. In Tables II.2.2 and II.2.3, values of Al, B, Ba, Ca, Fe, K, Mg, Mn, Na, S, Si Sr and Zn were measured by Inductively Coupled Plasma (ICP), while P was measured through Atomic Absorption Spectroscopy (AAS). The fifth column of Table5.41 evidences the percentages of minerals coming from the raw feedstock and dissolved in the liquid phase: these values were obtained accounting for the mass of solid utilized in the experimental runs and its ash content (Table 5.1). From 12% to 17% of the initial ash content was recovered in the liquid phase. This percentage increases with temperature and, to a lower extent, reaction time. This behavior resembles that of TOC.

Although water at these HTC conditions is a suitable solvent for minerals, their transfer from the solid seems quite limited. In general, it is not possible to appreciate a trend about the release of K, Ca, Si, Mg, S and Fe with respect to the process conditions. The only exception is represented by phosphorous, whose concentration tends to decrease with both residence time and temperature (Table II.2.1).

Tables 5.6 and 5.7 report the liquid phase analyses performed through a gas chromatograph with flame ionization detector (GC-FID). The data are related to the EWC 19.05.03 residue obtained at different process conditions and at B/W = 0.2.

Temp. (°C)	Res. time (h)	Guaiacol (mg/L)	Phenol (mg/L)	Acetic acid (mg/L)	Hydroxyacetone (mg/L)
180	1	<200	<200	980	213
	3	<200	<200	930	157
	8	<200	<200	992	116
220	1	<200	<200	1050	240
	3	<200	<200	1150	168
	8	233	<200	1300	107
250	1	253	<200	1330	206
	3	324	<200	1347	0
	8	305	<200	1263	0

Table 5.6. GC-FID analyses of the liquid phase (data related to EWC 19.05.03).

Temp. (°C)	Res. time (h)	2-Cyclopenten-1-one (mg/L)	Cyclopentanone (mg/L)
180	1	0	0
	3	0	0
	8	0	0
220	1	0	0
	3	0	0
	8	<100	<100
250	1	140	<100
	3	<100	<100
	8	<100	117

Table 5.7. GC-FID analyses of the liquid phase (data related to EWC 19.05.03).

Gaseous phase

Gas analyses were performed by means of a portable gas chromatograph (3000 micro-GC, SRA Instruments®), equipped with two columns: a Molsieve® column able to detect He, H_2, O_2, N_2, CH_4 and CO and a Plot-U® column able to detect CO_2, C_2H_4, C_2H_6 and C_3H_6/C_3H_8 (C_3's).

It was possible to have an indirect measure of gas production during HTC by observing the trend of pressure inside the reactor as a function of residence time. Such result was reported in Figure 5.4a. During the heating up, pressure steadily increases. Once the set temperature has been reached, each curve presents a peak of pressure which drops when the temperature stabilizes. During the whole initial temperature transient, the system pressure coincides with the vapor pressure of water at the variable temperature. As the time goes on, although the temperature is constant, pressure increases due to gas formation: gases are formed throughout the whole duration of the process. The rate of gas production appears to be higher in the first hours of reaction, while it generally tends to stabilize for longer residence times.

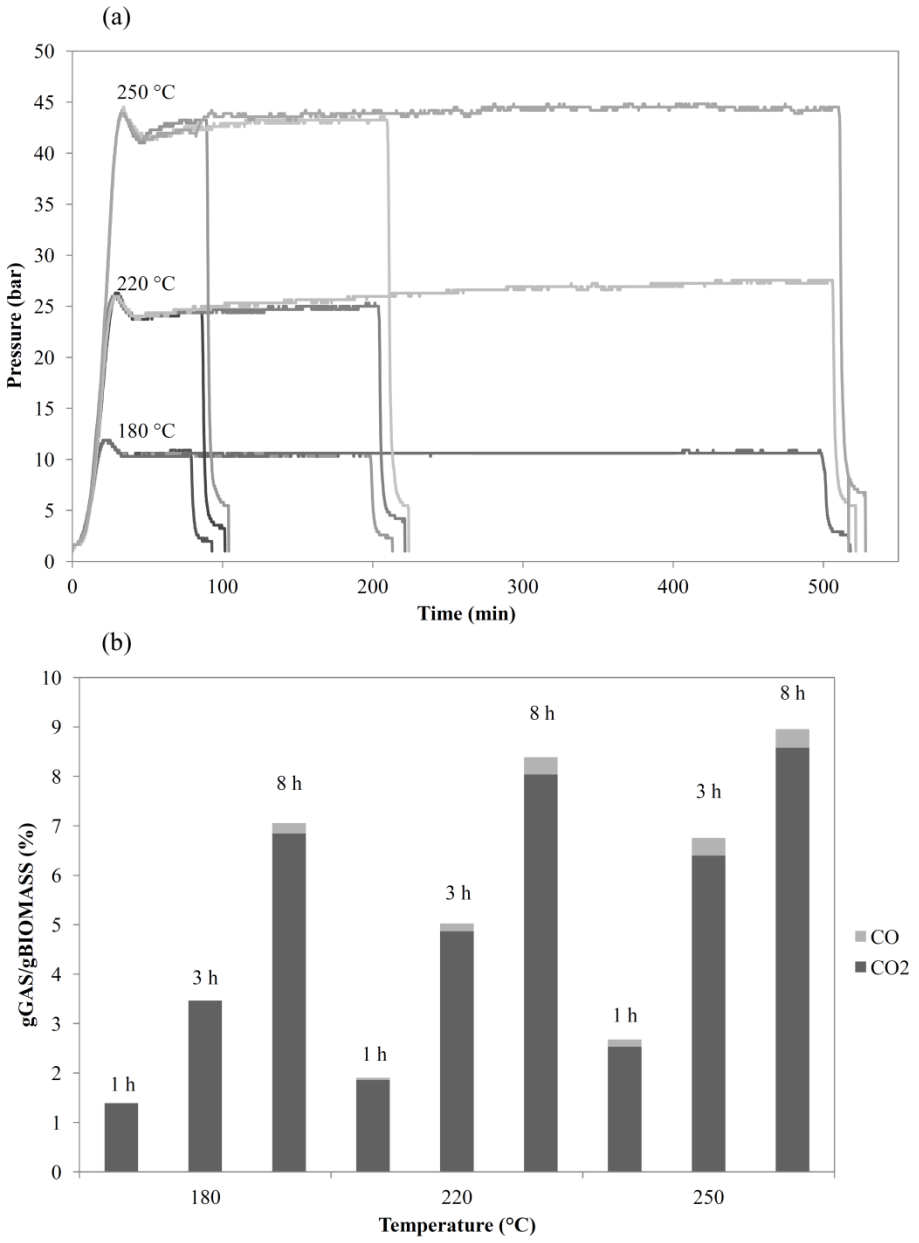

Figure 5.4. (a) Pressure behavior at different temperatures versus time; (b) CO_2 and CO production in percentage with respect to the dry feedstock at different temperatures and residence times.

The trends of Figure 5.4a testify the very good reproducibility of the gas pressure results, which reflect in the very good reproducibility of the gas yields.

As far as gas composition is concerned, the results from GC analyses showed that, for all the samples analyzed, more than 90 vol.% of the gas was composed by CO_2, followed by CO, which amounts at 3–8 vol.%. As a whole, more than 98 vol.% of the produced gas was composed by CO_2 and CO, the remaining part being represented by H_2 and CH_4. Traces of light hydrocarbons were detected in the gas formed at the most severe process conditions. This is in agreement with Lu et al. [7, 8], who reported that other permanent gases like ethylene, ethane, propene and butane are produced in small to negligible amounts.

Figure 5.4b shows the gas yields in percentage with respect to the mass of the dry feedstock as a function of the process conditions. Since the other gaseous products are yielded only in negligible amounts, only CO_2 and CO were included in the graph. The production of gases increases with both temperature and residence time. The large amounts of CO_2 produced allow concluding that decarboxylation is the main reaction involved in the production of gaseous products. However, at high temperatures or at long residence times, CO starts being produced in not negligible amount. This could be caused by the occurrence of decarbonylation, through which the organic compounds with a carbonyl group (i.e. aldehydes and ketones) loose oxygen by releasing a molecule of CO.

Finally, Figure 5.5 shows all the gases detected after the HTC process at different process conditions. In Appendix II, Table II.3, the complete set of data are reported.

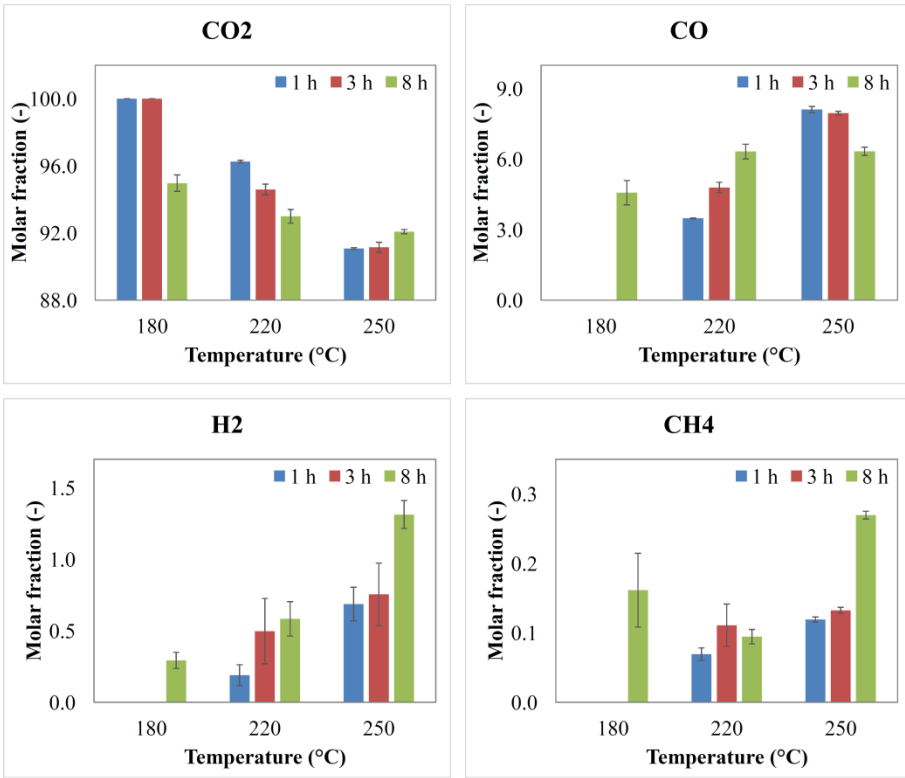

Figure 5.5. Molar fraction of the gases produced during HTC of EWC 19.05.03.

Overall balances

Figure 5.6 shows the total mass balance. The solid yield was determined in terms of amount of solid recovered with respect to the amount of dry substrate initially loaded into the reactor ($g_{HYDROCHAR}/g_{DRY\ FEEDSTOCK}$). The gas yield ($g_{GAS}/g_{DRY\ FEEDSTOCK}$) was calculated considering the volume of gas directly measured and the gas average molar mass computed considering the gas composition. The amount of raw biomass degraded and transferred into the liquid phase was determined by difference. Thus, the error bars of Figure 5.6 refer to the solid and gas phases only.

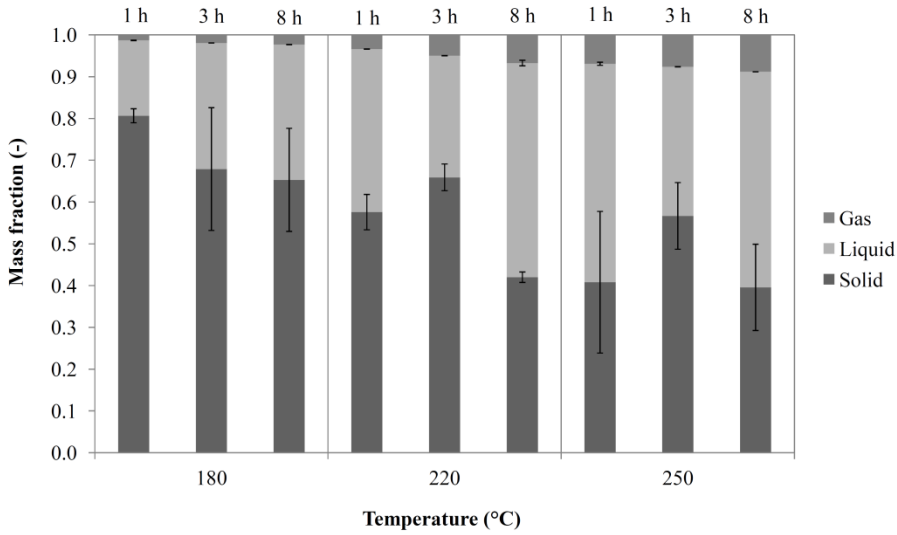

Figure 5.6. HTC mass balance. Yield of solid, gas and liquid (by difference) referred to the dry mass of the feedstock at different temperatures and residence times.

As reported in other works [9, 10, 11], temperature greatly influences the yield of solids. As obtained from the micro-GC analyses, at higher temperatures decarboxylation and decarbonylation reactions are more pronounced, bringing to higher CO_2 and CO production, while lowering the hydrochar yields. Moreover, an enhancement of the temperature promotes the dissolution of carbonaceous products into the aqueous phase, further decreasing the solid yields. As it was also found by Lu and Berge [12], at higher temperatures larger fractions of carbon are measured within the liquid and more gases are produced. Conversely, the influence of the residence time on the hydrochar yield seems to be less important (Figure 5.6), in agreement with previous results [2, 3, 13, 14]. This could be a clue that most reactions involved in HTC take place in the first hours of residence time. Similar results concerning product distribution within the three phases were obtained by several authors [15, 16, 17, 18]. It is worth noticing that solid yield values were affected by a remarkable scattering, due to the heterogeneous nature of the raw feedstock. Gas yield scattering was much lower than solid yield scattering, and almost negligible.

5.2 Carbonized EWC 19.05.03 for soil conditioning: comparison with the IBI limits for biochar

To study the applicability of hydrochar as a soil improver, the contribute given by the International Biochar Initiative [19] was considered. This choice was made mainly because of a current regulatory gap in the country where these analyses were done (i.e., Italy). As the title of the IBI manual suggests (i.e., *Standardized Product Definition and Product Testing Guidelines for Biochar That Is Used in Soil*), this document proposes a set of threshold limit values for the biochar to be used in soils. In this context, the term biochar refers to “a solid material obtained from the thermochemical conversion of biomass in an oxygen-limited environment” [19]. These threshold limit

values have been proposed by the IBI considering the maximum thresholds allowed in some jurisdictions (US, EU, UK, Australia and Canada).
Table 5.8 shows a comparison between the original feedstock and the hydrochar produced for the majority of the parameters proposed by the IBI. The fifth column of the table reports the IBI threshold limit values.

Parameter	**Unit**	**Values**		
		Original substrate	*Hydrochar*	*IBI threshold limit values*
Moisture	%	30.3	< 5	--
Organic carbon	%	23	48 – 85	> 30
$H:C_{ORG}$	-	0.19	0.08 – 0.12	< 0.7
Total Nitrogen	%	1.57	1.3 – 2.6	--
PAHs	mg/kg	< 0.1	0.1 – 0.3	6 – 20
PCBs	mg/kg	< 0.1	0.1 – 0.3	0.2 – 0.5
Arsenic (As)	mg/kg	< 5	6.2- 12.6	12 – 100
Cadmium (Cd)	mg/kg	< 2	2.5 – 5.1	1.4 – 39
Chromium (Cr)	mg/kg	< 16	19.8 – 40.4	64 – 1200
Cobalt (Co)	mg/kg	< 10	12.4 – 25.3	40 – 150
Copper (Cu)	mg/kg	32	39.7 – 80.9	63 – 1500
Lead (Pb)	mg/kg	< 10	12.4 – 25.3	70 – 500
Mercury (Hg)	mg/kg	< 1	1.2 – 2.5	1 – 17
Nickel (Ni)	mg/kg	< 10	12.4 – 25.3	47 – 600
Selenium (Se)	mg/kg	< 5	6.2 – 12.6	1 – 36
Zinc (Zn)	mg/kg	83	102.9 – 209.8	200 – 7000

Table 5.8. Parameters of the original feedstock and of the hydrochar and IBI threshold limit values.

The values reported the third column have been indicated by Contarina S.p.A., the company that manages the organic fraction of the municipal solid

waste of the province of Treviso (Italy), which provided the EWC 19.05.03 residue. For what concerns the four five parameters (moisture, organic carbon, H:C_{ORG} and total nitrogen), these values for hydrochar have been directly measured. For all the other parameters, it was considered that all these elements/compounds remain within the solid phase. Thus, the HTC process acts as a densificatior of these toxicants in the solid phase. The range of values reported in the fourth column of Table 5.8, was evaluated considering the hydrochar yields of the worst and of the best cases (i.e., when the yields are 40 and 81 %, respectively). Other parameters proposed by the IBI were not reported in Table 5.8, because of lack of data.

For what concerns the hydrochar produced, the results of this comparison clearly show that all the threshold limit values here considered are respected. Although preliminary, this is an interesting result because it supports the hypothesis to exploit the HTC process to recover a fraction of waste that is currently simply bio-stabilized and landfilled.

5.3 Phytotoxicity and germination tests

Phytotoxicity and germination tests were performed utilizing the hydrochar obtained from the EWC 19.05.03 residue at 250°C for 3 h. Another variant was made with composted hydrochar. To do this, hydrochar was put in socks and put inside small composting reactors for 30 days. This procedure was made to understand if the composting process is able to reduce possible toxic molecules within the hydrochar. The composition of the organic material to be composted, was reproduced using dog food, wood shavings, grass cuttings, fertig-compost, and water. The proportions are reported in Table 5.9.

Material	Water content (%)	Mass (g)	Mass percentage (%)
Dog food	8.3	180	42.9
Wood shavings	9.9	40	9.5
Grass cuttings	73.9	60	14.3
Fertig-compost	50.0	40	9.5
Water	100.0	80	19.0

Table 5.9. Composition of organic material to be composted..

In Figure 5.7, the composting apparatus is represented.

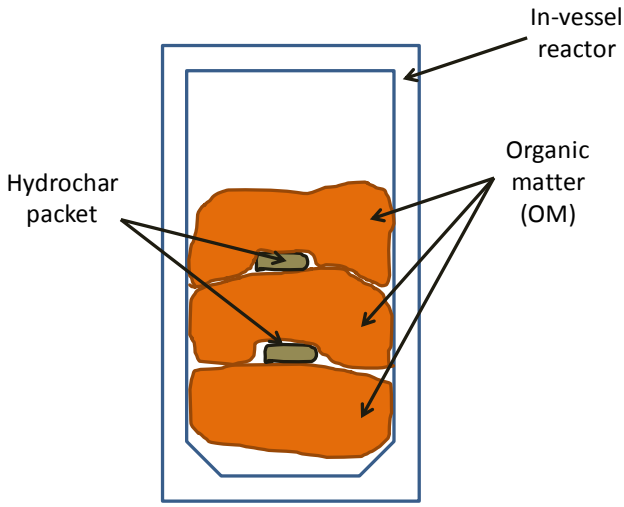

Figure 5.7. Schematic representation of the composting reactor filled with the hydrochar within nylon packets.

Two different types of seeds were tested: mustard and corn. Mustard was chosen because it is very sensitive to toxic substances [20]. Its seed is very small so it is more suitable for analyses in Petri dishes. Corn was chosen because it has a very thick seed and because it is more robust against toxic substances. These seeds were disposed in Petri dishes with sand. Prior to be used, sand was made to boil in distilled water for at least 1 h. Ten seeds were put in each Petri dish. Seven variants were made:

1. variant 0 or control: only with sand;
2. variant A: with hydrochar added in a mass percentage of 2.5%;
3. variant B: with composted hydrochar added in a mass percentage of 2.5%;
4. variant C: with hydrochar added in a mass percentage of 5%;
5. variant D: with composted hydrochar added in a mass percentage of 5%.

The control, variant A and variant B were tested both on mustard and corn seeds, while variants C and D were tested only on corn seeds. Figure 5.8 shows the Petri dishes after five days.

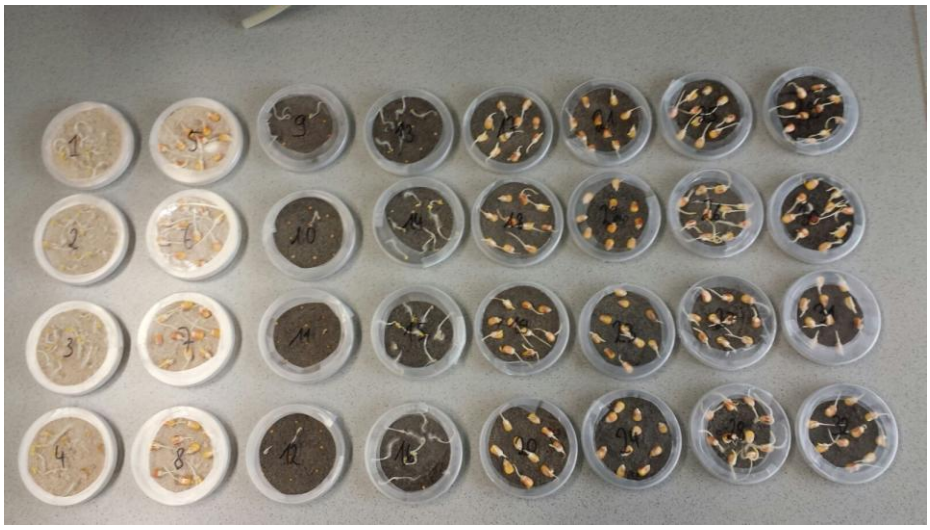

Figure 5.8. Phytotoxicity and germination tests. Results after five days.

The eight clearer Petri dishes on the left side of the figure are the control variants. In particular, those labeled from 1 to 4 are the control with mustard seeds, while those labeled from 5 to 8 are those filled with corn seeds. Petri dishes labeled from 9 to 12 are those filled with mustard seeds under variant A; from 13 to 16 are those with mustard seeds under variant B. Petri dishes from 17 to 20 are filled with corn seeds under variant A, while from 21 to 24 are corn seeds under variant B. Petri dishes from 25 to 28 are corn seeds under variant C and dishes labeled from 29 to 32 are filled with corn seeds under variant D.

Three main parameters were considered in performing these tests: germination rate, namely the number of seeds that after five days; roots length and shoots length.

Some statistical analyses were performed: average root and shoot length in each Petri dish for every replication; average root and shoot length for every variant; average germination rate of each variant. The complete set of results is reported in Appendix II (Tables II.4.1, II.4.2, II.5.1, II.5.2, II.5.3 and II.5.4). In Table 5.10, the main results are reported.

Test, Variant	**Average germination rate (%)**	**Average root length (cm)**	**Average shoot length (cm)**
Mustard, 0	97.5	1.87	3.07
Corn, 0	95.0	2.47	0.77
Mustard, A	17.5	2.03	1.27
Mustard, B	77.5	1.51	2.29
Corn, A	87.5	1.63	0.96
Corn, B	92.5	2.52	1.15
Corn, C	55.0	0.99	0.48
Corn, D	97.5	1.91	0.84

Table 5.10. Main results from phytotoxicity and germination tests.

Variants A and B effects on mustard seeds

Variant A strongly reduces the germination rate on the seeds, highlighting the presence of phytotoxic molecules on the hydrochar, mainly represented by volatile organic compounds. However, this effect is strongly reduced after 30 days composting of the hydrochar, demonstrating that the composting treatment can be an effective post-treatment for the hydrochar produced from the EWC 19.05.03 residue, although the germination rate sill remains lower with respect to the control. Applying variant A on mustard seeds, the average roots length is increased up to 8%, while variant B limits the roots length by a factor of 20%. For what concerns the shoots length, application of variant A reduces this parameter by a factor of 58%, confirming the presence of phytotoxic compounds in the hydrochar. Application of variant B, reduces the shoots length by a factor of 25%.

These results highlight the presence of phytotoxic compounds within the hydrochar, even though a composting treatment can effectively act to reduce these molecules. It has to be considered that mustard seeds are particularly sensitive to toxic substances [20]. Further investigations can regard the enhancement of the composting period to lower more and more the presence of toxic substances.

Variants A and B effects on corn seeds

Corn seeds are definitely more resistant to phytotoxicity effects. In particular, the germination rate passes from 95% (control) to 87.5% (variant A) and 92.5% (variant B). Considering that the standard deviations for the germination rates of corn seeds in control, variant A and variant B, calculated on 4 repetitions are all equal to 5%, the variations on the average germination rates reported above are statistically negligible. Thus, it is possible to conclude that both variation A and B do not affect the germination rate of corn seeds.

Variants C and D effects on corn seeds

The application of 5% in mass of hydrochar generates a decrement on germination rate of 42%, confirming again that the application of fresh hydrochar has phytotoxic affects on the seeds. Conversely, the application of composted hydrochar in a mass percentage of 5% promotes the germination of seeds, passing from a germination rate of 95% (control) to a germination rate of (97.5%). Even though this datum could lead to think of a beneficial effect of composted hydrochar, statistically this datum is not meaningful and cannot be considered strong enough to state this, because of a variance of 5%, which makes this datum completely comparable to the control one.
Both roots and shoots lengths are strongly reduced from the application of variant C. Roots lengths decreases of a percentage of 60%, while the shoots length is reduced of a 37.7%. The application of variant D (composted hydrochar) produces a reduction of the roots length of 22.7%, while the shoots length is increased of a 9%.
The phytotoxicity tests described in this paragraph were done in collaboration with: Dominik Wüst, Dennis Jung, Saskia Sachs of the Institute of Agricultural Engineering, Chair of Conversion Technology and LCA of Renewable Resources, University of Hohenheim (DE), and Juergen Franzaring of the Institute of Landscape and Plant Ecology, University of Hohenheim (DE).

5.4 Conclusions of Chapter 5

In this chapter, several analyses were performed on the products of HTC of the residue coded by the European Waste Catalogue as EWC 19.05.03. This material is a by-product of the composting treatment of the organic fraction of the municipal solid waste. At present, this material is disposed off, after having bio-stabilized it during the composting process. This residue is mainly composed by lignocellulosic material. In this chapter, carbonization tests were done at three temperatures (180 °C, 220 °C and 250 °C) and three

residence times (1 h, 3 h and 8 h). Analyses on the solid, liquid and gaseous phases were performed, with the target to get insights on the possibility to valorize this by-product, applying the HTC process. In particular, the hydrochars obtained were analyzed to assess the exploitability to use them both for energy production and for soil conditioning. The results obtained show that the energy valorization is always possible.

In addition, preliminary comparisons with international standards for biochar seem to validate the possibility to use carbonized EWC 19.05.03 as a soil conditioner, even though phytotoxicity and germination tests provided negative results, when applying fresh hydrochar as it is. These results highlight the presence of toxic substances (mainly volatiles) the inhibit or lower the germination and the growth of the seeds. Interestingly, when hydrochar undergoes a composting process, its toxic compounds are strongly reduced. Thus, when thinking about real scale applications, this suggest that one possibility can bes represented by the opportunity to reintroduce the hydrochar at the beginning of the composting plant, mixing it with the entering untreated organic fraction of MSW. In this way, phytotoxic molecules (such as volatile hydrocarbons) can be removed by stripping it from the hydrochar, during the composting process. In this case, the entire cycle of the OFMSW could be closed, with no residual waste to be managed or landfilled. Another possibility is represented by the washing of the hydrochar with air or water. In deep tests have to be performed to get more insights on this possibility.

References of Chapter 5

[1] Basso D., Weiss-Hortala E., Patuzzi F., Castello D., Baratieri M., Fiori L., 2015. Hydrothermal carbonization of off-specification compost: A byproduct of the organic municipal solid waste treatment. Bioresource technology, vol. 182, p. 217-224.

[2] Dinjus E., Kruse A., Tröger N., 2011. Hydrothermal carbonization - 1. Influence of lignin in lignocelluloses. Chemical Engineering & technology, vol. 34, p. 2037-2043.

[3] Heilmann S.M., Jader L.R., Sadowsky M.J., Schendel F.J., Keitz M.G.V., Valentas K.J., 2011. Hydrothermal carbonization of distiller's grains. Biomass Bioenergy, vol. 35, p. 2526-2533.

[4] Mumme J., Eckervogt L., Pielert J., Diakté M., Rupp F., Kern J., 2011. Hydrothermal carbonization of anaerobically digested maize silage. Bioresource Technology, vol. 102, p. 9255-9260.

[5] Pala M., Kantarli I.C., Buyukisik H.B., Yanik J., 2014. Hydrothermal carbonization and torrefaction of grape pomace: a comparative evaluation. Biresource Technology, vol. 161, p. 255-262.

[6] Gao Y., Chen H.-P., Wang J., Shi T., Yang H.-P., Wang X.H., 2011. Characterization of products from hydrothermal liquefaction and carbonization of biomass model compounds and real biomass. Journal of Fuel Chemistry and Technology, vol. 39, p. 893-900.

[7] Lu X., Jordan B., Berge N.D., 2012. Thermal conversion of municipal solid waste via hydrothermal carbonization: comparison of carbonization products to products from current waste management techniques. Waste Management, vol. 32, p. 1353-1365.

[8] Lu X., Pellechia P.J., Flora J.R.V., Berge N.D., 2013. Influence of reaction time and temperature on product formation and characteristics associated with the hydrothermal carbonization of cellulose. Bioresource Technology, vol. 138, p. 180-190.

[9] Funke A., Ziegler F., 2011. Heat of reaction measurements for hydrothermal carbonization of biomass. Bioresource Technology, vol. 102, p. 7595-7598.

[10] GajićA., Ramke H.G., Hendricks A., Koch H.-J., 2012. Microcosm study on the decomposability of hydrochar in a Cambisol. Biomass Bioenergy, vol. 47, p. 250-259.

[11] Liu Z., Balasubramanian R., 2012. Hydrothermal carbonization of waste biomass for energy generation. Procedia Environmental Sciences, vol. 16, p. 159-166.

[12] Lu X., Berge N.D., 2014. Influence of feedstock chemical composition on product formation and characteristics derived from hydrothermal carbonization of mixed feedstocks. Bioresource Technology, vol. 166, p. 120-131.

[13] Erlach B., Harder B., Tsatsaronis G., 2012. Combined hydrothermal carbonization and gasification of biomass with carbon capture. Energy, vol. 45, p. 329-338.

[14] Müller J.B., Vogel F., 2012. Tar and coke formation during hydrothermal processing of glycerol and glucose. Influence of temperature, residence time and feed concentration. The Journal of Supercritical Fluids, vol. 70, p. 126-136.

[15] Goto M., Obuchi R., Hirose T., Sakaki T., Shibata M., 2004. Hydrothermal conversion of municipal organic waste into resources. Bioresource Technology, vol. 93, p. 279-284.

[16] Sevilla M., Fuertes A.B., 2009. Theproduction of carbon materials by hydrothermal carbonization of cellulose. Carbon, vol. 47, p. 2281-2289.

[17] Berge N.D., Ro K.S., Mao J., Flora J.R.V., Chappell M.A., Bae S., 2011. Hydrothermal carbonization of municipal waste streams. Environmental Science Technology, vol. 45, p. 5696-5703.

[18] Hwang I., Aoyama H., Matsuto T., Nakagishi T., Matsuo T., 2012. Recovery of solid fuel from municipal solid waste by hydrothermal

treatment using subcritical water. Waste Management, vol. 32, p. 410-416.

[19] International Biochar Initiative, 2013. Standardized product definition and product testing guidelines for biochar that is used in soil. http://www.biochar-international.org/characterizationstandard. Version 2.1. Last access: 27.02.2016.

[20] Sverdrup L.E., Krogh P.H., Nielsen T., Kjær C., Stenersen J., 2003. Toxicity of eight polycyclic aromatic compounds to red clover (*Trifolium pratense*), ryegrass (*Lolium perenne*), and mustard (*Sianpsis alba*). Chemosphere, vol. 53(8), p. 993-1003.

Chapter 6

EWC 19.12.12: experimental tests and preliminary results

In this chapter, preliminary results regarding the application of the HTC process for the treatment of the EWC 19.12.12 residue are presented. The work on this substrate is still a work in progress.

6.1 Analyses and preliminary results

Figures III.1 and III.2 in Appendix III show the EWC 19.12.12 residue as received from Contarina S.p.a., which is the company that collects and treats the municipal solid waste in the province of Treviso (North-Eastern Italy). Although this residue presents a quite interesting amount of biodegradable material (Table 3.3 in Chapter 3), this residue is very heterogeneous.

Mass balance

Figure 6.1 reports the overall mass balance obtained carbonizing the EWC 19.12.12 residue at different process conditions.

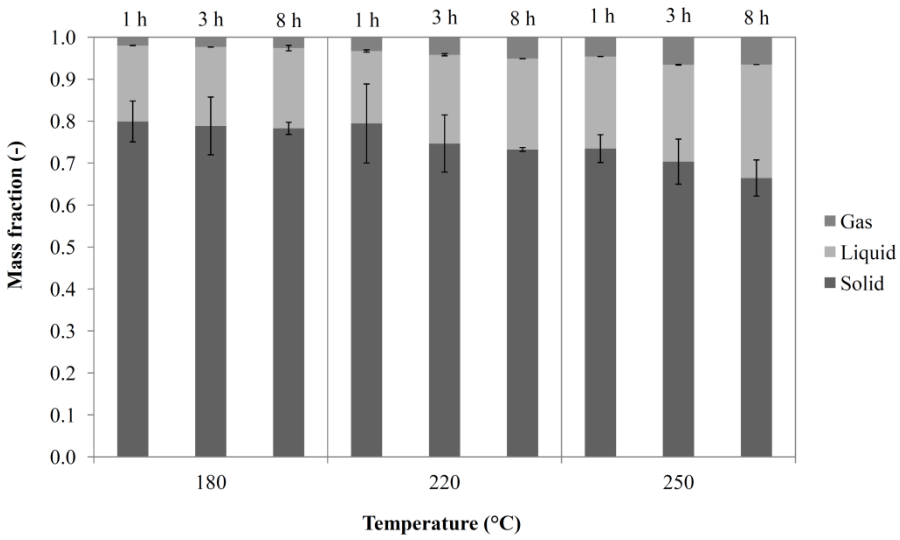

Figure 6.1. Mass balance.

The hydrochar yield ranges between 0.66 (HTC at 250 C° for 8 h) and 0.80 (HTC at 180 °C for 1 h). Even though the feedstock was quite heterogeneous, these results are interestingly coherent and follow a trend: at stronger process conditions, more liquid and more gas are produced, reducing the mass of hydrochar. From ultimate analysis (not yet completed) will be interesting to appreciate the behavior of C, H and O with respect to the process conditions, to try to find the best couple of temperature and time to be used to carbonize this material. Moreover, heating value measurements will suggest the best treatment conditions for the residue EWC 19.12.12. As a matter of fact, simply looking at the Figures III.1. and III.2 in Appendix III, the macro composition of this residue suggest to carbonize it to use it for energy production, more than other possible uses. The fact that this residue is a by-product of a specific waste treatment through which the raw waste is transformed into refuse derived fuel (RDF), support the idea to carbonize the wet residue coded as EWC 19.12.12, and mix it to the RDF produced. In this way, the EWC 19.12.12 residue will be reutilized and not landfilled, that is its

final destination at present. Moreover, if results of heating values measurements will report good HHV for the hydrochar obtained from this residue (i.e., HHV = 22 - 28 MJ/kg), mixing the hydrochar to the RDF will even increase the efficiency in energy production.

Liquid phase

Figure 6.2 reposts the TOC values measured on the process water obtained downstream of the process.

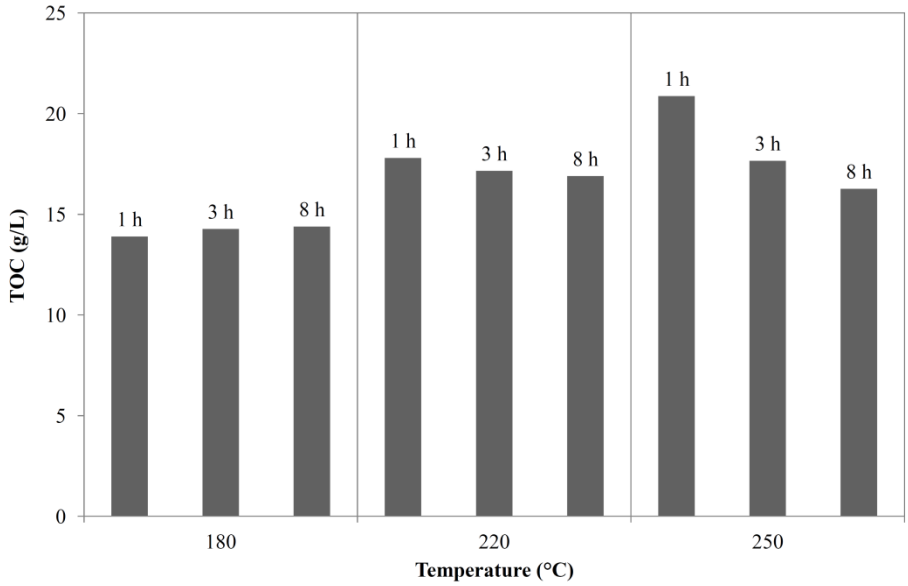

Figure 6.2. Total Organic Carbon.

At lower temperatures (180 °C) the TOC seems to be invariant with residence time, although looking at the data in Table III.1.1 in the Appendix, a slight increase is reported. Comparing the results at 180 °C both in terms of TOC and hydrochar yields, it is possible to think that only easily degradable compounds are affected by the process temperature and, once in the early

stages of the process these compounds are degraded, the whole process reaches an equilibrium independently from the residence time. This can suggest that, when running the process at lower temperatures, after about one hour, the carbonization can be thought to be mostly concluded.
At higher temperatures, namely 220 °C and 250 °C, the TOC lowers with the residence time, passing from 17.8 g/L to 16.9 g/L, at 220 °C, and from 20.9 g/L to 16.3 g/L, at 250 °C. This can be due to several mechanisms. First of all, considering that one main chemical reaction that occurs during hydrothermal carbonization is the dewatering of the feedstock, the lowering of the TOC with residence time can be due to a dilution effect. A second mechanism that can be responsible for the TOC to lower down could be the repolymerization of solved organic carbon into a solid substrate, in literature referred to be secondary char [1]. In this case, the amount of organic carbon that passes in the liquid phase is lower than that repolymerizes into secondary char. A third mechanism that occurs and can partly be responsible of the lowering of the TOC with residence time, is the gas production. It is not yet well understood if the HTC gas is directly formed from the solid feedstock, from the liquid phase, from both and in which percentages. What can be appreciated looking at both Figure 6.1 and 6.2 is that at longer residence times, more gas is produced and, because the HTC gas is mainly composed by carbon dioxide, both the carbon content in the solid phase and that in the liquid phase have to lower down. This is in agreement with what found by other authors [2, 3, 4].

Gaseous phase

Table 6.1 reports a short summary of the data obtained through a portable micro-GC (Agilent 3000), equipped with a MOLSIEVE and a PLOT U column was used. Detectable components were H_2, N_2, O_2, CO, CH_4, CO_2, C_2H_6 and C_2H_4.

Molecule	CO2	CO	CH4	H2
Mol fraction	93.23	4.94	0.57	1.26
St. dev.	0.60	0.55	0.27	0.39

Table 6.1. Total Organic Carbon.

Data concerning the gas composition are in agreement with the expectations: the gaseous phase is mainly composed by carbon dioxide. A small percentage of carbon monoxide was detected, along with traces of methane and hydrogen.

6.2 Conclusions of Chapter 6

The EWC 19.12.12 residue has been started to be investigated, by performing several carbonizations at different process conditions. In particular, the carbonizations have been performed at three temperatures, namely 180 °C, 220 °C and 250 °C and three residence times, 1 h, 3 h and 8 h. The overall mass balance has been assessed, highlighting that the hydrochar yield lower both with temperature and residence time, passing from 0.66 (HTC at 250 C° for 8 h) to 0.80 (HTC at 180 °C for 1 h). On the contrary, both the liquid phase and the gaseous phase increase with stronger process conditions. In terms of mass fractions, for what concerns the liquid phase, it passes from 0.18 (HTC at 180 °C for 1 h) to 0.27 (HTC at 250 C° for 8 h), while the gaseous phase passes from 0.02 (HTC at 180 °C for 1 h) to 0.07(HTC at 250 C° for 8 h).

The residence time does not influence the TOC when running HTC at lower temperatures (i.e., 180 °C), while when enhancing the temperature, residence time lower the TOC values. The lowering in the TOC content at higher temperatures, can be due to the production of water during the HTC process, the formation of secondary char and the gas production.

For what concerns the gaseous phase, micro-GC analyses show that it is mainly composed by carbon dioxide.

Further analyses have to be done on this substrate to assess the feasibility for it to be carbonized obtaining a hydrochar suitable to mixed to the refuse derived fuel (RDF), at present produced from the residual part of municipal solid waste. As a matter of fact, the EWC 19.12.12 residue is a by-product of RDF production and, at present, it is landfilled. Carbonizing it, increasing its heating value and mixing it to the RDF could enhance the performances of RDF itself, while avoiding the EWC 19.12.12 residue to be landfilled.

References of Chapter 6

[1] Müller J.B., Vogel F., 2012. Tar and coke formation during hydrothermal processing of glycerol and glucose. Influence of temperature, residence time and feed concentration. The Journal of Supercritical Fluids, vol. 70, p. 126-136.

[2] Funke A., Ziegler F., 2010. Hydrothermal carbonization of biomass: A summary and discussion of chemical mechanisms for processing engineering. Biofuels, Bioproducts and Biorefining, vol. 4, p. 160-177.

[3] Libra J.A., Ro K.S., Kammann C., Funke A., Berge N.D., Neubauer Y., Titirici M.-M., Fünher C., Bens O., Kern J., Emmerich K.-H., 2011. Hydrothermal carbonization of biomass residuals: a comparative review oft he chemistry, processes and applications of wet and dry pyrolysis. Biofuels, vol. 2(1), p. 89-124.

[4] Peterson A.A., Vogel F., Lachance R.P., Fröling M., Antal M.J., Tester J.W., 2008. Thermochemical biofuel production in hydrothermal media: A review of sub- and supercritical water technologies. Energy & Environmental Science, vol. 1, p. 32-65.

Chapter 7

Energy balance

In this chapter, a rigorous energy balance has been developed, on the basis of the data of grape seeds, reported both in Chapter 4 and in Appendix I.

7.1 Formulation of the problem

To evaluate the energy balance of the HTC reaction, the calculation of the enthalpy of reaction at different process conditions were performed. In particular, the equation that has been tried to solve was:

$$\Delta H_{HTC} = \Delta H_f(PRODUCTS) - \Delta H_f(REACTANTS) \quad (7.1)$$

In this chapter, the integration of Equation (7.1) in both temperature and pressure, to reach the actual process parameters, has been tried to performed. Some assumptions, mainly regarding the heat capacities of the molecules at the process conditions, have been made.

Assessment of the stoichiometric reaction

The whole reaction can be expressed in the general stoichiometric form

$$FS \rightarrow HC + LPC + H_2O + GAS \quad (7.2)$$

where:
FS, is the feedstock;
HC, is the hydrochar (solid phase product);
LPC, is a liquid pseudo-component;
H_2O, is the water formed during the process;
GAS, is the gaseous phase-

It is possible to express (7.2) in terms of chemical formulas:

$$FS = C_xH_yO_z \quad (7.3)$$

$$HC = C_lH_mO_n \quad (7.4)$$

$$LPC = C_aH_bO_c \quad (7.5)$$

$$GAS = CO_2 + CO + CH_4 + H_2 \quad (7.6)$$

thus obtaining:

$$\alpha C_x H_y O_z \rightarrow \beta C_l H_m O_n + \gamma C_a H_b O_c + \delta CO_2 + \varepsilon CO + \epsilon CH_4 + \theta H_2 + \vartheta H_2 O \quad (7.7)$$

in which:

$$x = \frac{1}{\alpha} \cdot (\beta \cdot l + \gamma \cdot a + \delta + \varepsilon + \epsilon) \quad (7.8)$$

$$y = \frac{1}{\alpha} \cdot (\beta \cdot m + \gamma \cdot b + 4 \cdot \epsilon + 2 \cdot \theta + 2 \cdot \vartheta) \quad (7.9)$$

$$z = \frac{1}{\alpha} \cdot (\beta \cdot n + \gamma \cdot c + 2 \cdot \delta + \varepsilon + \vartheta) \quad (7.10)$$

To assess the ΔHf° of each chemical compound, it is possible to state the following reactions.

Feedstock

$$C_x H_y O_z + hO_2 \rightarrow xCO_2 + \frac{y}{2} H_2 O + \frac{z+2h-2x-{}^{y}/_{2}}{2} O_2 \quad (7.11)$$

$$\Delta Hf,298°(C_x H_y O_z) = x \cdot \Delta Hf,298°(CO_2) + \frac{y}{2} \cdot \Delta Hf,298°(H_2 O) - Q(C_x H_y O_z) \quad (7.12)$$

where,

$$Q(C_x H_y O_z) = HHV(C_x H_y O_z) \cdot (molecular\ mass\ of\ C_x H_y O_z) \quad (7.13)$$

Hydrochar

$$C_lH_mO_n + jO_2 \rightarrow lCO_2 + \frac{m}{2}H_2O + \frac{n+2j-2l-{}^{m}/_{2}}{2}O_2 \quad (7.14)$$

$$\Delta Hf,298°(C_lH_mO_n) = l \cdot \Delta Hf,298°(CO_2) + \frac{m}{2} \cdot \Delta Hf,298°(H_2O) - Q(C_lH_mO_n) \quad (7.15)$$

where

$$Q(C_lH_mO_n) = HHV(C_lH_mO_n) \cdot (molecular\ mass\ of\ C_lH_mO_n) \quad (7.16)$$

Liquid pseudo-component

$$C_aH_bO_c + kO_2 \rightarrow aCO_2 + \frac{b}{2}H_2O + \frac{c+2k-2a-{}^{b}/_{2}}{2}O_2 \quad (7.17)$$

$$\Delta Hf,298°(C_aH_bO_c) = a \cdot \Delta Hf,298°(CO_2) + \frac{b}{2} \cdot \Delta Hf,298°(H_2O) - Q(C_aH_bO_c) \quad (7.18)$$

where,

$$Q(C_aH_bO_c) = HHV(C_aH_bO_c) \cdot (molecular\ mass\ of\ C_aH_bO_c) \quad (7.19)$$

Gaseous phase

The following data have been proposed by Poling et al. [1].
$\Delta Hf,298°(CO_2(g))$ = -393.51 kJ/mol
$\Delta Hf,298°(CO(g))$ = -110.53 kJ/mol
$\Delta Hf,298°(CH_4(g))$ = -74.52 kJ/mol
$\Delta Hf,298°(H_2(g))$ = 0 kJ/mol

Rigorously, the stoichiometric coefficients of the liquid pseudo-component can be assessed from equations (7.8), (7.9) and (7.10):

$$\gamma \cdot a = \alpha \cdot x - \beta \cdot l - \delta - \varepsilon - \epsilon \quad (7.20)$$

$$\gamma \cdot b = \alpha \cdot y - \beta \cdot m - 4 \cdot \epsilon - 2 \cdot \theta - 2 \cdot \vartheta \quad (7.21)$$

$$\gamma \cdot c = \alpha \cdot z - \beta \cdot n - 2 \cdot \delta - \varepsilon - \vartheta \quad (7.22)$$

From the ultimate analyses performed both on the feedstock and on the hydrochar, the following coefficients are known.
Feedstock:

$(\alpha \cdot x)$, $(\alpha \cdot y)$, $(\alpha \cdot z)$

Hydrochar:

$(\beta \cdot l)$, $(\beta \cdot m)$, $(\beta \cdot n)$

From the μ-GC analyses, the gaseous phase coefficients (δ, ε, ϵ and θ) are known.

In this way, it is possible to calculate the HHV($C_aH_bO_c$) through a suitable correlation between the calorific value of the compound and its elemental composition. Channiwala and Parikh [2] proposed a unified correlation for estimating HHV of solid, liquid and gaseous fuels. The correlation (7.23) can be used for 0.00% ≤ C ≤ 92.25%, 0.43% ≤ H ≤ 25.15%, 0.00% ≤ O ≤ 50.00%, 0.00% ≤ N ≤ 5.60%, 0.00% ≤ S ≤ 94.08%, 0.00% ≤ Ash ≤ 71.4% and for expected HHV values ranging between 4.745 MJ/kg and 55.345 MJ/kg.

$$HHV_{dry} = 0.3491\,X_C + 1.1783\,X_H + 0.1005\,X_S - 0.1034\,X_O - 0.0151\,X_N - 0.0211\,X_{Ash} \quad (7.23)$$

HHV_{dry} is expressed in MJ/kg and X_i are the mass percentages on dry basis of each element.

7.2 Identification of the molecules

The experimental data used in this discussion are those obtained through the HTC of grape seeds (Chapter 4 and Appendix I). These experimental data are reported in the following tables.

To perform all the tests, a 50 mL batch stainless-steel reactor was used (for more details, refer to Chapter 3). For each test, the reactor was filled with 6.1 ± 0.1 g of raw feedstock and with 20.4 ± 0.1 g of distilled water, thus obtaining a biomass to water ratio (B/W) of 0.3 ± 0.01.

Table 7.1 reports the three categories of products (solid, liquid and gas) obtained downstream of the HTC process.

Temperature (°C)	Time (h)	Hydrochar (g)	Liquid (L)	Gas (mol)
180	1	4.7	0.0211	0.0024
	3	4.6	0.0210	0.0034
	8	4.5	0.0201	0.0042
220	1	4.5	0.0203	0.0056
	3	4.3	0.0208	0.0071
	8	4.1	0.0201	0.0087
250	1	3.9	0.0207	0.0089
	3	3.7	0.0209	0.0098
	8	3.4	0.0205	0.0106

Table 7.1. HTC process products yields.

Several analyses have been performed, both on feedstock and products. In particular, ultimate analysis and calorific value of both feedstock and hydrochar, TOC analysis of the liquid and micro-GC analyses on the gases.

Table 7.2 and 7.3 report the results of the ultimate analyses and the corresponding amount of moles, evaluated multiplying the weight fractions

of C, H and O by the mass of feedstock or hydrochars, and assuming the molar weight of both feedstock and hydrochar to be equal to 100 g/mol. Temperature is indicated with "T", while residence time is indicated as "τ".

T (°C)	τ (h)	C (wt.%)	H (wt.%)	O (wt.%)	N (wt.%)	Ash (wt.%)	Mass (g)
180	1	60.24	6.62	27.84	1.32	3.98	4.7
	3	60.60	6.50	27.43	1.40	4.07	4.6
	8	62.30	6.80	25.35	1.40	4.15	4.5
220	1	63.40	6.70	23.96	1.60	4.34	4.5
	3	63.60	6.40	23.75	1.60	4.65	4.3
	8	68.40	6.70	18.28	1.90	4.72	4.1
250	1	66.50	6.40	20.54	1.80	4.76	3.9
	3	69.50	6.60	16.99	1.90	5.01	3.7
	8	70.70	6.50	15.66	2.00	5.14	3.4
Feedstock		54.40	6.60	34.20	1.60	3.20	6.1

Table 7.2. Ultimate analysis of feedstock and hydrochar.

T (°C)	τ (h)	C (mol)	H (mol)	O (mol)
180	1	0.234	0.306	0.081
	3	0.230	0.294	0.078
	8	0.233	0.304	0.071
220	1	0.239	0.301	0.068
	3	0.228	0.273	0.064
	8	0.232	0.271	0.047
250	1	0.216	0.248	0.050
	3	0.214	0.242	0.039
	8	0.202	0.221	0.034
Feedstock		0.276	0.399	0.130

Table 7.3. Moles of C, H and O within the feedstock and the hydrochar.

TOC analyses performed on the liquid, allowed the determination of the amount of carbon dissolved within this phase after each HTC process. In a similar way, micro-GC analyses gave information on the moles of C, H and O on the gaseous phase. Data of both the liquid and the gaseous phase are reported in Table 7.4.

Process conditions		**Liquid phase**	**Gaseous phase**			
T	**τ**	**TOC**	**CO_2**	**CO**	**CH_4**	**H_2**
(°C)	(h)	(g/L)	(mol %)	(mol %)	(mol %)	(mol %)
180	1	19.467	99.08	0.80	0.00	0.12
	3	17.181	98.37	1.16	0.00	0.47
	8	14.396	97.19	2.11	0.00	0.70
220	1	16.391	95.76	3.91	0.01	0.32
	3	17.622	95.41	4.27	0.03	0.29
	8	17.938	94.86	4.45	0.02	0.66
250	1	18.422	94.43	5.25	0.06	0.27
	3	20.206	94.60	4.87	0.08	0.45
	8	19.138	92.59	5.93	0.38	1.11

Table 7.4. Liquid and gaseous phases data.

Moldes et al. [3] reported that the chemical composition of grape seeds is 44% (w/w) lignin, 7% (w/w) cellulose and 31% (w/w) hemicellulose, the other 18% being oil and water. Moreover, many authors [4, 5, 6, 7] suggested that the main product of both cellulose and hemicellulose degradation is 5-hydroxymethylfurfural (5-HMF), while the hydrothermal degradation of lignin mainly results in the production of phenolic compounds. Therefore, starting from the TOC data, the moles of C have been divided proportionally between phenol (54%) and 5-HMF (46%). In this way, Equation (7.7) can be written as:

$$\alpha C_x H_y O_z \rightarrow \beta C_l H_m O_n + \mu C_6 H_6 O + \pi C_6 H_6 O_3 + \delta CO_2 + \varepsilon CO + \epsilon CH_4 + \theta H_2 + \vartheta H_2 O \quad (7.24)$$

In Equation (7.24), $\mu = 0.54 \cdot C_{TOC}$ and $\pi = 0.46 \cdot C_{TOC}$, where C_{TOC} represents the number of moles of carbon measured within the liquid phase, through the determination of the TOC. It is important to underline that this assumption considerably simplify the evaluation of the standard enthalpy of formation of the LPC, that will be discussed in section 7.3.

Hence, considering the moles of carbon measured through TOC analyses, the moles of both H and O were determined by proportion. In fact, knowing that in every mole of phenol there are 6 mol of H and 1 mol of O, and that in every mole of 5-HMF there are 6 mol of H and 3 mol of O, it was easy to calculate the total moles of H and O belonging to the two liquid components, respectively.

Moreover, knowing the moles of H and O introduced within the reactor by the feedstock and knowing their mole distribution within solid, liquid and gaseous products, it has been assessed that the moles of H obtained by difference between those insert within the reactor and those recovered in the products, have contributed to form water (Equation (7.25)).

$$\vartheta \ [mol] = \frac{1}{2}\left[H_{feedstock} - (H_{HC} + H_{LPC} + H_{GAS})\right] \quad (7.25)$$

In Equation (7.25), where ϑ is the parameter of Equation (7.7) and H_i refers to the moles of hydrogen measured within each substrate (feedstock,

hydrochar, LPC and gas, respectively). The moles of O belonging to the water were calculated by proportion.
Table 7.5 reports the molar composition of the LPC.

Process conditions		**5-HMF**			**Phenol**		
T (°C)	**τ (h)**	**C (mol)**	**H (mol)**	**O (mol)**	**C (mol)**	**H (mol)**	**O (mol)**
180	1	0.016	0.016	0.008	0.018	0.018	0.003
	3	0.014	0.014	0.007	0.016	0.016	0.003
	8	0.011	0.011	0.006	0.013	0.013	0.002
220	1	0.013	0.013	0.006	0.015	0.015	0.002
	3	0.014	0.014	0.007	0.016	0.016	0.003
	8	0.014	0.014	0.007	0.016	0.016	0.003
250	1	0.006	0.006	0.003	0.007	0.007	0.001
	3	0.016	0.016	0.008	0.019	0.019	0.003
	8	0.015	0.015	0.008	0.018	0.018	0.003

Table 7.5. Molar composition of the LPC.

The molar balance for each element (C, H, O) have been performed. In particular, the H balance is closed because of the assumption shown in Equation (7.25). On the contrary, both the C and O balances do not close, meaning that in this calculation few moles of both the elements are missed. Table 7.6 shows the moles of the two elements missed and the percentage errors. The last were calculated in relation to the moles of both C and O charged within the reactor through the feedstock.

T (°C)	τ (h)	Residual C		Residual O	
		(mol)	(%)	(mol)	(%)
180	1	0.006	2.0	0.010	7.6
	3	0.013	4.5	0.007	5.0
	8	0.015	5.3	0.017	13.3
220	1	0.004	1.3	0.021	16.0
	3	0.011	4.0	0.012	9.2
	8	0.005	2.0	0.029	22.1
250	1	0.038	13.7	0.011	8.2
	3	0.017	6.3	0.023	17.7
	8	0.031	11.2	0.018	14.0

Table 7.6. C and O balances.

The amount of carbon missed is satisfactorily low. This lost can be simply due to experimental errors. On the other hand, the oxygen balance closes with higher percentages of O missed. In this case, experimental errors can partially explain these higher errors, because the choice of representing the LPC with the two molecules 5-HMF and phenol could strongly affect the balance closure. As reported by some authors [4, 8], the liquid phase obtained during an HTC process is composed by a big number of chemical compounds, many of them being more oxygenated than the two chosen. Therefore, in the present case, the errors on the O balance can be related to the procedural choice done. Moreover, the O balance is affected also by the fact that the composition of the LPC has been calculated on the basis of the moles of carbon measured by the TOC. Hence, the underestimation of C propagates also on O, resulting in an underestimation of the moles of oxygen within the liquid phase.

7.3 Standard enthalpies of formation

Feedstock's standard enthalpy of formation

Using the data reported in Table 7.2 and considering a molecular mass of one pseudo-mole of feedstock of 100 g/mol, this mole will consist of

- C = 54.4 $g_C/mol_{molecule}$
- H = 6.6 $g_H/mol_{molecule}$
- O= 34.2 $g_O/mol_{molecule}$

and being the atomic and molecular masses:

- C = 12.011 g_C/mol_C
- H_2 = 2.01588 g_{H2}/mol_{H2}
- O_2 = 31.9988 g_{O2}/mol_{O2}

the stoichiometric coefficients of the feedstock are:

$\frac{x}{\alpha}$ = 54.4 $g_C/mol_{molecule}$ / 12.011 g_C/mol_C = 4.5292 $mol_C/mol_{molecule}$

$\frac{y}{\alpha}$ = 2 · 6.6 $g_H/mol_{molecule}$ / 2.01588 g_{H2}/mol_{H2} = 6.54801 $mol_H/mol_{molecule}$

$\frac{z}{\alpha}$ = 2 · 34.2 $g_O/mol_{molecule}$ / 31.9988 g_{O2}/mol_{O2} = 2.1376 $mol_O/mol_{molecule}$

The HHV_{dry} of the feedstock has been measured 23.584 kJ/g, according to UNI EN 14918, 2010.

Thus:

$Q(C_xH_yO_z)$ = HHVdry * 100 g/mol = 2358.3 kJ/mol

If, according to Reid et al. [1] $\Delta H_{f,298}°(H_2O_{(l)})$ = -241.81 kJ/mol, when considering the standard enthalpy of formation of the gases, which compose the gaseous phase, previously reported, it is possible to solve Equation (7.12):

$\Delta Hf,298°(C_xH_yO_z) = \frac{x}{\alpha} \cdot \Delta Hf,298°(CO_2) + \frac{y}{2\alpha} \cdot \Delta Hf,298°(H_2O\ (l)) - Q(C_xH_yO_z) =$

= 4.5292 $mol_C/mol_{molecule}$ · (-393.51 kJ/mol) + 3.274 $mol_H/mol_{molecule}$ · (-241.81 kJ/mol) - (-2358.4 kJ/mol) =

= -215.57 kJ/mol

Hence:

$\Delta H_{f,298}°(C_xH_yO_z)$ = -215.57 kJ/mol.

Hydrochar's standard enthalpy of formation

The hydrochar's standard enthalpy of formation has been calculated with the same procedure used to evaluate the feedstock's standard enthalpy of

formation and using data reported in Tables 7.2 and 7.3. Hydrochar's stoichiometric coefficients are those reported in Equation (7.4). Hydrochar's heating values were measured according to (UNI EN 14918, 2010). Table 7.7 reports the HHV, the stoichiometric coefficients and the standard enthalpies of formation of the hydrochar, evaluated at the different process conditions.

T (°C)	τ (h)	HHV (kJ/mol)	l (mol)	m (mol)	n (mol)	$\Delta H_{f,298}°(C_lH_mO_n)$ (kJ/mol)
180	1	2645.9	5.02	6.57	1.74	-121.80
	3	2682.5	5.05	6.45	1.71	-82.60
	8	2802.8	5.19	6.75	1.58	-53.98
220	1	2794.4	5.28	6.65	1.50	-86.42
	3	2849.8	5.30	6.35	1.48	-1.59
	8	2830.7	5.69	6.65	1.14	-213.94
250	1	2616.3	5.54	6.35	1.28	-330.10
	3	2986.6	5.79	6.55	1.06	-82.08
	8	2987.8	5.89	6.45	0.98	-108.20

Table 7.7. Calorific values and standard enthalpies of formation of hydrochar.

Hence, the average standard enthalpy of formation of the hydrochar was calculated according to Equation (7.15). Finally, the average value of $\Delta H_{f,298}°(C_lH_mO_n)$ has been calculated:

$\Delta H_{f,298}°(C_lH_mO_n)$ = -120.08 kJ/mol.

Liquid pseudo-component's standard enthalpy of formation

As previously described, phenol and 5-hydroxymethylfurfural (or 5-HMF) were chosen as representatives of the liquid compounds formed during HTC, which remain dissolved in water at the end of the process. Under this

assumption, the procedure for the evaluation of the standard enthalpy of formation of the LPC (i.e., Equations (7.17), (7.18), (7.19) and (7.23)) is considerably simplified. As a matter of fact, data on the standard enthalpy of formation of phenol are available in literature Poling et al. [1]. On the contrary, at our knowledge this datum related to the 5-HMF compound is not available in literature. Thus, the Benson group contribution method Poling et al. [1], was used for the determination of $\Delta H_{f,298}°(5-HMF)$. Thus,

$\Delta H_{f,298}°(C_6H_6O)$ = -96.4 kJ/mol

and

$\Delta H_{f,298}°(C_6H_6O_3)$ = -277.2 kJ/mol.

Finally, considering the distribution of the two chemical species within the liquid (54% phenol and 46% 5-HMF), the average standard enthalpy of formation of the LPC can be assessed:

$\Delta H_{f,298}°(C_aH_bO_c)$ = -179.6 kJ/mol.

7.4 Enthalpy of the HTC reaction

In this paragraph, the calculation of the enthalpy of reaction at the HTC operational conditions (T and τ) have been developed rigorously. This calculation is based on Equation (7.1), written in a different and compact form (Equation (7.26)).

$$\Delta H_{r,(T,P)} = \left[\sum\left(\Delta H_{f,(T,P),pi} \cdot q_{pi}\right) - \Delta H_{f,(T,P),fs} \cdot q_{fs}\right] / q_{fs} \qquad (7.26)$$

in which:
$\Delta H_{r,(T,P)}$, is the enthalpy of reaction at the actual HTC conditions of T and P [MJ/kg];
$\Delta H_{f,(T,P),pi}$, is the enthalpy of formation of the *i*-th product at T and P;
q_{pi}, is the amount of the *i*-th product formed during HTC (expressed in kg for both hydrochar and LPC, and in mol for both water and the gaseous products);
$\Delta H_{f,(T,P),fs}$, is the enthalpy of formation of the feedstock at T and P;
q_{fs}, is the amount of feedstock introduced within the reactor at the beginning of the process (expressed in kg).

To perform the calculation of Equation (7.26), the standard enthalpies of formation of both the products and the feedstock have been evaluated, as reported in the previous paragraph. Then, the enthalpies of formation at the actual process conditions have been calculated as

$$\Delta H_{f,(T,P)} = \Delta H_{f,298}{}^{\circ} + dH \qquad (7.27)$$

being $dH = \int_{298}^{T} C_p dT + \int_{1}^{P} V dP$, in which C_p is the heat capacity and V the molar volume.

Calculation of $\Delta H_{f,298}^{\circ}$

The enthalpies of formation of both the feedstock and the hydrochars, were calculated as:

$$\Delta H_f = mol_C \cdot \Delta H_f^0(CO_2) + \frac{1}{2} mol_H \cdot \Delta H_f^0(H_2O) + HHV \qquad (7.28)$$

where:
$\Delta H_f^0(CO_2)$ = -393.51 kJ/mol [1];
$\Delta H_f^0(H_2O)$ = -241.81 kJ/mol [1];
HHV, is the higher heating value of the feedstock or of the hydrochar, measured.

Equation (7.28) was even used for the calculation of the ΔH_f of the liquid pseudo-component, taking into account that it is composed of 46% by 5-HMF and 0.54% by phenol. The higher heating values of both 5-HMF and phenol were estimated through the formula proposed by Channiwala and Parikh [2].
The enthalpies of formation of carbon monoxide, methane and hydrogen used, were those proposed by Poling et al. [1]. In particular:

$\Delta H_f^0(CO)$ = -110.53 kJ/mol;
$\Delta H_f^0(CH_4)$ = -74.52 kJ/mol;
$\Delta H_f^0(H_0)$ = 0.00 kJ/mol;

Table 7.8 reports the results of the calculations of the enthalpies of HTC reaction as the carbonizations were performed at 25 °C and 1 bar.

Temperature	Res. time	ΔH
(°C)	(h)	(MJ/kg)
180 °C	1	-4.8
	3	-2.7
	8	-1.5
220 °C	1	-5.1
	3	-2.1
	8	-14.7
250 °C	1	-19.3
	3	-9.8
	8	-11.7

Table 7.8. Enthalpies of HTC reaction at 25 °C and 1 bar.

The average enthalpy of HTC reaction at 25 °C and 1 bar is -8.0 MJ/kg.

7.5 Solution of the temperature dependent integral

To solve the first integral for both the feedstock and all the products, different procedures have been followed.

Solution for the feedstock

Dupont et al. [9] measured the heat capacities of several wood samples, within the temperature range of 313 - 353 K and proposed a simple equation to evaluate the average biomass heat capacity. In addition, Simpson and TenWolde [10] proposed another correlation to evaluate the heat capacity of

wood, below fibre saturation and at temperatures between 280 and 420 K. Thus, to determine the variations of the heat capacity of the feedstock with temperature, for the actual HTC temperatures (i.e., up to 523 K), the literature data have been interpolated first linearly and then with a second order polynomial.

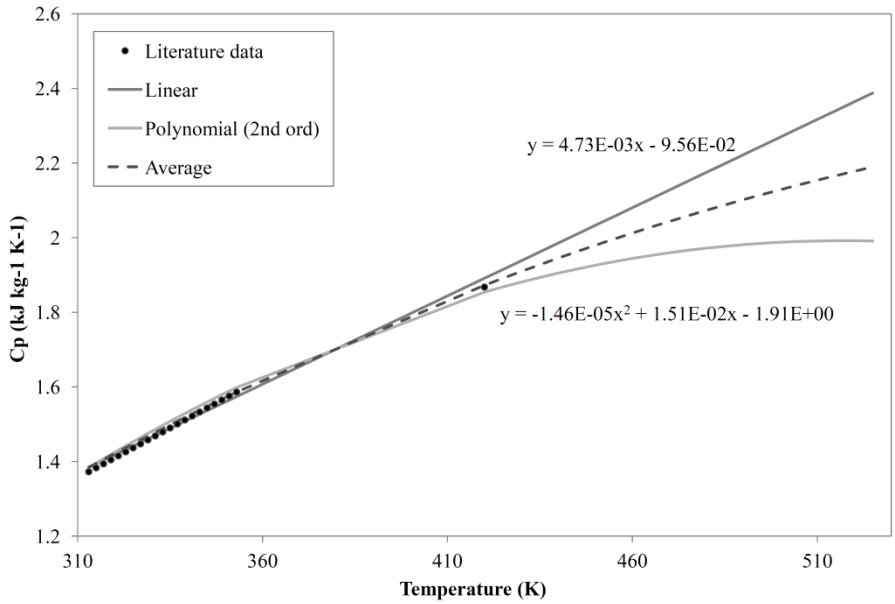

Figure 7.1. Determination of the heat capacity of the feedstock.

Finally, the heat capacity variations with temperature for the feedstock have been obtain as average values between those estimated through both the interpolations (Equation (7.29)).

$$C_{P,feedstock}(T) = -7.30E-06 \cdot T^2 + 9.92E-03 \cdot T - 1.00 \qquad (7.29)$$

Table 7.9 reports the results obtained following the procedure previously described.

Feedstock	
T	**Cp*ΔT**
(°C)	(kJ/kg)
180	259.95
220	342.03
250	406.49

Table 7.9. Heat capacities of the feedstock at different temperatures.

Solution for both the water and the gaseous phase

For both the water and the gaseous products, the integral has been solved using the empirical equation Smith et al. [11]:

$$\int_{T_0}^{T} \frac{C_p}{R} dT = A \cdot T_0 \cdot (t-1) + \frac{B}{2} \cdot T_0^2 \cdot (t^2-1) + \frac{C}{3} \cdot T_0^3 \cdot (t^3-1) + \frac{D}{T_0} \cdot \left(\frac{t-1}{t}\right) \quad (7.30)$$

where $t = \frac{T}{T_0}$.

To solve the right hand side of Equation (7.30), Smith et al. [11] proposed a function called ICPH(T0,T;A,B,C,D,) and gave the numerical values of the A, B, C and D parameters. Table 7.10 reports the values of the four parameters and the results of the integration.

	A	B	C	D	R x ICPH
		(x 10^{3})	(x 10^{6})	(x 10^{-5})	(kJ/mol)
Water	3.470	1.450	0.000	0.121	7.75x 10^{-3}
CO2	5.457	1.045	0.000	-1.157	9.62 x 10^{-3}
CO	3.376	0.557	0.000	-0.031	6.71 x 10^{-3}
CH4	1.702	9.081	-2.164	0.000	9.46 x 10^{-3}
H2	3.249	0.422	0.000	0.083	6.50 x 10^{-3}

Table 7.10. Heat capacities of both the water and the gaseous phase.

Solution for 5-HMF

To assess the heat capacity variations with temperature of 5-HMF, a regression equation has been recovered from data proposed by King [12], obtained using the Benson group contribution method [1]. The Benson group contribution method can be expressed through Equations (7.31) and (7.32).

$$\Delta H_f°(298.15\ K) = \sum_k N_k\left(\Delta H_{fk}°\right) \tag{7.31}$$

$$C_P°(T) = \sum_k N_k C_{pk}°(T) \tag{7.32}$$

where:
$\Delta H_f°$, is the enthalpy of formation at 298 K [kJ/mol];
$C_P°(T)$, is the heat capacity at temperature T [J/mol K];
N_k, is the incident number for group *k*;
$H_{fk}°$, is the group contribution for enthalpy formation [kJ/mol];
$C_{pk}°(T)$, is the group contribution for heat capacity at temperature T [J/molK].

Through Equations (7.31) and (7.32), King [12] calculated $C°_P$ data for 5-HMF at several temperatures (298 K, 400 K, 500 K, 600 K, 800 K and 1000 K). Thus, a second order polynomial equation has been recovered, allowing the integration of $C°_P$ from 298 K to the actual HTC temperatures. Figure 7.2 reports the interpolated data and shows the polynomial equation integrated to evaluate the heat capacity of 5-HMF. The equation is reported in the figure.

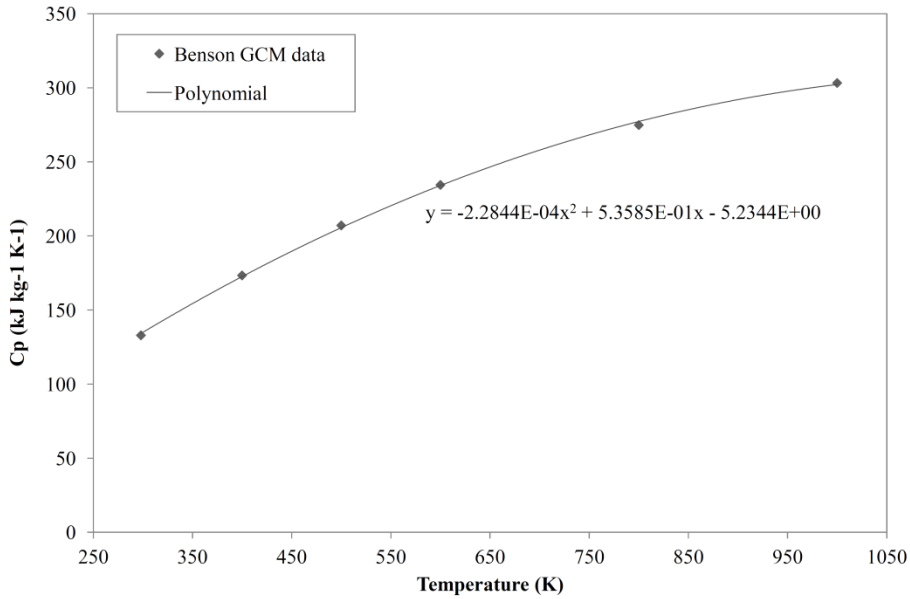

Figure 7.2. Determination of the heat capacity of 5-HMF.

Table 7.11 reports the results obtained for 5-HMF.

5-HMF	
T	**Cp*ΔT**
(°C)	(kJ/kg)
180	200.79
220	263.31
250	312.80

Table 7.11. Heat capacities of 5-HMF at different temperatures.

Solution for phenol

For the calculation of the heat capacity of phenol, the Joback $C°_P$ function from group contributions has been considered Poling et al. [1]. The property formula is reported below.

$$C_P°(T) = S_0 + S_1 \cdot T + S_2 \cdot T^2 + S_3 \cdot T^3 \quad (7.33)$$

in which:

$S_0 = [\sum_k N_k(CpAk) - 37.93]$
$S_1 = [\sum_k N_k(CpBk) + 0.21]$
$S_2 = [\sum_k N_k(CpCk) - 3.91E - 04]$
$S_3 = [\sum_k N_k(CpDk) + 2.06E - 07]$

and the coefficients $CpAk$, $CpBk$, $CpCk$ and $CpDk$ are reported in [1]. Thus, for the solution of the temperature dependence integral to be used in Equation (7.27) for what concerns phenol, Equation (7.33) has been integrated from 25 °C to the HTC temperature. Table 7.12 reports the results obtained for phenol.

Phenol	
T	**Cp*ΔT**
(°C)	(kJ/kg)
180	201.53
220	263.73
250	312.31

Table 7.12. Heat capacities of phenol at different temperatures.

Finally, the temperature dependence integral of the LPC has been calculated as a weighted sum of the contributions of both 5-HMF and phenol, according to the assumption made in Paragraph 7.2 (LPC composed by 54% phenol and 46% 5-HMF).

Solution for hydrochar

The heat capacity of the hydrochar has been evaluated through the correlation proposed by Lee [13]. The author experimentally measured the heat capacities of coal at temperatures from 588.7 K to 1088.7 K and pressures from 0 barg to 103.42 barg. Thus, based on the data obtained from his work and that available in the literature and assuming the heat capacity to

be a function of the volatile matter content of the coal, he proposed the following generalized correlation (7.34).

$$C_{P,m} = 0.17 + 1.1 \cdot 10^{-4} \cdot T + (3.2 \cdot 10^{-3} + 3.05 \cdot 10^{-6} \cdot T) \cdot VM \quad (7.34)$$

where

$C_{P,m}$,, is the mean heat capacity, expressed in Btu/lb/°F;

T, is the temperature, expressed in °F;

VM, is the volatile matter, expressed in weight percent (dry basis).

Table 7.12 reports the results obtained for phenol.

Hydrochar		
T	**Cp*ΔT**	**Cp*ΔT**
(°C)	(Btu/lb)	(kJ/kg)
180	201.53	127.03
220	263.73	163.09
250	312.31	191.02

Table 7.13. Heat capacities of hydrochar at different temperatures.

7.6 Main results

Figure 7.3 shows the behaviour of HTC reaction enthalpies at different process conditions.

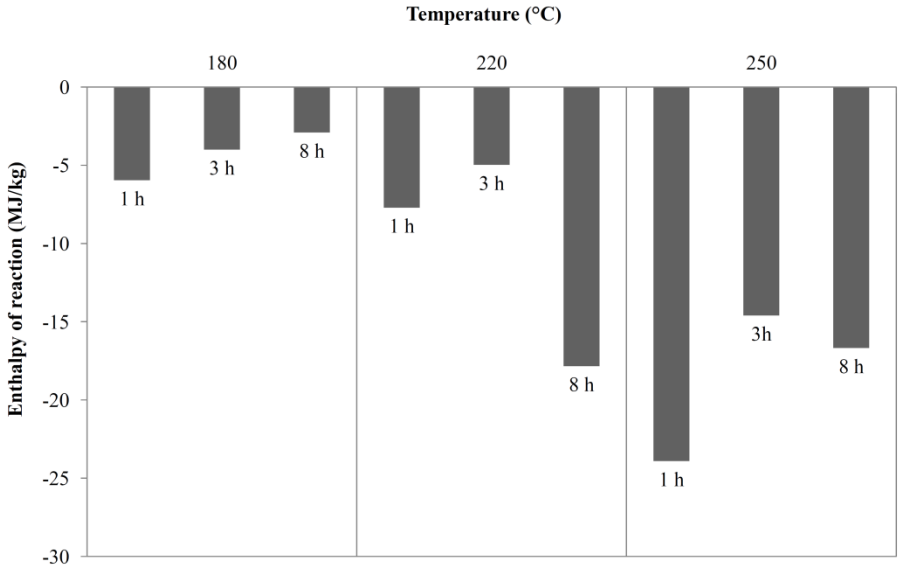

Figure 7.3. Enthalpy of HTC reaction at different process conditions.

The results obtained are similar with those proposed by Funke and Ziegler [14] and Ramke et al. [15]. In particular Funke and Ziegler measured values of HTC heat of reaction ranging between -0.76 and -1.08 MJ/kg_{daf}. Ramke et al. [15] reported values ranging between -4.3 and -5.7 MJ/kg_{daf}, for different types of biomass. Interestingly, all the authors correlated the heat of reaction with both temperature and residence time as process conditions. These lower values have been obtained carbonizing with biomass to water ratios of 0.2. The results shown in Figure 7.3 were obtained at biomass to water ratios of 0.3. In this case, the results obtained seem to support the thesis that higher

biomass to water ratios slightly increase the hydrothermal carbonization process. This is consistent with what found by [16, 17, 18].

7.7 Conclusions of Chapter 7

In this chapter a rigorous energy balance has been presented. The HTC reaction enthalpy at different process conditions has been evaluated and the two integrals of temperature and pressure have been solved with some assumptions and preliminary simplifications.

Data on grape seeds have been used to estimate the HTC reaction enthalpy and several hypothesis have been done. The results obtained seem to be in agreement both with the expectations and the literature. Further investigation and improvements can be done, to better understand the thermal nature of the process.

References of Chapter 7

[1] Poling B.E., Prausnitz J.M., O'Connell J.P. 2001. The Properties of Gases and Liquids, 5th Ed., McGraw-Hill.

[2] Channiwala, S.A., Parikh, P.P., 2002. A unified correlation for estimating HHV of solid , liquid and gaseous fuels q 81.

[3] Moldes D., Gallego P.P., Rodríguez Couto S., Sanromán A., 2003. Grape seeds: the best lignocellulosic waste to produce laccase by solid state cultures of Trametes hirsute. Biotechnology Letters, vol. 25, p. 491-495.

[4] Libra J.A., Ro K.S., Kammann C., Funke A., Berge N.D., Neubauer Y., Titirici M.-M., Fühner C., Bens O., Kern J., Emmerich K.-H., 2011. Hydrothermal carbonization of biomass residuals: a comparative review oft he chemistry, processes and applications of wet and dry pyrolysis. Biofuels, vol. 2(1), p. 89-124.

[5] Funke A., Ziegler F., 2010. Hydrothermal carbonization of biomass: A summary and discussion of chemical mechanisms for process engineering. Biofuels, Bioproducts and Biorefining, vol. 4, p. 160-177.

[6] Xiao L., Shi Z., Xu F., Sun R., 2012. Hydrothermal carbonization of lignocellulosic biomass. Bioresource Technology, vol. 118, p. 619-623.

[7] Titirici M.-M., Antonietti A., Baccile N., 2008. Hydrothermal carbon from biomass: a comparison of the local structure from poly-tomonosaccharides and pentoses. Green Chemistry, vol. 10, p. 1204-1212.

[8] Stemann J., Putschew A., Ziegler F., 2013. Hydrothermal carbonization: Process water characterization and effects of water recirculation. Bioresource Technology, vol. 143, p. 139-146.

[9] Dupont C., Chiriac R., Gauthier G., Toche F., 2014. Heat capacity measurements of various biomass types and pyrolysis residues. Fuel vol. 115, p. 644–651.

[10] Simpson W., TenWolde A., 1999. Physical properties and moisture relations of wood, in: Wood Handbook: Wood as an Engineering Material, p. 3.1–3.24.

[11] Smith J.M., Van Ness H.C., Abbott M.M., 2001. Introduction to chemical engineering thermodynamics. McGraw Hill, Sixth Edition.

[12] King Z.D., 2014. Aspen simulation of furfural and hydroxymethylfurfural production from biomass. M.Sc. Thesis, Missouri University of Science and Technology.

[13] Lee A.L., 1968. Heat capacity of coal. American Chemical Society, Div. Fuel Chem. 12(3). Conference paper: 156th national meeting on standards in nuclear chemistry and technology, Atlantic City, NJ, USA, 8 Sep 1968; Other Information: See CONF-680918--P1.

[14] Funke A., Ziegler F., 2011. Heat of reaction measurements for hydrothermal carbonization of biomass. Bioresource Technology, vol. 102, p. 7595-7598.

[15] Ramke H.-G., Blöhse D., Lehmann H.-J., Fettig J., 2010. Hydrothermale Carbonisierung organischer Siedlungsabfälle. Bio- und Sekundärrohstoffverwertung, V - 22. Kasseler Abfall- und Bioenergieforum, Kassel, p. 141–157.

[16] Sabio E., Álvarez-Murillo A., Román S., Ledesma B., 2016. Conversion of tomato-peel waste into solid fuel by hydrothermal carbonization: Influence of the processing variables. Waste Management, vol. 47, p. 122–132.

[17] Álvarez-Murillo A., Román S., Ledesma B., Sabio E., 2015. Study of variables in energy densification of olive stone by hydrothermal carbonization. Journal of Analytical and Applied Pyrolysis, vol. 113, p. 307–314.

[18] Sermyagina E., Saari J., Kaikko J., Vakkilainen E., 2015. Hydrothermal carbonization of coniferous biomass: Effect of process parameters on mass and energy yields. Journal of Analytical and Applied Pyrolysis, vol. 113, p. 551–556.

Chapter 8

Other thermodynamic considerations

Paragraphs 8.1, 8.2 and 8.3 were developed in collaboration with prof. Marco Baratieri and Ph.D. Francesco Patuzzi from the Free University of Bolzano (IT).

8.1 Reaction kinetics modelling

Few experiences can be found in the literature about the assessment of biomass hydrothermal carbonization kinetics. Braghiroli et al. [1] studied the kinetics of hydrothermal carbonization of aqueous solutions of condensed tannins, considering long reaction times (from 1 to 720 h) and relatively low HTC temperatures (130, 160, 180 and 200°C). The applied kinetic scheme involved a first-order reaction with an activation energy of 91 kJ/mol. Reza et al. [2], studying the hydrothermal carbonization of loblolly pine, investigated higher HTC temperature (200, 230, and 260°C) and lower reaction times (15s to 30 min) and applied a reaction mechanism involving the degradation of hemicellulose and cellulose in parallel first-order reactions. Activation energy of hemicellulose and cellulose degradation were determined to be 30 and 73 kJ/mol, respectively. 5 s to 30 min reaction times.

Danso-Boateng et al. [3] described the kinetics of faecal biomass hydrothermal carbonization by means of a first-order reaction. The investigated HTC temperature and reaction times were in the range 140 to 200 °C and 30 min to 4 h, respectively. The calculated activation energies

were 70 and 78 kJ/mol for primary sewage sludge and synthetic faeces, respectively.
Luo et al. [4] described the hydrothermal decomposition of water hyacinth with a similar reaction mechanism, nonetheless considering two temperature range. The calculated activation energies were 145 and 90 kJ/mol for the ranges of 150-210 °C (range I) and 200-280°C (range II).
In this chapter, a two-step kinetic mechanism is presented.

Experimental data

Data concerning grape marc have been used. In particular, grape marc has been carbonized at three different temperatures and three residence times. All the data used to calibrate the model are reported both in Chapter 4 and in Appendix I.

The two-step kinetic mechanism

The experimental results have been applied for the calibration of a two-step reaction scheme, based on the mechanism proposed by Di Blasi and Lanzetta investigating the thermal degradation of xylan [5] and applied by Prins for the kinetics of willow wood during torrefaction treatment [6]. The proposed two-step mechanism assumes that the original biomass (compound *A*) forms an intermediate product (compound *B*), whose degradation gives the final product (compound *C*) as char. The formation of volatiles (V_1 and V_2) products is assumed to take place through reactions in parallel to those giving the compounds *B* and *C* respectively (Figure 8.1).

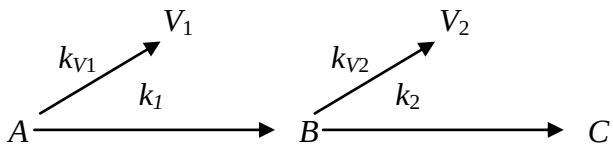

Figure 8.1. Two-step kinetic mechanism.

All the involved reactions are assumed to be of first order and the kinetic parameters are described by the usual Arrhenius equation (Equation 8.1).

$$k_i = k_{0,i} \cdot exp\left(-\frac{E_{a,i}}{RT}\right) \tag{8.1}$$

where:
$i = 1, 2, V_1, V_2$;
$k_{0,i}$, is the pre-exponential factor;
$E_{a,i}$, is the activation energy;
R ,is the universal gas constant;
T , is temperature in Kelvin.

The global kinetic reactions scheme is then described by the following equations (8.2 and 8.3).

$$\begin{cases} \frac{\partial M_A}{\partial t} = -K_1 \cdot M_A \\ \frac{\partial M_B}{\partial t} = k_1 \cdot M_A - K_2 \cdot M_B \\ \frac{\partial M_C}{\partial t} = k_2 \cdot M_B \end{cases} \quad \text{(solid phase)} \tag{8.2}$$

$$\begin{cases} \frac{\vartheta M_{V1}}{\vartheta t} = k_{V1} \cdot M_A \\ \frac{\vartheta M_{V2}}{\vartheta t} = k_{V2} \cdot M_B \end{cases} \quad \text{(liquid phase)} \tag{8.3}$$

where M_i $(i = A, B, C, V_1, V_2)$ represents the mass of each phase for the adopted scheme, while K_1 and K_2 are defined by the following relations:

$$K_1 = k_1 + k_{V1} \tag{8.4}$$

$$K_2 = k_2 + k_{V2} \tag{8.5}$$

The set of equations (8.2 and 8.3) can be integrated imposing the following initial conditions for *t*=0:

$$\begin{cases} M_A = M_0 \\ M_B = M_C = M_{V1} = M_{V2} = M_0 \end{cases} \tag{8.6}$$

where M_0 is the initial sample mass.

The calibration procedure has been carried out by means of a MatLab script. In this script, a function (receiving the applied temperature profile and the kinetic parameters as inputs) calculates for every experimental value (measured at a particular HTC temperature and after a certain time) the correspondent value predicted by the model.
The differential system (8.2 and 8.3) presents a stiff nature because of the different reaction rate of the two steps. Thus, a suitable solver was selected: the optimal set of kinetic parameters is determined by a nonlinear data-fitting, minimizing the square deviations between experimental and

predicted values. The used method (trust-region-reflective algorithm) requires that the number of equations is at least as great as the number of variables. In this case the requirement is satisfied. In fact the number of (independent) equations corresponds to the number of experimental measurements (three set of 9 solid yields), while the variables are 8, defined by the pre-exponential factor $k_{0,i}$ and the activation energy $E_{a,i}$ for each of the 4 kinetic equations. As initial values of the parameter to be calibrated, the values proposed by Prins [6] were used.

Results of the kinetic model calibration are reported in Figure 8.2. The values of the model parameters that give the best fit of the experimental data are: $3.34 \cdot 10^{7}$, $1.10 \cdot 10^{10}$, $9.15 \cdot 10^{6}$ and $1.55 \cdot 10^{10}$ s^{-1} for $k_{0,1}$, $k_{0,2}$, $k_{0,V1}$ and $k_{0,2}$ respectively, and 94.5, 139.7, 93.7 and 146.2 kJ/mol for $E_{a,1}$, $E_{a,2}$, $E_{a,V1}$ and $E_{a,V2}$ respectively. As it can be observed, the model fits with satisfying accuracy the experimental data. The first reaction step results significantly faster than the second, since the activation energies of the kinetic terms in the former are smaller than those in the latter. Consequently, for low temperature ranges the conversion yield of the compound *C* is very small and roughly negligible (i.e., the two-step scheme can be reduced to a single step reaction). This can be clearly shown in Figure 8.3, where the evolution in time at of the elements considered in the reaction scheme is reported for different HTC temperature. A further evidence of the difference between the two reaction steps can be seen in Figure 8.4, on which the global kinetic parameter of the first (K1) and the second (K2) step have been estimated applying Equations (8.4) and (8.5). The resulting apparent pre-exponential factor and activation energy are $4.24 \cdot 10^{7}$ s^{-1} and 94.3 kJ/mol, respectively, for the first step and $2.02 \cdot 10^{10}$ s^{-1} and 141.2 kJ/mol, respectively, for the second step.

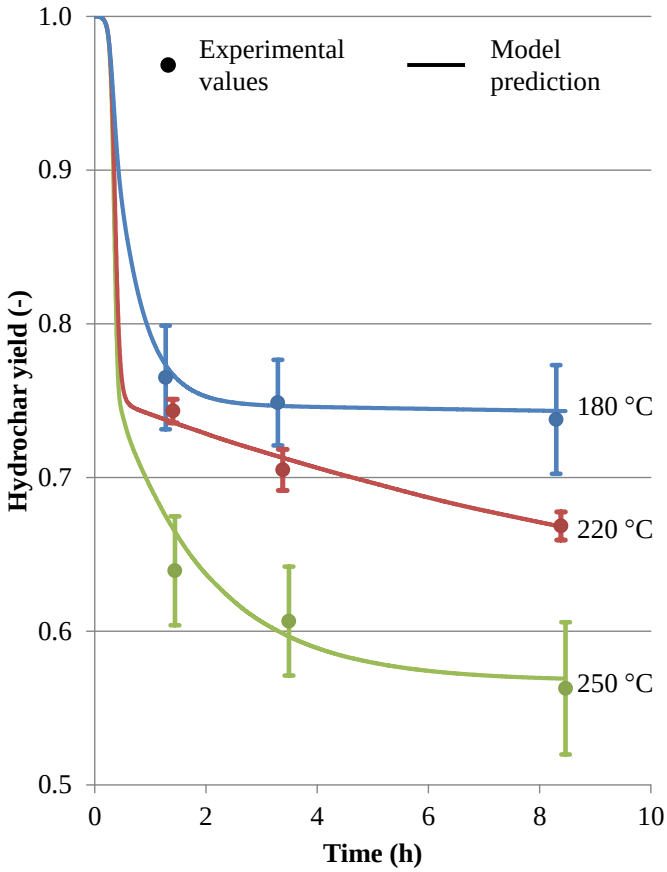

Figure 8.2. Comparison between the experimental hydrochar yields and the predictions of the calibrated two-step reaction model.

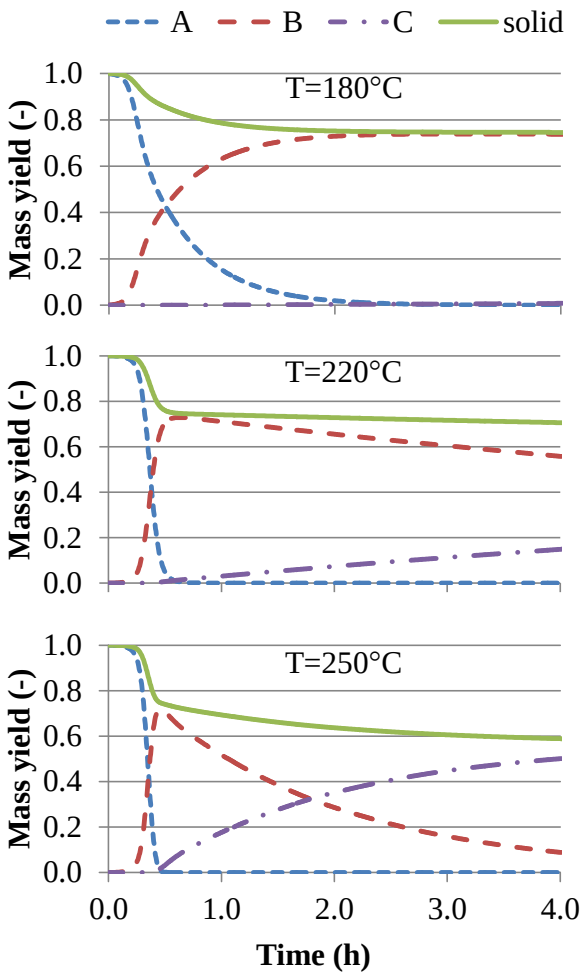

Figure 8.3. Evolution in time at different HTC temperature of the elements considered in the reaction scheme.

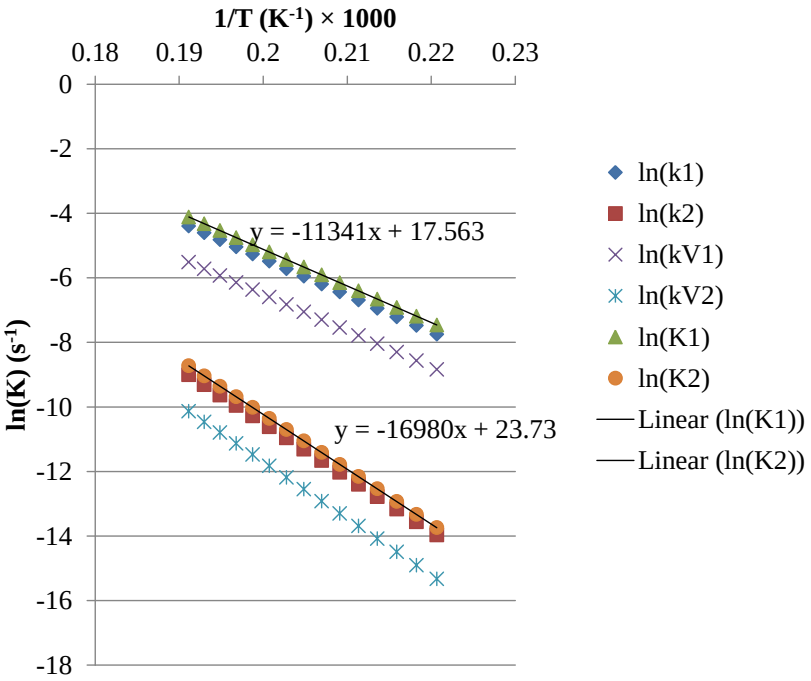

Figure 8.4. Arrhenius plot of the kinetic parameters of the considered reaction scheme.

The kinetic analysis showed that a two-step reaction mechanism can be suitably used to describe the evolution in time of the hydrochar yield at different process temperature.

8.2 Thermo-fluid model of a batch hydrothermal carbonization reactor

The 50 mL bench scale batch reactor described in Chapter 2, was modelled through a multi-physics commercial software and both mass, momentum and heat equations have been integrated within the domain. The temperature profiles in the external wall and inside the reactor together with pressure have been recorded to calibrate the model.

Figure 8.5 shows the temperature measurement points.

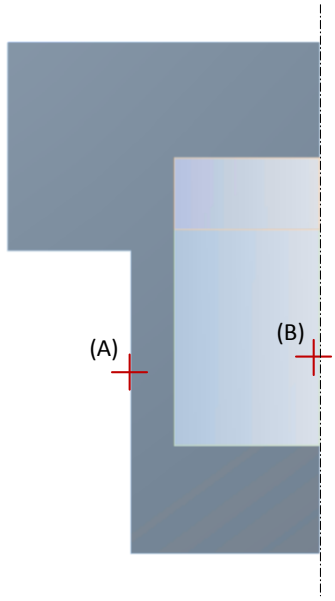

Figure 8.5. External (A) and internal (B) temperature sampling points.

Using a commercial multi-physics software, the HTC reactor has been modelled considering its axial symmetry. In the first stage of the modelling, a mono-phase and mono-component equivalent fluid has been considered. As boundary conditions, convection heat exchange with air along three surfaces have been imposed; on the bottom edge of the reactor conduction through 3 cm of stone, then convection heat exchange with air have been imposed. On

the boundary covered by the band heater, time-dependent temperature profile has been imposed. Figure 8.6 shows the reactor scheme and the boundary conditions.

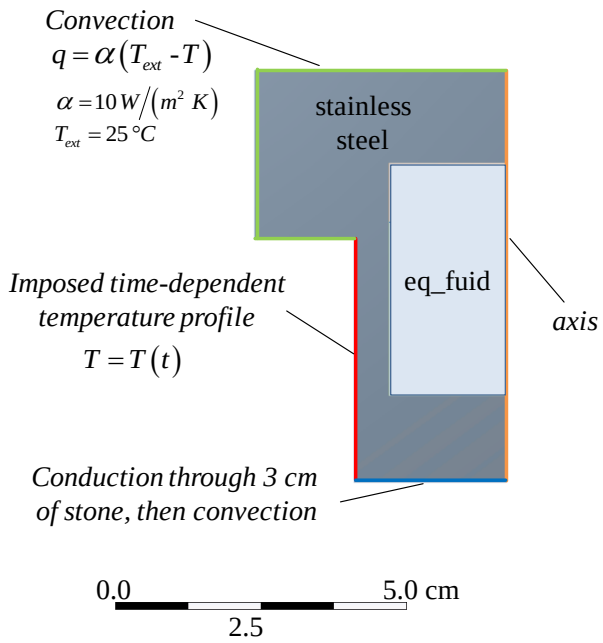

Figure 8.6. Reactor scheme and boundary conditions.

The simple geometry of the reactor allowed to obtain a good quality mesh (Minimum Orthogonal Quality = 0.9998, Maximum Aspect Ratio = 1.4286). Table 8.1 summarizes the mesh statistics.

Mesh statistics
37424 quadrilateral cells
73992 interior faces
948 wall faces
284 axis faces
Face area: 247.49 – 252.16 mm^2

Table 8.1. Mesh statistics summary.

The model has been calibrated using the temperature profiles on the two sampling points (A) and (B). Figure 8.7 shows the temperature profiles used.

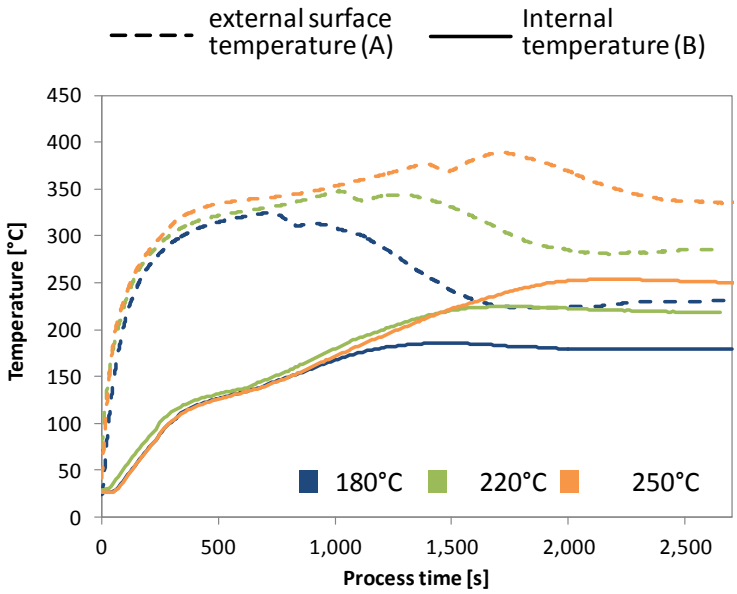

Figure 8.7. Temperature profiles on the external wall (dashed lines) and within the reactor (solid lines).

Under the assumption of having an equivalent fluid filling the reactor domain, the temperature profile within the reactor have been tried to be calculated. The temperatures registered at the sampling point (A) have been used as input data, while the outputs of the model have been compared to the temperature profiles at the sampling point (B). Results obtained using the input data referred to 180°C set point temperature, are shown in Figure 8.8.

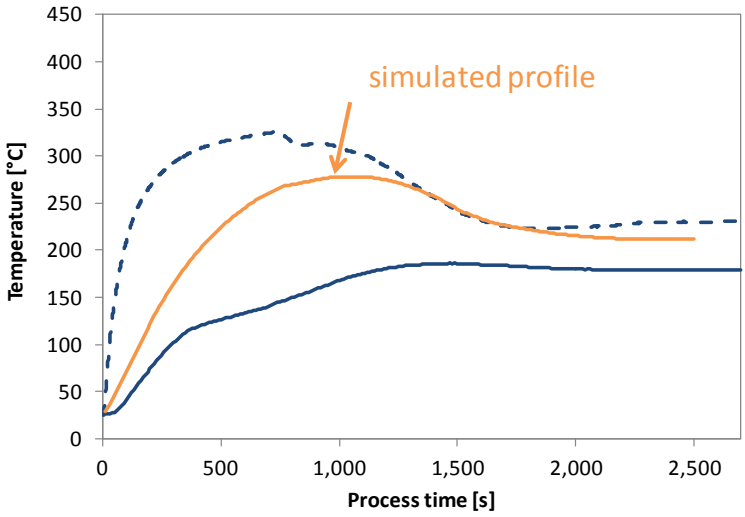

Figure 8.8. Modeling preliminary results.

In the figure reported above, the dashed line represent the temperature of the band heater, which heats up the reactor. The blue solid line shows the trend followed by the temperatures in the sampling point (B), while the orange solid line shows the output temperatures of the model.

The temperature profile calculated by the model is not in agreement with the real temperatures measured in (B). It is deemed that this not satisfactory prevision is mainly affected by the model strong assumption of working with a mono-phase equivalent fluid. As a matter of fact, the model predicts higher temperatures than the actual ones: thermo-physical properties (i.e., thermal diffusivity, thermal capacity) of the actual fluid significantly differ from the assumed ones. Furthermore, the model does not take into account the latent heat of vaporization of the mixture.

For these reason, to obtain better insights on the HTC process occurring within the experimental apparatus, some improvements are foreseen:

- the removal of the mono-component assumption, thus realizing a bi-phase model, able to predict the change of state;

- the removal of the mono-component assumption, considering a mix composed by a model substrate (i.e., the biomass) and water, even though remaining under liquid-vapor conditions (bi-phase model);
- the coupling of these two improvements, thus obtaining a tri-phase and multi-component model.

8.3 An improved thermal model

Part of this paragraph is reported in [7].

A simplified dynamic analytic model was built, based on lumped capacitance method, in order to simulate the thermal behaviour of the system, using the actual temperature profile imposed by the reactor external heater. A resistance-capacitance network was used to describe the system, taking into account the thermo-physical properties of the systems (i.,e., reactor shell, gaseous and liquid phase). This simplified tool supplemented with the calibrated kinetic model represents a first step in the characterization of the HTC process performance under different operative conditions.

This analytical model is based on lumped capacitance method, which reduces the thermal system to a number of discrete components, assuming that the temperature difference inside each object is negligible. In the present case it is considered just one component, i.e. the HTC reactor, with its overall heat capacity and thermal resistance, subjected to the external heat flux by the electrical heater. The basic assumption is of constant temperature inside the reactor (T). Besides the external heating system, the HTC reactor exchanges heat with the surroundings both through the upper (T_U) and the lower (T_D) surface.

A resistance-capacitance network has been used to describe the system, taking into account the thermo-physical properties of the liquid-gaseous water mixture, of the reactor shell and considering the thermal losses to the surroundings (Figure 8.9).

The energy balance reported in Equation (8.7), equals the variation of the internal energy of the system in time with the sum of the energy input of the external heater (i.e., term dependent on T_H) and the thermal losses (Q).

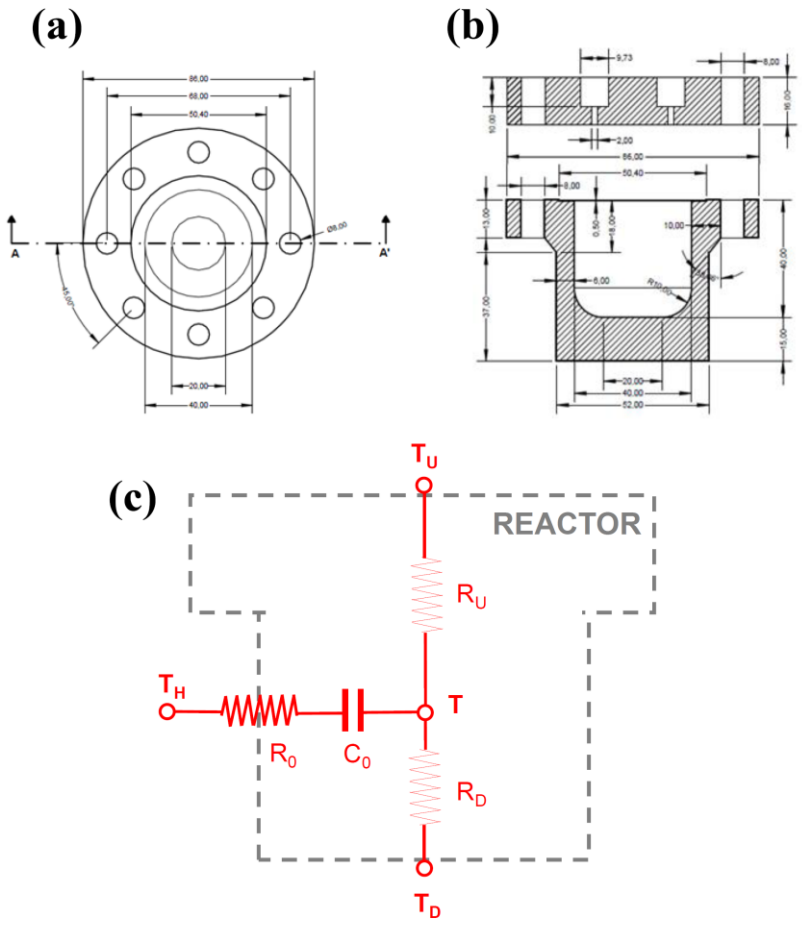

Figure 8.9. HTC reactor: a) top view; b) section; c) network of thermal resistances and capacities used to describe the lumped capacitance model of the HTC reactor.

$$C_0 \frac{dT}{d\tau} = \frac{T_H - T}{R_0} - Q \qquad (8.7)$$

This ordinary differential equation of the first order with constant coefficients - whose main variable is the internal temperature of the reactor *T* - can be solved by firstly substituting the variable.

$$T' = T_H - T \tag{8.8}$$

thus obtaining

$$\frac{dT'}{d\tau} = \frac{1}{\tau_0}(T' - QR_0) \tag{8.9}$$

where

$$\tau_0 = R_0 C_0 \tag{8.10}$$

is usually defined as the "time constant" of the system. The solution of Equation (8.7) is then reported in Equation (8.11).

$$T = (T_H - QR_0) + (T_0 - T_H + QR_0) \cdot exp\left(-\frac{\tau}{\tau_0}\right) \tag{8.11}$$

The overall thermal capacity (C_0) of the system is defined as the sum of the heat capacities of the water, i.e., considered as pure specie (C_W), of the stainless steel shell of the reactor (C_{ST}). Another heat storage term (C_{ST}, i.e., heat loss) is also foreseen, being the reactor positioned on a marble support.

$$C_0 = C_W + C_{ST} + \eta C_M \tag{8.12}$$

The different heat capacities have been computed by means of Equations (8.13), (8.14) and (8.15), where m_i and c_i are the mass and the specific heat of the *i-th* material and specie. In the calculation of the heat capacities for saturated liquid water, the specific heat at constant volume (i.e., $c_{V,LIQ.W}$) has been assumed to be equal to the one at constant pressure(i.e., $c_{P,LIQ.W}$) while the heat capacity of saturated steam has been neglected.

$$C_W = m_W c_{L,W} \quad \left(c_{P,LIQ.W} \approx c_{V,LIQ.W} \approx c_{L,W}\right) \tag{8.13}$$

$$C_{ST} = m_{ST} c_{ST} \tag{8.14}$$

$$C_M = m_M c_M \tag{8.15}$$

The additional heat storage term (i.e., marble support) is multiplied by a calibration factor, assessed through the experimental tests. The specific heat at constant pressure of water has been computed as a function of the temperature using Equation (8.16) [8]. Temperature values are expressed in Kelvin and c_p values in Joule per kmol per Kelvin. Only the liquid phase is considered.

$$C_{L,W} = 2.7637 \cdot 10^5 - 2.0901 \cdot 10^3 \cdot T + 8.1250 \cdot T^2 - 1.4416 \cdot 10^{-2} \cdot T^3 + 9.3701 \cdot 10^{-6} \cdot T^4 \tag{8.16}$$

The overall thermal resistance (R_0) of the system are defined as the sum of the thermal resistance of the reactor shell (i.e., stainless steel, R_{ST}) and the convective resistance of the water on the inner surface of the reactor (R_C).

$$R_0 = R_{ST} + R_C \tag{8.17}$$

$$R_{ST} = \frac{1}{2\pi L\lambda_{ST}} \cdot ln\left(\frac{r_{ext}}{r_{int}}\right) \tag{8.18}$$

$$R_C = \frac{1}{h_C(2\pi r_{int}L)} \tag{8.19}$$

The conductive resistance of the reactor shell (cylindrical layer) depends on the geometric parameters (see also Figure 8.9), as internal and external radius (r_{int}, r_{ext}) and height (L) subjected to the external heating. It also depends on the thermal conductivity of stainless steel (λ_{ST}). The convective resistance has been activated only for internal temperatures (i.e., water temperatures) greater than 110 °C. It depends on the internal surface area and on the conductive coefficient, indirectly assessed by means of the experimental tests.

The thermal losses are defined as the sum of the losses through the upper (Q_U) and the lower (Q_D) surfaces dependant on the relevant external temperature T_U and T_U

$$Q = Q_U + Q_D = \frac{T-T_U}{R_U} + \frac{T-T_D}{R_D} \tag{8.20}$$

where the conductive thermal resistances - Equations (8.21) and (8.22) - have been computed using geometric properties - as the reactor shell thickness (Δl_U, Δl_D, upper and lower, respectively), and the circular surface areas (upper and lower areas are considered equal) - and thermophysical (λ_{ST}) properties of the reactor shell.

$$R_U = \frac{\Delta l_U}{\lambda_{ST} \pi r_{int}^2} \tag{8.21}$$

$$R_D = \frac{\Delta l_D}{\lambda_{ST} \pi r_{int}^2} \tag{8.22}$$

To test the experimental condition, also the vapour pressure (P) has been computed through Equation (8.23) to be compared to the actual measured values. Equation (8.21) gives values in Pa and the constants can be found in [8]. The whole time domain has been discretized in unit domains of 10 seconds, where the solution Equation (8.9) has been computed keeping constant the input parameters within them.

$$P = exp\left(73.649 - \frac{7258.2}{T} - 7.3037 \cdot ln(T) + 4.1653 \cdot 10^{-6} \cdot T^2\right) \tag{8.23}$$

The temperatures and parameters introduced in the previous expressions are reported in Table 8.2.

To test the model, experimental tests were performed recording temperature data in different sections of the reactor. In particular, the temperature on the upper (T_U), lower (T_D) and side (T_H, i.e., the heating temperature) external surfaces of the reactor have been recorded during the experimental runs.

Thus, in order to simulate the thermal behaviour of the system, the actual temperature profile has been used to represent the input of the reactor external heater, while the temperature on the upper and lower surfaces have been used to compute the thermal losses through the shell.

Parameter	Value	U.o.M.	Description
m_w	0.026	kg	Mass of water
m_{ST}	0.842	kg	Mass of stainless steel (reactor)
m_M	1.245	kg	Mass of marble (support)
c_{ST}	500	$J\ kg^{-1}\ K^{-1}$	Specific heat of stainless steel (reactor)
c_M	880	$J\ kg^{-1}\ K^{-1}$	Specific heat of marble (support)
λ_{ST}	16.3	$W\ m^{-1}\ K^{-1}$	Thermal conductivity of stainless steel (AISI316)
h_C	1225	$W\ m^{-2}\ K^{-1}$	Thermal convection coefficient, water-reactor
r_{int}	0.020	m	Reactor internal radius
r_{ext}	0.026	m	Reactor external radius
L	0.04	m	Reactor height
η	0.1	-	Calibration parameter (heat loss to marble support)

Table 8.2. Thermal, physical and geometrical parameters of the thermal model.

Results of the thermal simulation - applied to a run having set point equal to 250 °C - are presented in Figure 8.10 where the actual measured temperature inside the reactor is compared with the modelled one.

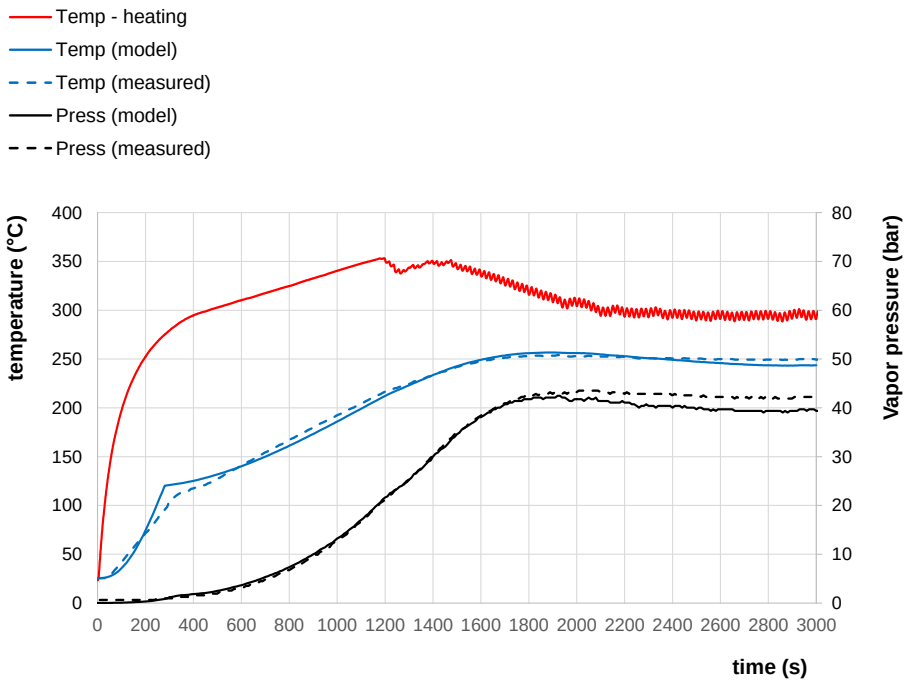

Figure 8.10. Thermal model: measured Vs model temperature inside the reactor (blue lines); actual heating temperature (red line); measured Vs model vapour pressure (black lines).

The actual heating temperature is also plotted in the figure, along with the curves of the vapour pressure, i.e., modelled and measured. The pressure values, confirm that the vapour is in saturated condition until the system reaches the setup temperature. After that, the generation of gas - given by the HTC reactions - occurs inside the water mixture and causes an increase of the vapour pressure with respect to the predicted values (e.g., increase of 2.8 bar, at 2,500 s).

The thermal behaviour of the system can be roughly represented by three different stages. A first stage of heating (until 100-110 °C), a second stage (until reaching the set point) and a plateau. The changing in the slope of the curve between the first and the second stage has been modelled introducing a convective resistance *Rc*.

8.4 The Henry's law and the measurements of the gaseous phase produced during HTC

In this paragraph, the Henry's law was studied to determine the mole fraction of gaseous phase dissolved in the process water, after a hydrothermal carbonization of biomass.
Henry's law can be written in the form of Equation (8.24).

$$c_W = \frac{P}{k_H} \tag{8.24}$$

where:
c_W , is the concentration of the gas in water, (mol/L);
P., is the actual pressure, (atm);
k_H , is the Van't Hoff constant at 25 °C, (L atm/mol).

The Van't Hoff constant at 25 °C for carbon dioxide is equal to 29.41 L atm/mol. Considering the data of the gaseous phase obtained after the carbonization of the EWC 19.05.03 residue (data reported in Chapter 5 and in Appendix II), the Henry's law was applied to evaluate the amount of carbon dioxide solved in water at the end of a HTC process. In this way, summing this amount of gas solved in the process water to the amount of gas measured in the gaseous phase, it was possible to assess the real total gas production during a hydrothermal carbonization process.

Figure 8.11 reports the results of the calculations made using the data coming from two different test campaign (the complete set of data are reported in Appendix IV, Tables IV.1, IV.2 and IV.3). In these calculations, it was supposed that the gas was composed only by carbon dioxide, thus the values of pressure considered are all referred to be only due to CO_2.

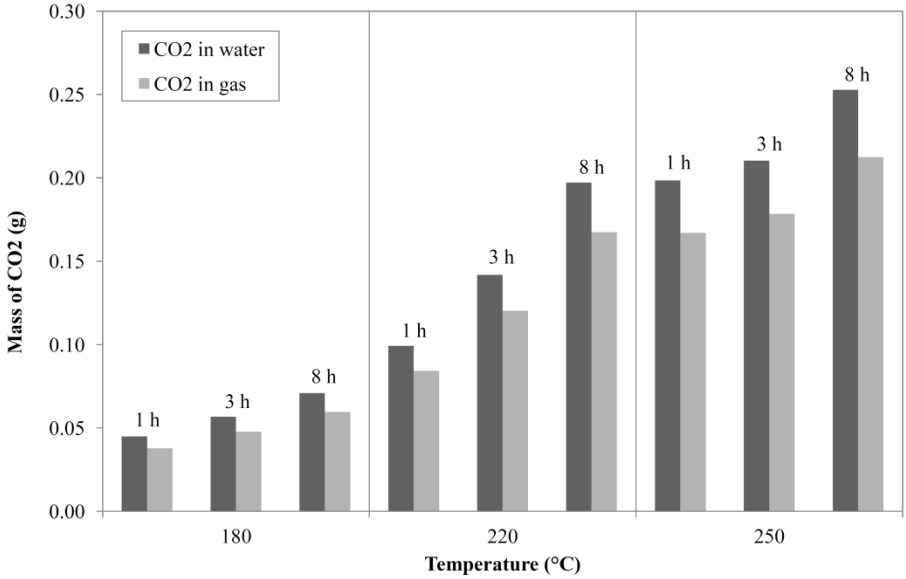

Figure 8.11. Mass of CO_2 in the gaseous phase and within the process water, after HTC at different process conditions (data related to the EWC 19.05.03 residue).

Figure 8.11 highlights the mass distribution of carbon dioxide between the process water and the gaseous phase. Interestingly, from these results it is possible to state that the volume of gas measured after each carbonization is only a fraction of the total gas formed during a HTC process. In Figure 8.12, a comparison between the amount of gas measured after each carbonization and the amount of gas calculated through the Henry's law is reported.

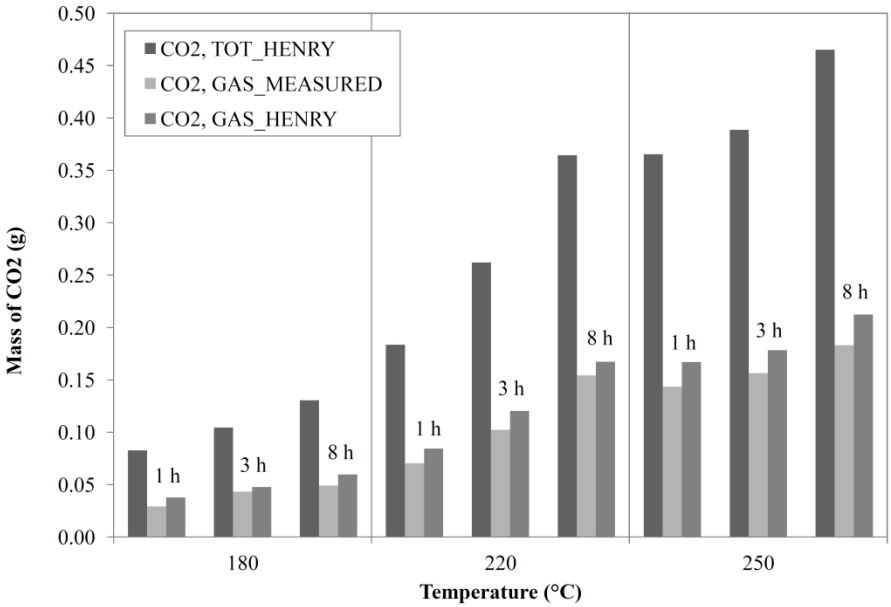

Figure 8.12. Comparison between the results of Henry's law and the direct gas measurements.

In Figure 8.12 "CO2, TOT_HENRY" refers to the total amount of carbon dioxide predicted by Henry's law; "CO2, GAS_MEASURED" refers to the actual amount of carbon dioxide directly measured after every HTC process, while "CO2, GAS_HENRY" refers to the amount of carbon dioxide in the gaseous phase, calculated by applying Henry's law. Interestingly, the amount of gas predicted by Henry's law is very similar to the amount measured, and this fact validate the predictions of the law. Moreover, this support the thesis that the amount of gas directly measured after every test is only a percentage (35 to 42%) of the total mass of gas formed.

8.5 Conclusions of chapter 8

In this chapter, the HTC process has been modelled both considering the kinetics occurring during a hydrothermal carbonization and evaluating the

thermal behaviour of the system. A simple model resembling the process kinetics has been described in paragraph 8.1. A thermo-fluid model describing the temperature profiles within the HTC reactor during the carbonization has been described in paragraph 8.2. This model was developed with a commercial multi-physics software. In paragraph 8.3, the thermal model was improved, describing the reactor behaviour through a simplified dynamic analytic model was built, based on lumped capacitance method. Finally, in paragraph 8.4 the Henry's law was used to investigate the gaseous phase formed during the HTC process. In particular, it was found that more than the carbon dioxide measured through the experimental apparatus should be produced by the process, because a part of it dissolves in the water.

References of Chapter 8

[1] Braghiroli F.L., Fierro V., Izquierdo M.T., Parmentier J., Pizzi A., Celzard A., 2014. Kinetics of the hydrothermal treatment of tannin for producing carbonaceous microspheres. Bioresource Technology, vol. 151, p. 271–277.

[2] Reza M.T., Yan W., Uddin M.H., Lynam J.G., Hoekman S.K., Coronella C.J., Vásquez V.R., 2013. Reaction kinetics of hydrothermal carbonization of loblolly pine. Bioresource Technology, vol. 139, p. 161–169.

[3] Danso-Boateng E., Holdich R.G., Shama G., Wheatley A.D., Sohail M., Martin S.J., 2013. Kinetics of faecal biomass hydrothermal carbonisation for hydrochar production. Applied Energy, vol. 111, p. 351–357.

[4] Luo G., Strong P.J., Wang H., Ni W., Shi W., 2011. Kinetics of the pyrolytic and hydrothermal decomposition of water hyacinth. Bioresource Technology, vol. 102, p. 6990–6994.

[5] Di Blasi C., Lanzetta M., 1997. Intrinsic kinetics of isothermal xylan degradation in inert atmosphere. Journal of Analytical and Applied Pyrolysis, vol. 40-41, p. 287–303.

[6] Prins M.J., Ptasinski K.J., Janssen F.J.J.G., 2006. Torrefaction of wood Part 1. Weight loss kinetics. Journal of Analytical and Applied Pyrolysis, vol. 77, p. 28–34.

[7] Baratieri M., Basso D., Patuzzi F., Castello D., Fiori L., 2015. Kinetic and thermal modelling of hydrothermal carbonization applied to grape marc. Chemical Engineering Transactions, vol. 43, p. 505-510.

[8] Liley P.E, Thomson G.H., Friend D.G., Daubert T.E., Buck E., 1997. Perry's Chemical Engineers' Handbook. Physical and Chemical Data, Section 2, 7th ed., McGraw-Hill, New York.

Chapter 9

Conclusions

9.1 Main conclusions

In this work, three different substrates have been investigated with the purposes to obtain insights on the application of the hydrothermal carbonization process as a viable alternative to valorise wet organic residues. In particular, grape marc (i.e., the residue of wine or distillates production), the EWC 19.05.03 residue and the EWC 19.12.12 residue, two by-products coming from common treatments of municipal solid waste, have been studied. The two main possibility that have been considered, for the exploitation of the hydrochar produced from these residues were: the energy production and the use of hydrochar as a potential soil conditioner. Energy can be produced because typically hydrochar has an energy content higher than the raw feedstock (22 - 28 MJ/kg). Moreover, its chemical and physical characteristics make it comparable to common fossil peats and coals, these similarities suggesting the possibility to co-combust hydrochar with fossil coals. The results reported in this work, support the possibility to exploit hydrochar for this purpose. Furthermore, the big amount of data recovered in studying HTC on grape marc, allowed to get in deep knowledge on this process and were used to calibrate the kinetic and thermal models described in Chapter 8.

According to the European concept of Circular Economy, the recovery of material from a potential waste, prior to use it for energy production,

constitute a more encouraged and noble alternative. For this reason, the hydrochar obtained from the EWC 19.05.03 residue, that is labelled as "off-specification compost", has been tested in phytotoxicity and germination tests. Although in deep analyses have to be done to ensure and validate this hypothesis, preliminary results have shown that the characteristics of this carbonized material have the potentials to provide benefits when applying hydrochar in soil. When considering that, at present, the final destination of the EWC 19.05.03 is the landfill, it is easily understandable that if HTC can transform this residue in a material that can be added to the compost, maybe even enhancing the performances of the compost itself, both economic and environmental benefits are easy to realize. These benefits can rise primarily from the fact that by applying the HTC process, the landfilling of a waste is avoided, moving towards the other European concept of zero waste. Furthermore, all the environmental drawbacks linked to the managing of a landfill are reduced.

Another residue that can be valorised apply the HTC process, while avoiding it to be landfilled, is the EWC 19.12.12. The chemical characteristics of this residue make it suitable for energy production. In fact, because it comes from the treatment of the residual fraction of MSW, that is a very heterogeneous fraction that is transformed into refuse derived fuel, the material entering a HTC plant can be fouled, for example, by the presence of plastics or other contaminating materials. Conversely, the raw EWC 19.12.12 residue cannot be directly used for energy production, because of its high humidity. Thus, the production of hydrochar from this material and the mixing of this hydrochar to RDF can represent a viable solution, that can strongly reduce the environmental impacts of landfills and can again allow to move towards the objective of zero waste.

Finally, this work provides the basis for the development of projects and business plans for real scale applications of the HTC process to valorise the feedstocks here studied.

Appendices

In the appendices, data regarding all the analyses performed on the materials investigated are reported.

Appendix I regards analyses and results obtained for grape seeds, grape skins and grape marc.

Appendix II regards analyses and results obtained for the residue EWC 19.05.03.

Appendix III regards analyses and results obtained for the residue EWC 19.12.12.

Appendix IV reports more information on Chapter 8.

Appendix I

More information on Chapter 4

SEM images

Figures from I.1 to I.4 show pictures of not carbonized grape seeds.

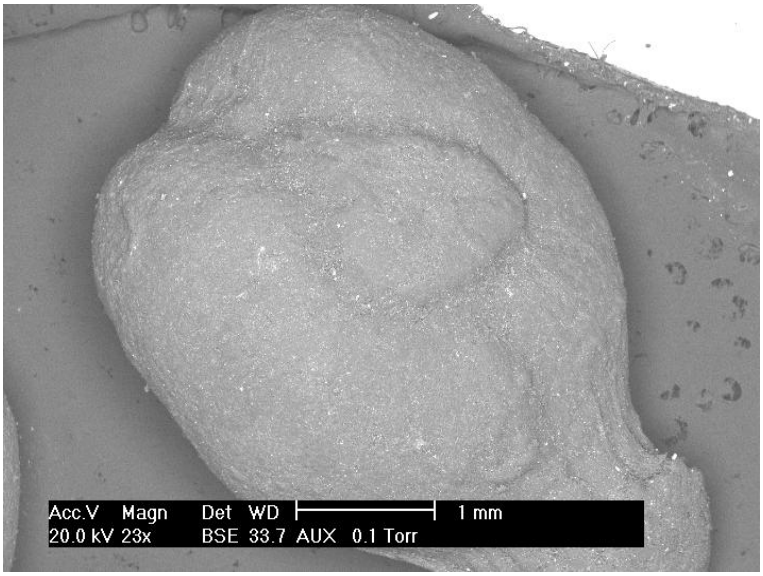

Figure I.1. Not carbonized grape seed.

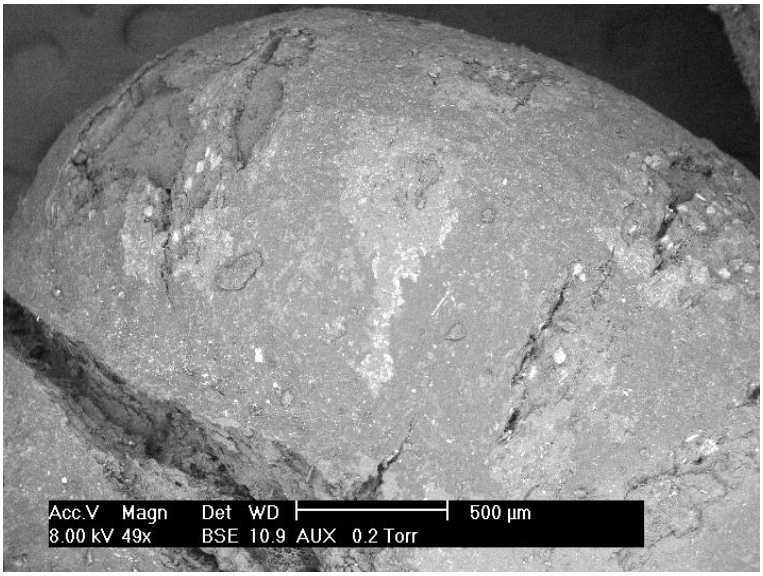

Figure I.2. Not carbonized grape seed (particular).

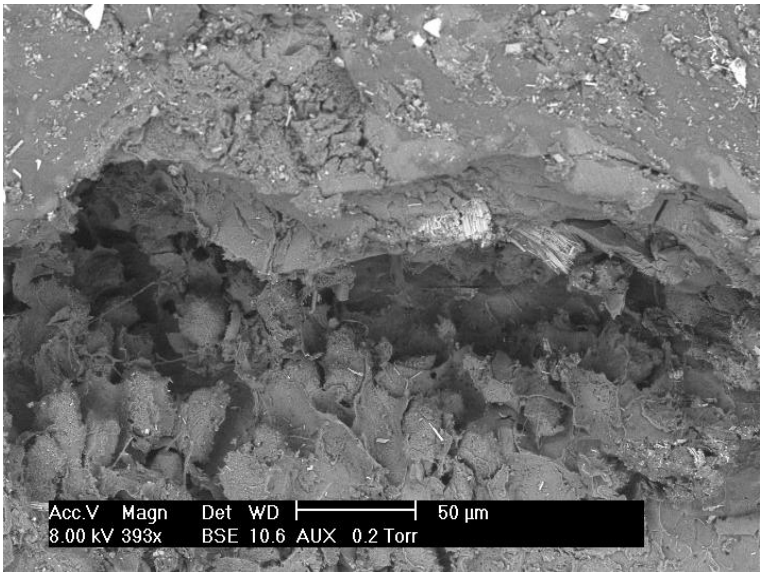

Figure I.3. Not carbonized grape seed (particular).

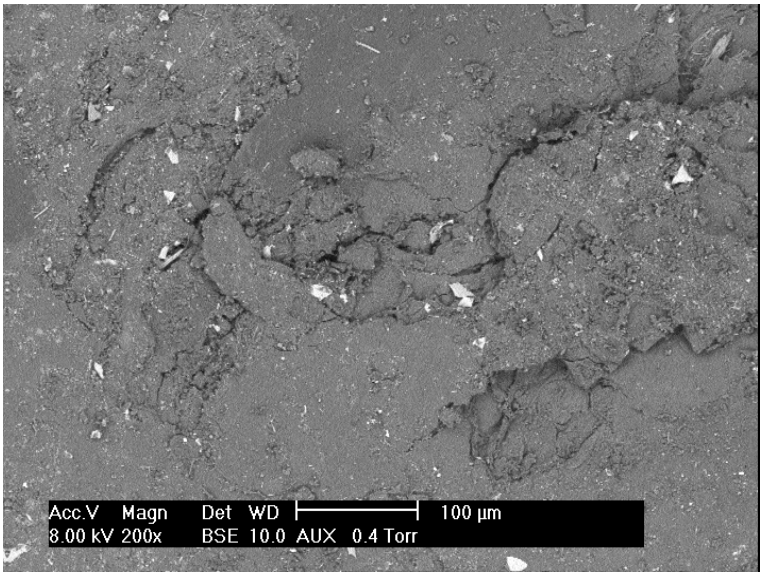

Figure I.4. Not carbonized grape seed (particular).

Figures from I.5 to I.10 show pictures of grape seeds carbonized at 180 °C.

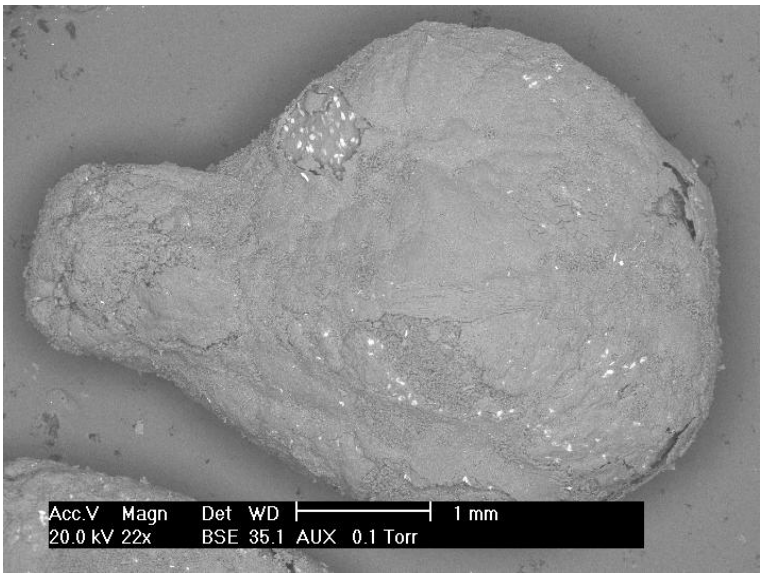

Figure I.5. Grape seeds after HTC at 180 °C for 1 h.

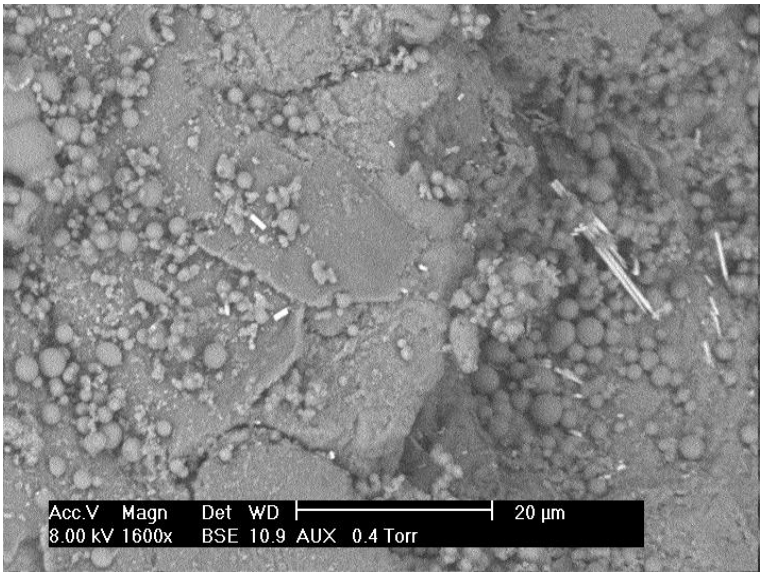

Figure I.6. Grape seeds after HTC at 180 °C for 1 h.

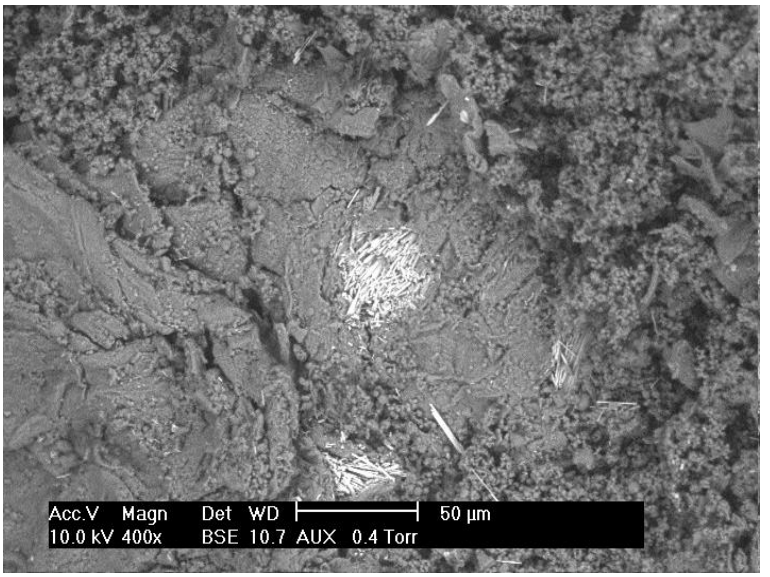

Figure I.7. Grape seeds after HTC at 180 °C for 1 h.

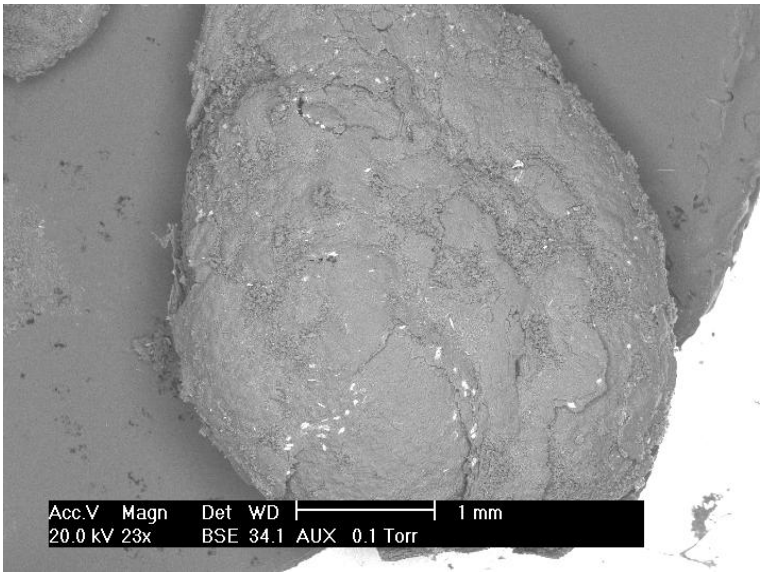

Figure I.8. Grape seeds after HTC at 180 °C for 8 h.

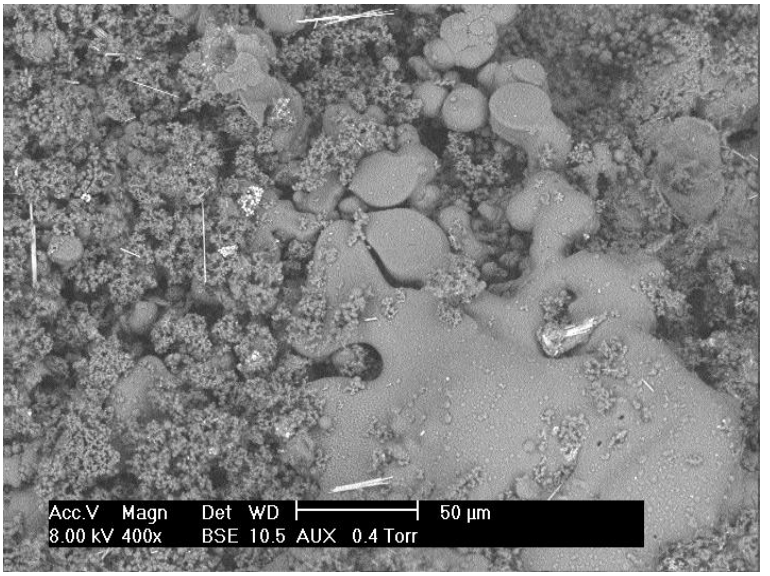

Figure I.9. Grape seeds after HTC at 180 °C for 8 h.

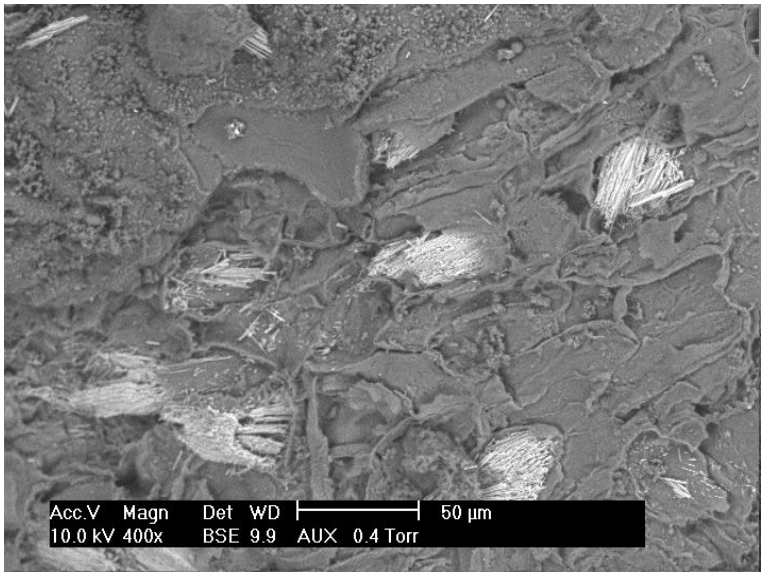

Figure I.10. Grape seeds after HTC at 180 °C for 8 h.

Figures from I.11 to I.23 show pictures of grape seeds carbonized at 250 °C.

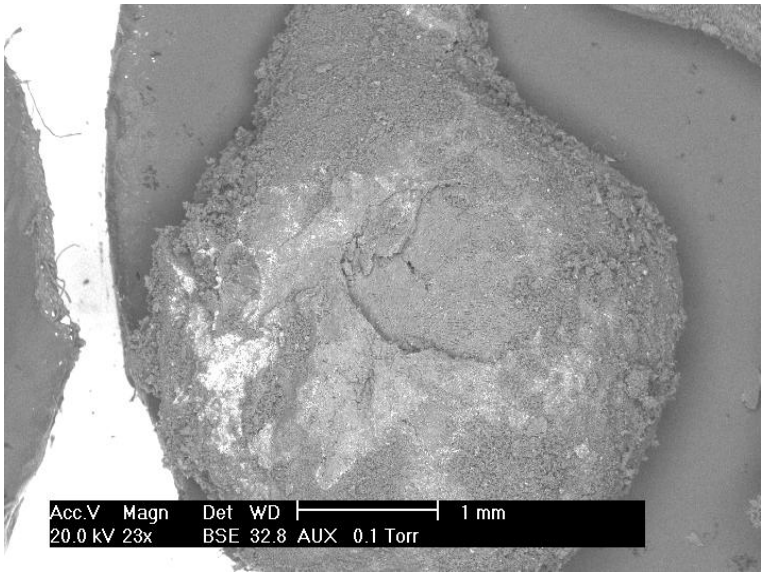

Figure I.11. Grape seeds after HTC at 250 °C for 1 h.

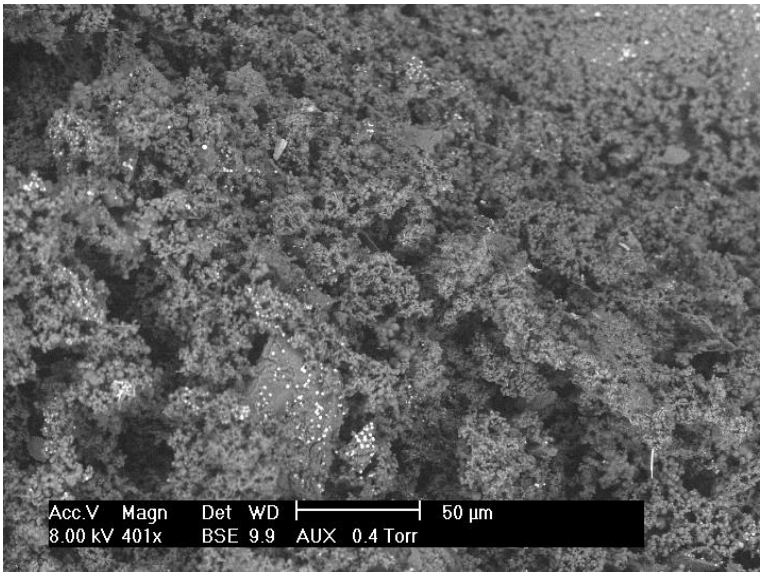

Figure I.12. Grape seeds after HTC at 250 °C for 1 h.

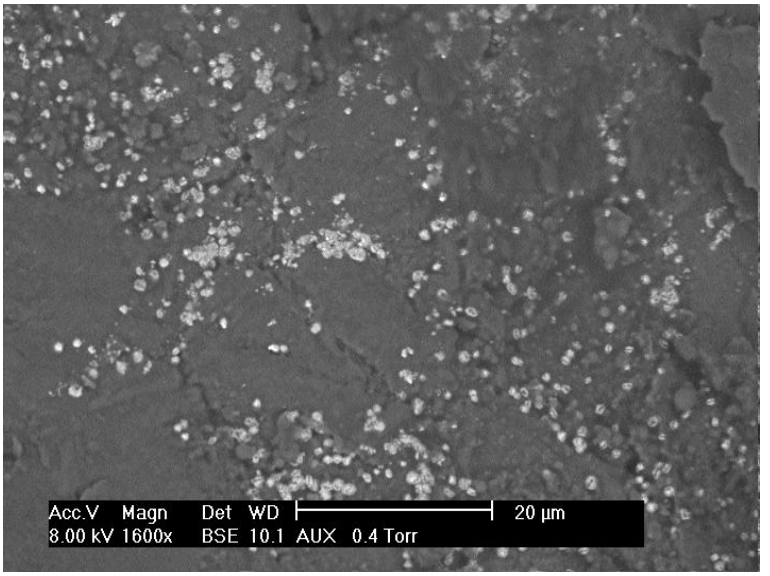

Figure I.13. Grape seeds after HTC at 250 °C for 1 h.

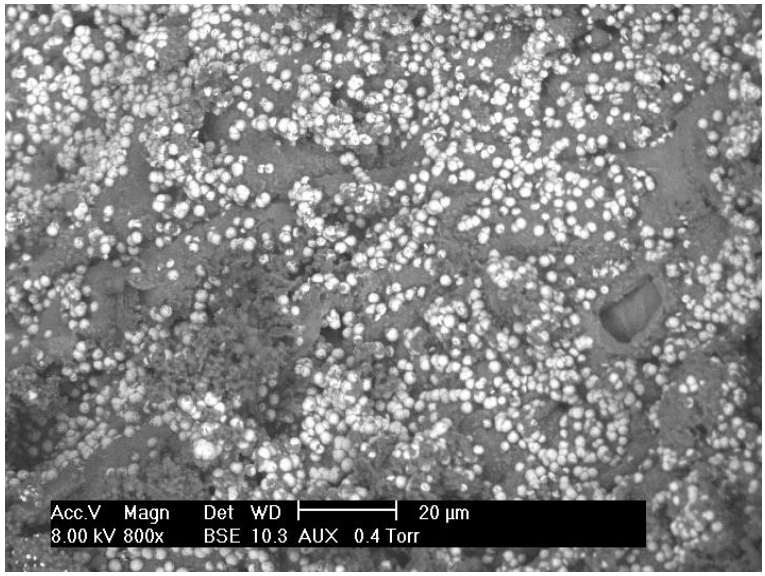

Figure I.14. Grape seeds after HTC at 250 °C for 1 h.

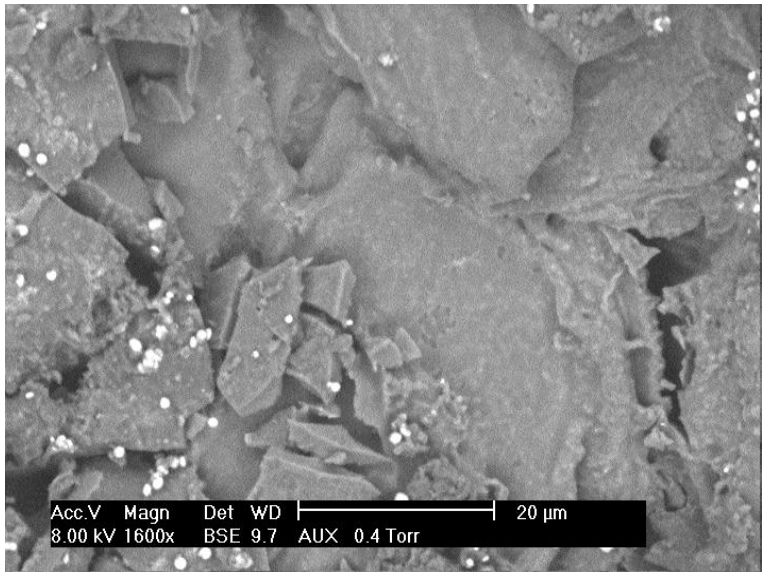

Figure I.15. Grape seeds after HTC at 250 °C for 1 h.

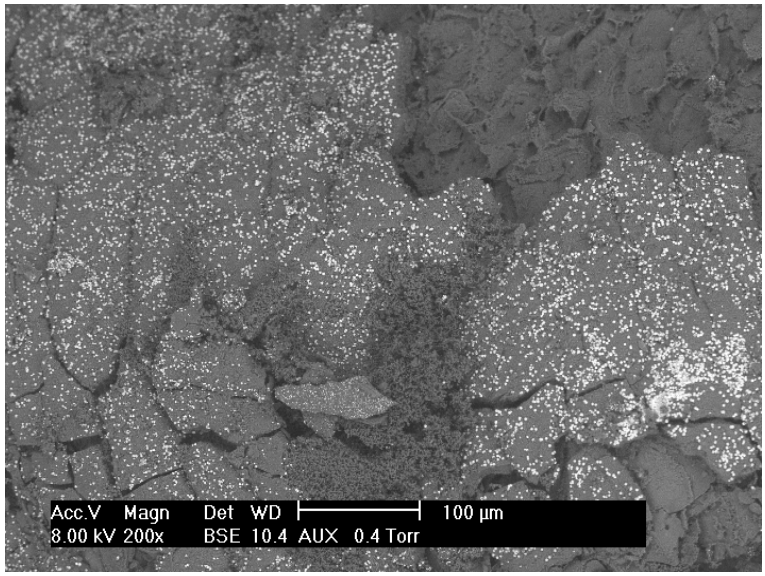

Figure I.16. Grape seeds after HTC at 250 °C for 8 h.

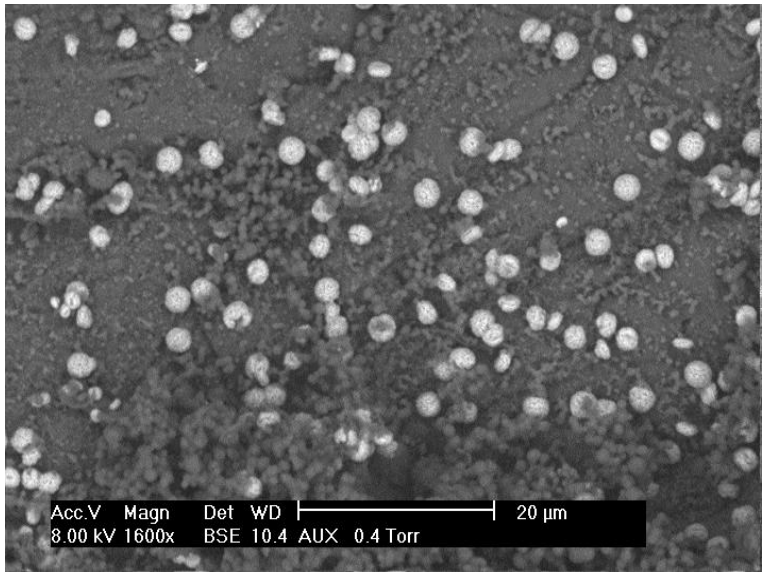

Figure I.17. Grape seeds after HTC at 250 °C for 8 h.

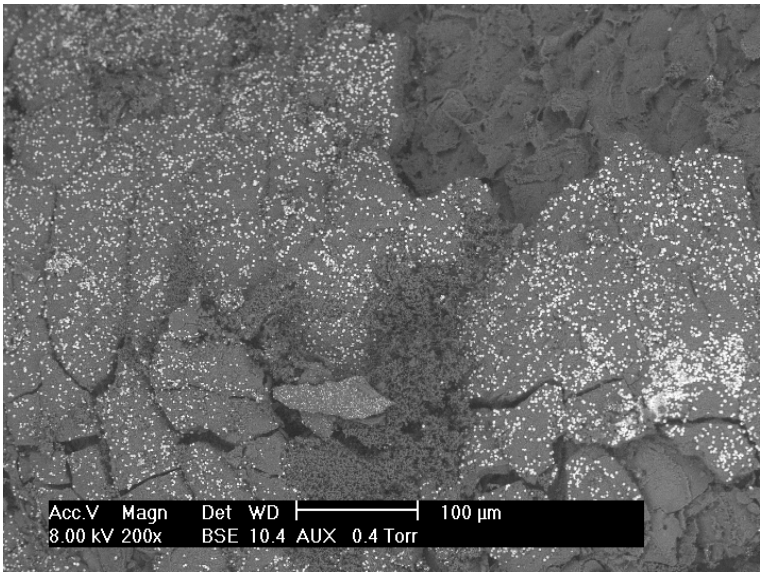

Figure I.18. Grape seeds after HTC at 250 °C for 8 h.

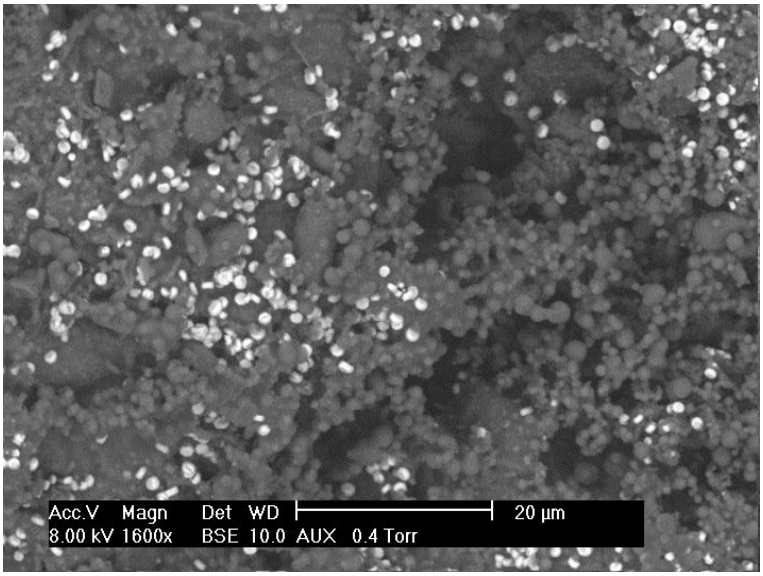

Figure I.19. Grape seeds after HTC at 250 °C for 8 h.

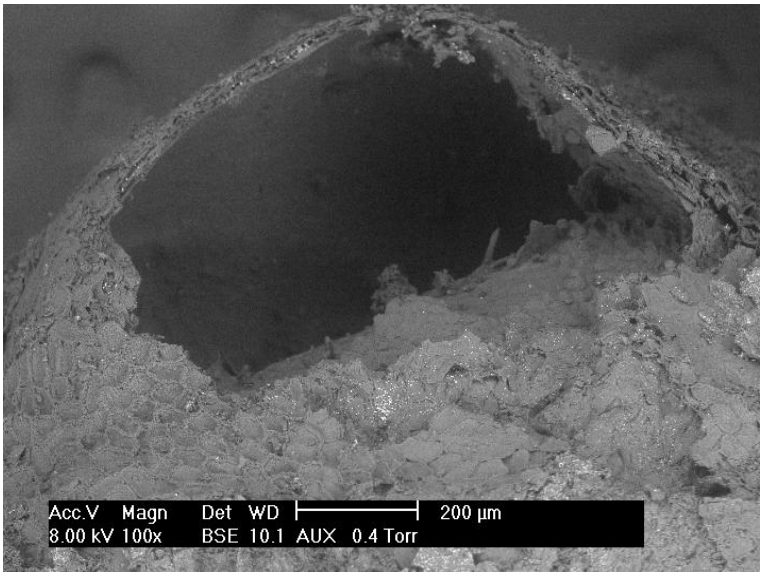

Figure I.20. Grape seeds after HTC at 250 °C for 8 h.

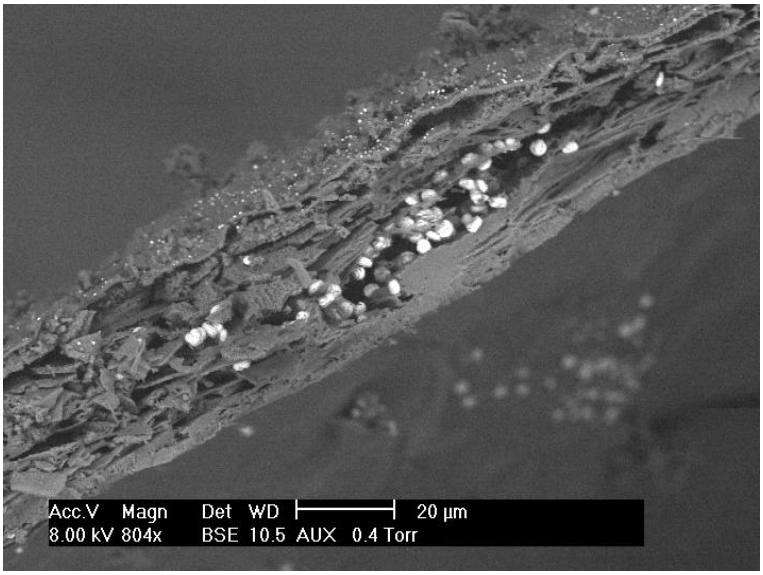

Figure I.21. Grape seeds after HTC at 250 °C for 8 h.

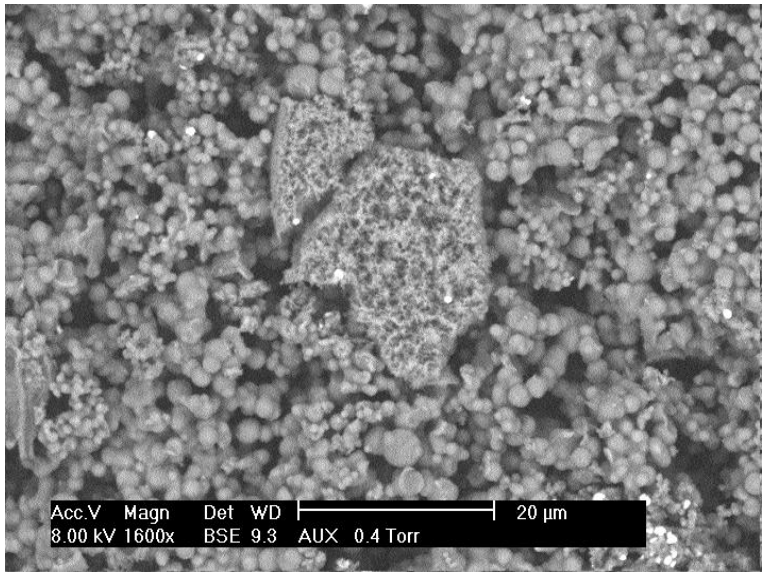

Figure I.22. Grape seeds after HTC at 250 °C for 8 h.

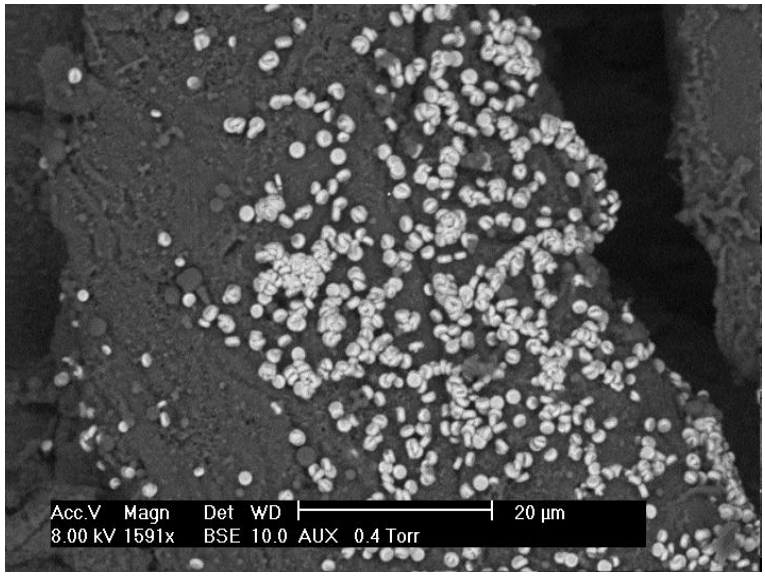

Figure I.23. Grape seeds after HTC at 250 °C for 8 h.

DTG curves

The following figures show the DTG curves obtained for grape marc the hydrochar obtained at different process conditions (180 °C, 220 °C and 250 °C).

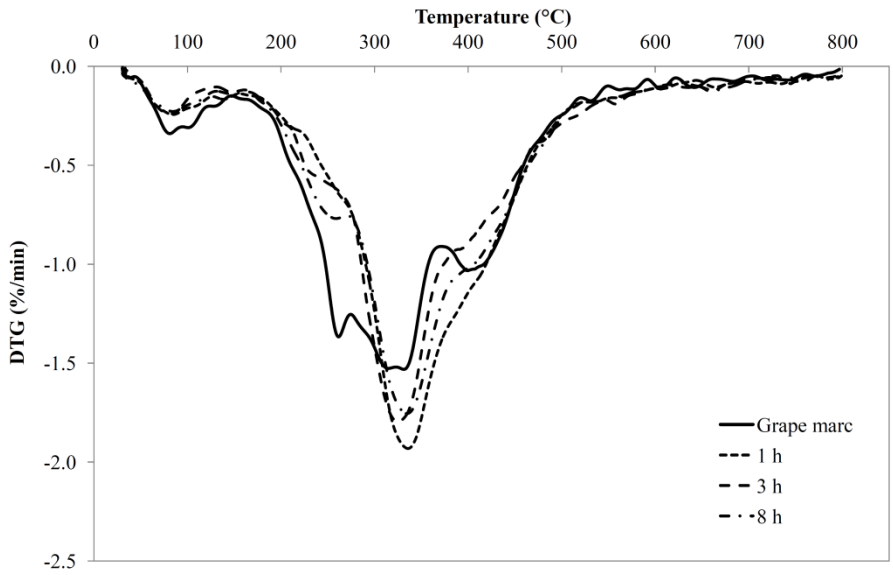

Figure I.24. DTG curves of grape marc and hydrochar from grape marc at 180 °C.

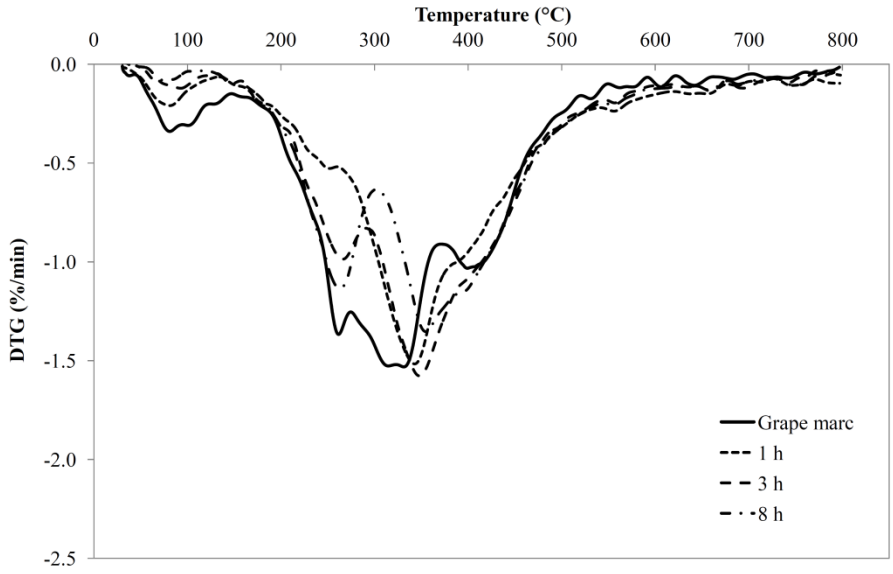

Figure I.25. DTG curves of grape marc and hydrochar from grape marc at 220 °C.

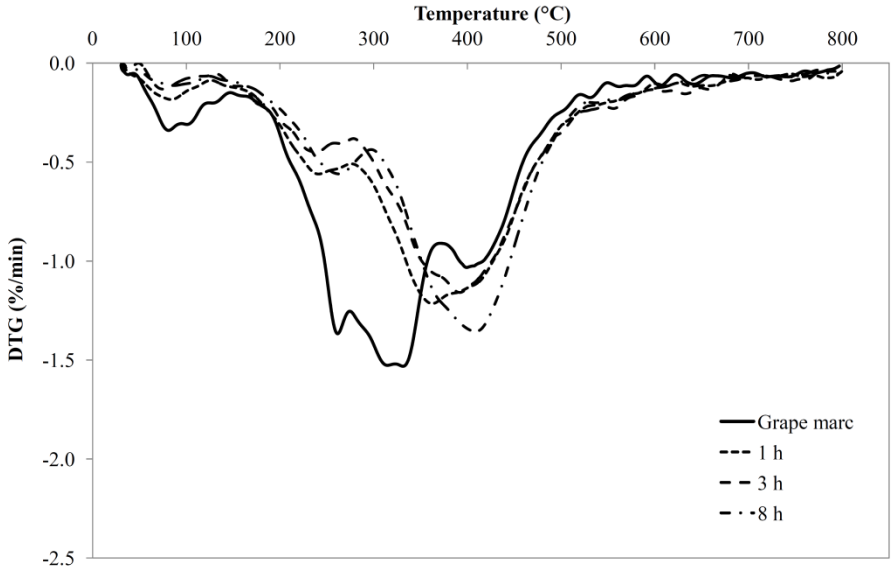

Figure I.26. DTG curves of grape marc and hydrochar from grape marc at 250 °C.

TOC data

		Grape seeds	Grape skins	Grape marc
T (°C)	**Res. time (h)**	**TOC (g/L)**	**TOC (g/L)**	**TOC (g/L)**
180	0.5	20.91	12.77	20.64
	1	19.47	12.97	20.11
	3	17.18	12.60	18.91
	8	14.40	11.63	14.22
220	0.5	16.15	12.75	18.26
	1	16.39	13.03	19.91
	3	17.62	12.72	20.39
	8	17.94	11.81	18.11
250	0.5	19.15	11.62	17.56
	1	18.42	12.41	19.86
	3	20.21	11.73	18.60
	8	19.14	11.80	18.92

Table I.1. TOC data of the liquid obtained after HTC of the three substrates (grape seeds, skins and marc).

Temp. (°C)	Res. time (h)	Al	Ca	Cu	Fe	K	Mg	P	S	Si	Zn	Total (mg/L)	Total (mg)	Ash (%)*
180	0.5	8.8	71.3	0.8	4.9	1767.2	145.2	156.7	12.0	9.3	3.0	2178.9	65.4	33.5
	1	0.0	54.8	0.4	32.2	2223.9	87.4	344.4	47.0	69.0	3.3	2862.4	85.9	44.0
	3	0.6	16.3	1.6	17.9	2247.5	83.2	279.4	43.0	51.1	2.4	2743.0	82.3	42.2
	8	0.3	6.6	0.2	22.0	2151.7	73.5	224.1	26.2	46.1	2.8	2553.5	76.6	39.2
220	0.5	9.3	25.8	0.1	6.3	1841.1	96.9	53.9	14.4	8.8	1.6	2057.9	61.7	31.6
	1	0.1	4.4	0.4	4.4	2031.7	47.9	74.4	38.4	59.4	1.1	2262.2	67.9	34.8
	3	0.0	3.8	0.1	3.5	1945.3	44.2	20.8	27.5	45.3	0.9	2091.4	62.7	32.1
	8	0.0	54.8	0.4	32.2	2223.9	87.4	344.4	47.0	69.0	3.3	2862.4	85.9	44.0
250	0.5	8.7	53.8	0.0	9.1	2662.0	93.1	7.2	20.4	24.5	2.2	2880.8	86.4	44.3
	1	0.0	127.2	0.3	3.3	2099.4	37.4	19.7	38.6	62.6	1.8	2390.3	71.7	36.7
	3	0.0	131.8	0.2	1.0	2233.4	37.4	9.9	14.9	57.5	0.9	2487.0	74.6	38.2
	8	0.0	54.8	0.4	32.2	2223.9	87.4	344.4	47.0	69.0	3.3	2862.4	85.9	44.0

*: Percentage of ash respect to the initial ash within the solid feedstock.

Table I.2. ICP data of the liquid obtained after HTC of grape seeds.

Temp. (°C)	Res. time (h)	Al	Ca	Cu	Fe	K	Mg	P	S	Si	Zn	Total (mg/L)	Total (mg)	Ash (%)*
180	0.5	8.6	135.7	0.3	0.0	2065.4	77.3	91.5	20.6	3.2	1.1	2403.5	72.1	26.7
	1	0.0	126.8	0.0	1.1	2145.1	36.5	129.4	54.8	18.5	2.8	2515.0	75.5	27.9
	3	0.0	69.9	0.0	1.2	2433.6	37.6	125.7	62.9	16.7	2.7	2750.3	82.5	30.6
	8	0.0	12.8	0.0	4.2	2541.7	38.7	102.6	56.7	19.3	2.0	2778.0	83.3	30.9
220	0.5	17.4	45.0	0.5	0.0	2689.8	54.7	54.8	26.5	2.1	1.1	2891.8	86.8	32.1
	1	0.0	4.4	0.0	1.5	2887.3	30.4	75.6	74.8	16.8	2.2	3093.0	92.8	34.4
	3	0.0	6.1	0.0	0.0	2936.3	27.2	51.6	65.8	18.4	2.1	3107.5	93.2	34.5
	8	0.0	3.1	0.0	0.0	2897.3	24.6	37.5	64.2	22.4	3.4	3052.5	91.6	33.9
250	0.5	10.7	34.0	0.5	0.0	2451.5	44.7	27.1	33.0	9.3	0.9	2611.4	78.3	29.0
	1	0.0	4.1	0.0	0.0	3001.2	20.0	39.3	72.7	22.9	1.7	3161.9	94.9	35.1
	3	0.0	20.2	0.0	0.0	3077.4	17.4	15.0	60.5	34.7	1.3	3226.5	96.8	35.9
	8	0.0	27.3	0.0	0.0	3012.8	15.7	23.9	56.5	27.5	1.0	3164.7	94.9	35.2

*: Percentage of ash respect to the initial ash within the solid feedstock.

Table I.3. ICP data of the liquid obtained after HTC of grape skins.

Temp. (°C)	Res. time (h)	Al	Ca	Cu	Fe	K	Mg	P	S	Si	Zn	Total (mg/L)	Total (mg)	Ash (%)*
180	0.5	10.5	164.6	0.2	0.6	2569.7	131.9	143.5	29.3	10.5	1.4	3062.0	91.9	27.9
	1	0.0	133.5	0.0	6.2	2522.5	65.1	216.9	197.9	25.1	3.3	3170.5	95.1	28.9
	3	0.0	39.2	0.0	7.2	3014.4	68.5	199.1	203.7	30.6	1.3	3564.0	106.9	32.5
	8	0.0	12.6	0.0	6.1	2425.2	52.9	144.0	146.2	29.3	1.2	2817.5	84.5	25.7
220	0.5	8.9	37.8	0.4	0.0	3062.7	88.7	67.1	22.1	7.9	0.9	3296.4	98.9	30.0
	1	0.0	11.9	0.0	2.8	3806.3	49.8	113.7	195.1	30.5	1.9	4212.0	126.4	38.4
	3	0.0	8.4	0.0	1.8	4159.9	45.9	72.9	178.8	36.6	3.2	4507.5	135.2	41.1
	8	0.0	8.4	0.0	0.0	3402.7	39.6	49.7	134.7	31.8	1.6	3668.5	110.1	33.4
250	0.5	8.8	23.0	1.0	0.0	2955.5	67.2	16.6	31.4	11.4	1.3	3116.0	93.5	28.4
	1	0.0	9.0	0.0	0.0	3616.4	35.6	44.9	143.0	34.5	1.6	3885.0	116.6	35.4
	3	0.0	42.1	0.0	0.0	3697.5	29.1	27.6	115.6	34.9	1.5	3948.3	118.4	36.0
	8	0.0	47.5	0.0	0.0	3577.5	28.9	14.3	96.5	41.3	1.0	3807.0	114.2	34.7

*: Percentage of ash respect to the initial ash within the solid feedstock. All the values are in μg/L.

Table I.4.1. ICP data of the liquid obtained after HTC of grape marc.

Temp. (°C)	Res. time (h)	TOC (mg/L)	Al (µg/L)	B (µg/L)	Ba (µg/L)	Ca (µg/L)	Fe (µg/L)	K (µg/L)
180	1	15215	0.75	5.4	0.29	85.5	7.85	2444
	3	14783	0.85	5.5	0.29	62.7	8	2695
	8	14727	1	5.8	0.41	7.35	8.1	3069
220	1	14754	<1.00	5.7	0.15	3.55	2.15	3622
	3	16731	<1.00	5	0.15	4	1.45	3125
	8	14695	<1.00	5.1	0.12	6.4	0.7	3020
250	1	15047	<1.00	5	<0.10	20.1	<0.20	3409
	3	14707	<1.00	4.7	<0.10	32.7	<0.20	3444
	8	12997	<1.00	4.7	<0.10	28.4	<0.20	3082

Table I.4.2. ICP data of the liquid obtained after HTC of grape marc.

Temp. (°C)	Res. time (h)	Mg (μg/L)	Mn (μg/L)	Na (μg/L)	P (μg/L)	S (μg/L)	Si (μg/L)	Sr (μg/L)	Zn (μg/L)
180	1	121.6	0.7	12.1	412	97.5	17	0.86	1290
	3	130.8	0.66	12.2	411	109	20.2	0.68	1210
	8	114.2	0.56	10.7	397	88.8	20.3	0.23	1180
220	1	91.75	0.15	13.5	181.5	112	25.3	0.04	0.58
	3	74.4	0.1	10.5	156	95.5	23	0.05	0.45
	8	64.5	0.08	10.4	109.5	106	22.6	0.05	0.37
250	1	63.6	0.07	12.2	78	123.5	26.7	0.07	0.18
	3	46.2	0.09	14	29.9	161.5	31.3	0.09	0.16
	8	11.9	0.07	10.7	54.4	155.5	31.6	0.1	0.19

Table I.4.3. ICP data of the liquid obtained after HTC of grape marc.

GC analyses on the gas phase

Tables I.5, I.6 and I.7 reports the data of the GC analyses performed on the three substrates (grape seeds, skins and marc).

Res. time (h)	180 °C				220 °C				250 °C			
	CO_2	**CO**	**CH_4**	**H_2**	**CO_2**	**CO**	**CH_4**	**H_2**	**CO_2**	**CO**	**CH_4**	**H_2**
0.5	97.65	2.09	0.00	0.26	96.79	3.06	0.00	0.15	94.91	4.85	0.03	0.20
1	99.08	0.80	0.00	0.12	95.76	3.91	0.01	0.32	94.43	5.25	0.06	0.27
3	98.37	1.16	0.00	0.47	95.41	4.27	0.03	0.29	94.60	4.87	0.08	0.45
8	97.19	2.11	0.00	0.70	94.86	4.45	0.02	0.66	92.59	5.93	0.38	1.11

Table I.5. Results of GC analyses of grape seeds, at different process conditions.

Res. time (h)	180 °C				220 °C				250 °C			
	CO_2	CO	CH_4	H_2	CO_2	CO	CH_4	H_2	CO_2	CO	CH_4	H_2
0.5	99.42	0.46	0.00	0.11	97.27	2.51	0.01	0.20	95.17	4.59	0.03	0.21
1	99.34	0.49	0.00	0.16	96.65	3.09	0.00	0.26	94.21	5.54	0.00	0.25
3	98.90	0.78	0.00	0.32	96.30	3.37	0.00	0.33	93.78	5.80	0.00	0.42
8	96.55	2.28	0.00	1.17	95.73	3.79	0.00	0.48	95.85	3.56	0.00	0.59

Table I.6. Results of GC analyses of grape skins, at different process conditions.

Res. time (h)	180 °C				220 °C				250 °C			
	CO_2	CO	CH_4	H_2	CO_2	CO	CH_4	H_2	CO_2	CO	CH_4	H_2
0.5	99.43	0.52	0.00	0.05	96.89	2.96	0.02	0.12	94.93	4.86	0.04	0.17
1	99.10	0.71	0.05	0.14	95.97	3.72	0.03	0.29	93.74	5.89	0.07	0.29
3	98.75	1.01	0.02	0.22	96.02	3.63	0.04	0.30	94.82	4.71	0.11	0.35
8	98.17	1.44	0.03	0.36	96.02	3.64	0.10	0.24	96.32	2.95	0.17	0.55

Table I.7. Results of GC analyses of grape marc, at different process conditions.

Figures from I.27 to I.32 graphically show the results of the GC analyses of grape seeds and skins. The histograms of grape marc are directly reported in Chapter 4.

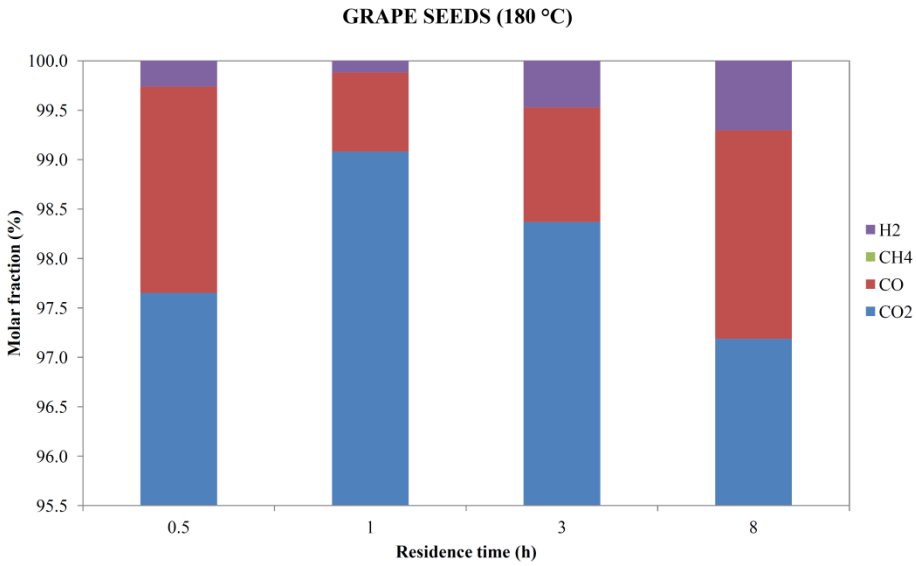

Figure I.27. HTC of grape seeds at 180 °C: gases molar fractions.

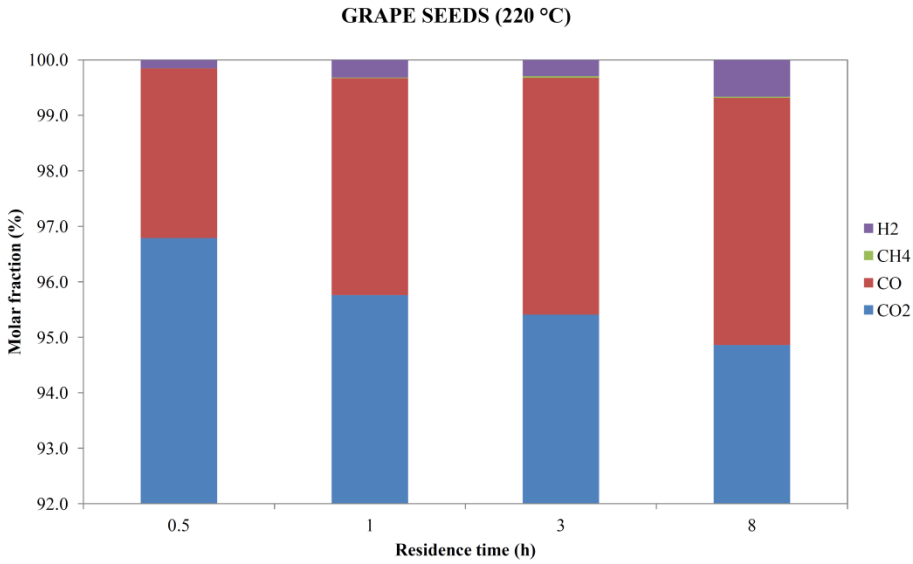

Figure I.28. HTC of grape seeds at 220 °C: gases molar fractions.

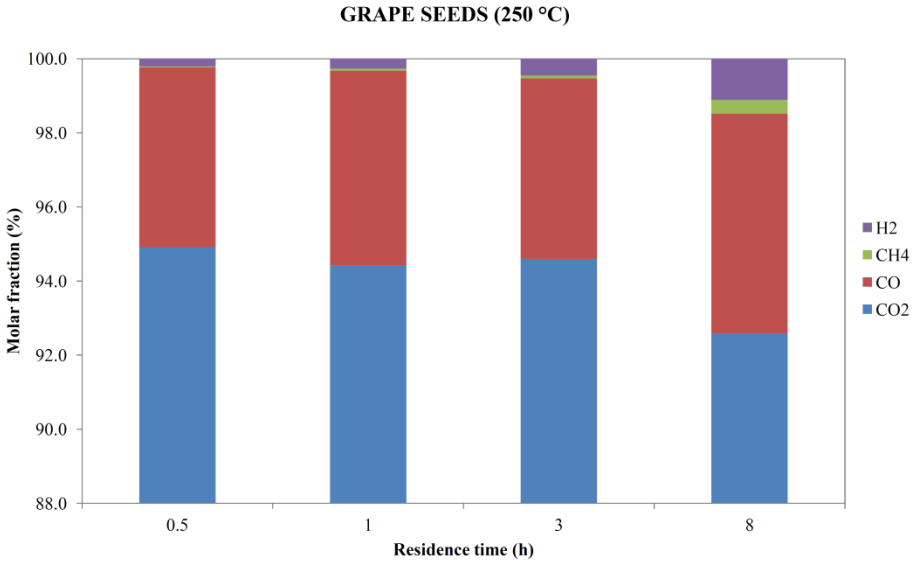

Figure I.29. HTC of grape seeds at 250 °C: gases molar fractions.

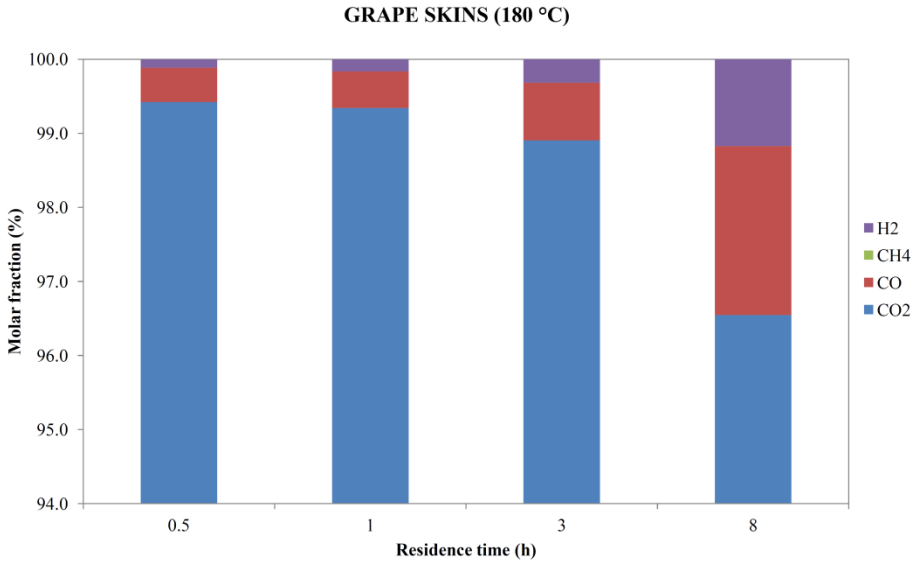

Figure I.30. HTC of grape skins at 180 °C: gases molar fractions.

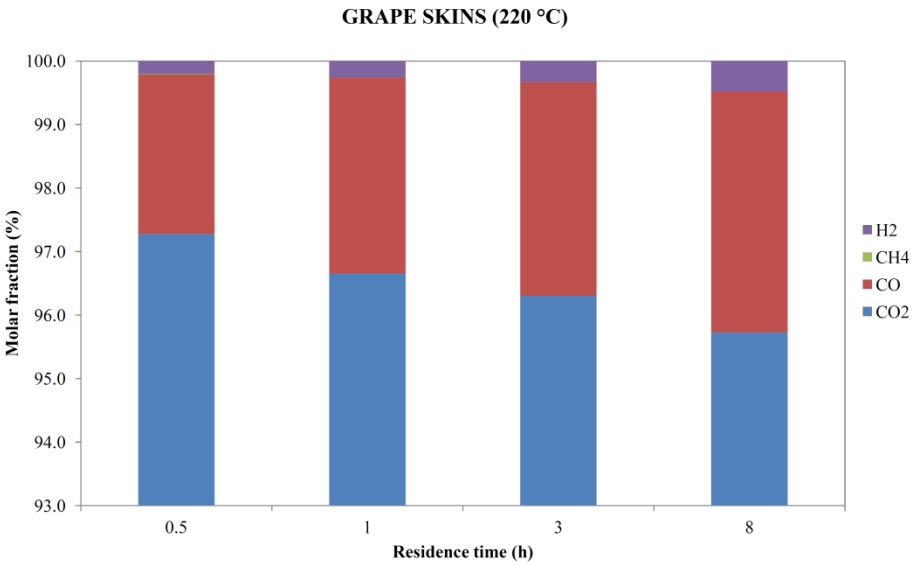

Figure I.31. HTC of grape skins at 220 °C: gases molar fractions.

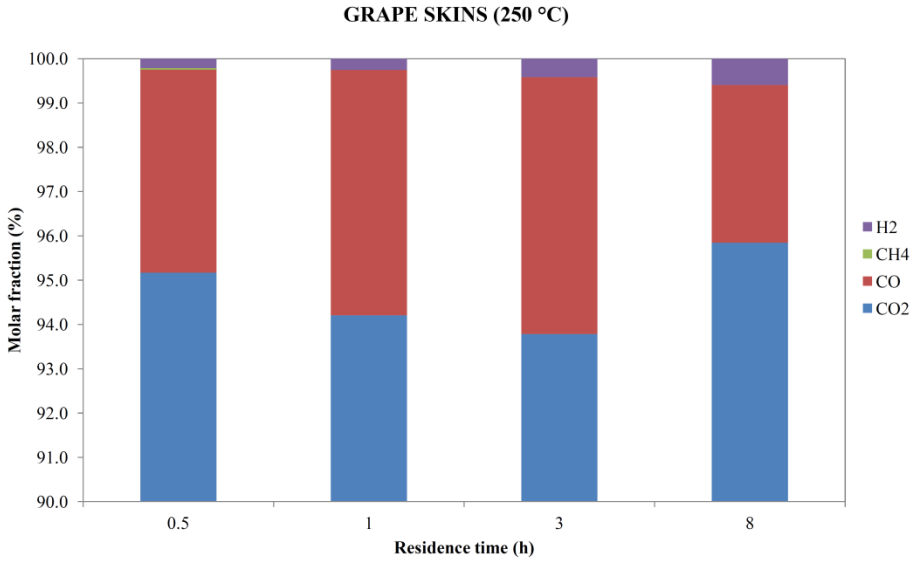

Figure I.32. HTC of grape skins at 250 °C: gases molar fractions.

Carbon balances of grape seeds, grape skins and grape marc

Tables I.8, I.9 and I.10 report the data relative to carbon balance of the three substrates.

GRAPE SEEDS					
T (°C)	**time (h)**	**C Solid (g)**	**C Liq (g)**	**C Gas (g)**	**C tot (g)**
180	0.5	2.73	0.44	0.025	3.19
	1	2.75	0.41	0.029	3.19
	3	2.77	0.37	0.040	3.17
	8	2.80	0.29	0.050	3.14
220	0.5	2.92	0.34	0.063	3.32
	1	2.87	0.33	0.067	3.28
	3	2.73	0.36	0.085	3.18
	8	2.80	0.36	0.103	3.27
250	0.5	2.78	0.39	0.100	3.27
	1	2.59	0.38	0.107	3.08
	3	2.57	0.42	0.117	3.11
	8	2.43	0.39	0.126	2.95

Table I.7. Results of GC analyses of grape marc, at different process conditions.

GRAPE SKINS					
T (°C)	**time (h)**	**C Solid (g)**	**C Liq (g)**	**C Gas (g)**	**C tot (g)**
180	0.5	1.13	0.38	0.021	1.53
	1	1.20	0.39	0.021	1.62
	3	1.11	0.38	0.026	1.52
	8	1.09	0.35	0.019	1.46
220	0.5	1.08	0.39	0.037	1.51
	1	1.09	0.40	0.041	1.53
	3	1.04	0.39	0.049	1.47
	8	1.06	0.36	0.060	1.48
250	0.5	1.02	0.35	0.059	1.43
	1	1.09	0.35	0.071	1.51
	3	0.99	0.35	0.076	1.42
	8	0.95	0.36	0.078	1.39

Table I.7. Results of GC analyses of grape marc, at different process conditions.

GRAPE MARC					
T (°C)	**time (h)**	**C Solid (g)**	**C Liq (g)**	**C Gas (g)**	**C tot (g)**
180	0.5	2.27	0.56	0.028	2.85
	1	2.16	0.55	0.030	2.74
	3	2.11	0.51	0.038	2.66
	8	2.11	0.39	0.046	2.55
220	0.5	2.30	0.51	0.058	2.87
	1	2.13	0.54	0.062	2.73
	3	2.10	0.56	0.080	2.74
	8	2.01	0.50	0.096	2.60
250	0.5	2.09	0.48	0.100	2.67
	1	2.09	0.55	0.098	2.74
	3	1.89	0.51	0.117	2.51
	8	1.85	0.52	0.123	2.49

Table I.7. Results of GC analyses of grape marc, at different process conditions.

Appendix II

More information on Chapter 5

Higher heating values of carbonized EWC 19.05.03

Table II.1 reports data on the HHVs of both the raw residue EWC 19.05.03 and the hydrochars obtained after its carbonizations at different process conditions.

Temperature (°C)	Residence time (h)	HHV (MJ/kg)
180	1	12.597
	3	14.743
	8	15.605
220	1	15.401
	3	17.225
	8	17.176
250	1	16.990
	3	17.620
	8	19.013
Raw material	0	11.736

Table II.1. HHVs of both EWC 19.05.03 and hydrochars.

Digital microscope images

Figures from II.1 to II.4 show digital microscope images of raw feedstock and hydrochars.

Figure II.1. Not carbonized EWC 19.05.03 residue.

Figure II.2. Hydrochar obtained at RT=1 h and T=180 °C.

Figure II.3. Hydrochar obtained at RT=3 h and T=220 °C.

Figure II.4. Hydrochar obtained at RT=8 h and T=250 °C.

SEM images

Figures from II.5 to II.10 show the raw material, namely the EWC 19.05.03 residue, not carbonized.

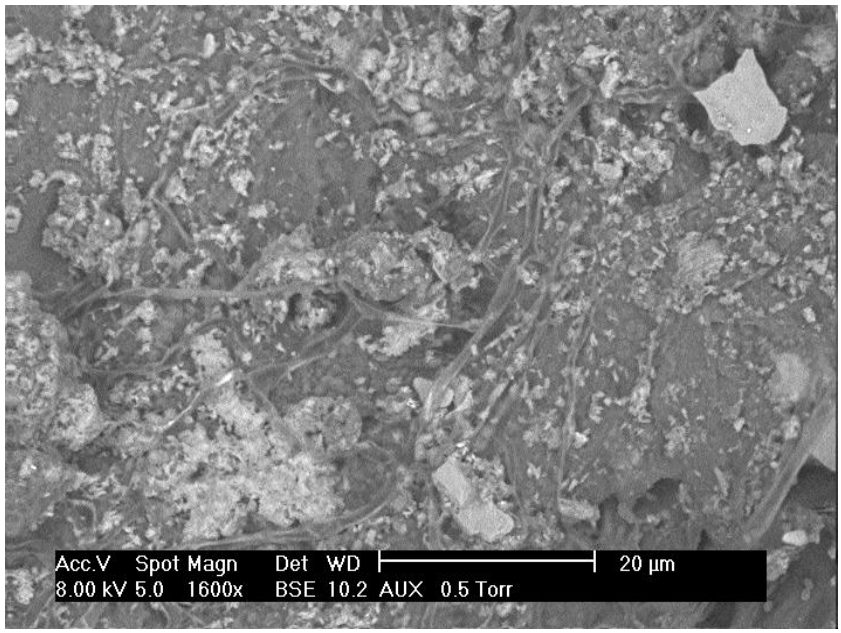

Figure II.5. Not carbonized EWC 19.05.03 residue.

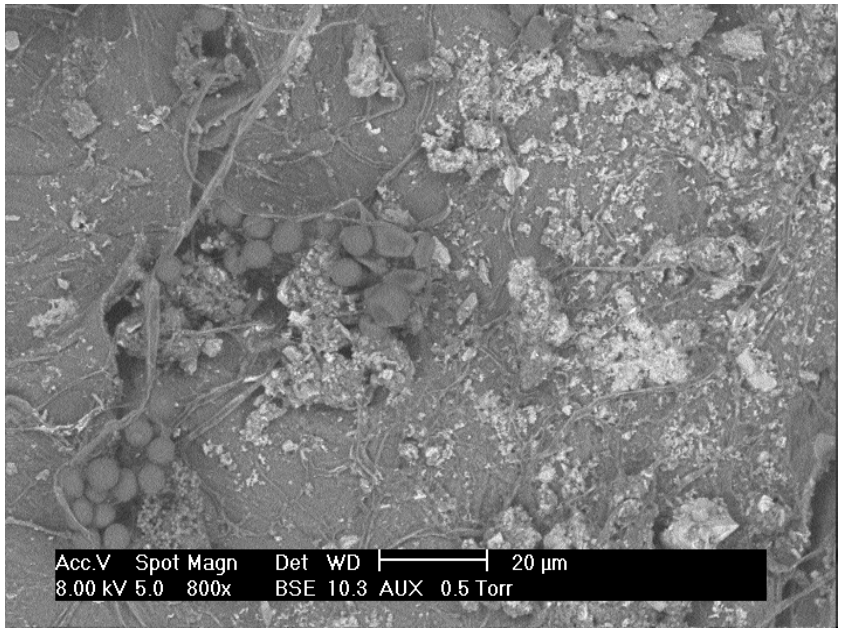

Figure II.6. Not carbonized EWC 19.05.03 residue.

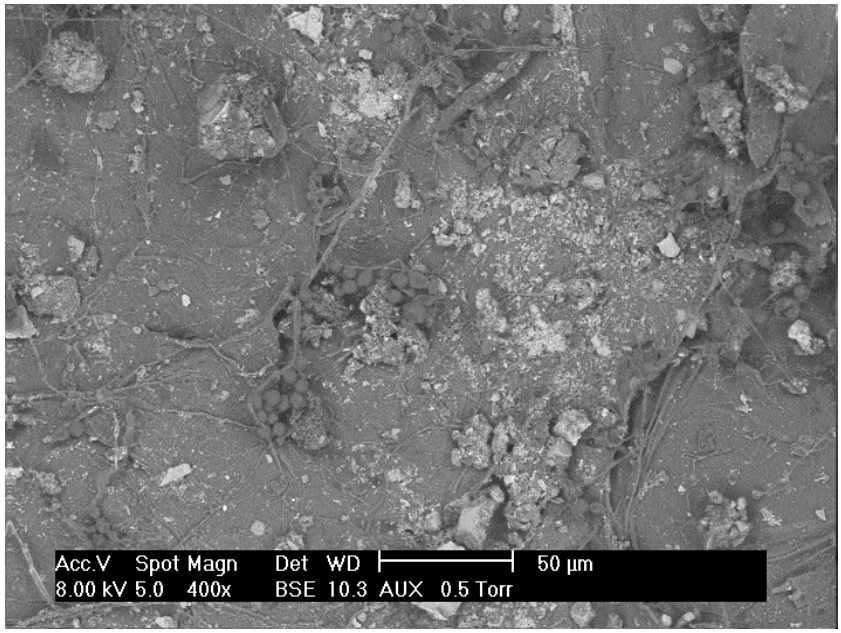

Figure II.7. Not carbonized EWC 19.05.03 residue.

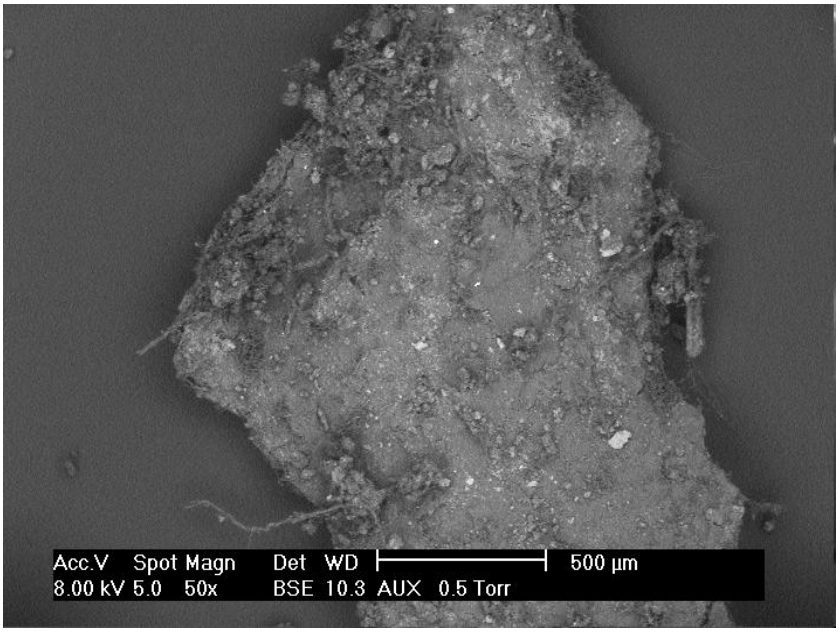

Figure II.8. Not carbonized EWC 19.05.03 residue.

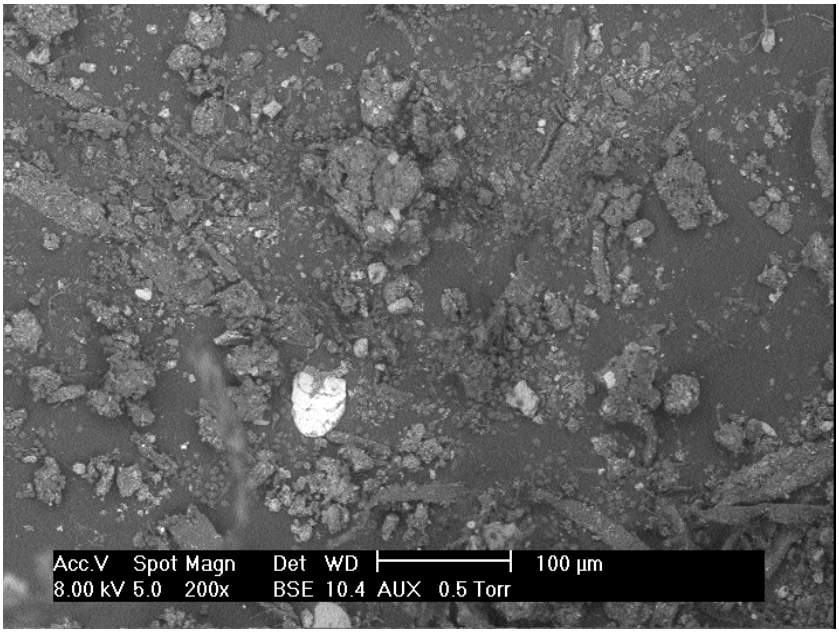

Figure II.9. Not carbonized EWC 19.05.03 residue.

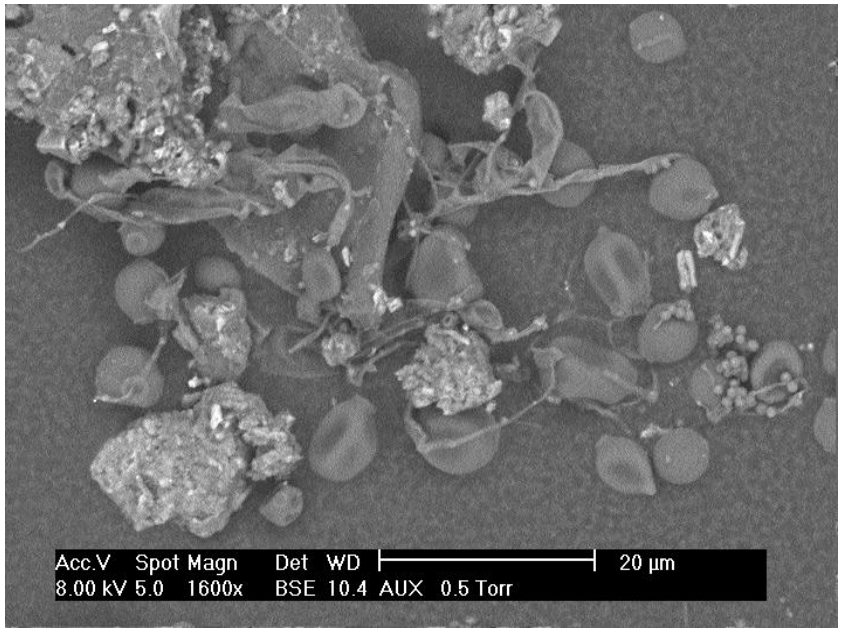

Figure II.10. Not carbonized EWC 19.05.03 residue.

Figures from II.11 to II.15 show the EWC 19.05.03 residue carbonized at 180 °C for 1 h.

Figure II.11. EWC 19.05.03 residue carbonized at 180 °C for 1 h.

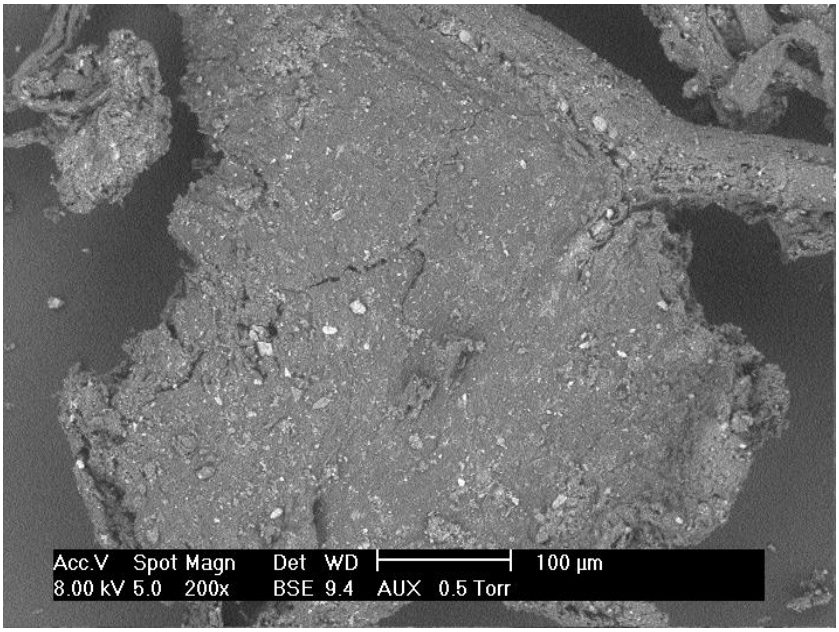

Figure II.12. EWC 19.05.03 residue carbonized at 180 °C for 1 h.

Figure II.13. EWC 19.05.03 residue carbonized at 180 °C for 1 h.

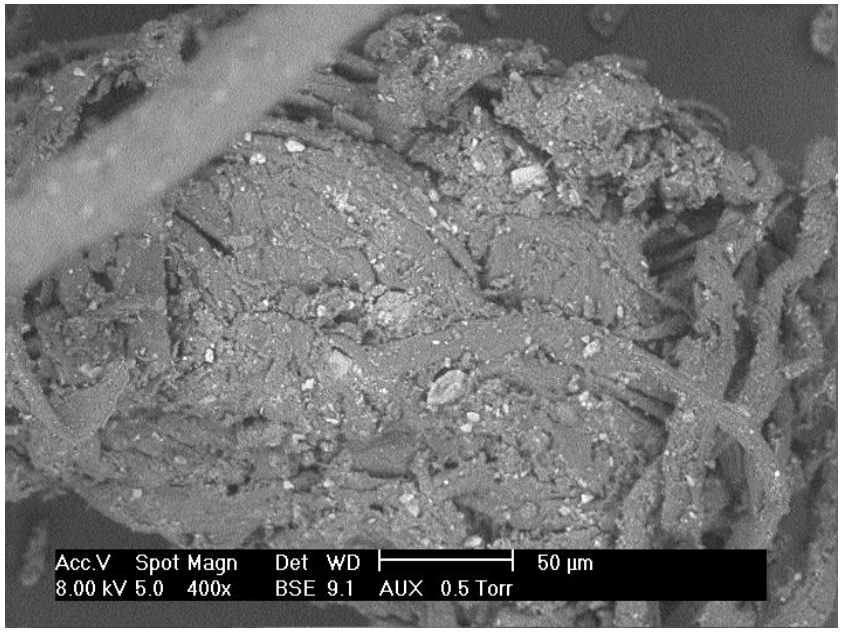

Figure II.14. EWC 19.05.03 residue carbonized at 180 °C for 1 h.

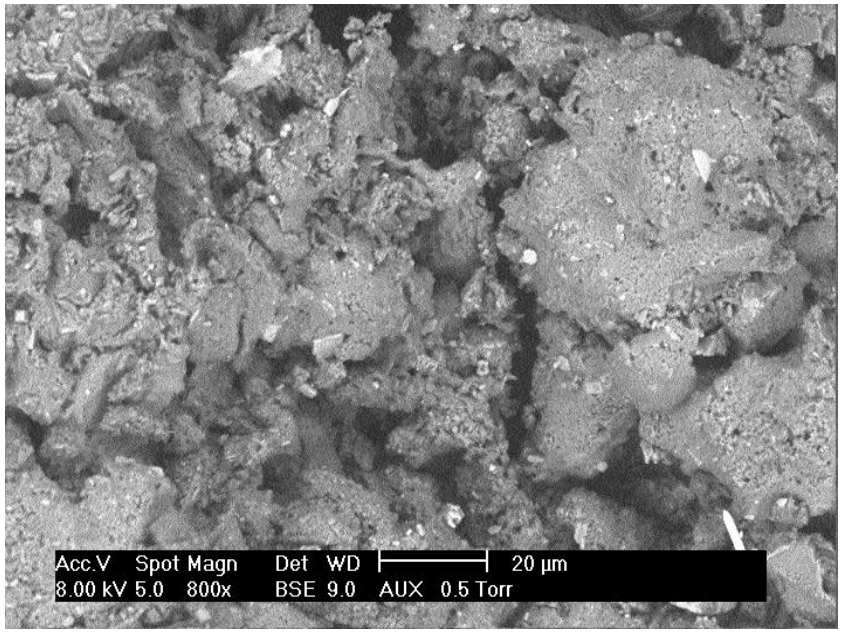

Figure II.15. EWC 19.05.03 residue carbonized at 180 °C for 1 h.

Figures from II.16 to II.20 show the EWC 19.05.03 residue carbonized at 250 °C for 8 h.

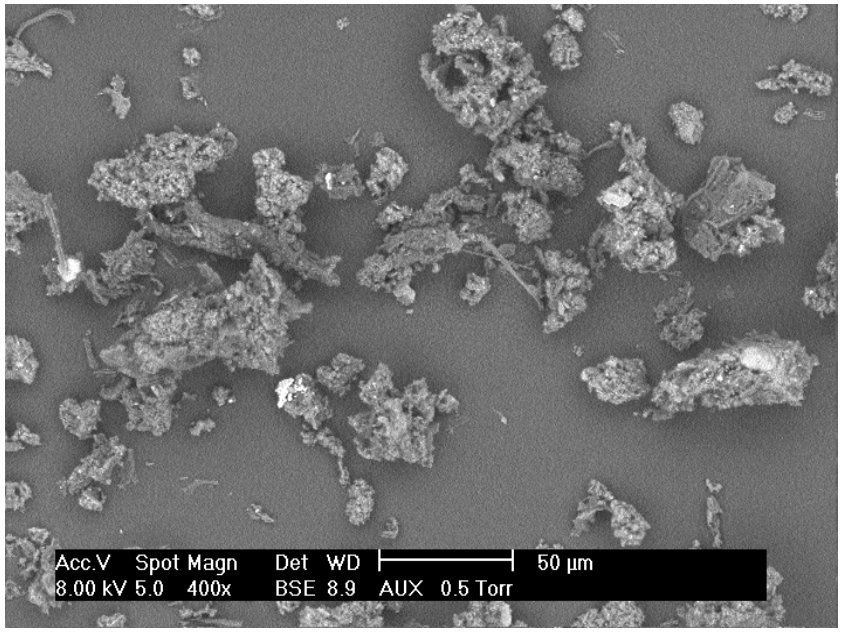

Figure II.16. EWC 19.05.03 residue carbonized at 250 °C for 8 h.

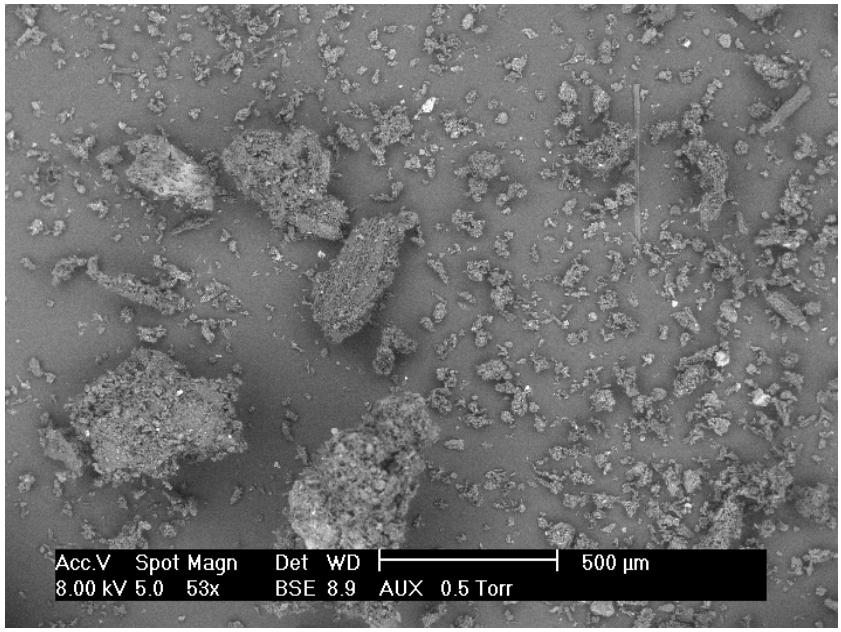

Figure II.17. EWC 19.05.03 residue carbonized at 250 °C for 8 h.

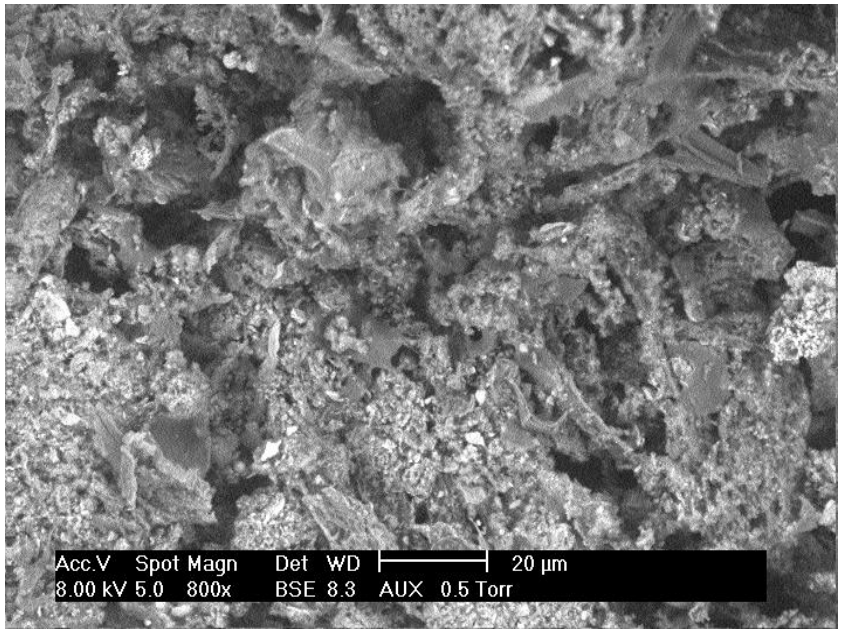

Figure II.18. EWC 19.05.03 residue carbonized at 250 °C for 8 h.

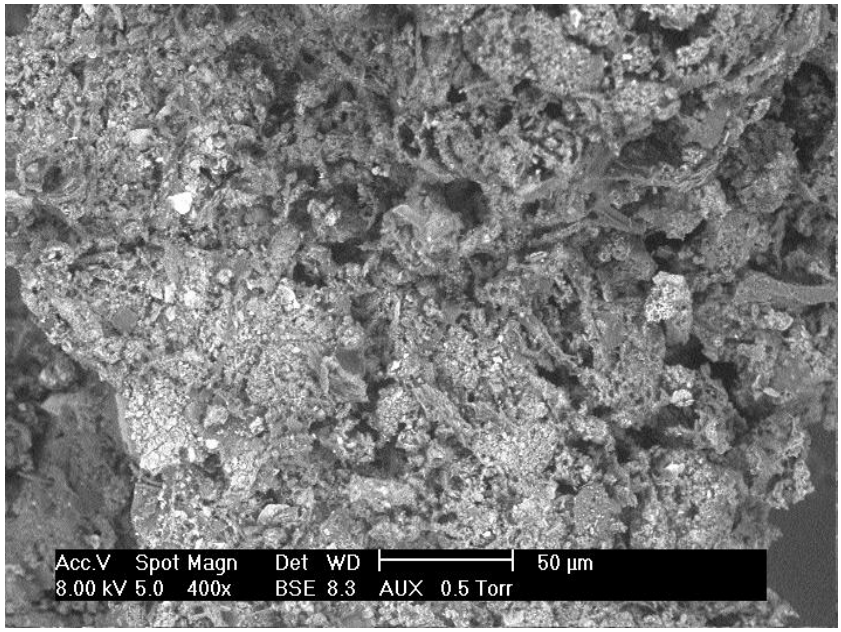

Figure II.19. EWC 19.05.03 residue carbonized at 250 °C for 8 h.

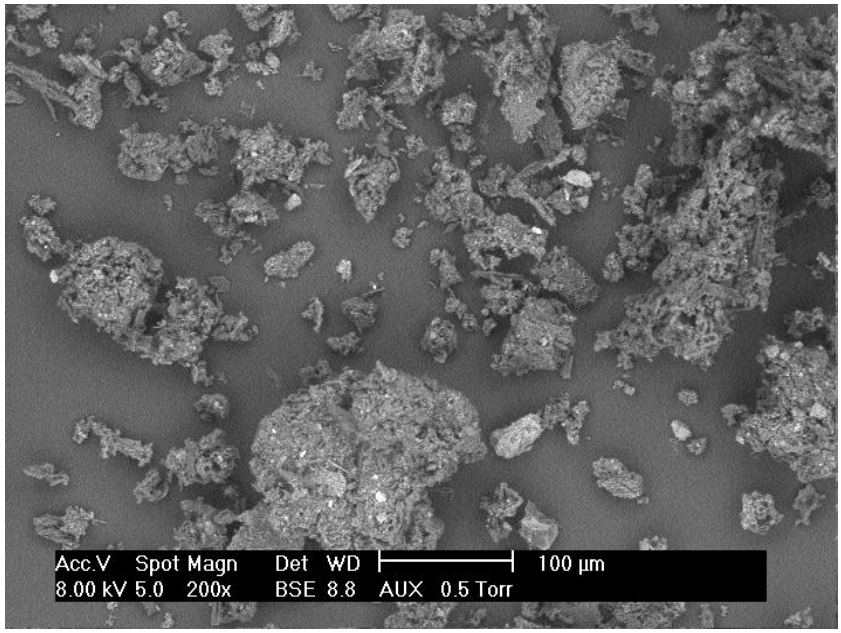

Figure II.20. EWC 19.05.03 residue carbonized at 250 °C for 8 h.

ICP data of the liquid phase obtained at different process conditions

Table II.2 reports data on the minerals found within the liquid phase, produced carbonizing the residue EWC 19.05.03 at different process conditions.

Temp. (°C)	Res. time (h)	Al (mg/L)	Ca (mg/L)	Cu (mg/L)	Fe (mg/L)	K (mg/L)	Mg (mg/L)	P (mg/L)	S (mg/L)	Si (mg/L)	Zn (mg/L)
180	1	0.0	221.5	0.1	6.6	1096.0	80.3	7.8	31.1	112.1	0.7
	3	0.0	257.1	0.1	7.2	1162.8	87.2	4.5	34.2	90.7	0.6
	8	0.0	335.6	0.3	9.2	1093.9	90.0	1.8	26.0	86.2	0.7
220	1	0.0	348.0	0.8	9.1	1059.7	84.4	3.6	33.25	100.6	1.8
	3	0.0	443.5	0.7	5.4	1231.5	104.1	1.9	34.65	106	1.6
	8	0.0	468.9	0.2	5.0	1198.1	94.0	1.7	24.8	117.5	1.3
250	1	0.0	570.3	0.0	3.2	1236.9	71.5	4.1	29.05	110.6	1.5
	3	0.0	308.0	0.0	10.5	1433.8	133.7	2.2	22.25	155.2	1.1
	8	0.0	827.9	0.9	0.8	1253.7	35.7	0.6	16.2	102.4	0.9

Table II.2.1. Mineral content in the aqueous phase from HTC at different operating conditions.

Temp. (°C)	Res. time (h)	TOC (mg/L)	Al (µg/L)	B (µg/L)	Ba (µg/L)	Ca (µg/L)	Fe (µg/L)	K (µg/L)
180	1	13489	2.2	6.2	1.7	1001	27.7	2444
	3	14103	2.3	5.7	0.66	536.9	19.6	2303
	8	13407	2.1	6.3	2.6	1078.5	32.3	2580
220	1	14682	1.5	6.1	3.75	1148.5	21.9	2587
	3	15687	1	6.3	4.35	1103.5	23.4	2778
	8	15405	1	5.8	4.95	1090	12.6	2653
250	1	17473	1	5.8	5.5	1412	15.5	2818
	3	16205	<1.00	4.7	4.7	1129	5.25	2752
	8	14950	<1.00	4.3	5.2	962	1.15	2783

Table II.2.2. ICP data of the liquid obtained after HTC of EWC 19.05.03.

Temp. (°C)	Res. time (h)	Mg (µg/L)	Mn (µg/L)	Na (µg/L)	P (µg/L)	S (µg/L)	Si (µg/L)	Sr (µg/L)	Zn (µg/L)
180	1	337.5	1.85	1014	20.2	116	148	3470	1100
	3	245.7	0.86	961.3	26.9	93	113	1860	0.78
	8	361	2.15	1073	11	147	162	4100	1000
220	1	285	2.4	1071	8.6	163	141	4450	0.9
	3	233.5	2.55	1158	5	170	154	4400	0.85
	8	191	2.1	1098	<5.00	199	123	4450	0.53
250	1	164	3.2	1172	6.5	202	138	5150	0.66
	3	104	2.1	1158	<5.00	216	137	4200	0.24
	8	59.5	1.7	1156	<5.00	262.5	112.5	4100	<0.200

Table II.2.3. ICP data of the liquid obtained after HTC of EWC 19.05.03.

Gaseous phase analysis

Table II.3 reports data on the gases formed during the carbonization of the residue EWC 19.05.03 at different

Temperature (°C)	Residence time (h)	CO_2	σ	CO	σ	H_2	σ	CH_4	σ
180	1	100.0000	0.0000	0.0000	0.0000	0.0000	0.0000	0.0000	0.0000
	3	100.0000	0.0000	0.0000	0.0000	0.0000	0.0000	0.0000	0.0000
	8	94.9711	0.4879	4.5743	0.5187	0.2931	0.0566	0.1614	0.0532
220	1	96.2535	0.0791	3.4869	0.0155	0.1901	0.0726	0.0694	0.0090
	3	94.5971	0.3216	4.7942	0.2228	0.4977	0.2284	0.1110	0.0305
	8	92.9966	0.4067	6.3253	0.3137	0.5836	0.1207	0.0945	0.0105
250	1	91.0809	0.0529	8.1128	0.1284	0.6871	0.1177	0.1192	0.0036
	3	91.1548	0.2923	7.9573	0.0818	0.7554	0.2188	0.1325	0.0043
	8	92.0840	0.1289	6.3332	0.1772	1.3132	0.0974	0.2696	0.0056

Table II.3. Gaseous phase composition.

Seed:			1		2		3		4		5	
Crop	**Variant**	**Germination rate (/10)**	**Root (cm)**	**Shoot (cm)**	**Root (cm)**	**Shoot (cm)**	**Root (cm)**	**Shoot (cm)**	**Root (cm)**	**Shoot (cm)**	**Root (cm)**	**Shoot (cm)**
Mustard	0	10	1.5	2.6	1.2	3.5	4.8	3.7	1.9	4.5	1.4	1.9
	0	10	1.5	2.4	0.8	3.9	2.0	3.0	3.7	3.5	1.4	3.1
	0	10	1.1	3.7	1.7	2.5	2.4	3.2	1.8	3.9	1.2	3.7
	0	9	2.0	2.0	1.5	1.5	1.3	3.5	1.2	2.3	0.9	2.5
	A	3	4.3	2.9	2.4	2	2.2	1.1				
	A	1	1.7	1.8								
	A	1	0.5	0.0								
	A	2	1.2	0.5	1.9	0.6						
	B	5	1.8	2.2	1.6	2.2	1.4	2.2	2.0	2.0	1.5	1.8
	B	8	2.5	3.6	1.1	2.5	1.1	2.8	1.1	2.8	2.2	3.6
	B	10	1.9	2.5	1.6	2.0	2.1	3.3	1.4	2.2	1.3	1.9
	B	8	2.2	2.5	2.6	2.8	2.1	2.3	1.4	2.8	1.8	2.9

Table II.4.1. Phytotoxicity and germination tests results (mustard).

Seed:		6		7		8		9		10	
Crop	**Variant**	**Root (cm)**	**Shoot (cm)**	**Root (cm)**	**Shoot (cm)**	**Root (cm)**	**Shoot (cm)**	**Root (cm)**	**Shoot (cm)**	**Root (cm)**	**Shoot (cm)**
Mustard	0										
	0										
	0										
	0										
	A										
	A	1.7	2.8	0.6	2.1	0.5	2.2				
	A	1.4	2.4	1.0	2.1	0.8	0.0	0.8	1.4	1.5	1.5
	A	1.7	2.0	1.2	2.6	0.8	1.0				
	B										
	B										
	B										
	B										

Table II.4.2. Phytotoxicity and germination tests results (mustard).

Seed:			1		2		3		4		5	
Crop	**Variant**	**Germination rate (/10)**	**Root (cm)**	**Shoot (cm)**	**Root (cm)**	**Shoot (cm)**	**Root (cm)**	**Shoot (cm)**	**Root (cm)**	**Shoot (cm)**	**Root (cm)**	**Shoot (cm)**
Corn	0	9	1.4	0.6	3.3	1.0	3.6	1.1	2.9	0.7	2.1	0.4
	0	10	1.2	1.0	2.7	0.8	2.6	0.9	2.6	0.7	2.0	1.0
	0	9	4.5	0.7	1.7	0.6	0.4	0.6	4.1	0.7	1.5	0.7
	0	10	1.8	0.0	2.0	0.7	2.5	1.1	2.1	0.7	2.6	1.1
	A	8	1.5	0.9	1.6	1.2	1.5	0.9	1.7	0.8	1.2	0.8
	A	9	2.9	0.6	3.0	1.0	2.5	0.7	2.7	0.8	0.5	0.6
	A	9	2.4	0.7	2.7	0.7	1.1	0.8	0.4	0.9	1.6	1.0
	A	9	1.4	0.8	2.0	0.8	1.5	0.8	0.4	0.5	0.0	0.7
	B	9	2.0	0.6	2.2	0.6	2.3	0.6	2.5	0.5	2.5	0.5
	B	9	5.5	0.8	3.0	1.1	3.0	1.1	4.8	0.9	2.7	3.5
	B	10	1.9	0.7	1.8	0.7	1.8	0.0	1.7	0.9	2.4	0.7
	B	9	2.5	1.8	3.0	1.0	2.5	2.5	2.7	1.1	3.9	3.6

Table II.5.1. Phytotoxicity and germination tests results (corn).

Seed:		6		7		8		9		10	
Crop	**Variant**	**Root (cm)**	**Shoot (cm)**	**Root (cm)**	**Shoot (cm)**	**Root (cm)**	**Shoot (cm)**	**Root (cm)**	**Shoot (cm)**	**Root (cm)**	**Shoot (cm)**
Corn	0	2.2	1.2	1.7	0.3	2.3	0.7	0.6	0.5		
	0	2.5	0.8	2.3	0.7	3.3	1.1	3.1	1.0	2.0	0.8
	0	5.3	1.2	3.5	0.5	2.9	0.7	5.9	1.1		
	0	1.8	0.8	2.0	0.8	2.1	0.7	0.9	0.7	1.9	0.7
	A	1.7	0.9	1.2	1.3	1.1	1.4				
	A	1.7	1.0	1.7	0.8	1.2	2.3	2.1	0.7		
	A	2.6	1.5	1.8	2.0	1.7	1.0	1.5	1.0		
	A	1.4	0.9	1.8	1.0	1.5	0.9	1.6	0.8		
	B	2.7	0.6	2.1	0.0	0.9	1.0	2.4	1.0		
	B	4.0	1.5	2.2	3.3	3.4	1.6	2.6	0.7		
	B	1.6	0.9	1.7	0.7	1.8	0.7	1.3	1.4	1.4	0.5
	B	2.2	0.8	2.9	1.1	2.5	1.5	2.9	2.1		

Table II.5.2. Phytotoxicity and germination tests results (corn).

Seed:			1		2		3		4		5	
Crop	**Variant**	**Germination rate (/10)**	**Root (cm)**	**Shoot (cm)**	**Root (cm)**	**Shoot (cm)**	**Root (cm)**	**Shoot (cm)**	**Root (cm)**	**Shoot (cm)**	**Root (cm)**	**Shoot (cm)**
Corn	C	8	3.0	0.8	3.1	0.6	1.7	0.6	1.9	1.1	1.0	0.9
	C	2	0.1	0.0	0.1	0.0						
	C	6	1.6	0.5	1.1	0.6	1.4	0.6	1.0	0.0	1.1	1.0
	C	6	0.1	0.0	0.1	0.0	0.1	0.0	0.1	0.0	0.1	0.0
	D	10	2.2	0.6	2.1	0.7	2.0	0.5	2.8	0.7	1.5	0.8
	D	10	4.0	0.9	3.1	0.7	3.0	1.0	3.0	1.9	3.5	1.5
	D	9	1.1	0.8	0.7	0.6	1.0	0.8	1.1	0.6	1.6	0.9
	D	10	2.1	0.9	2.0	0.6	1.7	0.8	1.4	0.6	1.7	0.7

Table II.5.3. Phytotoxicity and germination tests results (corn).

Seed:		6		7		8		9		10	
Crop	**Variant**	**Root (cm)**	**Shoot (cm)**	**Root (cm)**	**Shoot (cm)**	**Root (cm)**	**Shoot (cm)**	**Root (cm)**	**Shoot (cm)**	**Root (cm)**	**Shoot (cm)**
Corn	C	0.3	0.9	0.9	0.8	1.7	1.5				
	C										
	C	1.1	0.7								
	C	0.1	0.0								
	D	2.3	0.0	2.8	0.7	2.5	0.8	1.9	0.7	0.5	0.7
	D	2.0	1.9	0.7	0.6	1.8	1.2	2.1	1.1	2.5	1.1
	D	1.4	0.8	0.9	0.7	1.2	0.8	1.0	0.8		
	D	1.6	0.8	2.6	0.7	2.3	0.8	1.6	0.7	1.1	1.3

Table II.5.4. Phytotoxicity and germination tests results (corn).

Appendix III

More information on Chapter 6

Figure III.1. Picture of the EWC 19.12.12 residue as received.

Figure III.2. Picture of the EWC 19.12.12 residue as received (detail).

Liquid phase obtained from HTC of the EWC 19.12.12 residue

Tables III.1.1 and III.1.2 report data on the liquid phase, obtained after the carbonization of the EWC 19.12.12 residue.

Temp. (°C)	Res. time (h)	TOC (mg/L)	Al (µg/L)	B (µg/L)	Ba (µg/L)	Ca (µg/L)	Fe (µg/L)	K (µg/L)
180	1	13893	4.2	5.2	1.95	2051	96.9	720
	3	14270	4.2	5.6	3.35	2568	131.4	724
	8	14390	3.15	5.6		2485	125	655
220	1	17798	4	5.6	4.75	3030	145.5	953
	3	17154	2.6	5.6	5.7	3345	85.3	739
	8	16896	2	5.9	3.2	3235	59.2	783
250	1	20870	4.3	5.6	4.8	3877	80.4	759
	3	17654	1.7	6.7	6.3	3180	27.5	761
	8	16260	<1.00	7	7.65	2930	8.2	752

Table III.1.1. ICP data of the liquid obtained after HTC of EWC 19.12.12.

Temp. (°C)	Res. time (h)	Mg (µg/L)	Mn (µg/L)	Na (µg/L)	P (µg/L)	S (µg/L)	Si (µg/L)	Sr (µg/L)	Zn (µg/L)
180	1	250.9	6.77	1458	28.2	461.5	160	5000	6300
	3	256.6	7.83	1463	16.6	398.3	197	6200	5700
	8	233	16.3	1345	11.5	325	240	9100	4
220	1	283	9	1770	22.3	365	156	7400	5300
	3	201	8.2	1555	14.3	380	199	9000	3900
	8	163	8.1	1732	10.4	450	172	11800	1700
250	1	182	8.25	1570	15.2	286	240.5	10500	7800
	3	108.6	6.9	1716	7.9	273	243	13000	1900
	8	58	5	1839	5.2	279	268	14800	0.73

Table III.1.2. ICP data of the liquid obtained after HTC of EWC 19.12.12.

Temp. (°C)	Res. time (h)	Guaiacol (mg/L)	Phenol (mg/L)	Acetic acid (mg/L)	Hydroxyacetone (mg/L)	2-Cyclopenten-1-one (mg/L)	Cyclopentanone (mg/L)
180	1	<200	<200	1360	165	n.d.	n.d.
	3	<200	<200	1600	181	n.d.	n.d.
	8	<200	<200	1622	149	< 100	0
220	1	<200	<200	2120	319	n.d.	n.d.
	3	<200	<200	1930	243	n.d.	n.d.
	8	<200	<200	1700	125	n.d.	n.d.
250	1	<200	<200	2090	560	204	n.d.
	3	240	<200	1935	0	139	n.d.
	8	246	<200	1900	0	<100	141

n.d.: Not detected.

Table III.2. GC-FID results for the liquid obtained after HTC of EWC 19.12.12.

Appendix IV

More information on Chapter 8

Residence time (h)			**1**			**3**			**8**	
Temperature (°C)		**180**	**220**	**250**	**180**	**220**	**250**	**180**	**220**	**250**
1st test campaign	P_{RES} (atm)	1.053	2.211	4.422	1.263	3.158	5.106	1.842	4.422	5.685
	c_{WATER} (mol/L)	0.036	0.075	0.150	0.043	0.107	0.174	0.063	0.150	0.193
	n_{WATER} (mol)	0.001	0.002	0.005	0.001	0.003	0.005	0.002	0.005	0.006
	$CO_{2,WATER}$ (g)	**0.047**	**0.099**	**0.198**	**0.057**	**0.142**	**0.229**	**0.083**	**0.198**	**0.255**
	c_{GAS} (mol/L)	0.043	0.090	0.181	0.052	0.129	0.209	0.075	0.181	0.232
	Void volume (L)	0.021	0.021	0.021	0.021	0.021	0.021	0.021	0.021	0.021
	$CO_{2,GAS}$ (g)	**0.040**	**0.084**	**0.167**	**0.048**	**0.120**	**0.195**	**0.070**	**0.169**	**0.215**
	Gaseous phase (g)	0.028	0.070	0.146	0.039	0.104	0.177	0.056	0.143	0.188

Table IV.1. Henry's law. Results of the 1st test campaing.

Residence time (h)			**1**			**3**			**8**	
Temperature (°C)		**180**	**220**	**250**	**180**	**220**	**250**	**180**	**220**	**250**
2nd test campaign	P_{RES} (atm)	0.948	2.211	4.422	1.263	3.158	4.264	1.316	4.364	5.580
	c_{WATER} (mol/L)	0.032	0.075	0.150	0.043	0.107	0.145	0.045	0.148	0.190
	n_{WATER} (mol)	0.001	0.002	0.005	0.001	0.003	0.004	0.001	0.004	0.006
	CO_2 (g)	**0.043**	**0.099**	**0.198**	**0.057**	**0.142**	**0.191**	**0.059**	**0.196**	**0.250**
	c_{GAS} (mol/L)	0.039	0.090	0.181	0.052	0.129	0.174	0.054	0.178	0.228
	Void volume (L)	0.021	0.021	0.021	0.021	0.021	0.021	0.021	0.021	0.021
	$CO_{2,GAS}$ (g)	**0.036**	**0.084**	**0.167**	**0.048**	**0.120**	**0.162**	**0.050**	**0.166**	**0.210**
	Gaseous phase (g)	0.030	0.070	0.141	0.047	0.101	0.136	0.042	0.165	0.178

Table IV.2. Henry's law. Results of the 2nd test campaing.

Residence time (h)			**1**			**3**			**8**	
Temperature (°C)		**180**	**220**	**250**	**180**	**220**	**250**	**180**	**220**	**250**
AVERAGE	$CO_{2,WATER}$ (g)	0.045	0.099	0.198	0.057	0.142	0.210	0.071	0.197	0.253
	$CO_{2,GAS}$ (g)	0.038	0.084	0.167	0.048	0.120	0.178	0.060	0.167	0.212

Table IV.3. Henry's law. Average results of the two test campaigns.